

Some pages of this thesis may have been removed for copyright restrictions.

If you have discovered material in AURA which is unlawful e.g. breaches copyright, (either yours or that of a third party) or any other law, including but not limited to those relating to patent, trademark, confidentiality, data protection, obscenity, defamation, libel, then please read our [Takedown Policy](#) and [contact the service](#) immediately

THE MECHANICS OF THE CONFORM CONTINUOUS EXTRUSION PROCESS

PAUL KALEVI CLARKSON WOOD

Doctor of Philosophy

THE UNIVERSITY OF ASTON IN BIRMINGHAM

April 1990

This copy of the thesis has been supplied on condition that anyone who consults it is understood to recognise that its copyright rests with its author and that no quotation from the thesis and no information derived from it may be published without the author's prior, written consent.

THE MECHANICS OF THE CONFORM CONTINUOUS EXTRUSION PROCESS

PAUL KALEVI CLARKSON WOOD

Doctor of philosophy

April 1990

Summary

The work describes the programme of activities relating to a mechanical study of the Conform extrusion process. The main objective was to provide a basic understanding of the mechanics of the Conform process with particular emphasis placed on modelling using experimental and theoretical considerations.

The experimental equipment used includes a state of the art computer-aided data-logging system and high temperature loadcells (up to 260 °C) manufactured from tungsten carbide. Full details of the experimental equipment is presented in sections 3 and 4.

A theoretical model is given in Section 5. The model presented is based on the upper bound theorem using a variation of the existing extrusion theories combined with temperature changes in the feed metal across the deformation zone. In addition, constitutive equations used in the model have been generated from existing experimental data.

Theoretical and experimental data are presented in tabular form in Section 6.

The discussion of results includes a comprehensive graphical presentation of the experimental and theoretical data.

The main findings are:

- (i) The establishment of stress/strain relationships and an energy balance in order to study the factors affecting redundant work, and hence a model suitable for design purposes.
- (ii) Optimisation of the process, by determination of the extrusion pressure for the range of reduction and changes in the extrusion chamber geometry at lower wheel speeds.
- (iii) An understanding of the control of the peak temperature reach during extrusion.

KEY WORDS:

CONFORM
EXTRUSION
LOADCELLS
EXPERIMENTATION
MODELLING

Dedicated to my parents and my son

ACKNOWLEDGEMENTS

I should like to thank the United Kingdom Atomic Energy Authority for providing the funding to make this project possible. My special thanks to Mr. H. K. Slater on behalf of the Springfields Laboratory of the United Kingdom Atomic Energy Authority, for the support and guidance given throughout the duration of the contract.

My sincere thanks to my supervisor Dr. I. M. Cole of Aston University, for his support and technical guidance given throughout the duration of the programme.

I should like to thank Mr. L. W. Crane of Aston University, for co-ordinating the project from inception to completion, and his support given during this time.

CONTENTS

Page No.

Figures (incl. graphs)	9
Tables	13
Computer print print out (hard copy)	13
Symbols	14
1. Introduction	16
1.1. The Conform Concept	16
2. Literature survey	19
2.1. The Mk 2F Conform machine	20
2.2. Radial and tangential die extrusion	22
2.3. Extrusion die and tooling chamber design	23
2.4. The early Conform extrusion die	23
2.4.1. The early radial die	25
2.4.2. The expanding chamber die	26
2.4.3. Tube production	27
2.4.4. Multi-port/multi-abutment die arrangement	30
2.4.5. Other methods of extrusion	33
2.5. Aluminium and copper extrusion	35
2.6. The Mk 2B Conform machine	36
2.7. Machine Instrumentation	36
2.8. Practical difficulties associated copper feed	37
2.8.1. Wheel fatigue	38
2.8.2. Tool fatigue	40
2.8.3. Wheel cooling	41
2.8.4. Abutment cooling	42
2.8.5. Die cooling	44
3. Experimental equipment	45
3.1. Features of the Conform machine	48
3.2. Recording equipment	55
3.3. Feed stock	56
3.4. Preliminary experimental tests	59

3.5.	Measuring equipment	61
3.5.1.	Design of radial die loadcell transducer	61
3.5.1.1.	Considerations	62
3.5.1.2.	Constraints on the die loadcell spring element	62
3.5.1.3.	Choice of strain gauge for the die loadcell	69
3.5.2.	Design of abutment transducer	75
3.5.2.1.	Considerations	75
3.5.2.2.	Strain gauge selection	79
3.5.2.3.	Connection of flying leadwire	79
3.5.2.4.	New tools to accommodate the abutment loadcell	81
3.5.2.5.	Total direct load sensed by the abutment loadcell	83
3.5.2.6.	Friction at the abutment tool/wheel groove interface and its effect on the loadcell test results	85
3.5.2.7.	Isolation of different loads on the abutment tool	86
3.5.2.8.	Ingress of feed metal between the DHUP and abutment tool	87
4.0.	Instrumentation and calibration	89
4.1.	Assembling the hardware	89
4.2.	The test programme	91
4.3.	Installation of instrumentation and connection to sensing devices	96
4.4.	Calibration of measuring equipment	100
4.4.1.	Die loadcell	102
4.4.2.	Abutment loadcell	113
4.4.3.	Pressure transducers	118
4.4.4.	Tachometer	118
4.4.5.	Thermocouple probes	118

5.0.	Theoretical Analysis	123
5.1.	Existing theories	123
5.2.	Elements of the theory of plasticity	125
5.2.1.	Equation for effective stress and strain	125
5.2.2.	Determination of friction conditions	126
5.3.	Upper bound expression for internal work of deformation	128
5.4.	Constitutive equations	134
5.4.1.	Constitutive equation derived from the compression test	137
5.4.2.	Constitutive equation derived from the hot torsion test	139
5.4.3.	Flow softening	140
5.5.	Equation for strain rate	141
5.6.	Effect of temperature and speed	143
5.7.	Work done due to unknown external forces	149
5.7.1.	Abutment force	151
5.7.2.	Die force	152
5.8.	Effect of metal leakage	152
5.9.	Torque and power requirements	154
5.10.	Solution to upper bound expressions	156
5.11.	Equations used for basic machine design criteria	164
6.0.	Experimental and theoretical test data layout	166
6.1.	Experimental data	167
6.1.1.	Geometric constants and variables (measured values)	167
6.1.2.	Deformation (calculations based on measured values)	168
6.1.3.	Loads and pressures	169
6.2.	Theoretical data (based on calculated values)	169
6.2.1.	Geometric variables	169
6.2.2.	Deformation variables	170
6.2.3.	Loads and pressures	170
6.3.	Tabulated experimental data	171
6.4.	Tabulated analytical data	197

7.0.	Discussion of results	221
7.1.	Abutment force	221
7.2.	Die force	234
7.3.	Die temperature	247
7.4.	Torque measurement	259
7.5.	Grip length	267
8.0.	Concluding summary	270
8.1.	Deformation modes	270
8.2.	Force and pressure measurement	271
8.3.	Temperature considerations	273
8.4.	Measuring equipment	274
9.0.	Suggestions for further work	276
	References	279
	Appendices	284
A1		284
A2		291
A3		296
B1		297
B2		303
C1		316
C2		316
C3		317
C4		318
C5		320
D1		322

LIST OF FIGURES INCLUDING GRAPHS

Fig. No.	Description	Page No.
1.0	Main components of the Conform machine	17
2.0	Schematic of Mk 2F Conform machine	21
2.1	Location of die-insert in tool-block	24
2.2	Expanding chamber and die-insert	26
2.3	The bridge-die arrangement	27
2.4	Components of tube-die assembly	28
2.5	Tube extrusion set-up	29
2.6	Twin-port die arrangement	30
2.7	Twin-port/stepped abutment die arrangement	31
2.8	Tool-block assembly	32
2.9	Tube-die arrangement, fed from two grooves	33
2.10	Tangential extrusion with an abutment-die	34
2.11	The axial-die arrangement	35
2.12	Cooling resevoirs in Tool-block	43
3.0	Removal of Conform wheel	46
3.1	A schematic of the Conform machine	46
3.2	Feed rod supply to the wheel	47
3.3	Feed rod cooling	49
3.4	Automatic wire coiling unit	50
3.5	Assembly of tools in the shoe	51
3.6a	Tooling arrangement in the shoe	53
3.6b	Deformation zone in 2-D	53
3.7	Removal of oxide film	54
3.8	Measurement of wheel speed	57
3.9	Measurement of product speed from die	58
3.10a	Die-loadcell and housing assembly (photograph)	63
3.10b	Die-loadcell and housing assembly (schematic)	64
3.11a	Tooling set-up illustrating assembly of tools and abutment-loadcell (photograph)	76
3.11b	Tooling set-up illustrating assembly of tools and abutment-loadcell (photograph)	77

cont

Fig. No.	Description	Page No.
3.12	Residual metal attached to tools after each test	78
3.13	Part tool removal in shoe	80
3.14	Abutment loadcell and tool set-up	82
4.0	Computer stand layout	90
4.1	Base-board unit	90
4.2	Flow chart for data acquisition system	93
4.3	Schematic display of data-logging on computer screen	94
4.4	The work station	97
4.5	Main circuit diagram for base-board unit and measuring equipments connected to all module cards	99
4.6	Main circuit diagram for equipments connected directly to A/D module (AMM1)	101
4.7	Display of data on VDU for calibration	103
4.8	General calibration equipment layout	104
4.9	Heating system for calibration of loadcells	106
4.10a	Calibration of first EN 24 die-loadcell	107
4.10b	Calibration of first EN 24 die-loadcell	108
4.11a	Calibration of first tungsten carbide die-loadcell	110
4.11b	Calibration of first tungsten carbide die-loadcell	111
4.11c	Calibration of first tungsten carbide die-loadcell	112
4.12a	Calibration of first tungsten carbide abutment-loadcell	114
4.12b	Calibration of first tungsten carbide abutment-loadcell	115
4.13a	Calibration of third tungsten carbide abutment-loadcell	116
4.13b	Calibration of third tungsten carbide abutment-loadcell	117
4.14	Calibration of high pressure transducer	120

cont....

Fig. No.	Description	Page No.
4.15	Calibration of low pressure transducer	120
4.16	Calibration conversion factor	121
4.17	Calibration of tachometer	122
5.0	Geometry of deformation zone	129
5.1	Minimum upper bound value for work done	131
5.2	Schematic of deformation zone	133
5.3	Typical stress against strain plasticity curve	136
5.4	Flow chart for processing analytical test data	157
7.0	Abutment force against abutment clearance	222
7.1	Abutment force against reduction ratio	225
7.2	Abutment force against reduction ratio	227
7.3	Abutment force against reduction ratio	228
7.4	Abutment force against reduction ratio	229
7.5	Abutment pressure against reduction ratio	230
7.6	Abutment force against wheel speed	232
7.7	Total pressure against reduction ratio	233
7.8	Abutment pressure against reduction ratio	233
7.9	Macro-examination of discards in die-chamber	235
7.10	Macro-examination of discards in die-chamber	237
7.11	Dead-zone angle against reduction ratio	238
7.12	Die force against reduction ratio	241
7.13	Die force against reduction ratio	242
7.14	Die force against reduction ratio	243
7.15	Die force against wheel speed	245
7.16	Die pressure against reduction ratio	246
7.17	Die temperature against abutment depth setting	249
7.18	Die temperature against reduction ratio	250
7.19	Die temperature against reduction ratio	252
7.20	Die temperature against abutment depth setting	254
7.21	Die temperature against abutment depth setting	254
7.22	Die temperature against reduction ratio	256
7.23	Product temperature against wheel speed	257
7.24	Product temperature against wheel speed	258
7.25	Temperature against reduction ratio	261
7.26	Temperature against wheel speed	262

cont

7.27	Temperature against reduction ratio	266
7.28	Grip length against reduction ratio	269
C.1	Plane boundaries of deformation	318

LIST OF TABLES

Table No.	Description	Page No.
1	Conform wheel design criteria	39
2	Variables considered for preliminary experimental tests	60
3	Temperature and load survey on loadcell washer	65
4	Mechanical properties of tungsten carbide	68
5	Temperature survey on die loadcell	70
6.3	Experimental tabulated data	171
6.4	Theoretical tabulated data	197
B.1	Hard copy print out from computer on completion of each test	297
B.2	Software test programme for data-logging	303
C.3	Constant values for constitutive data	317
C.5	Constant values in heat loss equations	320
D.6	Software test programme for generating theoretical data	322

SYMBOLS

T	torque, temperature
F	force
P	pressure
σ	true stress in uniaxial tension (or compression)
τ	von Mises shear stress using a friction factor
K	von Mises shear stress without friction factor (or $m = 1$)
ϵ	component of true strain, effective strain
$\dot{\epsilon}$	mean effective strain rate
W	work done per unit volume per unit time
R	extrusion ratio (based on final and initial area reduction)
\dot{V}	mean feed metal velocity
\dot{V}	volume flow rate
$\dot{\Delta}$	mass flow rate
Δ	mass
ζ	fraction of feed metal remaining in the deformation zone after metal leakage
t	time
S	wheel speed
ρ	specific volume
C	specific heat capacity
J	mechanical equivalent of heat
α	angle of dead zone
μ	coefficient of friction
m	constant for friction factor, strain rate sensitivity index
n	strain hardening index
$\dot{\theta}$	rate of heat loss per unit area, or length
θ	heat loss
k	thermal conductivity
λ	thermal diffusivity = $k/\rho C$
β	fraction of heat transferred to feed metal

d diameter
L length
V volume
A cross-sectional area
W width of primary extrusion chamber
H abutment penetration depth
SA surface area of the wheel groove in the primary extrusion chamber per unit length
D wheel diameter
A,B,C,D,E constants relating to constitutive equations

Subscripts

L,R,C longitudinal (or uniaxial), radial and circumferential directions respectively
T total
t tooling, total corresponding to a given stage in the deformation zone
h homogeneous deformation
r redundant deformation
i ideal, initial
f friction deformation, final, feed metal
H homologous
1,2,2a,2b,3,4,5 refer to stages in the deformation zone pertaining to changes in the direction of plastic flow
d die, dead zone
a abutment
c container
m mean value
f1,f2 dead zone and land friction force respectively

1 INTRODUCTION

The Conform 'continuous extrusion' process offers a new dimension to the non-ferrous sector of the metal forming industry. In particular, it lends itself to the extrusion of aluminium, copper and aluminium alloys.

Development of the Conform process at the Springfield Laboratory of the United Kingdom Atomic Energy Authority has been synonymous with the enhancement in materials technology over recent years. As a consequence, new tool materials i.e. Niamic alloys, have permitted the efficient mass production of a wide range of sections and hollows from aluminium feed stock.

A Conform extrusion machine will accept feed in either rod or particulate form. Thereby, through the nature of its relatively simple operation, it will permit the production of sections from reclaimed waste (either prime metal waste from manufacturing operations, or used secondary scrap) particulate feed materials. Development in this field has been intense, so that the Conform process is presently considered to be a commercially acceptable alternative to traditional routes in non-ferrous metal processing.

1.1 THE CONFORM CONCEPT

The principle employed in using Conform for the extrusion of solid and hollow sections from non-ferrous metals, in either rod or particulate form, is illustrated in fig. 1.0 The main components are a rotating wheel with a circumferential groove and a stationary shoe. The shoe overlaps a part of the wheel surface and houses the tooling in relation to the wheel groove to form a 'mini-extrusion' chamber. Into this chamber the feed is drawn by frictional grip. The tooling can be of different forms but essentially consists of a grip segment, abutment and die-piece. The grip segment is allowed to penetrate into the wheel groove to ensure that a closed

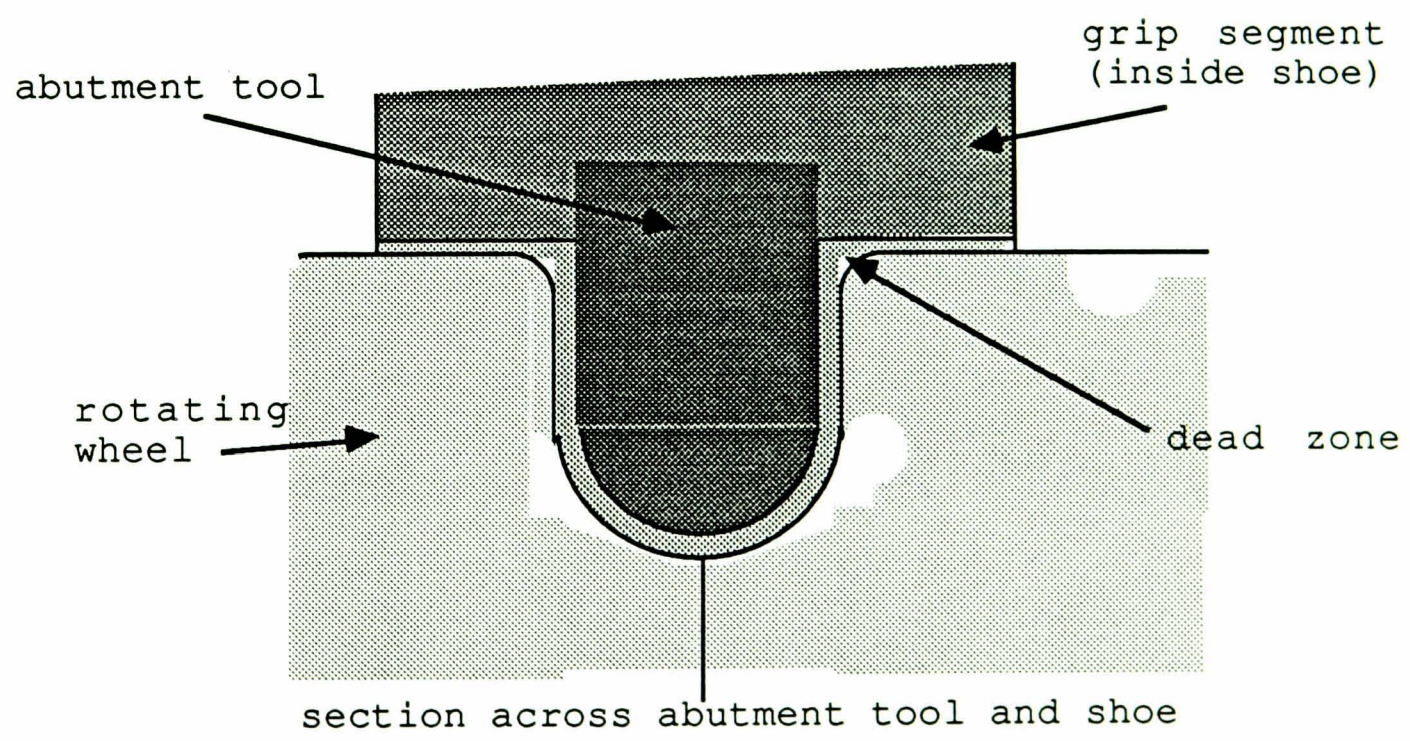
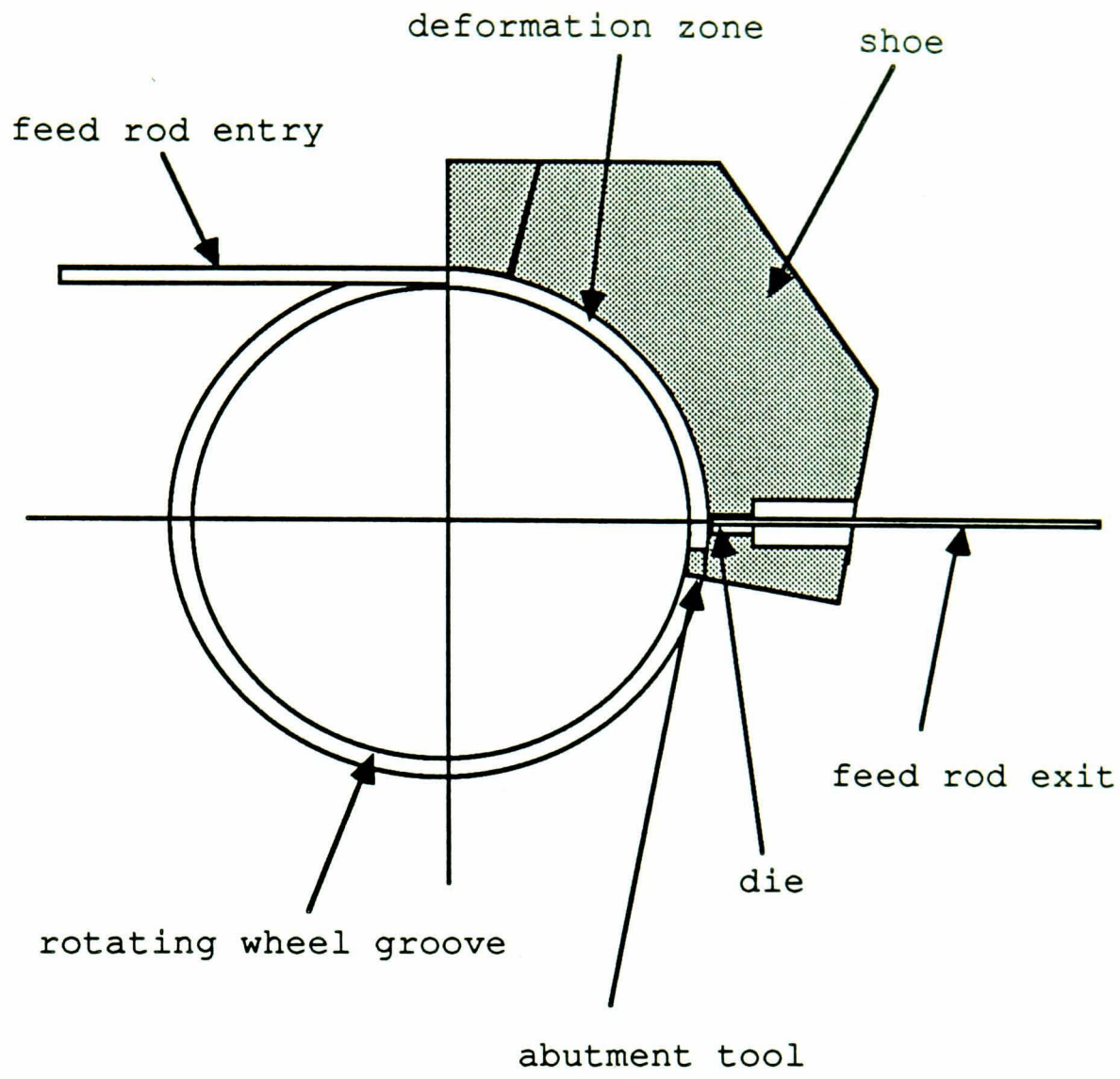


Figure 1.0 The diagram illustrates the main components on the Conform machine

extrusion vessel is provided, the abutment, which penetrates further to the root of the groove as shown in the illustration, is intended to arrest the 'forward' motion of the feed to produce an 'upset zone' in front of the die. Extrusion through a die orifice is then initiated when the flow stress within the feed metal is reached. The die orifice may be situated in a separate segment positioned between the grip segment and the abutment (for radial extrusion) or, alternatively, incorporated in the abutment itself (for tangential extrusion).

Although development of the process has been successfully achieved this was based on short term, specific projects. It was decided that a long term fundamental project was needed to establish the deformation mechanisms involved in the process in order to provide a sound basis for future development work. The work described in this thesis was the result of discussions between staff at the United Kingdom Atomic Energy Authority and Aston University.

2 LITERATURE SURVEY

The review mainly centres on the development work carried out at the Springfields Laboratory of United Kingdom Atomic Energy Authority, since the invention of the Conform process which was attributed to Green⁽¹⁾ in 1972.

Systematic development has demanded many changes to machine design since the first Conform machine was installed at the Springfields Laboratory in early 1974. Particular emphasis has been placed on tool design, materials and their cost. These changes have been necessary in order to enable the extrusion of a wide range of product sections and materials, suitable for commercial applications at a competitive price. Above all, their viability as production machines in industry has demanded an acceptable tool life so that an otherwise continuous extrusion operation is not inhibited.

The development work at Springfields has centred on two Conform machines which were installed in the mid 1970's. The Mk 2F was principally designed for the extrusion of aluminium and its alloys. The Mk 2B machine was employed in the development of copper-based alloys and, in general, harder feed materials.

This survey provides an insight into the development activities carried out at Springfields in a chronological order. For example, the Mk 2F machine was used in the development of aluminium alloys with particular emphasis given to product design, metallography and production capability. The Mk 2B machine, used in conjunction with harder feed materials, was reserved primarily as a test bed for the testing of tools and dies, with consideration given to improvements in tooling materials and design in order to extend fatigue life.

2.1 THE MK 2F CONFORM MACHINE

The mechanical design of the Mk 2F machine is centred on a long shaft which is supported by two large bearings in the framework of the machine, see figure 2.0. At one end of the shaft is a motor unit which induces angular momentum in order to drive the wheel unit situated at the other end of the shaft. The wheel and shoe arrangement overhang the support bearings in order to provide accessibility to the die tools. A disadvantage with this set-up is the magnitude of deflection of the shaft at high load.

The Mk 2F Conform machine was initially intended for use in the production of extruded sections from commercial purity aluminium feed stock of up to 9.5 mm diameter. The machine has been modified subsequently in order to accommodate a particulate feed input from either recycled powder, granular or droplet aluminium alloys.

Initial development work⁽²⁾ on the the Mk 2F Conform machine accepted a rod feed up to 6.35 mm (1/4 in) diameter. At a later date it was considered more economical to use a 9.5 mm diameter feed rod. This is, in the main, attributed to the range of standard feed stock sizes available from the manufacturer, and also limitations on the diameter of the rod feed stock due to the size of the wheel groove and the torque available from the drive unit.

The Mk 2F was capable of producing round wire sections ranging from 3 to 0.5 mm diameter from 9.5 mm diameter rod feed stock (a reduction ratio up to 360 : 1). The corresponding feed rates reached 25 m/s for round wire sections of 0.5 mm diameter (wheel speed of the order 5 rev/min). A higher wheel speed is attainable for smaller reductions, since it is possible to exercise better control on product coiling. The wire products were found to exhibit the mechanical properties expected of annealed aluminium, with matching electrical conductivity of 62% IACS.

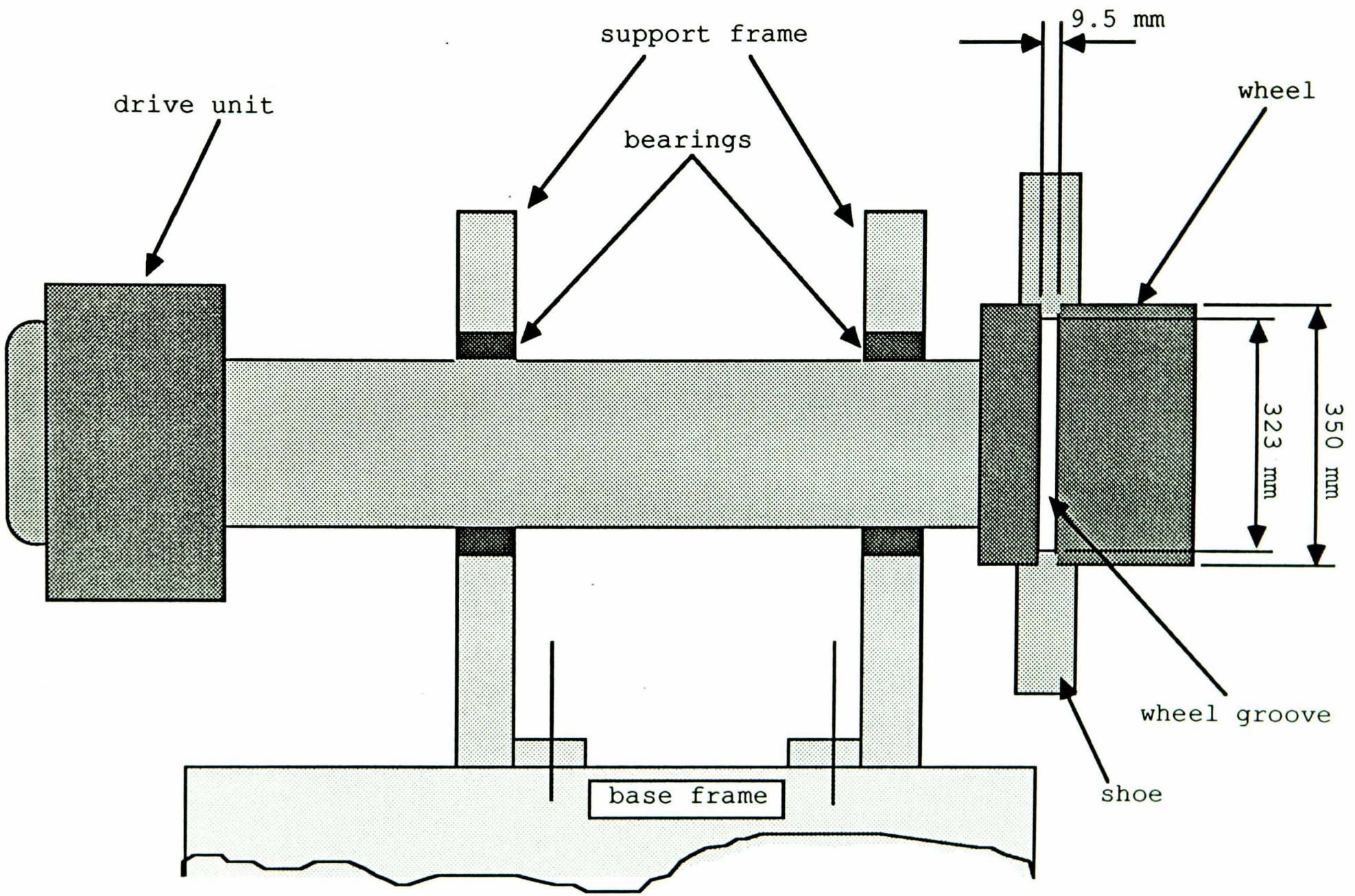


Figure 2.0 Schematic of the Mk 2F Conform machine.

The operational difficulty associated with the production of wire at high reduction ratio was the temperature induced by friction and deformation work in the die zone. This was measured to be of the order of 400 °C in the deformation zone, and under continuous production conditions, heat conduction to the tooling chamber, wheel and other machine parts required consideration.

A cooling facility was consequently introduced by suitable modification to the tools to incorporate cooling passages. This was found to be useful in two ways,

- 1) to reduce and control the temperature of the tool and wheel under continuous production conditions
- 2) to exercise some control over the mechanical properties of the extrudate

2.2 RADIAL AND TANGENTIAL DIE EXTRUSION

The Mk 2F machine was designed with a radial and tangential die extrusion capability. It is reported⁽³⁾ that the positioning of the radial die in the shoe provides better accessibility in terms of die size and rigidity compared to the tangential die. This is because the tangential die must be housed within the abutment tool which is designed to match the wheel groove, and is therefore limited in size and configuration.

A limitation with the radial die, however, is an appreciable increase in pressure in the tooling chamber to effect extrusion from a specified extrusion schedule. The configuration of the radial die in the tooling chamber is such that the die must be placed at a small distance in front of the abutment tool. The distance between the radial die and the abutment tool will be a function of the die orifice size i.e. extrusion ratio. Therefore an increase in the pressure

required to effect extrusion is necessary since the pressure at the abutment tool face is greater than at the die face due to increased friction and redundant deformation.

An additional limitation with the radial die is attributed to the dead zone which deposits itself between the abutment tool face and the die orifice⁽⁴⁾. Macro-examinations of various discards removed from the deformation zone highlight this feature.

2.3 EXTRUSION DIE AND TOOLING CHAMBER DESIGN

The die and housing arrangements have been the subject of intense investigation. This is because the product quality, configuration, extrusion ratio and speed of operation will depend on the strength and the design of the die tooling arrangement under continuous production conditions. The quality of the product is attributed to the surface finish and the product integrity in terms of metallography and quality control.

Rapid tool change-over is another essential feature in terms of reducing machine down-time. Therefore, the commercial viability of the machine under continuous production conditions in relation to the die system employed is determined from all the above considerations.

2.4 THE EARLY CONFORM EXTRUSION DIE

The radial die is the focal point of discussion since it offered scope for much improvement, and it was accepted early in the development work that commercial exploitation of the process will depend primarily on significant cost savings compared to traditional manufacturing routes.

Extrusion dies designed in-house at the Springfields Laboratories to extrude a variety of plain aluminium sections

were principally based on a standard die shape, which is used in the conventional extrusion processing of aluminium and its alloys.

A standard aluminium extrusion die used in industry incorporates the following design characteristics; a semi-cone die angle included at 180° , a small entry radius to the aperture (this is deemed necessary in order to provide additional die strength and, in particular, to allow an even flow of metal through the die orifice⁽⁵⁾). A suitable land and die material are chosen by considering factors such as operating temperature, stress and period of operation.

The die was placed adjacent to the tooling chamber ahead of the abutment tool as indicated in figure 2.1.

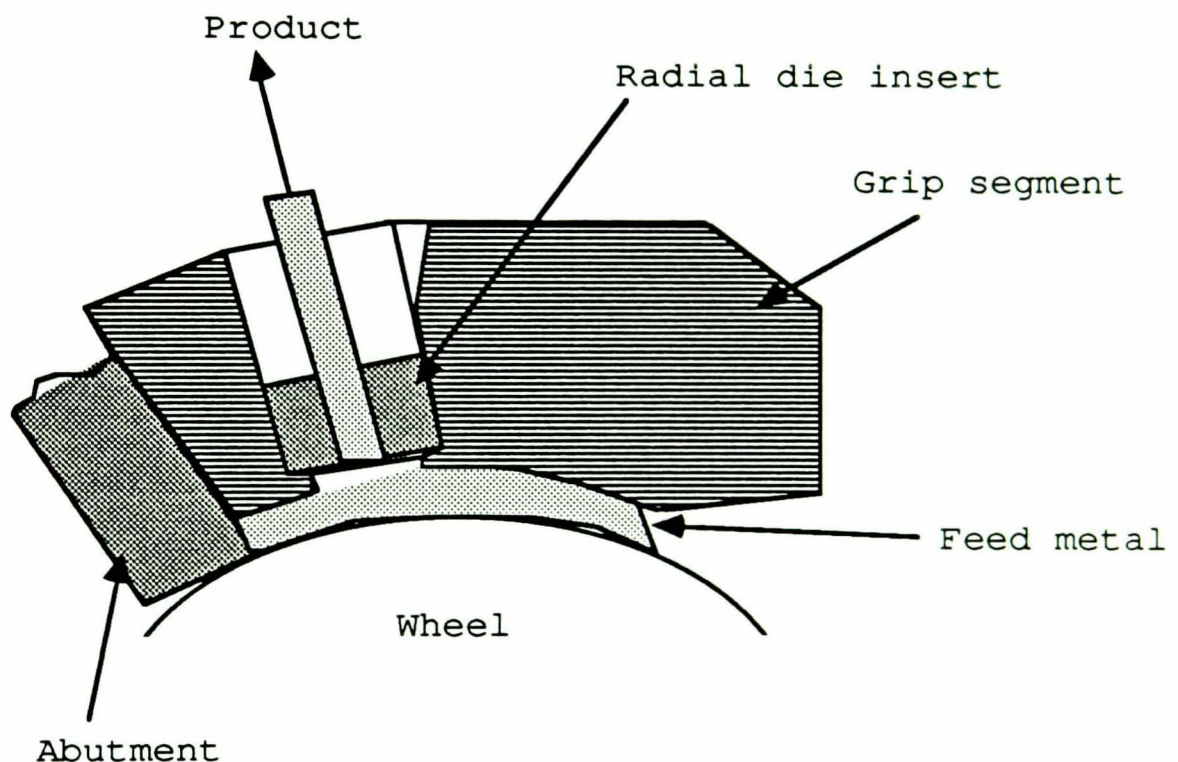


Figure 2.1
Location of die insert in tool block

Experimentation proceeded on the Mk 2F machine and the die arrangement was tested under simulated production conditions without cooling. The emphasis was on each test⁽⁶⁾ being

quality controlled in terms of dimensional stability and product surface finish.

Subsequent examination of the wire product on completion of experimentation⁽⁷⁾ revealed that the plain circular wire product exhibited a small degree of ovality of the order of 1.5%. Further examination of the product indicated that a non-uniform surface texture was present around its periphery at a given cross-section. Post-examination of the die also revealed asymmetric die hole wear, with appreciable wear arising in a direction perpendicular to the abutment tool face.

The reason for this peculiar phenomenon is attributed to the uneven flow of the feed metal across the die orifice. This, in turn, is directly related to the differential pressure which exists over the radial die face and which increases as it approaches the abutment tool.

2.4.1 THE EARLY RADIAL DIE

In an attempt⁽⁷⁾ to obtain a balanced pressure distribution across the radial die orifice, directing experimentation toward the positioning of the die in the tooling segment was proposed.

The initial suggestion was to vary the depth of the die insert in the tooling chamber. This was achieved by placing the die insert at a depth of 2 mm below its present position in the tooling segment.

The results from these tests were reported to be encouraging⁽²⁾. It was suggested that further adjustments to the depth of the die in the tool segment would eventually yield a balanced pressure distribution across the die orifice.

2.4.2 THE EXPANDING CHAMBER DIE

Provision for a secondary extrusion chamber which would house the die in a separate compartment from the tool segment was then conceived.

The secondary extrusion chamber is intended to provide a region where the metal can flow and mix uniformly prior to entering the die orifice. It is noted, however, that an increase the extrusion force at the die and abutment will result due to further redundant and friction deformation in the secondary extrusion chamber.

The chamber was designed to expand rather like a diverging funnel toward the die. This feature is useful in two ways since it can provide a larger surface area for extrusion at the die face than the present wheel groove dimension of 9.5 mm, see figure 2.2, and also a larger die insert can be used giving increased strength to the die tool insert.

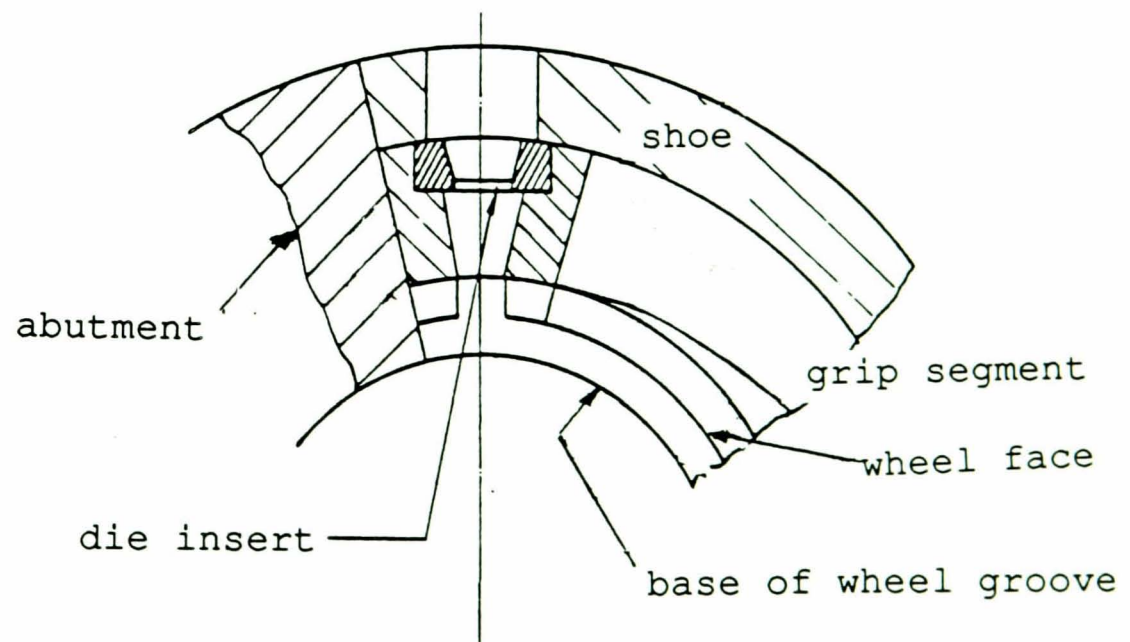


Figure 2.2 Expanding chamber and die insert

Experimentation carried out using this die arrangement showed a significant improvement in the product quality.

2.4.3 TUBE PRODUCTION

Initial attempts to extrude hollow sections employing a standard bridge die similar to those used in conventional extrusion processes was unsuccessful. The bridge die, which is located in the wheel groove see figure 2.3, is intended to separate the metal into two streams before it reaches the die orifice. The metal then rewelds as it flows through the die aperture to form a hollow section.

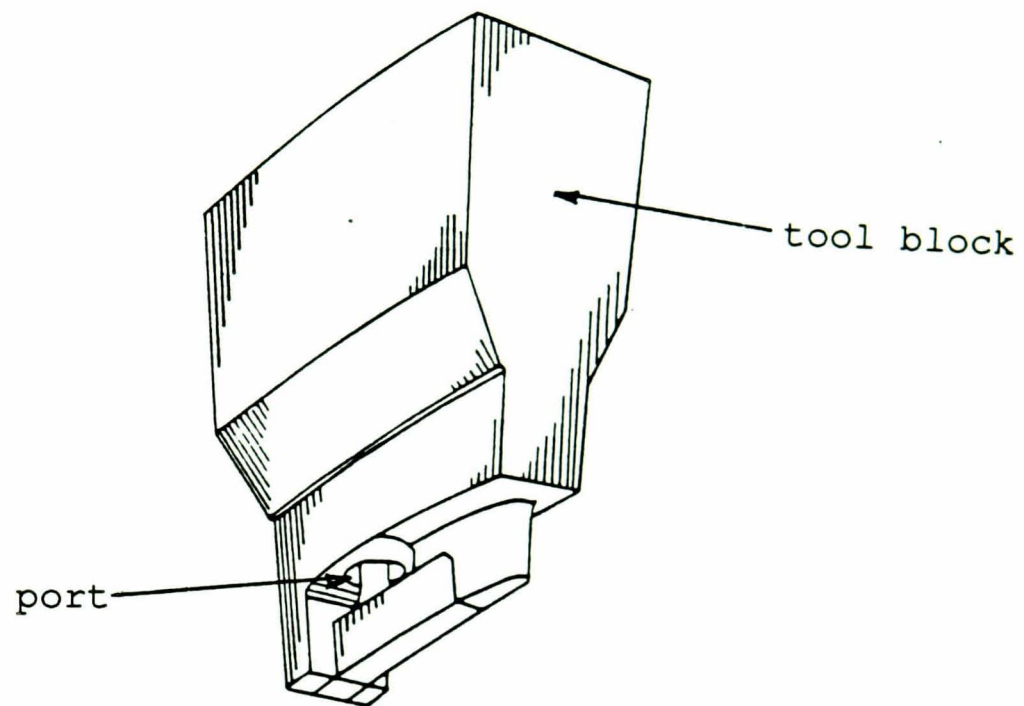


Figure 2.3 The bridge-die arrangement

The failure of the bridge die was due to its poor strength which was mainly attributed to its design configuration in the wheel groove.

An alternative approach entailed the use of an integral die and mandrel insert, see figure 2.4. In this illustration, the die consists of two main components, excluding the split casing (dieholder), which are generally referred to as the die ring and mandrel. The smaller section of the mandrel sits inside the die ring, and the larger section contains three separate kidney-shaped ports as shown in the illustration. The ports are provided to ensure that the metal separates into three streams.

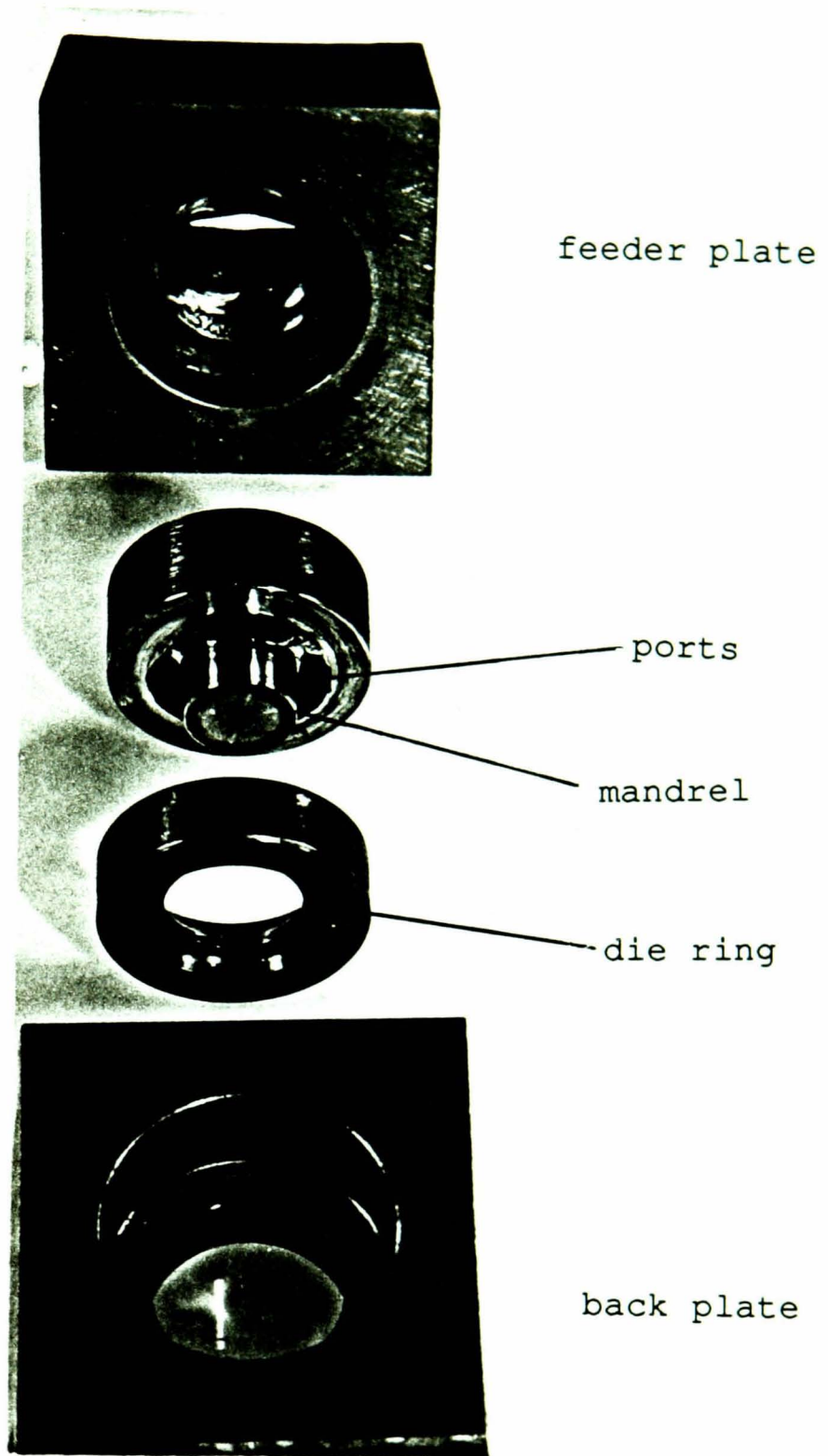


Figure 2.4 Components of the tube-die assembly

In general, the number of ports, their shape and location in the mandrel will be determined by the tube wall thickness, extrusion ratio and product aspect ratio. The split dieholder comprises two separate components; the feeder plate and back stop plate. The mandrel and die ring insert are seated concentrically in the back plate. The pre-determined annular space made available between the mandrel and the die ring finally determines the tube cross-section dimensions at the respective working temperature. The assembly of die tools is placed in the secondary extrusion chamber, see figure 2.5.

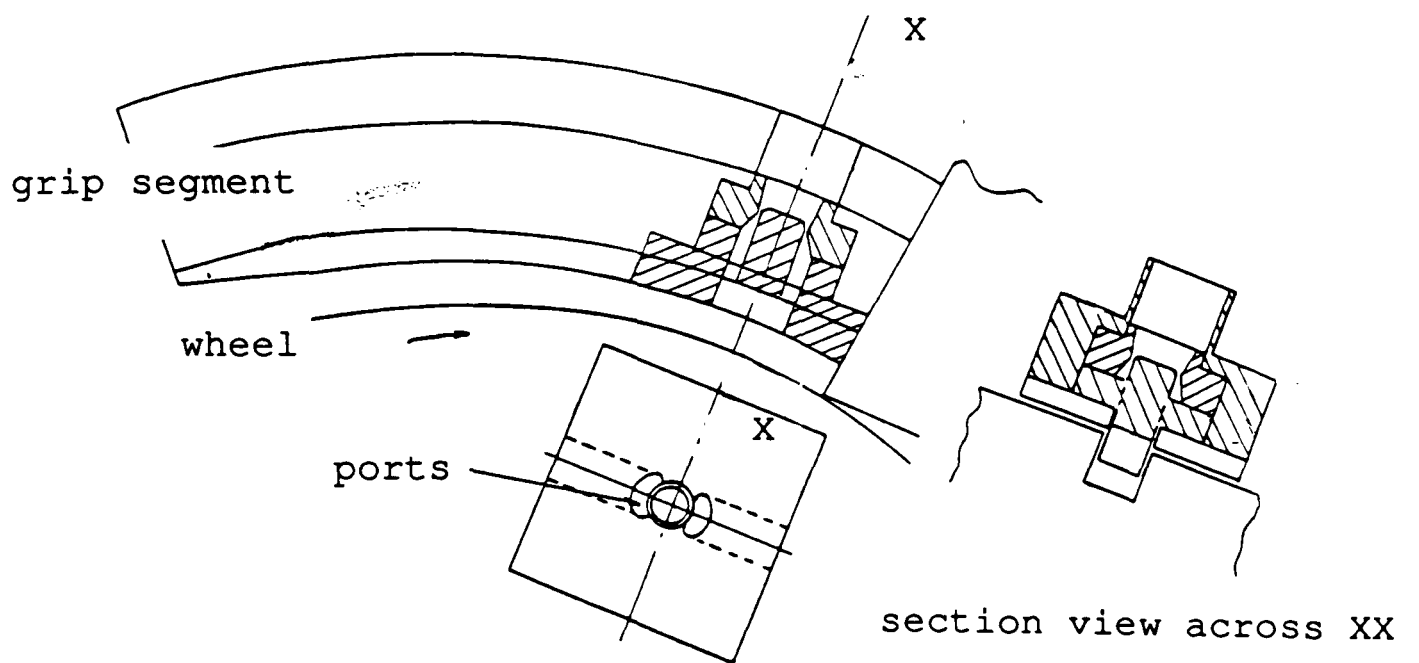


Figure 2.5 Tube extrusion arrangement

Hollow sections ranging from 3 mm outside diameter with a 0.5 mm wall thickness up to 16 mm outside diameter with a 1.5 mm wall thickness were produced using the mandrel-die tube insert. The results were reported as being encouraging, particularly the smaller section tubes below 10 mm outside diameter exhibiting a measured variation in wall thickness below 50 μm . However, the larger hollow sections showed a significant increase in the wall thickness variation and variation in surface texture at a given section. The cause of this phenomenon was once again attributed to the uneven metal flow through the tube die insert.

2.4.4 MULTI-PORT/MULTI-ABUTMENT DIE ARRANGEMENT

An alternative tube die arrangement is provided by the introduction of two separate feeder ports in the tooling segment, see figure 2.6. An even metal flow through the die orifice is maintained by the appropriate sizing of each port. This feature allows better control over the separation of the feed metal to the die orifice.

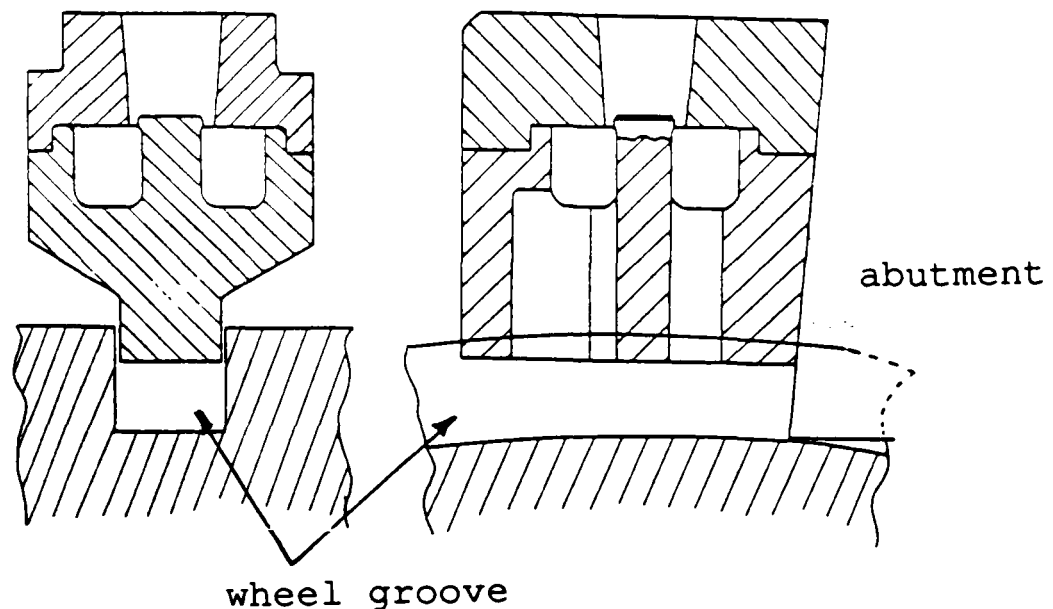


Figure 2.6 Twin-port die arrangement

A limitation in this die arrangement is attributed to the maximum diameter of each port, which is restricted to the width of the wheel groove. This does not, however, limit the size of port holes since they can be elongated in the plane of the extrusion chamber where larger sections are concerned or, alternatively, more ports can be incorporated.

When large hollow sections were produced, however, an unsatisfactory variation in the tube wall thickness at a given section was noted. Again, the fault was attributed to the uneven metal flow through the die orifice.

A further improvement to the twin/multi port die arrangement was achieved by using a stepped abutment coupled with twin

feeder ports, see figure 2.7. In effect, each port has been provided with its own mini-abutment. The correct combination of abutment steps and port sizing will ensure a balanced metal flow at the die orifice. Preliminary experimentation has shown that large plane, hollow and flat sections were successfully produced. These products were subsequently examined for dimensional stability, and the results were encouraging.

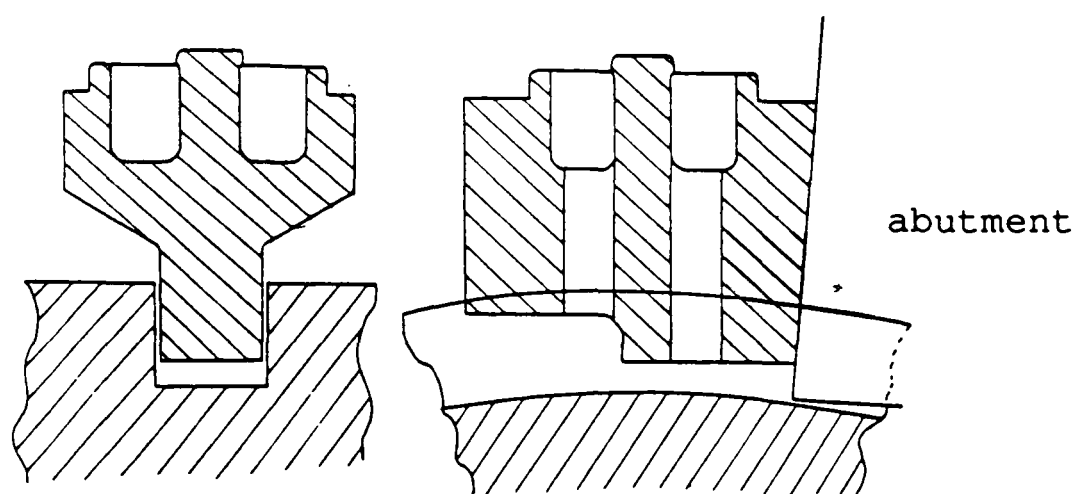


Figure 2.7 Twin-port/stepped abutment die arrangement

A further modification to this die system is a separate tool-block which houses the feeder plate, mandrel and die, see figure 2.8. This arrangement is not dissimilar to the integral mandrel-die system in terms of its versatility and flexibility. However, the essential feature of the die system, shown in figure 2.8, is the retention of the twin/multi port and stepped abutment as a redress for the differential metal flow through the die orifice. The effectiveness of the tool-block die system has provided a very efficient and simple procedure for rapid tool and die changeover.

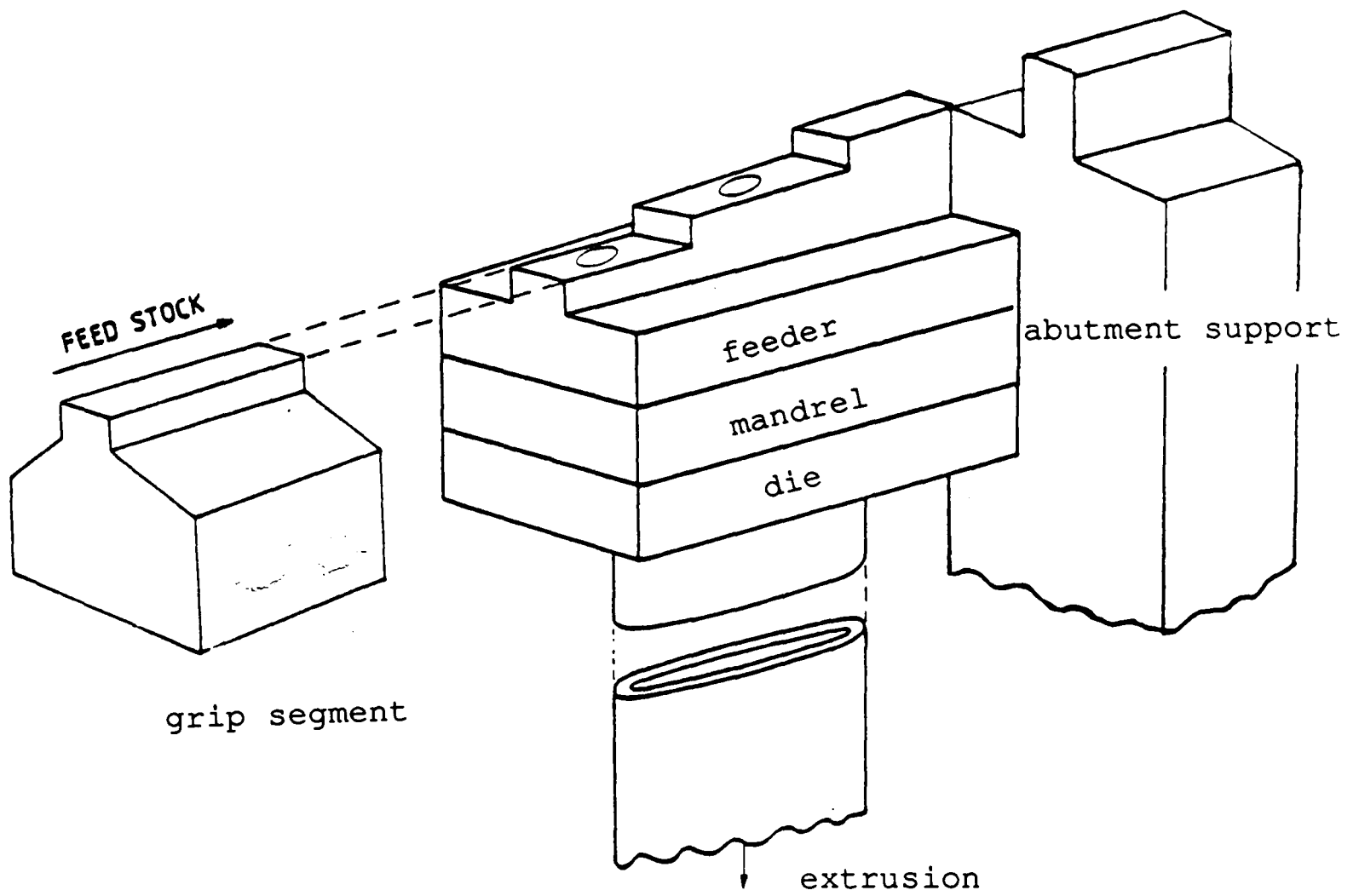


Figure 2.8 Tooling die arrangement with stepped feeder plate for wide extrusions

2.4.5 OTHER METHODS OF EXTRUSION

An alternative method of tube extrusion has been proposed⁽⁸⁾, whereby the die assembly can be fed with metal from two separate grooves, see figure 2.9. The theory suggests that that this method will yield improved metal mixing in the die chamber.

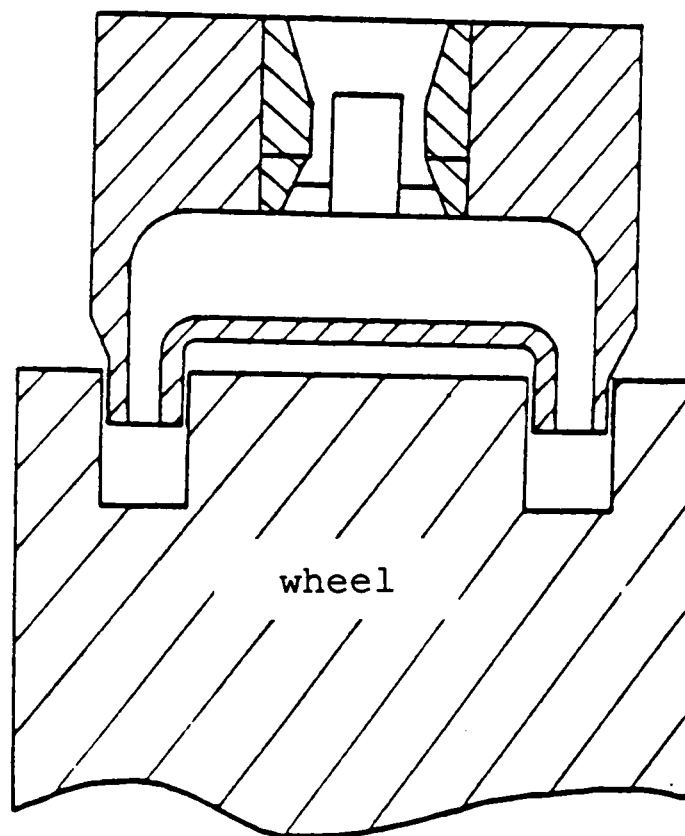


Figure 2.9 Tube-die arrangement, fed from two grooves

Other methods of tube extrusion⁽⁹⁾ are from a tangential or axial position relative to the axis of the drive shaft. Tangential extrusion requires the abutment to accommodate the die, see figure 2.10. The feed metal is directed into an expanding chamber between the tool-segment and the abutment.

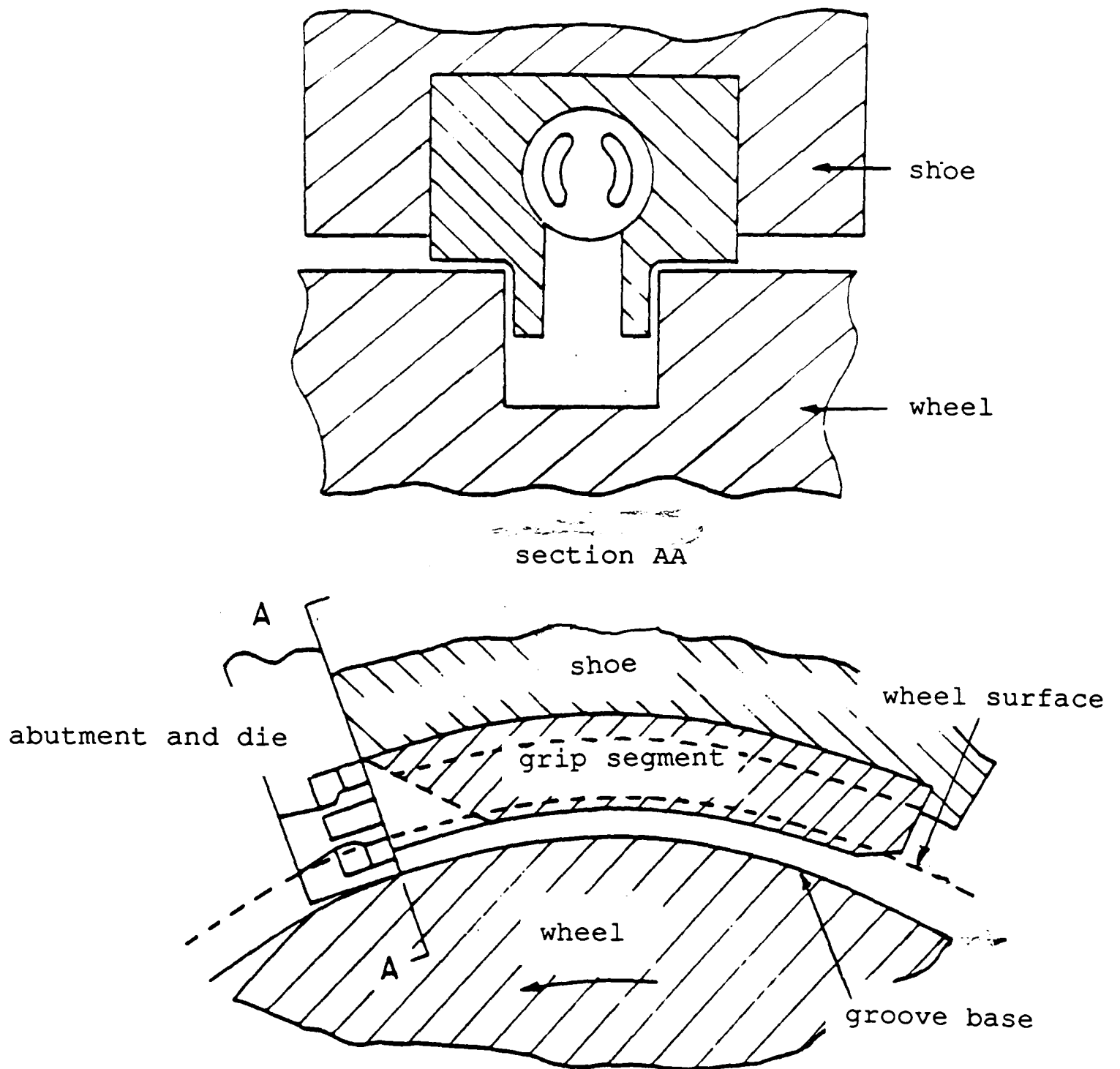


Figure 2.10 Abutment tube-die arrangement using the tangential extrusion method

The axial extrusion arrangement is illustrated in figure 2.11. The product leaves the die in a direction parallel to the axis of the drive shaft. This particular die system lends itself readily to the Conform machine with a cantilevered wheel.

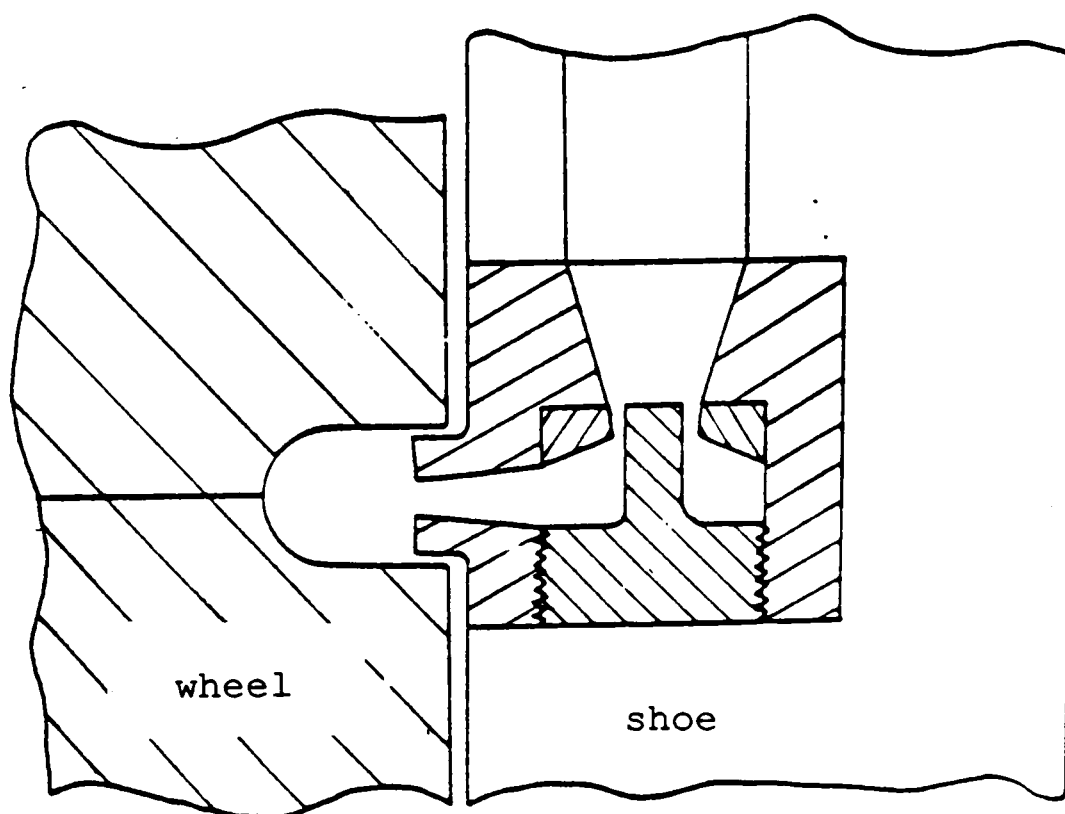


Figure 2.11 The axial-die arrangement

2.5 ALUMINIUM AND COPPER EXTRUSION

An advantage in using aluminium feed stock over copper is that the aluminium and steel tools gall in the extrusion chamber when subjected to mechanical and thermal processing. Subsequently, an adherent coat of aluminium feed is formed on the surface of the wheel groove as it passes through the extrusion chamber. The dead zone will provide a protective barrier on the wheel groove surface, since it provides a

cushion to high localised stress and heat spots in the extrusion chamber. Also an increase in the coefficient of friction between the ingoing rod feed and the wheel groove is evident.

Unfortunately, copper does not naturally form an adherent coat on the wheel groove surface. Therefore the wheel groove will be subjected to the full magnitude of the thermal and mechanical cyclic loads. In addition, relative slip between the wheel groove and feed stock, generates localised stress regions on the wheel groove surface, which eventually promotes small surface cracks leading to premature wheel failure.

2.6 THE MK 2B CONFORM MACHINE

The Mk 2B machine is designed with the wheel supported by a shaft between the bearings in the framework, unlike the Mk 2F machine. The advantage with this arrangement is that a greater load-bearing capability can be achieved. However, a distinct disadvantage is inaccessibility in terms of tool and wheel replacement in a production environment.

The Mk 2B Conform machine was primarily used for development in copper and some copper-based alloys. The higher hardness of copper compared with aluminium presented many practical difficulties, in particular premature tool and wheel fatigue. Because of this, the Mk 2B machine was reserved as a test bed to study the factors which affect tool and wheel fatigue.

2.7 MACHINE INSTRUMENTATION

The Mk 2B Conform machine was instrumented with the necessary equipment in order to monitor the following variables,

- a) torque
- b) temperature
- c) wheel speed
- d) feed rod speed
- e) product speed
- f) flow meter (cooling water)
- g) shoe constraining force
- h) shoe deflection

The equipments a) to c) were connected to a multi-pen mechanical chart recorder; a detailed review of the measuring equipment is given in section 4.

2.8 PRACTICAL DIFFICULTIES ASSOCIATED WITH COPPER FEED

The commercial success of Conform is partly attributed to the aluminium coat which naturally deposits itself on the wheel groove surface. As a consequence, an acceptable tool life is attained for the extrusion of aluminium - but not with copper-based feed stock. In view of this, attempts have been made to coat the wheel groove with a copper liner for the extrusion of copper-based feed stock ref.(10).

Initially, a copper sleeve was chemically plated to the wheel groove surface, see figure 6, prior to machine operation, this, however, proved to be unsuccessful. The reason being attributed to the liner being torn off by the ingoing feed rod.

In later development, it was revealed that, by using particulate feed, the inherent tendency was for the feed particles to stick to the wheel groove surface. This technique was used to coat a 'clean' wheel directly after re-assembly. Unfortunately, however, the subsequent use of a direct rod feed stock tended to tear fragments from the freshly placed liner. Although, with each cycle of the wheel as it passes the extrusion chamber, the previously torn fragments were replaced by the ingoing feed metal entering the extrusion chamber.

2.8.1 WHEEL FATIGUE

A comprehensive report was compiled by Marsh⁽¹¹⁾ on tool and wheel fatigue associated with the extrusion of copper feed stock. A practical study of wheel cycle life was initially carried out by Marsh. This consisted of a series of experimental tests in which different wheel designs and materials were repeatedly tested to failure.

During these tests it was revealed that the wheel material was required to possess mechanical properties of high fracture toughness and hardness (typically 550 VPN). This was necessary to ensure that the wheel could withstand the high cyclic stresses which it encounters over a given time. A suitable wheel design and material specification were determined from further experimentation, in which a wheel composed of either two or three separate discs was assembled, see figure 7.

The assemblage of discs is held tightly together by a uniaxial hydraulic nut (Pilgrim nut), which is screwed onto the end of the main shaft. The stresses developed in the rotating wheel arise mainly from a combined pressure and thermal cycle during machine operation. However, an additional stress is imposed due to the wheel being clamped in an axial position against a bearing shoulder. This is deemed necessary in order to prevent slip between the wheel and the main drive shaft. A

standard multi-keyed shaft was used in early experimentation in conjunction with a single-piece wheel, however tests proved this feature to be unsuitable.

The wheel assembly must be securely fastened to prevent the back extrusion of the feed metal at the adjoining interface of each disc. The initial assumption was that the wheel clamp force must be at least equal in magnitude to the total extrusion force. The maximum extrusion force was estimated to be equivalent to a pressure of the order 1.2 GPa acting on the abutment tool face.

A wheel cycle life acceptable under continuous production conditions was suggested by Marsh to be of the order 20×10^3 cycles. The criteria for wheel design are given in table 1 below,

Table 1

The extrusion of copper based rod feed stock 9.5 mm dia.

Wheel cycle	Max. extrusion ratio	Max. wheel life speed
20×10^3	20 : 1	15 rev/min

It was later discovered that plastic deformation of the wheel groove surface occurred during extended periods of machine operation. This, coupled with a high reduction and high wheel speed had the effect of reducing the overall wheel cycle life below the design limit.

In view of this, and the limited fundamental understanding of the mechanics of the Conform process, in particular how the cyclic stresses influence the performance of the wheel under continuous production conditions, further examination was carried out by Marsh.

The report contained an analytical and experimental study which attempts to predict the wheel cycle life by determining the number of revolutions to failure i.e. a fatigue curve. The analytical results were determined by considering the principal stresses acting on a cubic element of material just below the wheel groove surface.

Comparison of the experimental and theoretical results obtained for determining the wheel cycle life showed poor correlation. Marsh assessed the reliability of his approach, and suggested that an alternative analytical technique may prove more successful.

The problem of yielding which readily occurred at the wheel groove surface was, however, satisfactorily resolved. It became apparent that the axial stress due to the constraint of the wheel pre-load and, in addition, the thermally induced stress developed during machine operation, were, in total, sufficient to exceed the wheel material yield strength. This was overcome by reducing the wheel pre-load to account for the increase in thermally induced stress.

2.8.2 TOOL FATIGUE

Other tools which are prone to failure by fatigue are the abutment and die. The abutment and die tools must endure a high static load at elevated temperature. Because the abutment and die tools are required to be comparatively small in size, the stress imposed on these tools is high at the normal operating temperature.

Under normal operating conditions the abutment tool is subjected to a higher direct force than the die. Furthermore, the abutment tool is subjected to a high shear force, which eventually promotes failure by shear rather than by wear particularly while extruding the harder feed metals. The abutment and die tool life were also examined by Marsh⁽⁸⁾ in terms of increasing fatigue life.

A series of experimental tests were used to determine the optimum abutment design under continuous production conditions. The selection of a suitable material to manufacture the abutment tool, however, presented initial difficulties.

As previously mentioned, the machine operating conditions determine the abutment and die tool fatigue life. For example, if the machine is operated at a high reduction ratio and wheel speed, a higher temperature is generated in the extrusion chamber. It has been shown that the abutment tool life is significantly enhanced, if the temperature is controlled and maintained low by cooling. The influence of cooling effectiveness on the abutment and die tool materials is discussed in the following section.

2.8.3 WHEEL COOLING

To reduce the high thermally-induced stress in the wheel during long machine operation, various cooling methods were examined. Initially, a direct cooling technique in which the coolant consisting of a range of chemical compositions was directed straight into the wheel groove. The objective being to control the friction generated heat which arises mainly from the shoe/feed interface.

It was anticipated that, by applying the coolant directly into the heat source, the wheel temperature can be controlled and maintained to an acceptable level. It was subsequently discovered that this cooling method provided a lubricant film

at the wheel groove and feed metal interface. This feature is highly undesirable since it encourages greater slip between the wheel groove and the feed metal entering the extrusion chamber. In any event, coolant in the mini-extrusion chamber must be avoided when used in conjunction with particulate feed stock.

Another disadvantage associated with direct cooling is related to the increase in the amplitude of the temperature cycle experienced at the wheel groove surface, resulting in a notable increase in the thermally-induced stress developed in the wheel.

It is, however, possible to apply coolant to the wheel surface away from the immediate vicinity of wheel groove, for example, directly to the outer wheel discs. This is a feasible alternative, since heat transfer will cool the wheel groove by conduction. The final bulk temperature of the wheel assembly is then dependent on the temperature, flow rate and chemical composition of the coolant. In general, water coolant has proved to be a successful cooling medium when applied directly to the outer wheel discs.

Another solution is to cool the wheel assembly from an internal passage which is aligned axially along the inside of the main shaft. The theory being that heat conduction from the centre of the main shaft is sufficient to cool the wheel assembly to a steady and reduced bulk temperature during long machine operation. The cooling fluid used is water and this method also proved to be successful.

2.8.4 ABUTMENT COOLING

The abutment tool and tool holder was redesigned to accommodate a water-cooling passage to allow the controlled circulation of cooling fluid, see figure 2.12. The abutment bulk temperature is maintained constant by the use of flow/temperature sensing devices.

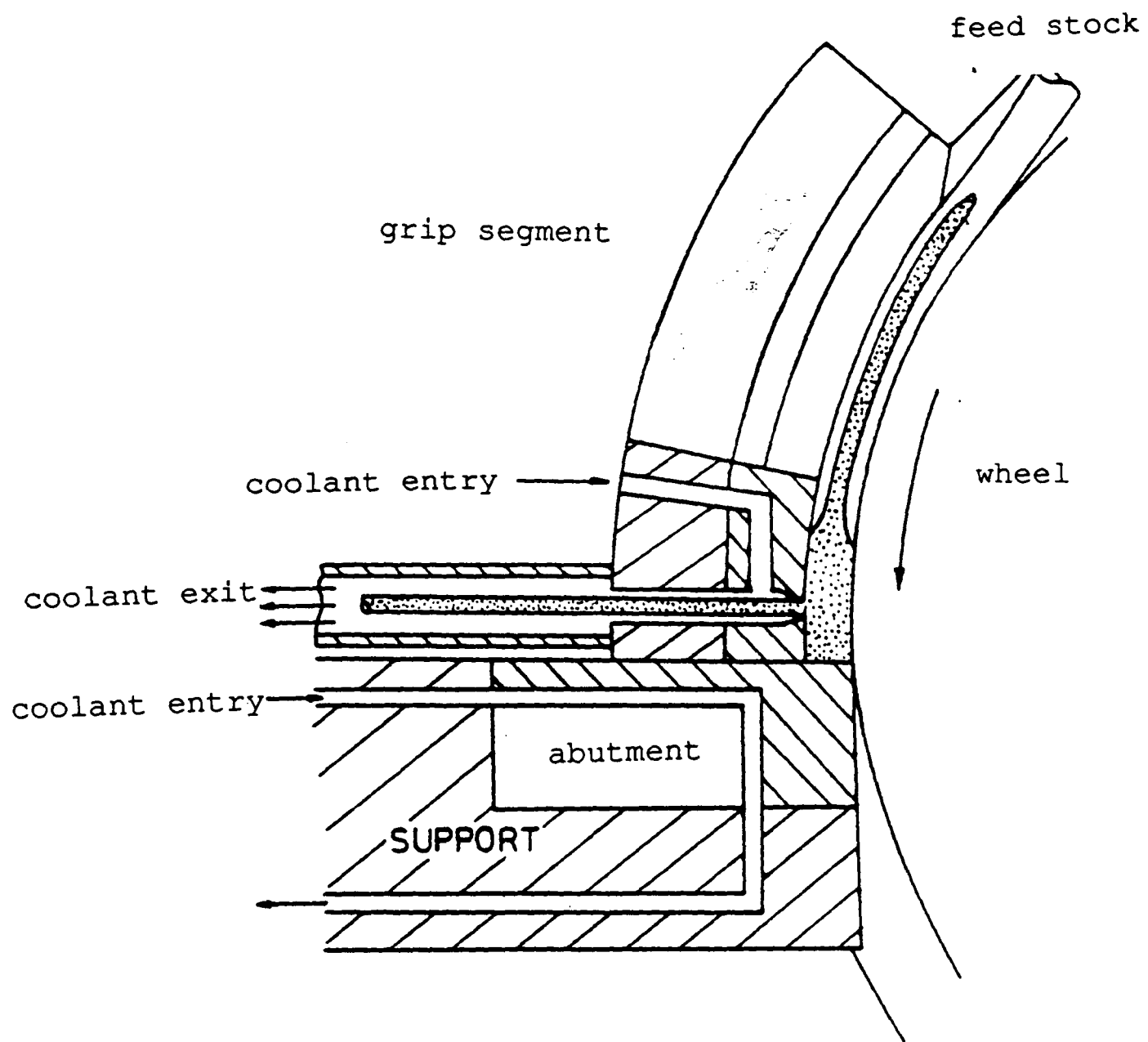


Figure 2.12 Cooling passages in shoe arrangement

Subsequent experimentation revealed that there was no increase in the fatigue life of the abutment tool at a reduced operating temperature. The cause being attributed to a reduction in bulk strength due to the removal of metal in order to introduce the cooling passages in the tool. However, this limitation was overcome by the further modification of reducing the port size of cooling holes.

Abutment bulk temperatures considerably in excess of 500°C have been recorded under continuous production conditions, and reduced to half that value by the implementation of water cooling. The water-cooled abutment tool has enabled a significant improvement in tool life.

2.8.5 DIE COOLING

It was also considered necessary to cool the die, die holder, together with the grip segment⁽¹²⁾ which is situated in the shoe adjacent to the die holder. Initially, a single tool which incorporated the die holder and grip segment was manufactured leaving a series of cooling passages to allow the controlled circulation of water, see figure 2.12 for details.

The coolant is to discharge directly on to the product at the rear of the die face, whilst a constant supply is maintained through the grip segment.

A notable increase in die and grip segment fatigue life was observed. An additional advantage to be gained by quenching the product directly after leaving the die is an appreciable change in the mechanical properties of the product. An oxide-free surface can also be maintained on the product using the appropriate coolant. The coolant used, was a water-based solution consisting of 1.5% industrial ethanol, mixed with a benzotriazole solution with a density of 4.4 kg/m³.

3 EXPERIMENTAL EQUIPMENT

The equipment supplied to the University for experimentation was a Conform machine complete with a hydraulic power pack and basic instrumentation. This particular machine was previously used for development with the extrusion of various aluminium alloys, and accepted feed stock in the rod or particulate form.

The basic elements of the Conform machine are a shaft with a grooved wheel which is powered by a hydraulic drive unit and a shoe which houses the tooling. The shaft is supported by bearings and is arranged in a cantilever in order to allow good accessibility for quick wheel removal and set-up, see fig 3.0 and 3.1 for details. The shoe contains the tooling which overlaps a small portion of the grooved wheel in order to form the extrusion chamber. The shoe is actuated by a hydraulic pump and pivots around a spigot so that it can be quickly released from the wheel for tool removal and subsequent tool set-up.

The hydraulic power drive unit is manufactured by Staffa (spec: GB 800) and is capable of developing a torque up to 40.6 kNm which in turn, can develop a maximum power output of 93 kW. The power pack which supplies the hydraulic motor is manufactured by Lucas (112 kW) and has a variable delivery pump unit with reverse flow capability. The pump will deliver 255 l/min at a pressure of 21 MPa (3000 lbf/in²).

Additional equipment includes a coil straightening stand situated behind the entrance to the extrusion chamber, see fig 3.2 for details. A rotating decoiler unit is also provided to allow the rod feed stock to be freely drawn into the coil-straightening stand without snagging by the driving force imparted from the feed rod, in turn, being drawn into the extrusion chamber.

The last stage of the rod-straightening stand incorporates an adjustable two-stage reduction unit by employing two sets of

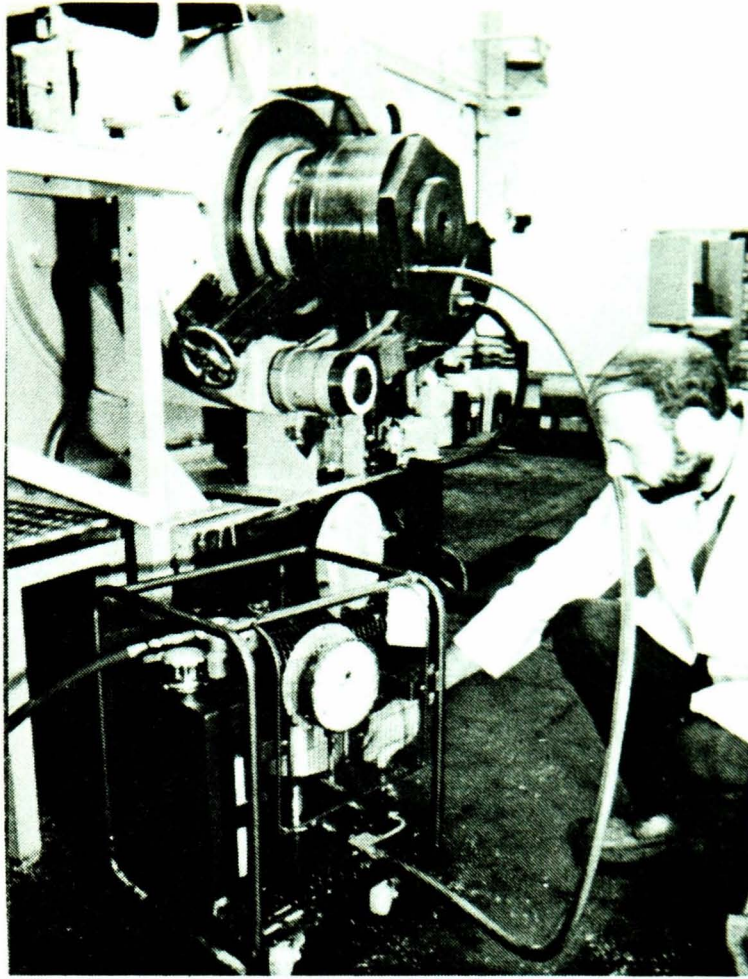


Figure 3.0. Shows the use of the pressure intensifier to release the shims for removal of the pilgrim nut.

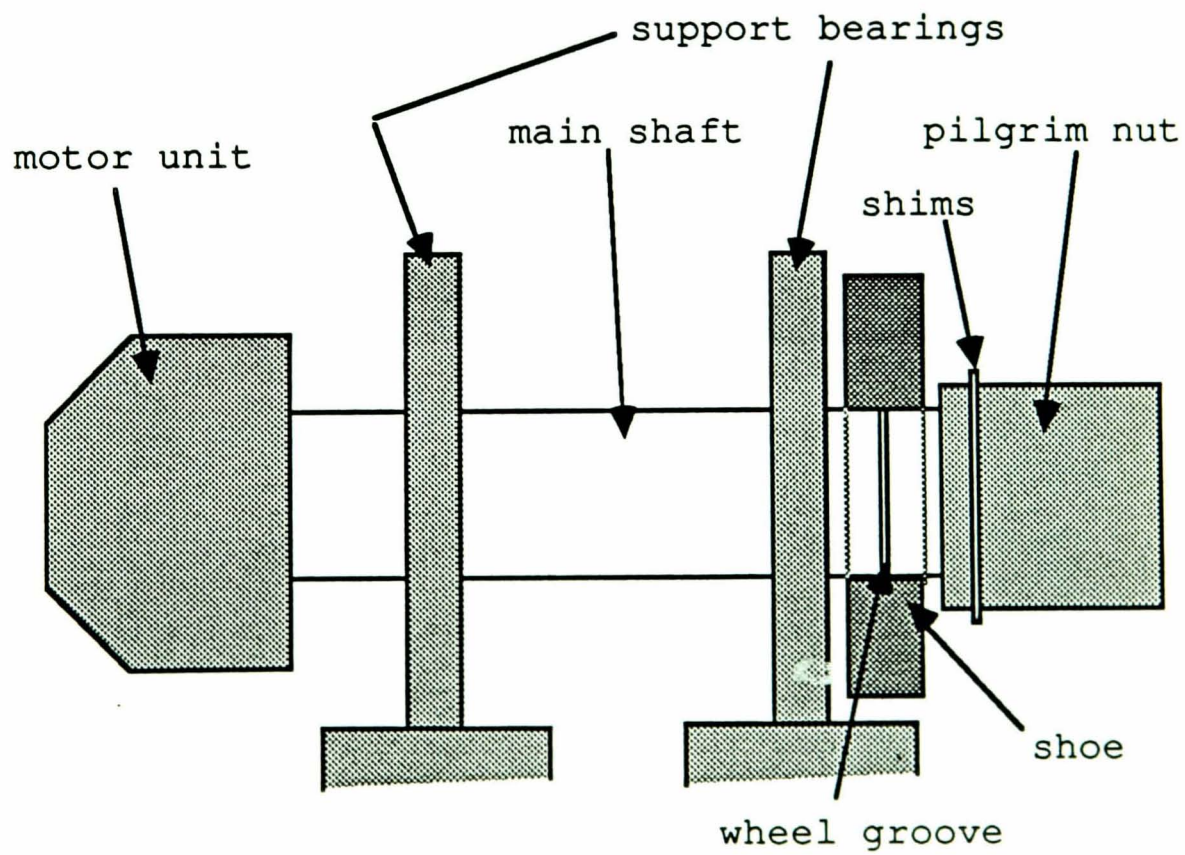
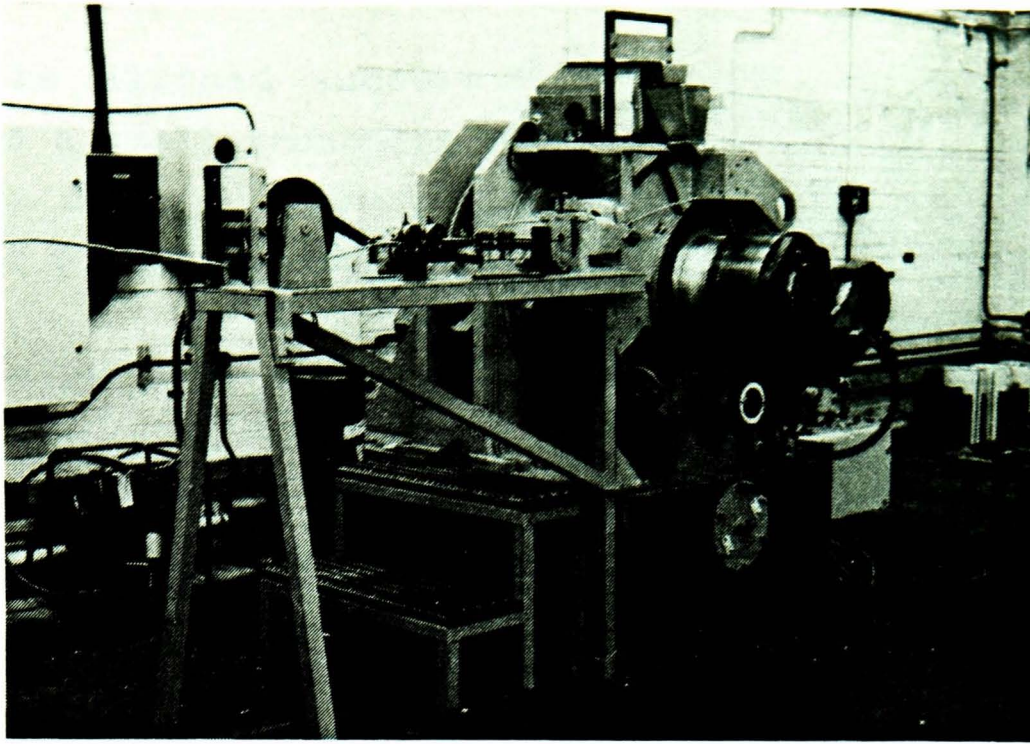
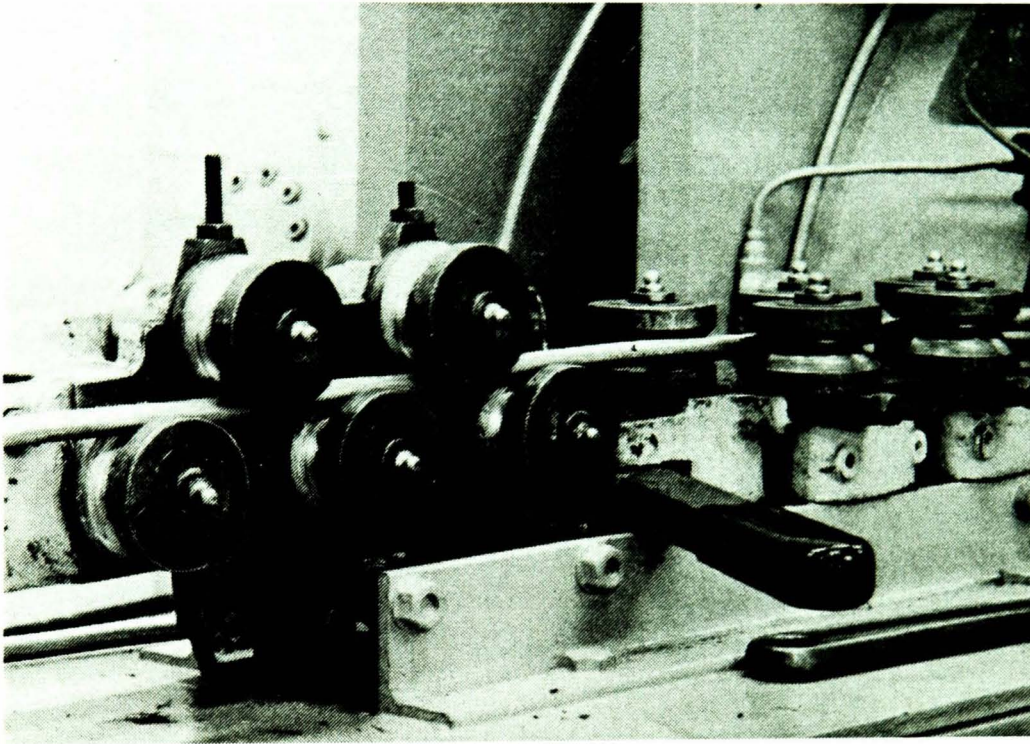


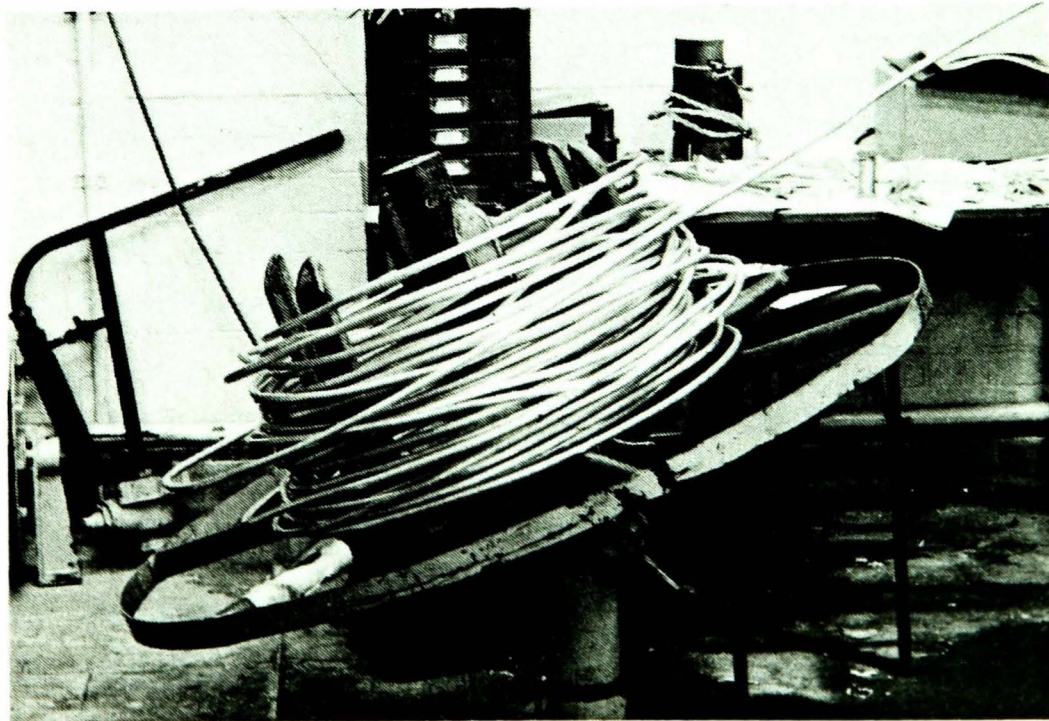
Figure 3.1. A schematic of the Conform machine.



a



b



c

Figure 3.2. Showing a) the coil straightening stand
b) two stage roller straightening unit
c) decoiler unit

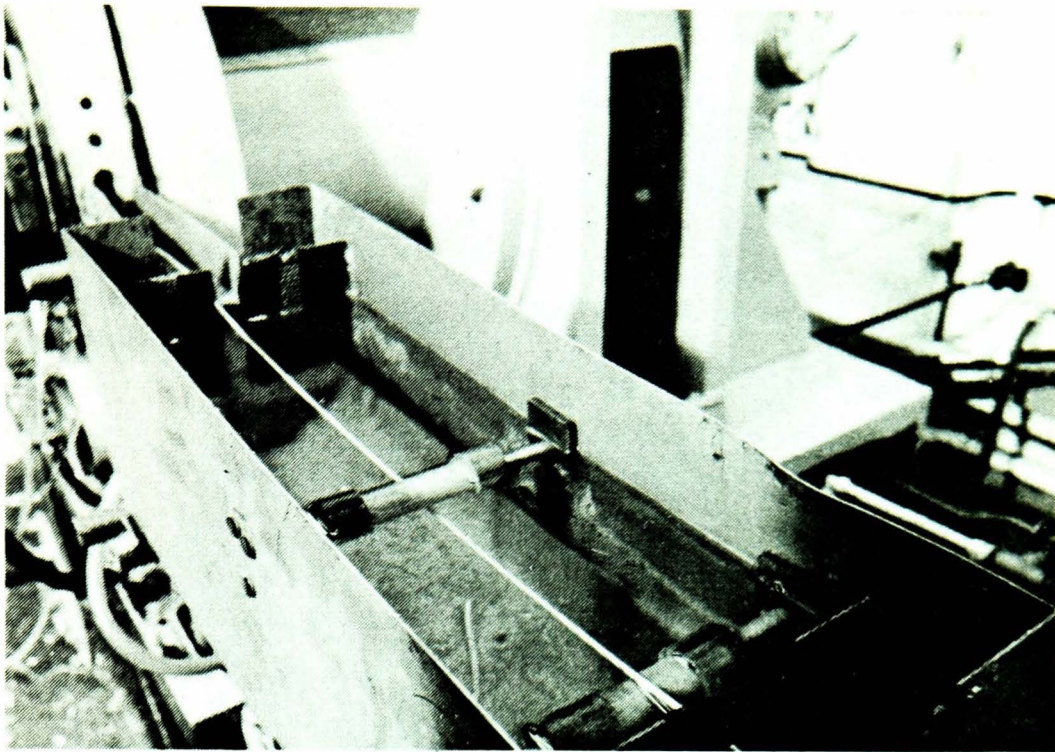
rollers aligned successively at 90° to each other. This allows a small reduction in the cross-section area of the feed rod in order to ensure that entry into the extrusion chamber is not prohibited by the otherwise tight interference fit.

A cooling water tank is situated ahead of the die to quench the product directly it emerges from the die. A subsequent modification to the cooling tank incorporated two rollers placed below the water level to ensure that the product is suitably submerged and therefore cooled as it exits the water tank, see fig 3.3.

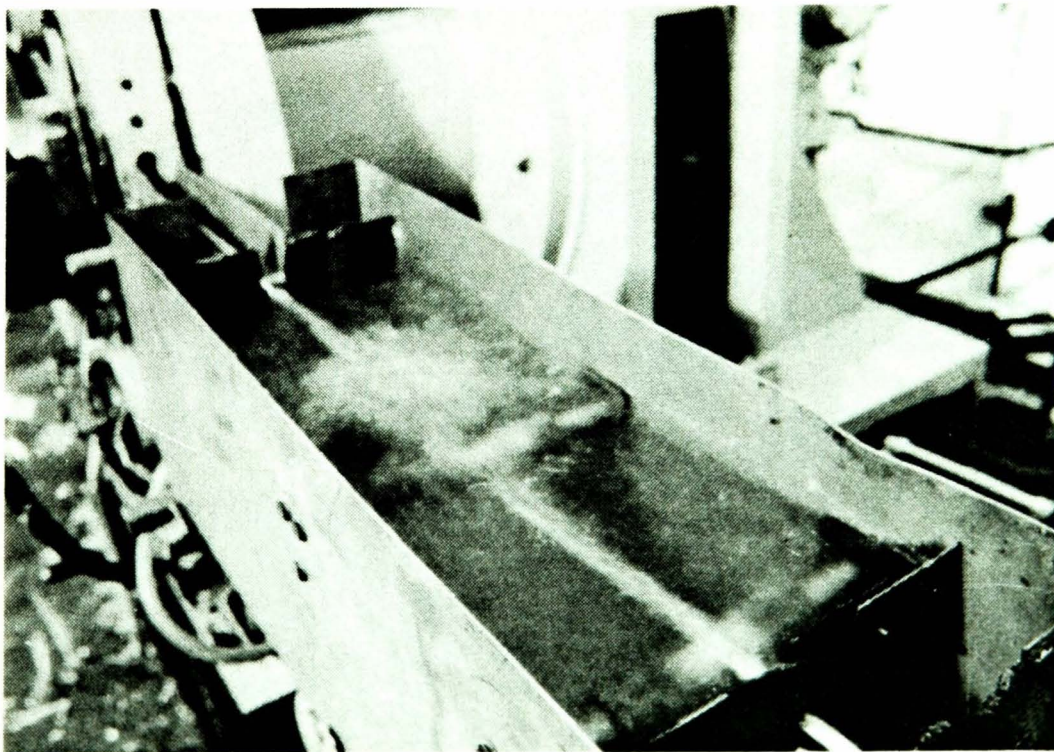
Finally, a variable speed coiling unit was provided by the University to coil the product after leaving the cooling tank. The control unit for this equipment is by a hand-operated knob which allowed 280° of rotation for the full range of speeds. The power unit used for this equipment is a variable-speed electric motor. In order to allow coiling at high speed, corresponding to high reduction, the pulley arrangement which connects the motor to the coiler was modified to provide a speed range from 0 - 3 m/s. In addition, a trip switch device was installed ahead of the coiler unit to provide semi-automatic control for the coiling operation, see fig 3.4.

3.1 FEATURES OF THE CONFORM MACHINE

The tooling in the shoe is flexible in order to accommodate a range of different die sizes and the subsequent replacement of worn parts. The tooling consisted mainly of a die, die housing, grip segment, abutment tool holder and abutment tool, see fig 3.5. The abutment tool is located in the wheel groove during machine operation in order to arrest the forward motion of the feed metal and constrain it to flow into the die chamber and subsequently through the die orifice. It is the abutment tool and die which require frequent changing in long production schedules, due to wear and fatigue of these parts.

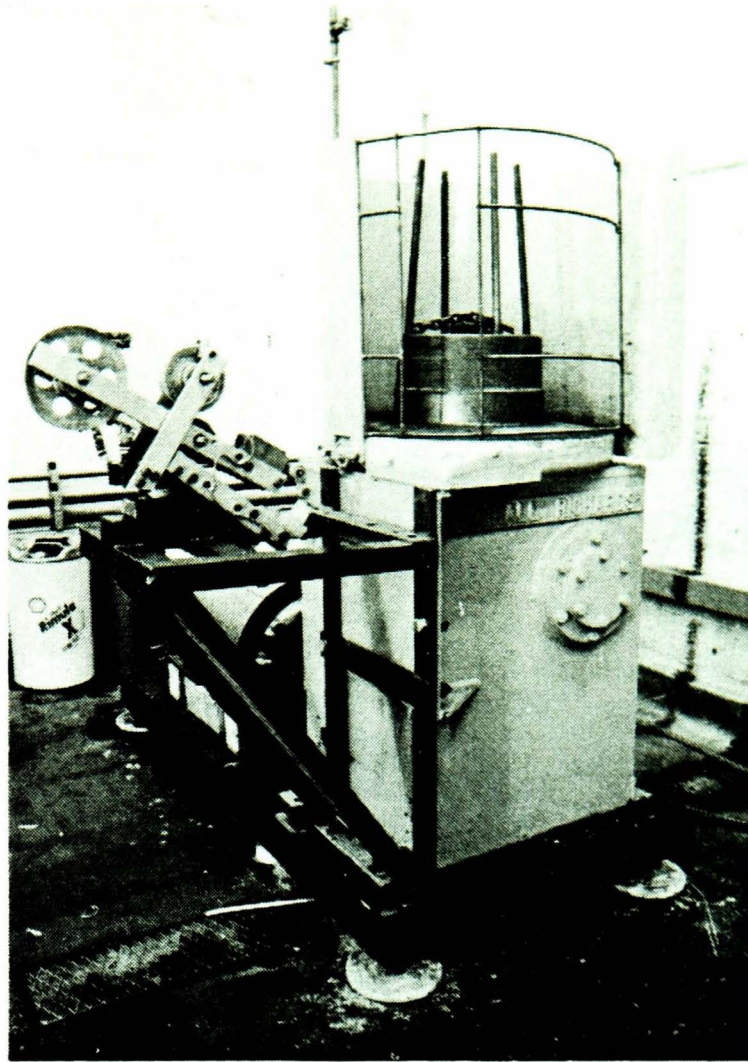


a

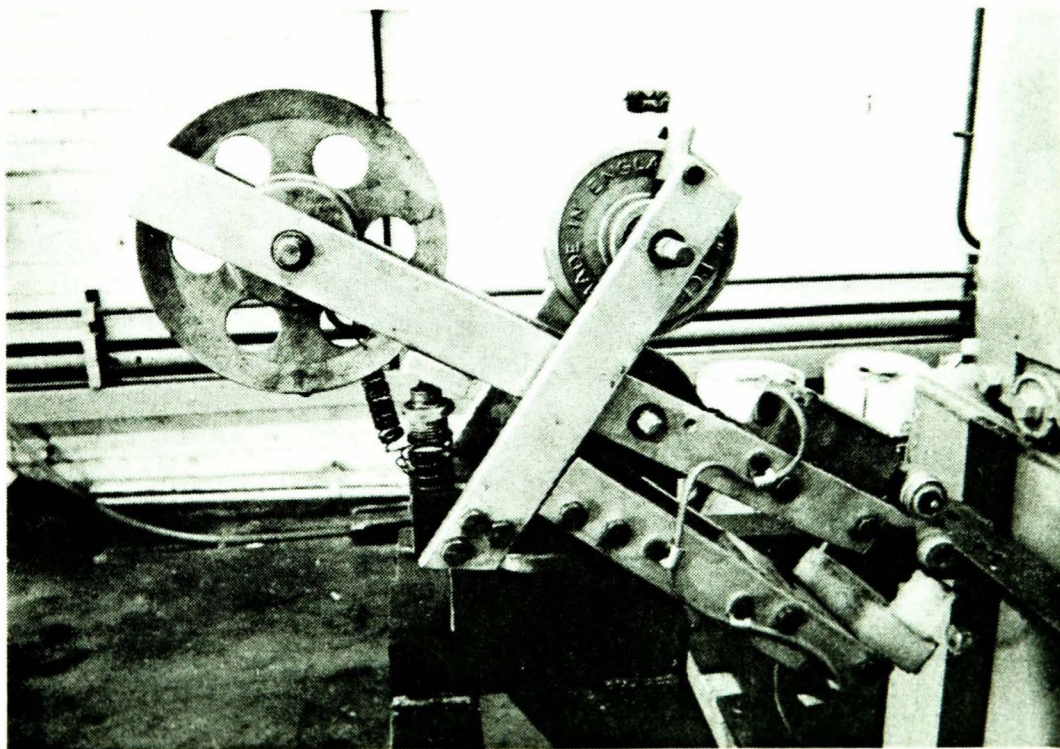


b

Figure 3.3. Showing a) stationary product in the cooling water tank
b) moving product in the cooling tank

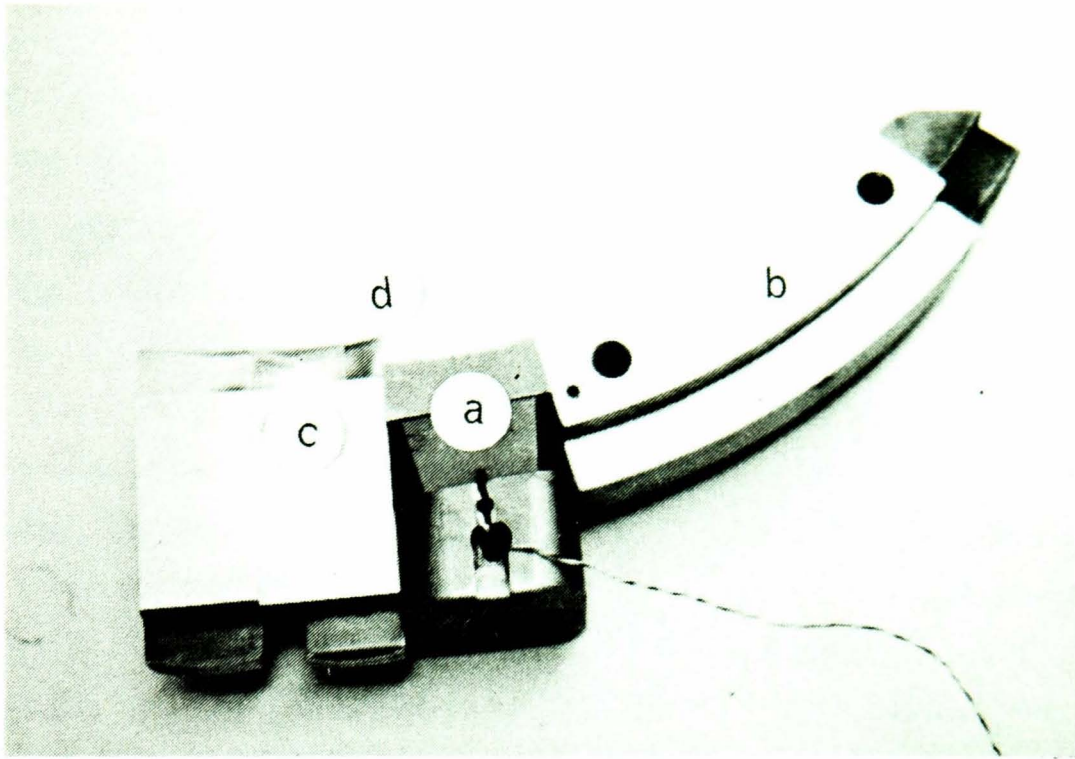


a



b

Figure 3.4. Showing a) the coiler unit
b) the automatic trip assembly



- a. die housing
- b. grip segment
- c. abutment tool holder
- d. abutment tool

Figure 3.5. The assembly of tools in the shoe

The tooling is held in position by a single retaining screw situated at the entrance to the grip segment. In effect, the retaining screw clamps the grip segment, die housing and abutment tool holder to a rigid tapered wedge as illustrated in fig 3.6a. The abutment holder is seated on a rigid block which can be adjusted by a single screw in order to vary the depth of the abutment tool in the wheel groove (in the range 0 - 14 mm). The grip segment and die housing upper part (DHUP) penetrate into the wheel groove to a measured depth of 4.5 mm. This is considered necessary to increase the rigidity of the tooling and also reduce the metal leakage (flash) from the tooling chamber as the feed metal traverses the deformation zone. It is noted that the actual abutment depth setting is the distance between the tip of the abutment tool and the shoulder of the DHUP (i.e. the protrusion of the abutment tool in the wheel groove, see fig 3.6b, the maximum abutment depth setting $H = 9.5$ mm). The depth of the abutment tool in the wheel groove is measured by using a setting block.

A scraper tool has also been installed on the machine in order to remove the oxide coat which develops on the surface of the dead zone in the wheel groove, see fig 3.7. The scraper tool is essentially a form tool in which the depth can be adjusted to remove a desired level of metal from the dead zone. Under normal conditions, the minimum amount of flash is removed to ensure a reduced level of waste is generated by the presence of this tool in the wheel groove; also the scraper tool removes any unwanted clusters of flash which may develop in the wheel groove as a result of the imperfect operation of the abutment tool.

The shoe pivots around a spigot so that it can be removed from the wheel for tool removal and subsequent tool set-up. The spigot is linked to a manually operated hand wheel, which allows fine adjustment of the shoe in relation to the grooved wheel. A graduated scale (calibrated in degrees from 0 - 90°) on the spigot indicates the position of the tooling in the shoe as it closes on the grooved wheel during the tool set-up procedure.

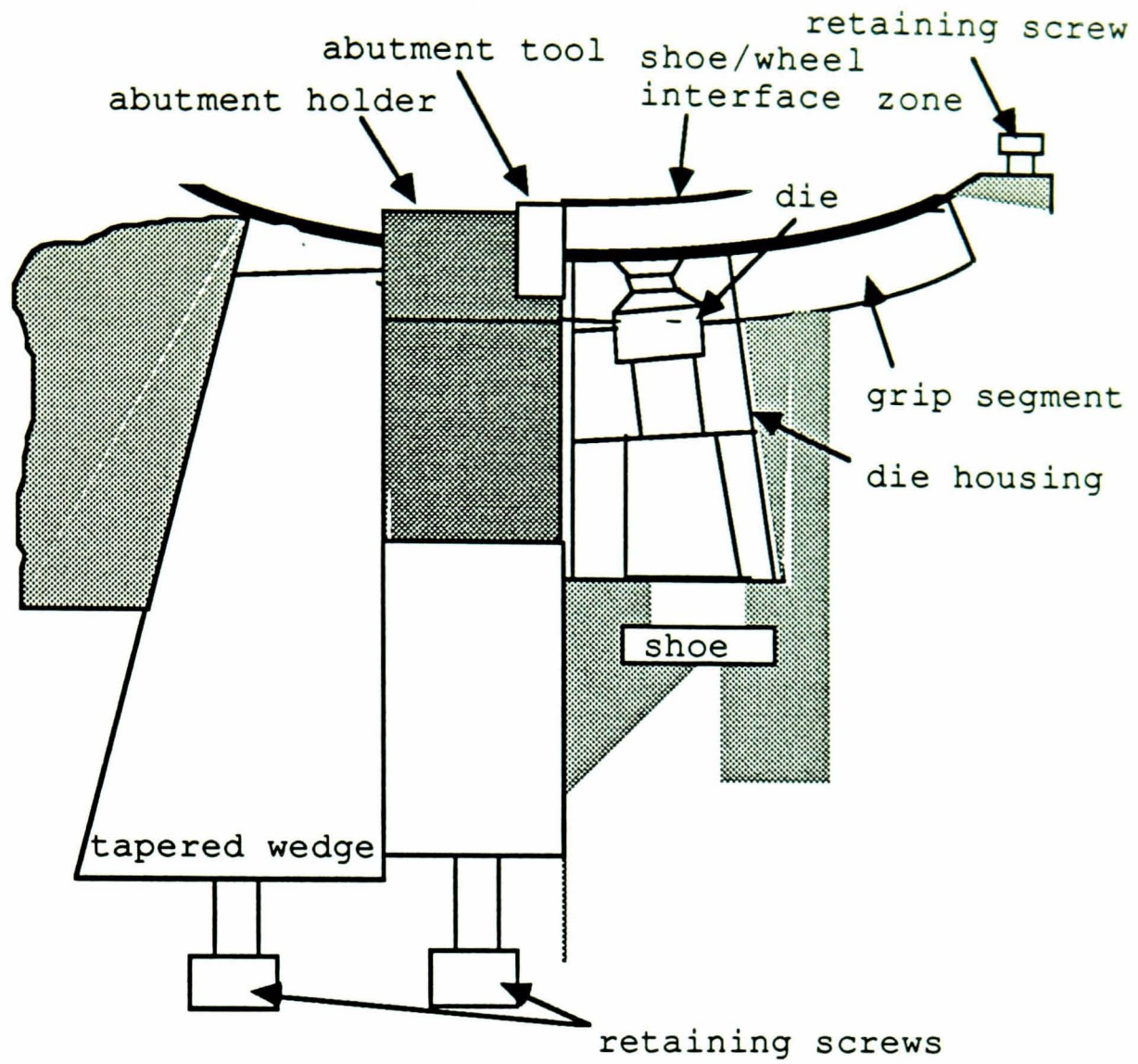


Figure 3.6a Tooling arrangement in the shoe

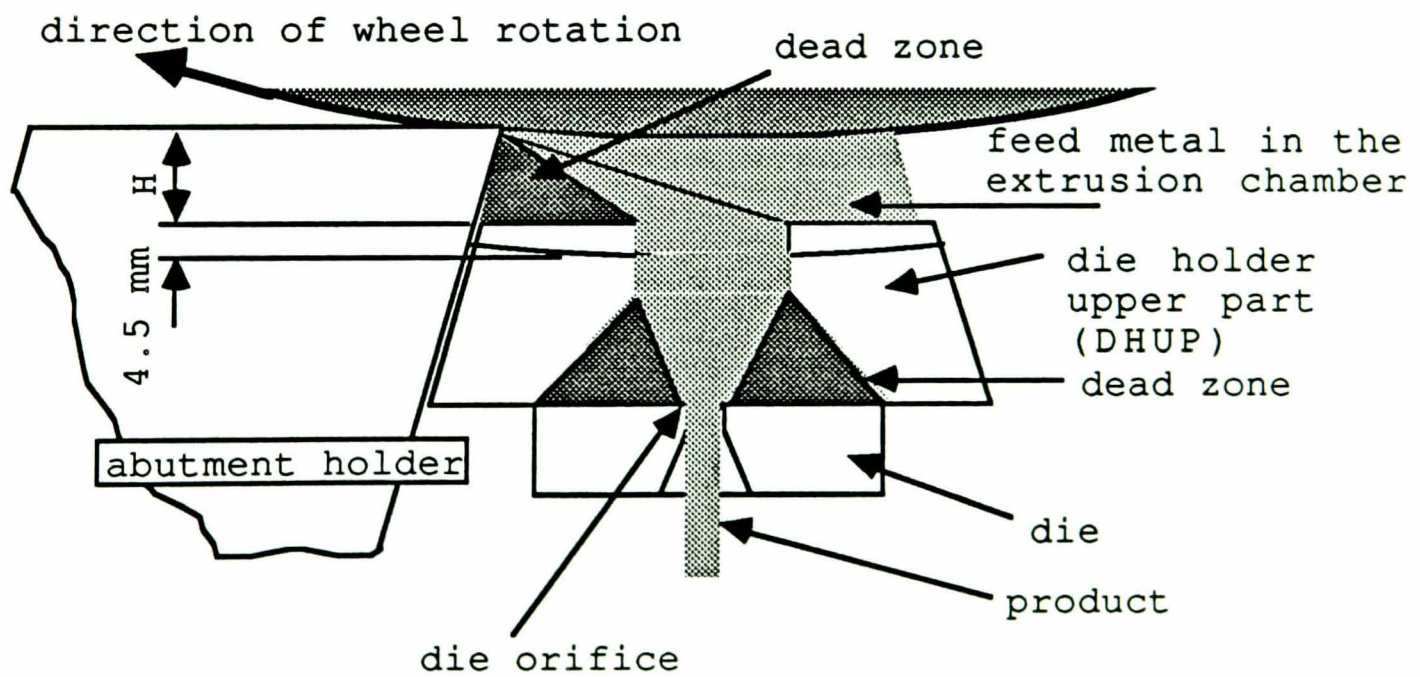


Figure 3.6b the diagram shows part of the deformation zone in 2-D.

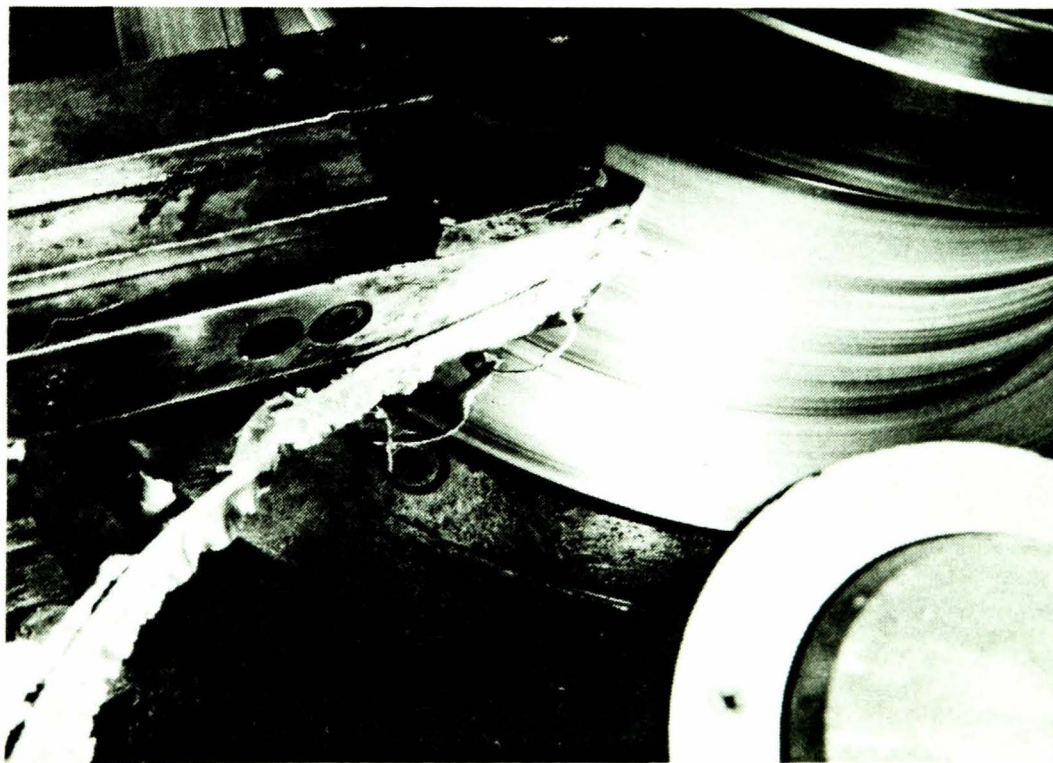
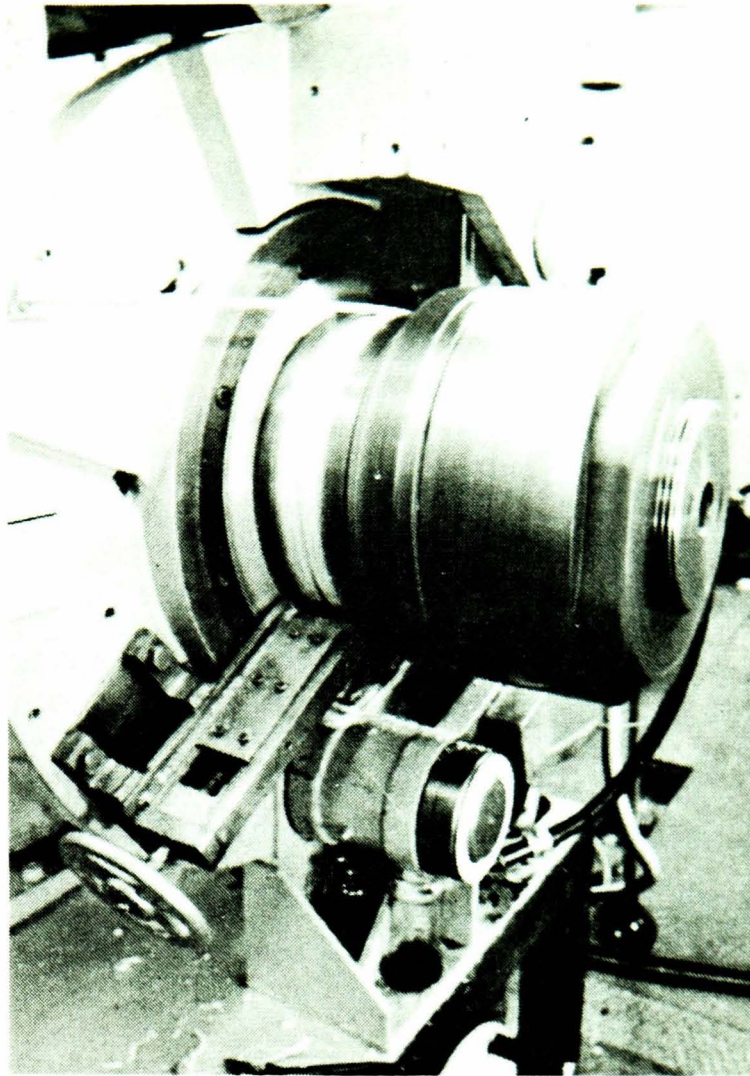


Figure 3.7. Showing the scraper tool in action, continuously removing the unwanted flash from the wheel groove.

It is imperative to ensure that minimum clearance is available between these different components during a production operation, because the level of flash generated is also influenced by the pre-set clearance between the moving wheel and stationary tooling.

Another complication which arises due to the friction heat generated in the deformation zone, is the expansion of the tools at elevated temperature, and the corresponding reduction in running clearances. Provision must be made to allow for thermal expansion of these components during tool set-up, since no adjustment can be made to the shoe during machine operation. Therefore a greater quantity of flash per unit time will be generated at the start of each test for the ambient temperature condition, and a corresponding reduction as steady state operation prevails over the transient condition.

It is noted that, unlike the shoe, the scraper tool can be adjusted during machine operation to allow for thermal expansion.

3.2 RECORDING EQUIPMENT

The Conform machine was supplied with instrumentation in the form of a Rikadenki Mitsui multi-pen mechanical chart recorder. In addition, various sensing devices were also provided, which are described as follows;

- a) High pressure (H.P.) hydraulic transducer connected to inlet pipe of motor.
- b) Low pressure (L.P.) hydraulic transducer connected to outlet pipe of motor.
- c) Tachometer which is placed in direct contact with the rotating shaft of the Conform machine.

- d) Three thermocouple probes attached to the die, abutment holder and grip segment tools.

These various devices are connected to the appropriate signal conditioning amplifiers and, in turn, to the multi-channel chart recorder. The chart recorder is a six-channel pen-operated recording device in which each pen produces a different colour trace on a graduated sheet. The speed of the trace can be varied, and it is essentially determined by the length of the production operation.

In order to prevent oil, grease or unwanted particles from coming into contact with the rotating wheel of the tachometer, a pressure pad has been installed adjacent to the rotating wheel of the tachometer, see fig 3.8. A solvent-based cleaning solution is applied to a small piece of absorbent tissue, which in turn is then placed on the pressure pad before the start of each test.

In addition, a hand-held tachometer is used to monitor the rod feed entry and product exit speed from the die, see fig 3.9 for details.

3.3 FEED STOCK

The feed stock supplied for experimentation is commercial purity aluminium in the annealed and half hard condition. The feed stock is supplied in coiled rod (nominally 9.6 mm diameter) and particulate form. A spectrograph test was carried out on various samples of rod feed stock in order to determine the percentage of impurity level. The spectrograph test revealed that the purity level is in the range 99.3 - 99.7 %. This is equivalent to the commercially pure aluminium grade AA 1050 (99.5 % purity).

The feed rod diameter is nominally 9.6 mm diameter. However, this was checked by cutting sections (approx 200 mm lengths)

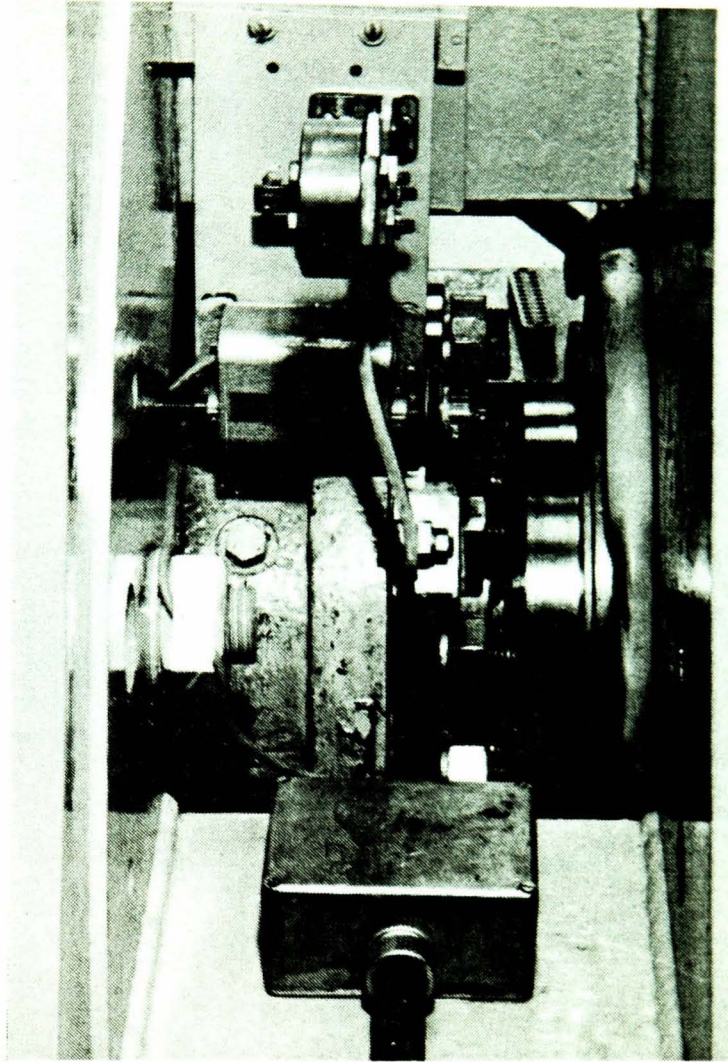


Figure 3.8. Showing the position of the tachometer, and pressure pad in contact with the rotating shaft.

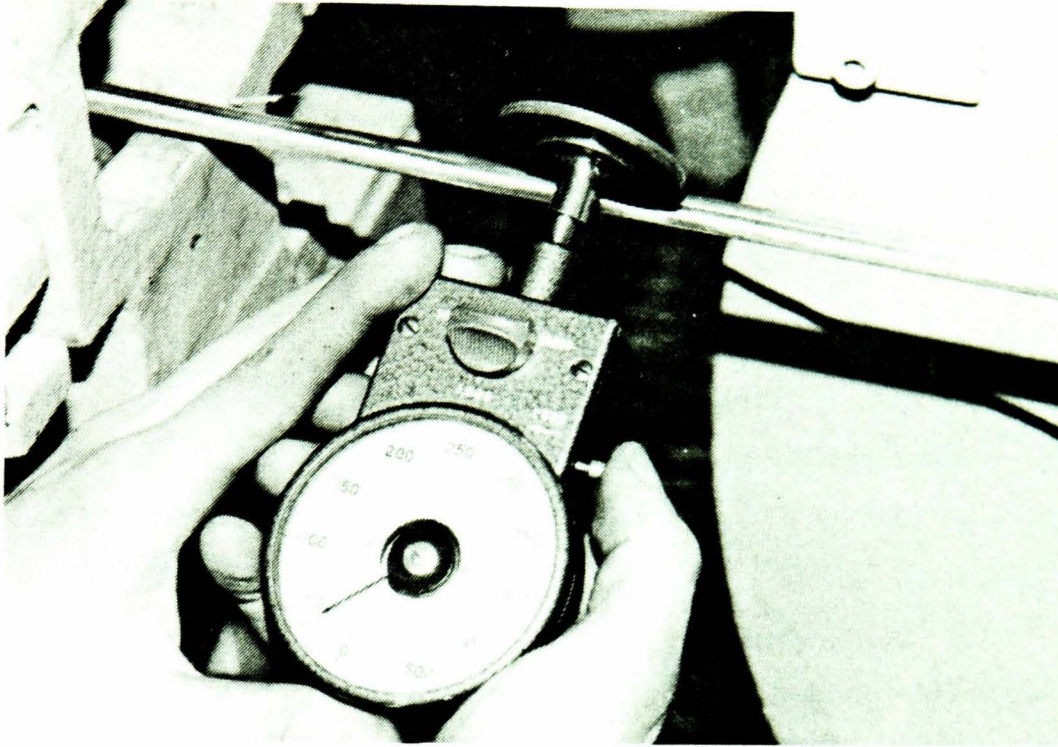


Figure 3.9. The portable tachometer monitoring the product exit speed from the die.

of feed rod from the coils, and measuring the length with a rule. The sections were weighed individually on a highly sensitive apparatus and, from knowledge of the density, the mean diameter was determined using the following equation,

$$\text{mean diameter, } d = \sqrt{(4\Delta / L\pi\rho)}$$

where Δ = mass (kg)

L = length (m)

ρ = density (kg/m³)

The mean diameter was found to be 9.6 mm (\pm 0.05) for the range of random samples taken from the batches of coiled feed rod. The accuracy of this technique is determined mainly by the lengths of rod samples chopped from various coils. The length of 200 mm was measured to an accuracy of \pm 0.5 mm using a scaled rule, and ensuring that the faces of the rod are flat and square to the rod length. The percentage error using the rule and weighing measurement will not be greater than 1/200, i.e. 0.5 %, compared with the micrometer measurements which yielded errors of the order 5 % due to the out-of-roundness of the rod feed stock.

The particulate feed stock was used solely for pre-heating the tooling at the start of each test and is not a variable in the present investigation.

3.4 PRELIMINARY EXPERIMENTAL TESTS

Preliminary experimental tests were carried out using the instrumentation detailed above in order to observe the behaviour of the machine under different setting and operating conditions.

Initially, these tests were carried out using the existing tools supplied with the Conform machine and set-up in the

normal configuration employed by UKAEA, to observe the torque and die temperature corresponding to changes in wheel speed for a range of different die sizes. In particular, the time taken for the change from the transient to the steady state operating condition was an important feature of these tests.

The variables considered are given in table 2 below.

Table 2

Setting variables (determined by geometry only)

feed stock: particulate (granular) spec. AA1050
 rod 9.6 mm dia. spec AA1050

die size (diameter in mm)	1, 2, 3.6, 6.2, 11
abutment depth setting	7 and 8 mm
shoe angle	60°, 70°, 80°, 90°

Operating variable

speed of wheel (rev/min)	5, 10, 15, 20
--------------------------	---------------

A typical test required the following procedure to be strictly adhered to, not only as a safety precaution but to prevent premature tool damage. A small reduction was initially selected for experimentation. The machine was set-up using the procedure described above. Particulate feed was then used to heat the machine tools until a steady state operation condition prevailed (after a period of approximately 10 minutes) at low wheel speed ($S = 5$ rev/min). The steady state operation was determined by observation of the reduction in torque and reduction in the rate of increase in die

temperature from the chart recorder.

The hopper funnel was then removed and the rod feed stock directed into the extrusion chamber by hand, after which the rod is drawn in by the frictional grip imparted to the feed rod by the rotating wheel. The two rollers on the last stage of the rod-straightening stand were then adjusted to impart a small reduction in cross-sectional area of the rod feed. This was necessary in order to prevent premature yielding of the feed rod entering the extrusion chamber.

The existing instrumentation supplied by the Springfield Laboratory was used to provide details of the power requirements and, in particular, the temperature at various stages in the extrusion chamber (the reasons for this will be described under Section 3.5).

3.5 MEASURING EQUIPMENT

It was proposed to install two loadcells at the die and abutment in order to monitor forces in the deformation zone. The test data acquired from the two loadcells are needed to compare the data derived from the theoretical analysis which is detailed in Section 5.

Interchangeability between the original tools in the shoe of the Conform machine supplied by the UKAEA and the modified tools which will accommodate the sensing equipment was the starting point for design.

3.5.1 RADIAL DIE LOADCELL TRANSDUCER

Two compression loadcell transducers were designed and manufactured from tungsten carbide and EN 24 steel. They were carefully designed to ensure that calibration can take place away from the machine. The original tools required suitable modification in order to house a single loadcell for

experimentation, see fig 3.10a and 3.10b, which is an assembly drawing of the modified tool housing and die loadcell.

3.5.1.1 CONSIDERATIONS

On close inspection, it was observed from the tool and die loadcell assembly, that no provision has been made to prevent feed metal entering the clearance zone between the moving die and the rigid die holder upper part (DHUP).

The ingress of feed metal takes place during normal machine operation for the range of reduction and speeds. The effect of this is to prevent free movement of the die insert in the die housing and is an unavoidable situation inherent in the design. However, by minimising this clearance zone and allowing for thermal expansion, it is feasible to minimise the influence of the ingress of feed metal on the measured load.

In addition, it was anticipated that the ingress of feed metal will influence the operation of the die by a minimum (numerically $\ll 5\%$ of the actual load). This is because a dead zone formation in the die chamber ahead of the die orifice will prohibit the feed metal from entering this clearance zone.

3.5.1.2 CONSTRAINTS ON DIE LOADCELL SPRING ELEMENT

To ensure that the die loadcell yields accurate and reliable measurements, it was necessary to allow freedom of movement of the loadcell in the lateral direction. In other words, there must be no constraints to the loadcell in any direction other than in the compressive position. In addition, limited access in the shoe has assigned a maximum dimension of approximately 25 mm on the gauge diameter of the loadcell (noting that sufficient space must be made available for the attachment of strain gauges on the gauge diameter). Provision for the

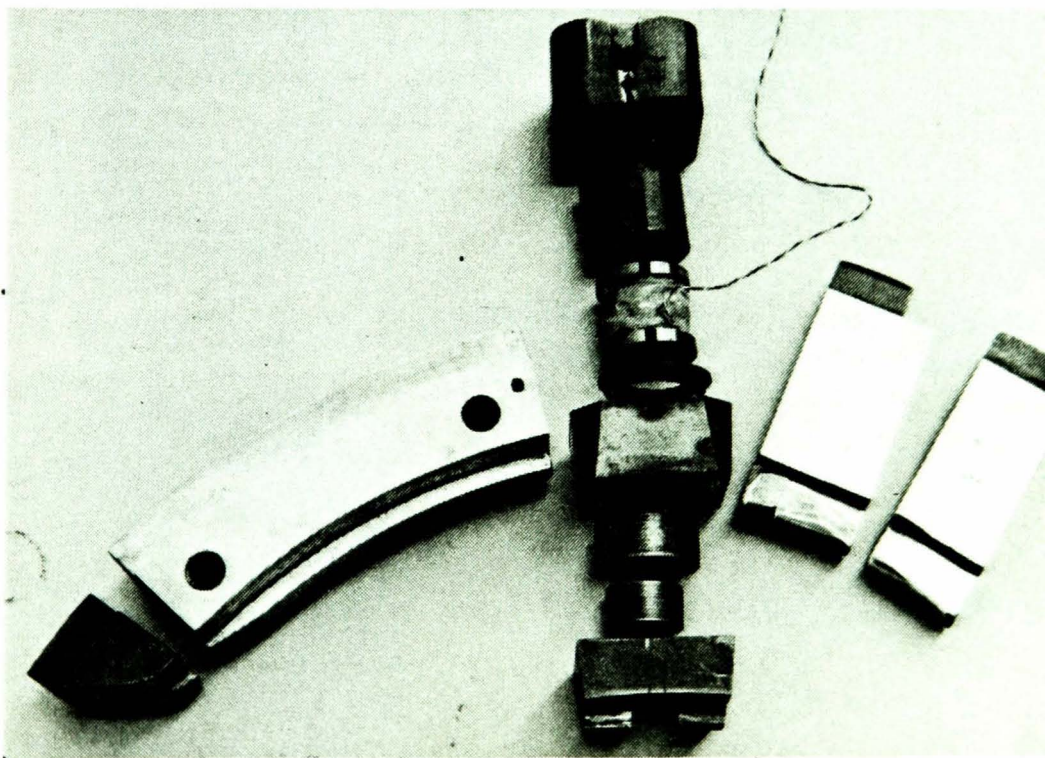
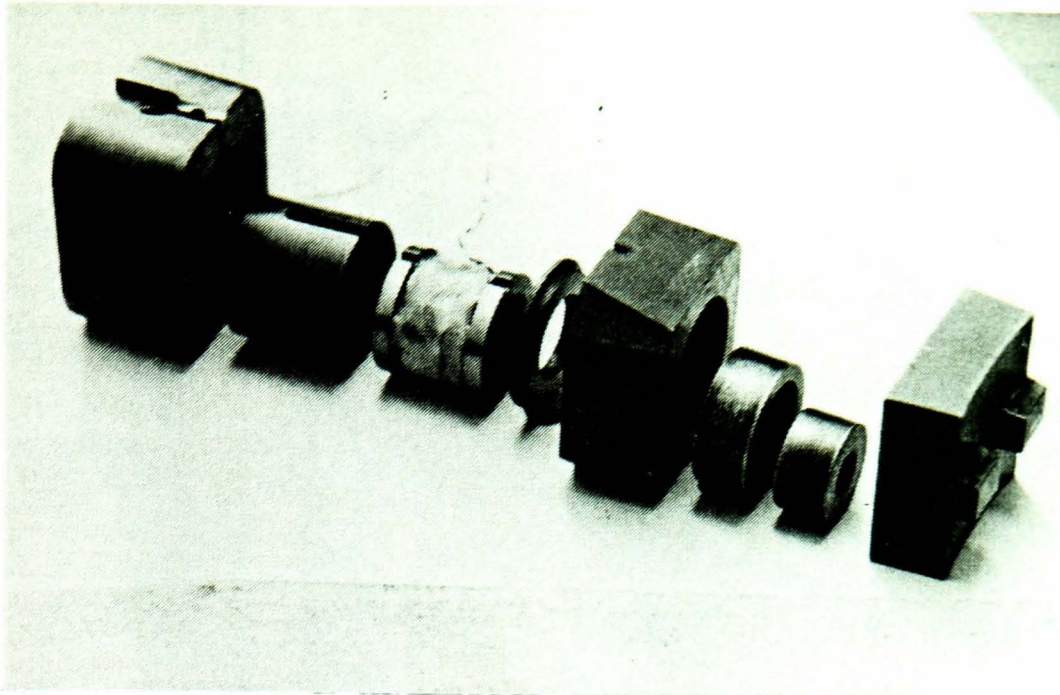


Figure 3.10a. The die loadcell and housing assembly

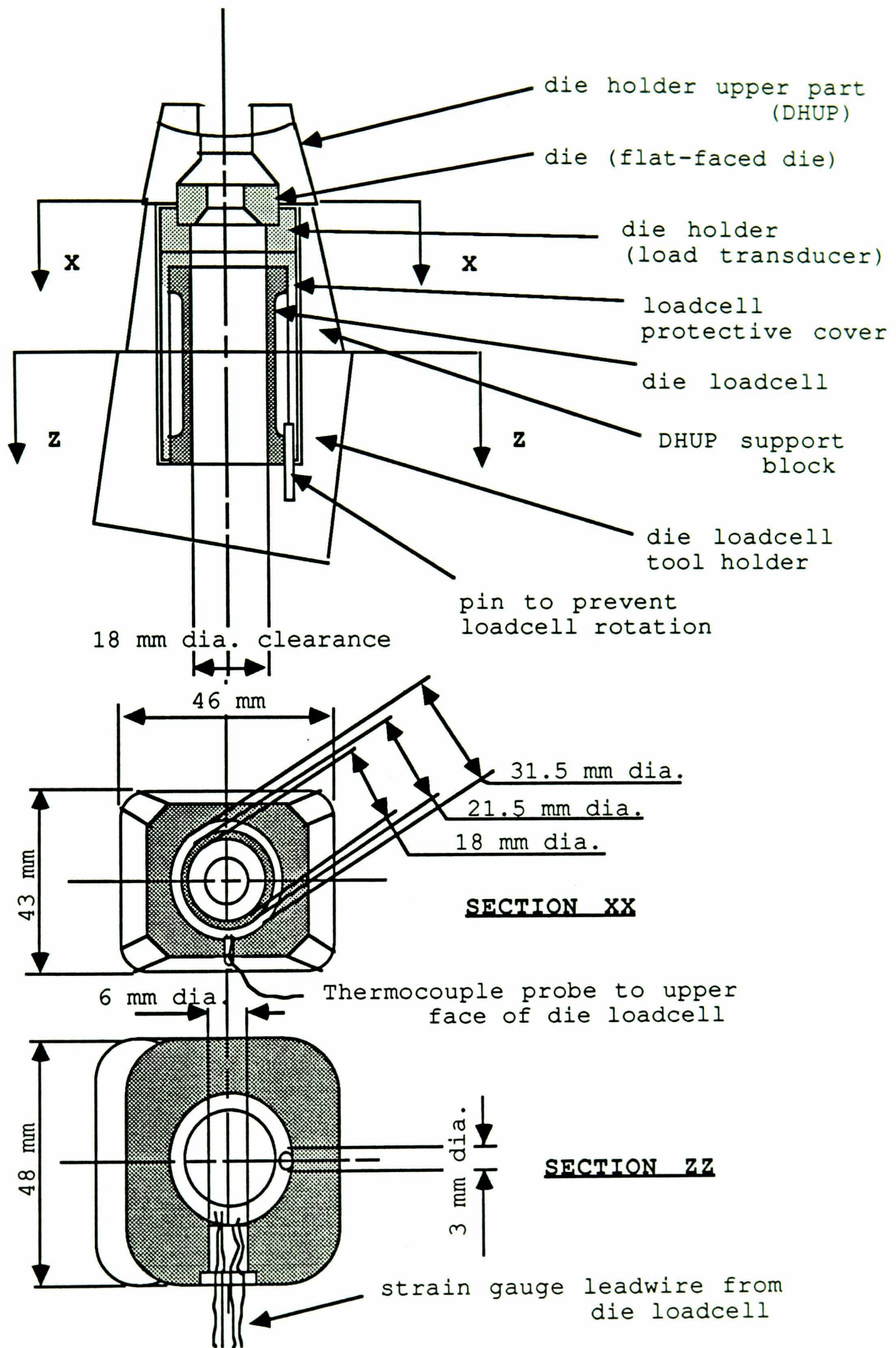


Figure 3.10b The diagram illustrates the die loadcell and housing

extrusion of rod section up to 10 mm diameter required the loadcell to be designed with a central hole of 18 mm diameter to allow a 4 mm minimum radial clearance.

In order to design the loadcell transducer to support a given load at an elevated temperature for the range of reduction, knowledge was gained of the environment in which the die loadcell should perform. This was achieved by conducting a series of experimental tests to determine the maximum force and force range that the proposed die loadcell will endure, using a variety of different-sized hollow steel washers. The following information in table 3 has been deduced from these tests using a 2 mm diameter die (reduction ratio = 23.0).

Table 3

reduction ratio;	23
wheel speed;	12 rev/min
abutment height;	8 mm
shoe angle;	75°
a normal operating temperature of washer approx. 200/300 °C	
b load range 0 to 90 kN at ambient temperature (machine start-up, 5 min. duration)	
c load range 0 to 60 kN at elevated temperature (static loading, 40 min. duration)	

Initially, a die loadcell was designed and manufactured from EN24 steel, hardened and tempered for the toughness condition 350 VPN (yield stress = 650 N/mm²). Under the heat treatment condition and dimensions as detailed above, the loadcell can sustain a maximum assumed load of 160 kN, this implies a design safety factor of 1.8. However, for the actual load of

90 kN at machine start-up, a compressive induced strain of 0.16 % will be sensed by the loadcell.

In this particular case a low profile loadcell is desirable, i.e. the height of the loadcell must be kept to a minimum (nominally 24 mm), the reasons for which will be described later. However, standard guidelines⁽¹³⁾ for the general case in column loadcell design, stipulate that the product of the height and the reciprocal of the gauge diameter (ie H/d_0) must lie between 1.1 and 1.5. This rule should be enforced in order to prevent;

a) 'End effects' influencing the uniform strain field on the gauge length if $H/d_0 < 1.1$. The end conditions generally imply the existence of friction at the loadcell/workpiece interface, inaccurate machining where the loadcell contact faces are not flat, parallel and square with the cylindrical gauge length, or indeed the positioning of the loadcell 'in situ', i.e. the application of offset loading on the column loadcell itself regardless of manufacturing accuracy.

b) 'Axial bending' if the column height becomes too large in relation to the gauge diameter ie $H/d_0 > 1.5$. The column becomes unstable in the longitudinal direction and, if unsupported, the column in the extreme case will preferentially bend about its longitudinal axis.

These rules are only generalised, since they apply to a particular case in column loadcell design and, as previously stipulated, are guidelines for the general case only. However, it is apparent that these rules have been extended to cover all types of column loadcell design, with some degree of confusion prevailing over the validity of these statements for the exceptional cases. As a result, further examination of the above criterion was considered necessary and is reported in ref (14).

The importance of this discussion on the design of the die loadcell in question is brought about by the constraints on the maximum allowable height of the die loadcell. This is because a maximum height of 24 mm has been assigned to the die loadcell in order to provide suitable accommodation in the tool holder. The die loadcell manufactured from EN24 steel was therefore modified, since the height did not fall into the design criterion namely $H/d_o > 1.1$. To do this the external and internal diameter of the die loadcell were reduced in order to support the same maximum load of 160 kN, at the expense of reducing the radial clearance made available between the 10 mm diameter product exiting the die and the internal diameter of the loadcell.

To overcome the limitations of the EN 24 loadcell, a material was employed with an elastic modulus (E) much greater than that of steel. This feature will allow a reduction in the minimum necessary gauge diameter (whilst maintaining the same, or reduced level of strain of approximately 0.15 %) and, in turn, reduce the minimum height of the loadcell required to adhere to the design criterion $H/d_o > 1.1$.

The material selected for this application was tungsten carbide with a 6% Co content⁽¹⁵⁾. The 'E' value for the carbide material chosen is three times that of EN24 steel. Further details of the physical and mechanical properties of the carbide material are given in table 4 below,

A hot isostatic pressing (HIP) treatment was called for the manufacture of the carbide. This is necessary because the sintering process involved with the manufacture of the carbide can generate porosity < 1%. The HIP process reduces the porosity in the loadcell spring element to a minimum i.e. 0 %.

The design drawing of the loadcell manufactured from tungsten carbide is detailed in appendix A1. This loadcell was designed to endure a compressive strain at ambient temperature of 0.14 % for the machine start-up condition. Assuming that the loadcell is held rigid under a given load in the

compressive position within the tooling, the temperature induced compressive strain will be negligible. As a result, it is expected that the actual compressive (longitudinal) strain in the loadcell will reduce to below 0.07 % at elevated temperature, due to the corresponding reduction in load for the steady-state machine operating condition. However, barrelling of the loadcell will be further pronounced due an increase in the circumferential (transverse) strain in the portion of the loadcell which remains unconstrained for the elevated temperature condition. The effect of this increase in transverse strain is to increase the output signal from the bridge circuit, this will be discussed in more detail under 'Choice of strain gauge for the loadcell', section 3.5.1.3.

Table 4

tungsten carbide (main elements: 94% WC, 6% Co)	
density;	15 Mg/m ³
hardness;	1560-1600 VPN
compressive strength;	5.85 kN/mm ²
Young's modulus;	630 kN/mm ²
Poisson's ratio;	0.22
linear coefficient of expansion;	5.2*10 ⁻⁶ /K
resistivity;	0.2 μΩm
thermal conductivity;	110 W/mK

The column loadcell has a reputation for inherent non-linearity. The deviation from linear behaviour is commonly ascribed to the change in cross-sectional area of the column (barrelling) which occurs with deformation under load. Because of this effect, the stiffness of the spring element continually increases as it is loaded in compression. It has also been shown that the elastic modulus (E) will increase⁽¹³⁾

for the column loadcell in the compressive condition due to small changes in the density. However, this will be partially offset by a reduction in the elastic modulus which is accompanied by an increase in temperature. Furthermore, it was anticipated that the application of heat to the loadcell under certain loading conditions (assuming that the loadcell is held rigidly in the compressive position and free to expand laterally) would serve only to aggravate the area effect.

3.5.1.3 CHOICE OF STRAIN GAUGE FOR THE DIE LOADCELL

It is commonly established in column loadcell design⁽¹³⁾ that all four arms of a full bridge circuit are not 'equally' active. This is due to the effect of Poisson strain on the transverse gauges, which register only a quarter or less strain than the gauges aligned longitudinally (noting that a steel spring element has a Poisson strain equal to approximately one third of the longitudinal strain). As a result, the increase in circumferential strain due to the inherent barrelling of the column loadcell when deformed, would generate a non-linear response from the unbalanced bridge circuit. This is because the change in strain of the 'non-active' gauge in one arm of the bridge is not matched by an equal and opposite change in the 'active' gauge in the adjacent arm. However, the combined effect of the transverse and longitudinal strain gauges in the bridge circuit serves to increase the overall sensitivity of the loadcell.

The main purpose of the non-active gauge arranged in the bridge circuit of the column loadcell is to provide a temperature-compensating medium. It should be noted however, that the transverse gauges are not strictly passive gauges since the Poisson strain can amount to one quarter of the longitudinal strain. However, the full bridge circuit consisting of two active and two passive gauges was the only arrangement likely to yield the best possible results for temperature compensation. If however, the loadcell gauge diameter was greater, then it is possible that two or more

gauges in each arm of the bridge (implying a total of eight or more gauges) would be a more suitable arrangement in terms of temperature compensation.

In addition, temperature variations arising across the die loadcell faces (the upper face of the loadcell was at a higher temperature than the lower face) deemed it imperative to use a full bridge circuit.

In order to determine the temperature of the die loadcell for a range of different operating conditions, it was considered necessary to manufacture a prototype loadcell from EN24 steel for experimentation. The loadcell was designed to be kept as far from the heat source (the die) as possible, and subsequently this placed restrictions on its overall dimensions, in particular the height of the loadcell in the tool holder. Thermocouple probes were attached to the upper and lower flange faces of the die loadcell. Preliminary tests were carried out by operating the Conform machine for a range of different setting conditions. The information in table 5 has been deduced for the worst operating condition using a 2 mm (reduction ratio = 23.0) diameter die,

Table 5

Reduction ratio;	23
wheel speed;	12 rev/min
Abutment height;	8 mm
Shoe angle;	75°
highest temperature recorded	250 °C
highest temperature differential recorded	45 °C

The effect of high temperature on the choice of strain gauge for the die loadcell has been considerably limiting. Indeed,

it is apparent that Modified 'Karma' alloy is the only suitable strain gauge presently available from the manufacturer⁽¹⁶⁾, which exhibits good resistive stability over the temperature range concerned. Furthermore, the fatigue life of the Karma alloy (or K-alloy) is much greater than its standard counterpart, the Constantan strain gauge. Unfortunately, the K-alloy is considerably more expensive to manufacture and install on the loadcell spring element.

The design of the loadcell required it to be small and compact which implied further restrictions on the choice of strain gauges presently available from the manufacturer. This in turn placed a further increase in the manufacturing and installation cost of the strain gauges on the loadcell spring element.

Other gauges however, were available, these include Self Temperature Compensated strain (STC) gauges, which compensate for temperature variation independently of the bridge circuit configuration. These gauges are selected for their STC number which corresponds to the thermal coefficient of expansion of the loadcell spring element. If this type of gauge had been employed, a quarter-bridge circuit (incorporating a single active longitudinally aligned strain gauge) would be sufficient to provide temperature compensation. However, a single gauge cannot compensate for temperature variation across the loadcell upper and lower faces. Although this feature is undesirable to a lesser extent in the full-bridge arrangement, it would nonetheless lead to non-uniform temperature-induced strain (thermal gradients) and, in turn, yield an unreliable and inaccurate output from the bridge circuit.

Above all, the reproducibility of results from the output of the bridge circuit on the die loadcell was the most important consideration. Regardless of deviations from linearity due to temperature and the loading condition, if the loadcell failed to provide repeatable results it is deemed unreliable and should not be used. Another important consideration is the

initial design criterion namely,

$$1.1 \leq H/d_0 \leq 1.5$$

Also the maximum induced compressive strain should be no greater than 0.15 %. This is considered necessary since the fatigue life of the strain gauge decreases significantly with increasing strain beyond that limit. This is more important where dynamic strains are concerned. However, the operation of the die loadcell is virtually static and it is important, therefore, that the strain gauges and loadcell spring element were selected for the 'minimum creep' condition.

Another important factor requiring consideration is the rate of heat transfer across the loadcell from the upper face (close to the die) to the lower face. It is noted that EN24 steel has a thermal conductivity of 40 W/mK at ambient temperature. Tungsten carbide with the physical properties detailed above, is shown to be a better conductor of heat than EN24 steel. The die loadcell manufactured from the tungsten carbide material, will take a shorter time to reach a steady state operation for a change in the machine operating conditions, and also a reduced temperature differential across the loadcell faces will exist.

The tungsten carbide material has a much lower coefficient of thermal expansion than steel. This implies that the radial expansion of the die loadcell due to an increase in temperature, is smaller than the protective cover designed to enclose the die loadcell within the tool holder, see fig 3.10a and 3.10b. The protective cover was designed with sufficient space made available for thermal expansion within the tool holder.

Other considerations included flying leadwire access from the loadcell bridge circuit to the monitoring equipment. Also, the need to ensure that ease of assembly and removal for both the tools and loadcell from the shoe for constant inspection was imperative. As a result, the protective cover was

designed with a longitudinal slot for access to the bridge circuit to attach the flying leadwire when assembled. The tool holder was designed with a port to allow access for the 4-core leadwire to the terminal box on the side of the shoe.

The upper and lower faces of the loadcell were lubricated with a high temperature MoS₂-based lubricating oil. This was necessary in order to allow a more uniform pressure to be distributed across the faces of the loadcell with deformation under load and to allow free radial expansion which accompanies any increase in temperature. As a consequence, it was considered that the vibrations transmitted to the loadcell from the machine, in particular the die during normal operation, are sufficient in magnitude to cause the loadcell to rotate in the tool holder. Such rotation must be avoided, because minimum space has been allocated for flying leadwire access to the terminal box on the shoe. If the loadcell were allowed to rotate relative to the tool holder, it is probable that the flying leadwire would be severed, or at least damaged. To overcome this difficulty, the die loadcell was slotted on both its upper and lower flange diameters. The intention of this feature was to locate the slotted region of the loadcell flange over a pin at the base of the tool holder, and so prevent any rotation of the loadcell and protective cover relative to the tool holder. The location pin is situated adjacent to the port at the base of the tool holder to allow the routing of leadwire direct from the loadcell, through the slot in the protective loadcell cover to the terminal box on the shoe.

Provision was made for the attachment of thermocouple probes to the upper and lower faces of the die loadcell. This implied that a hole is required in the upper part of the die loadcell protective cover, in order to feed a thermocouple probe to the loadcell spring element. A second thermocouple probe was fed through the longitudinal slot at the base of the protective cover to the loadcell.

The resistance of the strain gauges selected for installation was initially 500 Ω . An important consideration was the desensitivity factor associated with the length of leadwire connecting the sensing devices to the instrumentation. Because of this, high resistance gauges were selected. Another consideration is leadwire temperature compensation. Since the leadwires are routed through the shoe of the machine, a small change in temperature will arise from their point of connection on the strain gauges of the loadcell to the monitoring equipment. However, this feature affects the output signal from the strain gauges to a lesser extent, provided that the leadwires which form the bridge circuit are maintained at the same temperature. Leadwire temperature compensation, can be accomplished by two methods; a) twisting together all the leadwires that form the bridge circuit from their point of connection to the instrumentation baseboard and, b) employing a strain gauge module for the instrumentation baseboard, which has a built-in leadwire temperature compensating terminal for the connection of an additional dummy leadwire; the instrumentation system is discussed in full under Section 4.

High resistance strain gauges, chosen to allow maximum possible bridge excitation voltage (up to 10 V) by the die loadcell, was the initial suggestion. As a result, amplification of the output signal from the unbalanced bridge circuit is reduced accordingly. The amplification is then selected to return the signal to the recording equipment within an acceptable working range of the order 0 to 10 V.

Unfortunately, it was not possible to obtain miniature high resistance gauges from the manufacturers⁽¹⁾ with an acceptable short delivery time. The alternative was to select strain gauges presently in the manufacturer's stock, and therefore 350 Ω gauges were the only option. A gain $G < 150$ used in conjunction with a 10 V bridge excitation voltage was sufficient to generate the output signal to below 10 V at maximum strain (or load).

3.5.2 DESIGN OF ABUTMENT TRANSDUCER

A compression loadcell transducer was designed and manufactured from tungsten carbide to provide a measurement of the direct force imparted to the abutment tool face, see fig 3.11a and 3.11b. The abutment loadcell is a hollow column, designed to function with strain gauges cemented to the gauge diameter in the appropriate configuration as in the previous case with the die loadcell. The design criterion for the abutment loadcell therefore incorporated the same basic principles as outlined for the die loadcell.

3.5.2.1 CONSIDERATIONS

Similar difficulties were encountered with the design of the abutment loadcell spring element. For example the ingress of feed metal between the DHUP and the abutment tool which occurred during machine operation, see fig 3.12, and space restriction - where the height of the abutment loadcell is limited to 16.5 mm in length.

Regarding the latter, it is noted that the height, gauge diameter and internal diameter assigned to the die loadcell are 24 mm, 21.5 mm and 18 mm respectively. The internal diameter of the abutment loadcell is determined by the diameter of the location pin situated on the abutment seat, which constrains the abutment loadcell from free movement in the lateral directions. The location pin is 7 mm diameter and manufactured from silver steel. The gauge diameter of the abutment loadcell required to support the same load as the die loadcell is 14 mm, the resulting design is shown in appendix A2. The height to gauge diameter ratio is 1.4, and a load of 100 kN will generate a compressive strain equivalent to 0.14 %.

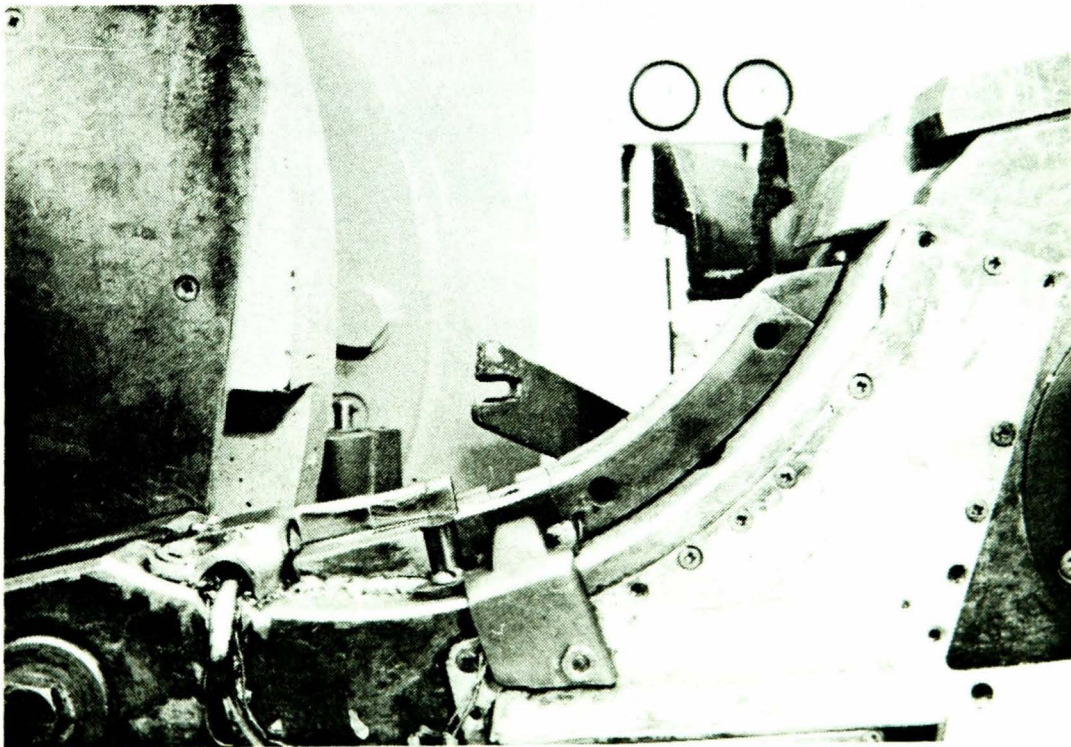
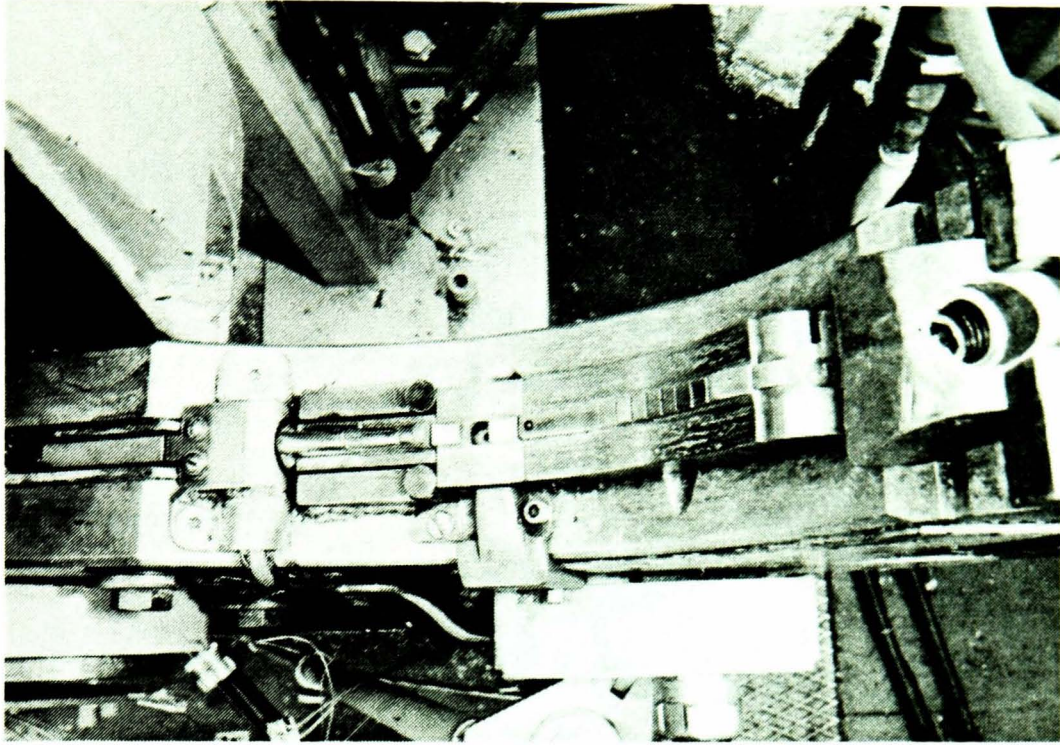


Figure 3.11a. Illustrating the tool set-up surrounding the abutment loadcell.

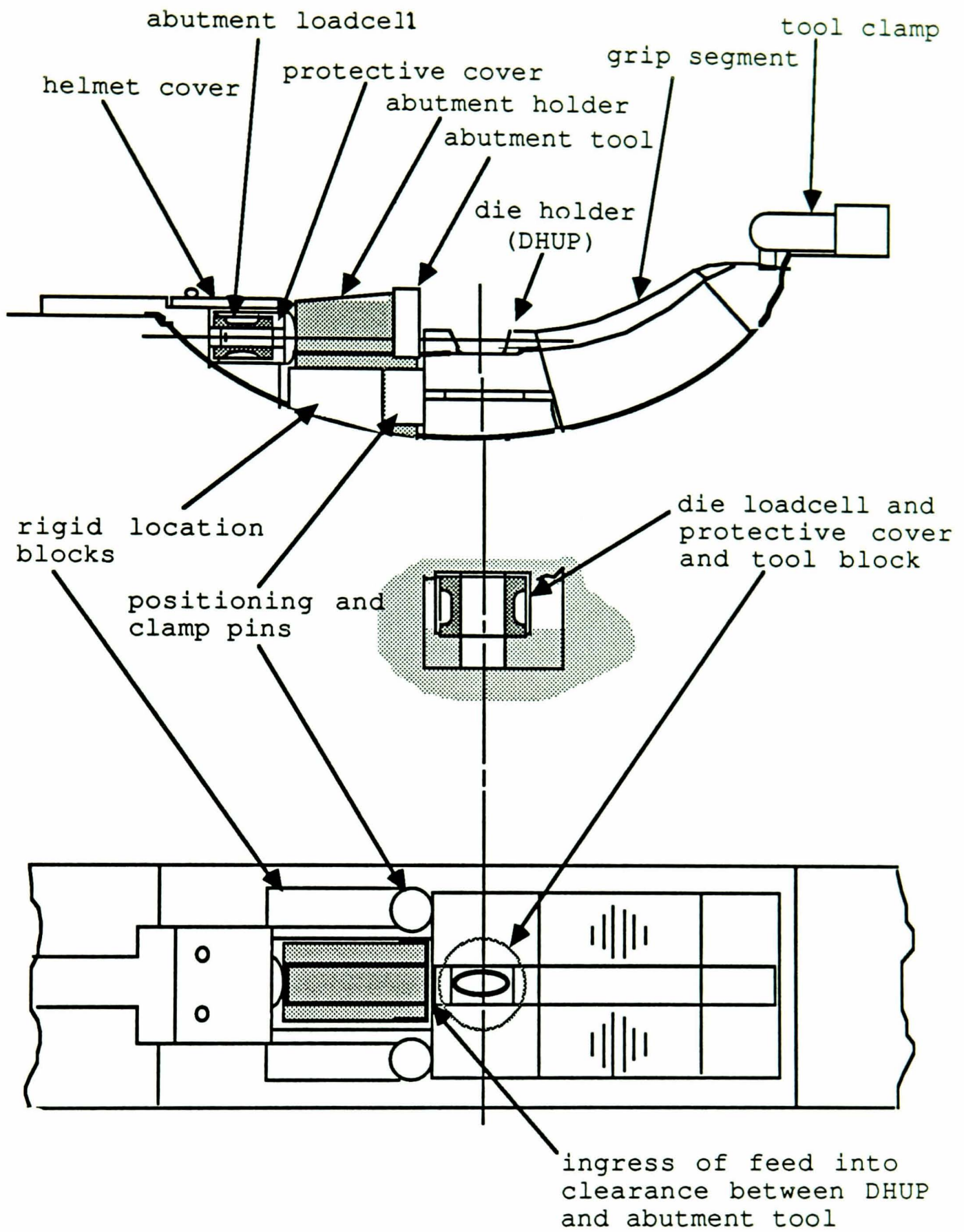


Figure 3.11b Tool and loadcell set-up in the shoe of the Conform machine

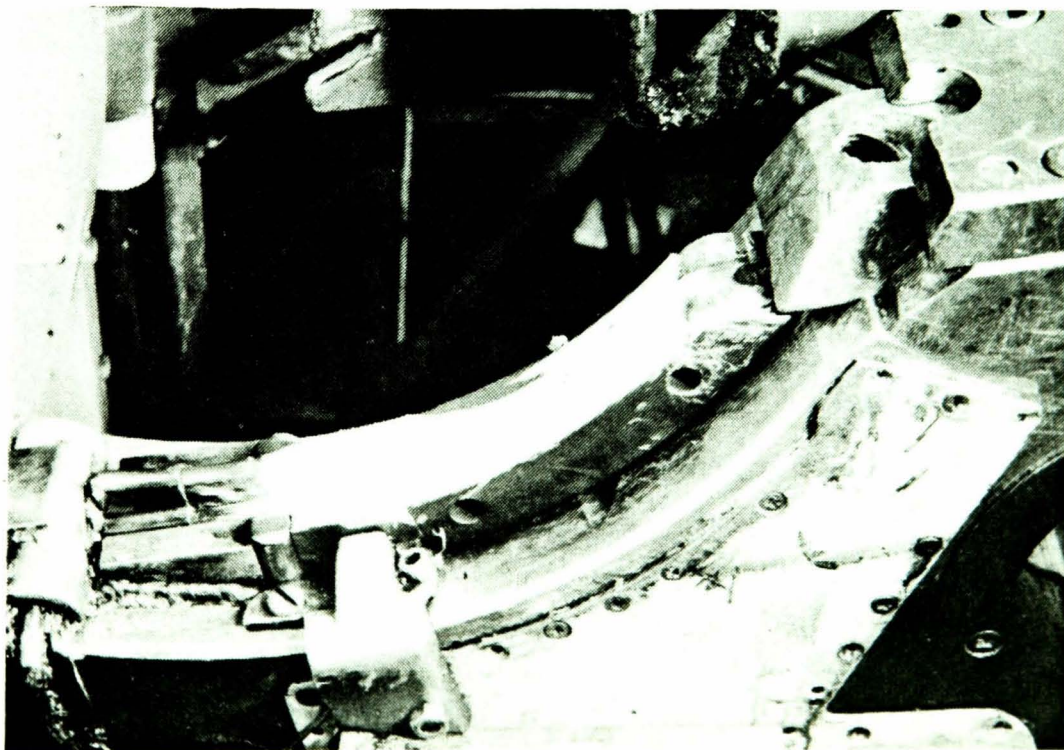
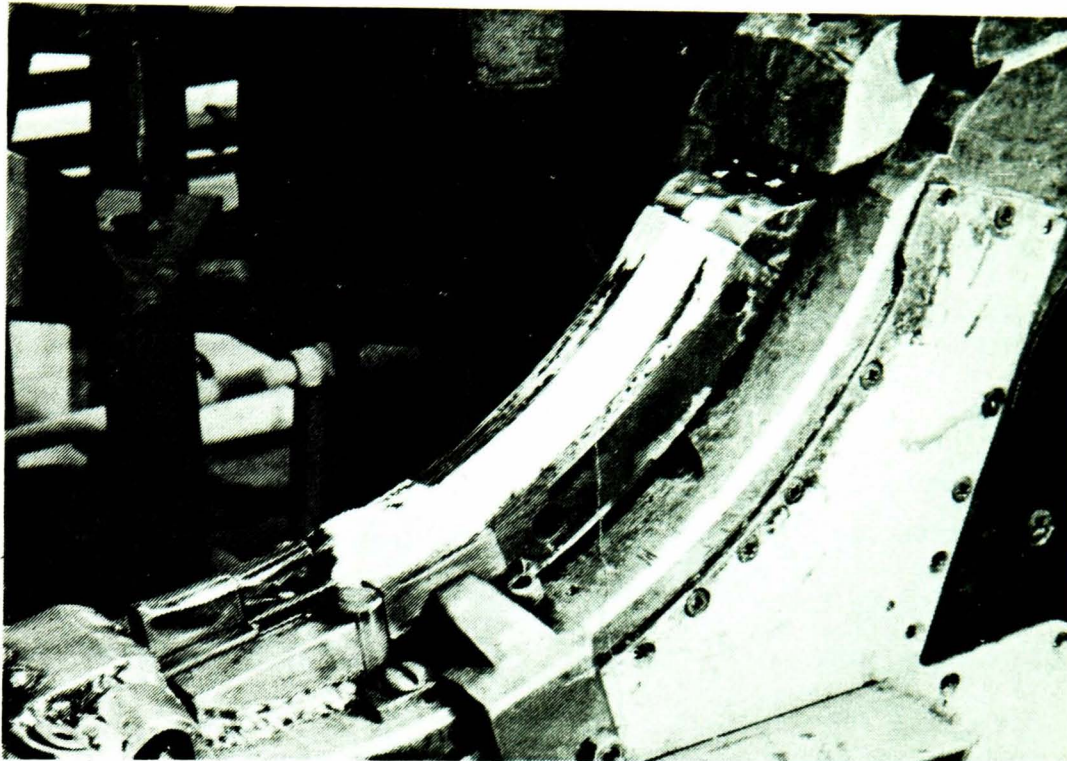


Figure 3.12. Showing the residual metal attached to the tools, after the shoe has been removed from the wheel on completion of each test.

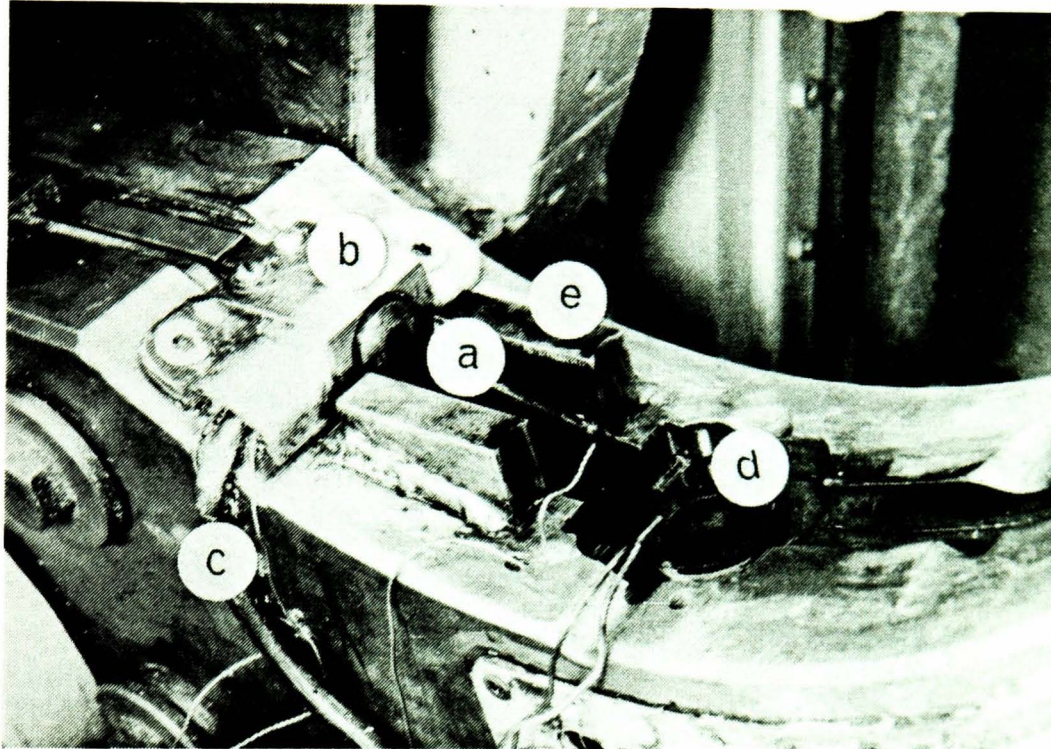
3.5.2.2 STRAIN GAUGE SELECTION

The strain gauge specification for the abutment loadcell is a full bridge circuit incorporating two active and two passive 350 Ω strain gauges. The gauges are manufactured from K-alloy and are of the miniature type. Further details are given in appendix A3.

3.5.2.3 CONNECTION OF FLYING LEADWIRE

A protective cover was provided to enclose the abutment loadcell. Provision was also made for a longitudinal slot and hole in the protective cover to allow routing of 4-core flying leadwire and thermocouple probes to the loadcell spring element.

Space restriction is not critical in the immediate region surrounding the abutment loadcell. In other words, the abutment loadcell and protective cover are not fully encapsulated within a tool holder as was the die loadcell. However, a helmet cover manufactured from EN5 (mild steel) was designed to protect the abutment loadcell and protective cover from the hot flash which arises from the deformation zone during normal machine operation (the hot flash becomes more pronounced for the larger reduction ratio i.e. $R > 8$). The helmet cover was case-hardened on all faces which are prone to attack from hot flash. A screwed hole is provided on the side face of the helmet cover to support the conduit in which the flying leadwire is routed from the terminal box on the shoe to the strain gauges on the loadcell, see fig 3.13. Thermocouple probes which sense the temperature on the upper and lower flange faces of the abutment loadcell are also supported by the helmet cover.



- a. abutment loadcell spherical cap
- b. helmet cover
- c. small bore conduit
- d. die loadcell (exposed)
- e. rigid location blocks

Figure 3.13. The shoe after part tool removal

3.5.2.4 NEW TOOLS TO ACCOMMODATE THE ABUTMENT LOADCELL

It was necessary to modify the original tools in the shoe of the Conform machine to accommodate the abutment loadcell. Initially, the tapered wedge which provided a rigid securing block to clamp the grip segment, DHUP and abutment tool holder in position was removed. In its place a shorter tapered wedge was located in order to provide a rigid clamping medium for support at the base of the abutment holder only, see fig 3.14.

In addition, a rigid and secure base was required to support the abutment loadcell in position adjacent to the abutment holder and directly 'in line' with the abutment tool ('in line' implies that the total direct force vector on the abutment is transmitted to the centre of the loadcell column). However, the latter was not possible since the abutment tool height has been designated as a geometric variable for experimentation. Consequently, variations in the depth setting of the abutment tool would require corresponding adjustments to the position of the loadcell in line with abutment tool. Also, the height of the abutment tool was such that the helmet cover, which protects the abutment loadcell, would make contact with the surface of the rotating wheel if the loadcell was placed directly in line with the abutment tool face. Therefore, the position of the loadcell was adjusted until it fell short of contacting the wheel (allowance also made for the helmet cover) for a minimum abutment tool depth setting of 6 mm.

A rigid support for the abutment loadcell (abutment loadcell seat) was designed and manufactured from EN5 steel and case-hardened. The rigid support is clamped to the shoe and can be adjusted to fit neatly in position by slackening the two Allen screws to the rear of the unit, see appendix C4 for details. In addition, the angle which the front face of the abutment loadcell seat subtends from the abutment tool face can be adjusted. The loadcell seat was set flat and parallel with respect to the abutment tool face during tool set-up.

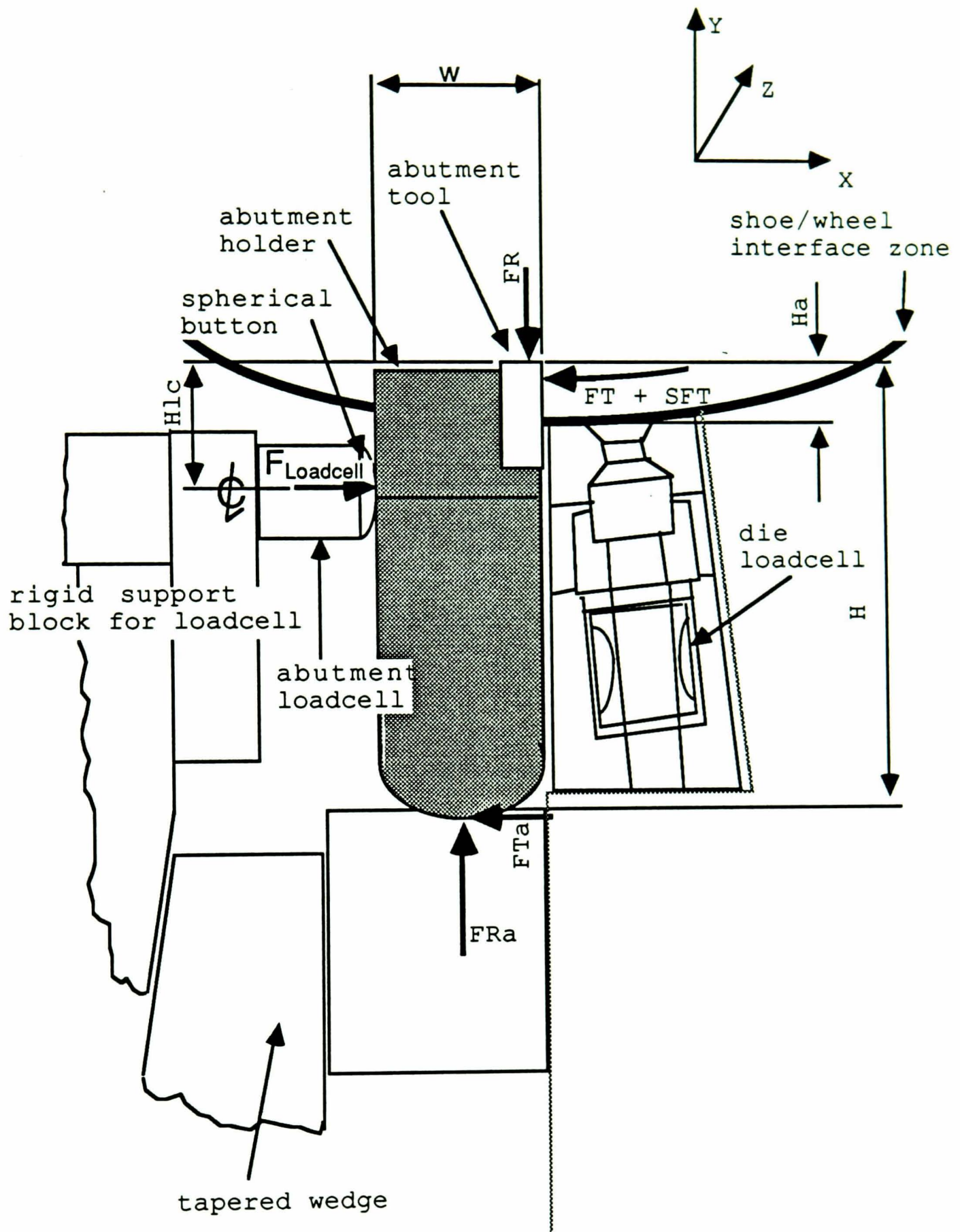


Figure 3.14 Abutment loadcell and Tool set-up

3.5.2.5 TOTAL DIRECT LOAD SENSED BY THE ABUTMENT LOADCELL

The load sensed by the abutment loadcell (F_{Loadcell}) is not the true direct force that is sensed by the abutment tool ($F_T + SFT$), see fig 3.14. This is due to the positioning of the loadcell behind the abutment tool. In fact, the true direct force is partially offset by the amount $H_{1c} - H_a/2$ (assuming uniform hydrostatic pressure acting over the abutment tool face). The actual loading on the abutment tool face is a combination of forces arising from (a) variations in tangential and radial stresses acting across the face of the abutment tool due to the relative motion of feed material and (b) friction (SFT) at the wheel groove and abutment tool interface and (c) additional offset loading due to the ingress of aluminium feed into the clearance between the DHUP and the abutment tool holder.

The true load on the abutment loadcell was determined by calculation. Initially, however, modification to the tools which physically constrain the operation of the abutment loadcell was necessary in order to simplify these calculations. For example, a spherical button was designed and manufactured from EN24 steel (heat treatment condition; hardness = 350 VPN, equivalent yield stress = 650 N/mm²). The spherical button is seated on the upper face of the abutment loadcell in order to minimise offset forces being transmitted to the abutment loadcell.

It is observed from fig 3.14, that the abutment holder pivots about its base (or seat) due to the tangential load (F_{Ta}) and the radial thrust (F_{Ra}). Also, the external surfaces of the abutment tool holder, which are in contact with the inside surface of the shoe, were sized to prevent contact between these components at elevated temperature. The abutment tool holder is therefore constrained only by its seating at the base, the loadcell button and the abutment tool in the wheel groove during normal machine operation.

In order to provide a suitable seat for the abutment tool holder to pivot about its base, the optimum condition is a frictionless pivot where,

$$F_{Ta} = \mu F_{Ra}$$

and,

$$\mu \approx 0$$

however this is not possible in practice. But with the application of suitable lubrication i.e. a graphite-based lubricant (or MoS_2) for elevated temperature operation, a significant reduction in the coefficient of friction is feasible.

If the abutment holder is considered to be rigid, then the force transmitted to the loadcell is determined by summing all the forces in the X - direction i.e.,

$$F_T + S_{FT} + F_{Ta} - F_{\text{Loadcell}} = 0$$

By assuming a frictionless pivot motion about the abutment tool holder base, then the tangential force ($F_{Ta} = 0$) is equated to zero,

therefore,

$$F_T + S_{FT} = F_{\text{loadcell}}$$

It is observed that the force on the loadcell is the same as the total load sensed by the abutment tool.

3.5.2.6 FRICTION AT THE ABUTMENT TOOL/WHEEL GROOVE INTERFACE

A coating of feed material is deposited on the inside surfaces of the wheel groove and on the peripheral surfaces of the wheel to form a dead zone during normal machine operation. The dead zone profile in the wheel groove is initially determined by the abutment tool shape and then by the scraper tool setting. The scraper tool is used to remove part of the feed material coating the inside surfaces of the wheel groove and, in turn, the oxide film formed on the surface of the dead zone. However, the operation of the scraper tool will be neglected in the following analysis in order to simplify the theory.

The abutment tool is essentially a form tool since it continuously shears the feed metal at the abutment tool/wheel groove interface. In other words, the feed which impinges on the face of the abutment tool is forced to leave the extrusion chamber through the die to form a product, or, alternatively, through the running clearance to produce flash. The feed which by-passes the abutment tool/wheel groove interface, will remain stationary on the wheel groove surface to form a dead zone. Relief angles have therefore been introduced at the top and side faces of the abutment tool, in order to provide a suitable clearance and, in turn, to minimise the friction force on the abutment tool. The theoretical treatment of the friction force on the total abutment force is described in full in Section 5.

It is noted, however, that a dead zone of feed material exists ahead of the abutment tool face, see Section 5 for details. This implies that the feed material entering the extrusion chamber shears as it impinges on the face of the dead zone ahead of the abutment (not when it reaches the abutment face). Indeed, the feed material entering the extrusion chamber will never make contact with the abutment tool face except at machine start-up, although there will be contact between the top and side faces of the abutment tool in the wheel groove,

as described previously.

3.5.2.7 ISOLATION OF DIFFERENT LOADS ON THE ABUTMENT TOOL

The 'original' tools in the shoe of the Conform machine supplied by the UKAEA were designed for manufacturing flexibility. As such, the grip segment, DHUP and the abutment tool holder are clamped together by a single fastening screw and tool clamp. This design implies that the thrust imparted on the grip segment and the DHUP is, in part, transmitted to the abutment tool holder. The resulting effect on the abutment tool is an increase in the total direct force sensed by the abutment loadcell.

It was necessary to isolate the additional loading on the abutment tool from the direct load due to the feed which impinges on the abutment tool face. Otherwise these combined loads serve only to increase the total direct force on the abutment tool. Consequently, the data obtained from the abutment loadcell during subsequent experimentation will be meaningless in terms of providing accurate details for modelling the process. Therefore modification to the existing tools incorporated two rigid location blocks and two 12.7 mm diameter by 23 mm long pins situated adjacent to the abutment tool holder, see fig 3.11a and 3.11b. The DHUP is now isolated from making contact with the abutment tool holder, instead the pins provide a rigid clamping medium for the DHUP, grip segment and tool clamp. Initially the additional loading on the abutment tool due to the combined force of the DHUP and grip segment tool was estimated for the maximum load operating condition. The maximum load was estimated by considering the geometry of the extrusion chamber, reduction ratio, and thereby the mean radial and tangential thrust transmitted by the feed metal to the grip segment and then to the abutment tool. Then, tests were carried out to determine the pin size necessary to accommodate the additional direct loading from these tools.

Prototype pins measuring 12.7 mm diameter by 23 mm long, were manufactured from EN24 steel, hardened and tempered to provide a yield stress of 850 MPa in order to sustain a maximum estimated force of 30 kN (this includes a design safety factor of 3). To study the effect of the pin subjected to lateral compression during normal machine operation, tests were carried out using a 500 kN Instron testing machine. A direct load was then applied in small increments to the pin up to 30 kN, to observe deformation in lateral compression. Small 'flats' on the surface of the pin under load became pronounced as the load was increased beyond 20 kN. Indeed these flats measured approximately 0.3 mm (mean dimension taken due to slight tapering (tapering < 0.05 mm across the length of the pin), for the 20 kN loading condition.

Tests were also carried out using the two 12.7 mm diameter pins in position between the rigid location blocks and the DHUP on the shoe of the machine for the worst operating condition. It was noted that the flats imparted on the pin surface were tapered - at the base of the pin the dimension of the flat measured 0.4 mm and this tapered off to zero towards the centre of the pin length. The reason being due to the loading and positioning of the DHUP and grip segment on the pins which are secured by the rigid location blocks. In other words, the pressure across each pin varied from the base to the central height and was greater in magnitude at the base of the pin. The variation in pressure across the pin length is ascribed to slight misalignment between the DHUP and the pins situated in position on the rigid location blocks. Modification to the rigid location blocks provided correct alignment. The direct thrust on the two pins was estimated at approximately 15 kN (7.5 kN on each pin).

3.5.2.8 INGRESS OF FEED BETWEEN THE D.H.U.P. AND THE ABUTMENT TOOL

It was anticipated that the ingress of feed metal into the clearance zone available between the DHUP and the abutment

tool holder will influence the force measured by the abutment loadcell. The clearance available using 12.7 mm diameter pins at ambient temperature was 0.5 mm. In order to study the effect of feed metal entering this clearance and the subsequent increase in direct force, it was necessary to vary the pin sizes used in order to prevent contact between the abutment tool and DHUP. This feature would correspondingly reduce or increase the size of the clearance made available for the ingress of feed to take place. It is then possible to determine the additional loading on the abutment tool which is described under Section 7.

4 INSTRUMENTATION AND CALIBRATION

The measuring equipment installed on the Conform machine were connected directly to signal conditioning amplifiers and voltage energisers (namely module cards) and subsequently to a 12-bit Analogue to Digital converter - all conveniently arranged within a single box (or baseboard unit), see fig 4.0 and 4.1 for details. The baseboard unit was then interfaced with a 640 kbyte RAM IBM PC AT which has a colour graphics display. An FX 800 series printer has been selected to print out the processed test results from the computer on completion of each test. The computer and peripheral equipment are all housed within a multi-shelf security stand, which contains four power points and quick release (DB 25) connectors for attachment of flying leadwires from the sensing devices.

The instrumentation system was selected for the following reasons;

- a) to reduce the time involved in manual processing of experimental test data.
- b) to increase the overall time beyond that initially allocated to experimentation.
- c) to gain a 'hands-on' insight into the use of computer-aided manufacture.

The data acquisition system chosen to meet the particular demands of this research programme is a Keithley series 500 work station: This system incorporates the baseboard and a range of modules within a single unit. The details of this system will be described in full later.

4.1 ASSEMBLING THE HARDWARE

The main computer casing was removed in order to gain access to the interface card slot locations. The interface cards for

- a. VDU
- b. computer
- c. keyboard
- d. printer
- e. work station
- f. AMM1
- g. AIM3
- h. AIM6



Figure 4.0 Computer stand layout

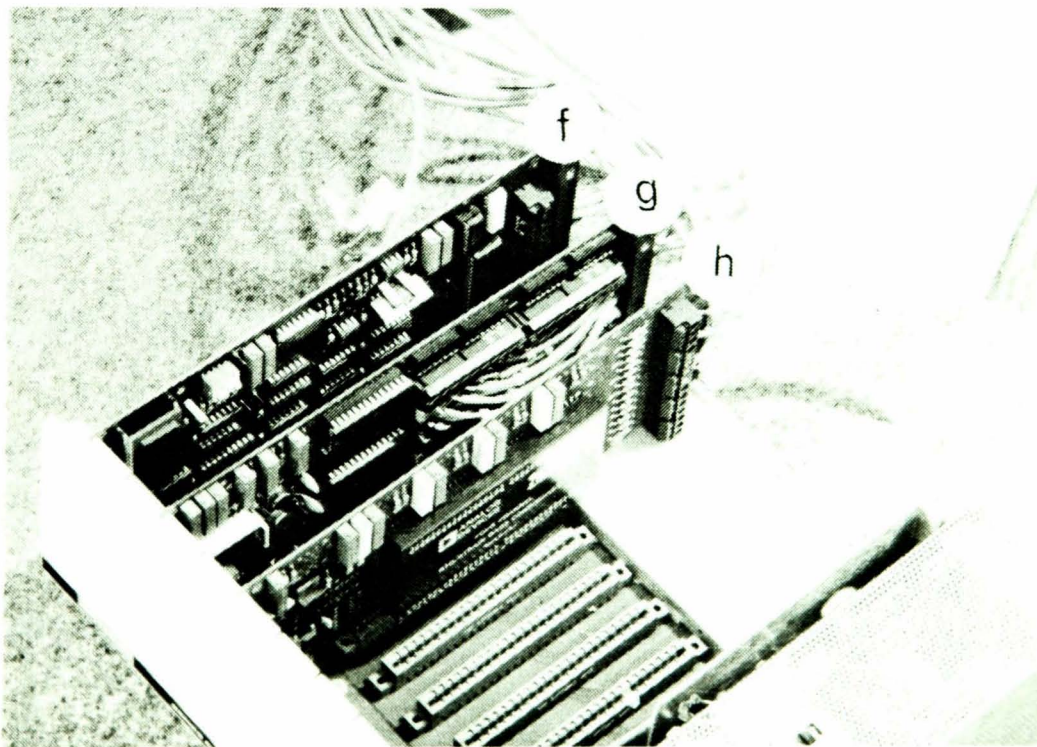


Figure 4.1 The computer and peripheral equipment.

the computer VDU terminal, Keithley baseboard, printer and enhanced colour graphics adapter were inserted into slot 1,2,7 and 8 of the computer respectively. A memory expansion card was also installed in slot 4 of the computer, which boosted the RAM size from 512k to 640k. The computer and peripheral devices were then assembled.

The next step was to switch on the new hardware and insert the diagnostics floppy disk which accompanied the new equipment in disk drive A. The user-friendly software then prompted the user to select the computer configuration (computer software set-up) menu. This is necessary since the hardware must be given details of interfacing modules, RAM size, keyboard type (UK) and others. The next step was to install the floppy disk-operating-system (DOS) disk in drive A and, transfer the information to the route directory of the hard (or fixed) disk. The DOS version supplied with the new hardware equipment is version 3.30. Also, the information from the software soft500 version 5.1 was installed to the subdirectory on the hard disk together with the BASIC and the BASICA programming commands. The advantages of transferring floppy disk information to a hard disk are that start-up time of the computer is shorter, and it is convenient for the user, since the computer operator is not required to insert disks each time the computer is re-booted.

4.2 THE TEST PROGRAMME (SOFTWARE)

The sampling rate selected was 800 ms. The software simply informs the computer to retrieve data from the background after successive 800 ms steps based on the the computer interrupting its internal clock mechanism.

The number of samples collected each time the computer retrieves data from the background at the specified sample rate is selected by varying the depth parameter in the analogue-input command (CALL ANIN).

It was anticipated that the duration of each test was not expected to exceed 50 min. Therefore, the amount of data retrieved and stored in the BASICA arrays should not exceed the maximum storage space allocated by the array software dimensioning. The array dimensioning was designed to reserve the maximum amount of data equivalent to that retrieved in a 40 min logging period, given the memory size of the hardware. However, this can be adjusted according to the specific demands of each test. Provision was made for a total of 11 variables to be logged in the software, these include 6 thermocouple probes, two loadcells, two pressure transducers (torque) and a tachometer.

A flow chart given in figure 4.2 illustrates the format of the software test programme

A menu was designed to appear at given time intervals during each test depending on the selection of the timer at (c). The menu is deemed necessary to allow the user the option of a real-time graphical display (e) or the data logging mode (g). The graphical display provides the user with a visual 'high resolution' real-time colour plot on a continuous time base. The units are in degrees for temperature measurement and volts corresponding to the force, torque and speed measurements. The option of the data logging mode provides a visual display of the real-time data at 5 second intervals in SI units while simultaneously logging the information into the computer memory. The colour display was used to highlight the data from all the variables displayed in the data logging mode on computer screen, see fig 4.3 for details.

The data logging mode was used for the most part of each test, bearing in mind that if the memory limit reserved in the basic array dimensions for each variable is exceeded, the test programme would terminate data logging and display a menu and indicating completion of test. The real-time graph display, however, can retrieve and display the data for an indefinite period but will not store any of this information in the computer memory.

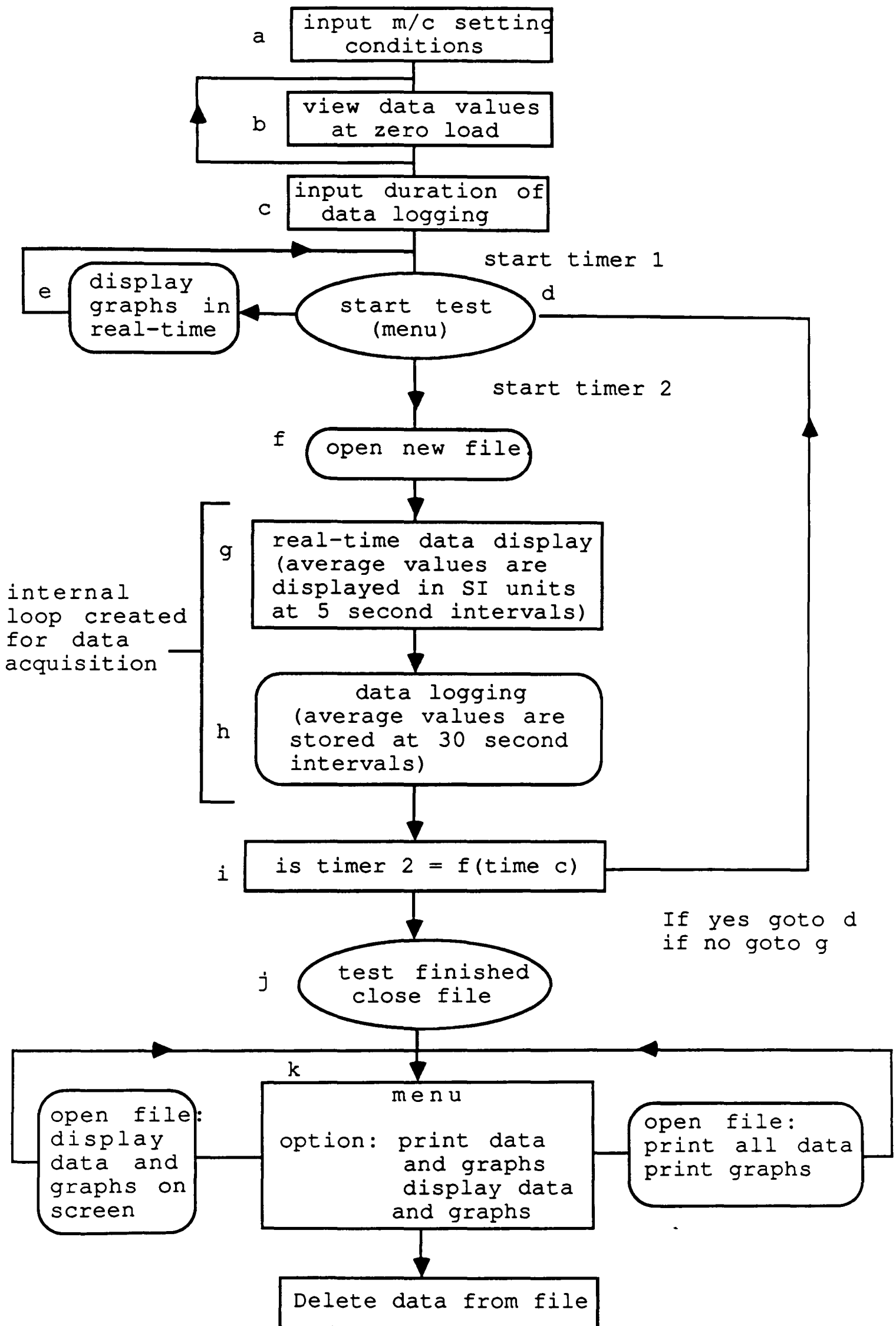


Figure 4.2 The flow chart illustrates the real-time data acquisition software

Real time data display

time	temp1	temp2	temp3	temp4	temp5	temp6	wheelspeed	Torque	load A	load D
S	oC	oC	oC	oC	oC	oC	rev/min	kNm	kN	kN
256	226	220	198	51	155	159	5.1	22	45	64

data logging count: 256
when count = 2600 then
data logging is complete

Figure 4.3 Computer screen in real-time data display and data logging procedure

In order to increase the time period for the data logging mode, an internal command loop was created in which the data was collected and successively added for up to 30 samples corresponding to each variable, and then divided by the number of loops for each variable collected. This provides a mean value for each variable corresponding to an incremental time-base of 30 seconds, which is subsequently, stored to memory. Meanwhile, the real-time data is displayed on the computer screen at 5 second time intervals.

It was later found that a limitation with the data logging mode is the speed at which the data can be retrieved from the background of the computer. This is due to the number of commands created in the loop for averaging these data values. Subsequently it was necessary to reduce the speed of real-time data collection to 1 second time intervals, in order to avoid a time-delay through switching. An average of 5 data values were then taken for the real-time data display which implied a 5 second time increment on the computer screen between the display of new data. However, a smaller time increment could be selected, but greater than a one second time interval.

The stored data were printed out on a 30 second time-base, on completion of each test in a tabulated and graphical format for all variables, see appendix B1 for details.

A software-driven configuration table is provided in a subdirectory with the various soft500 commands separate to the main test programme, which incidently, is stored in the root directory on the fixed disk. This feature provides a menu in which details of the input terminal numbers for the three modules and the corresponding sensing devices are allocated.

Details of the software test programme are given in appendix B2.

4.3 INSTALLATION OF INSTRUMENTATION AND CONNECTION TO SENSING DEVICES

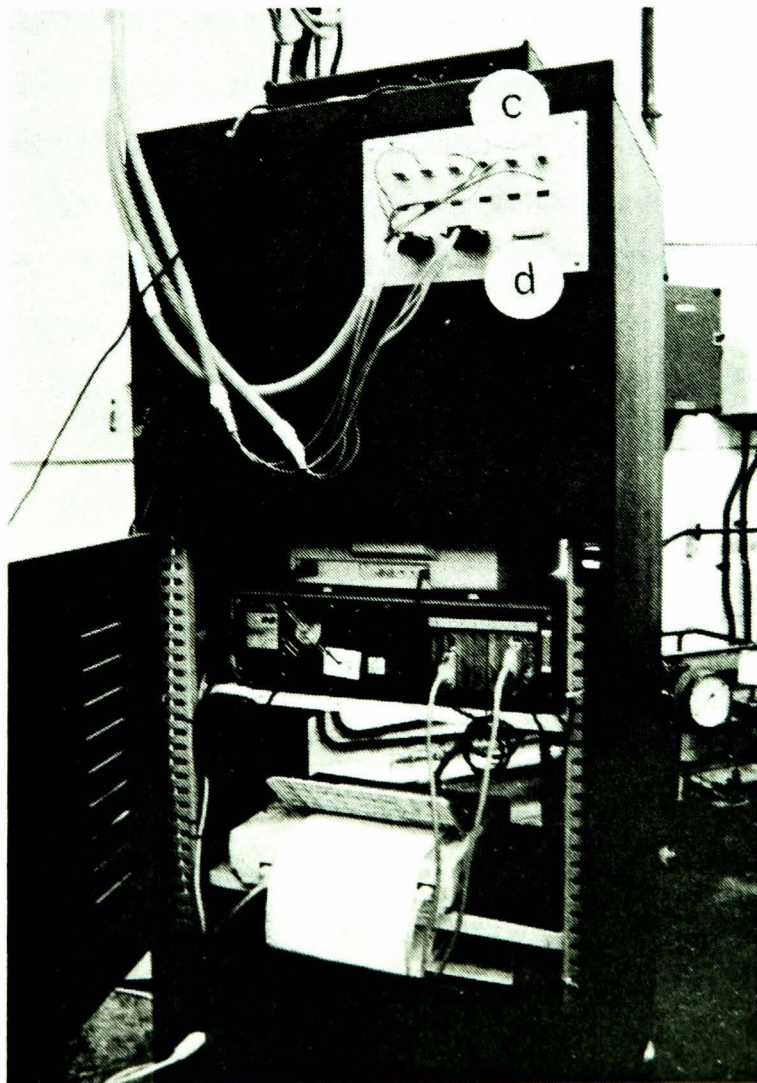
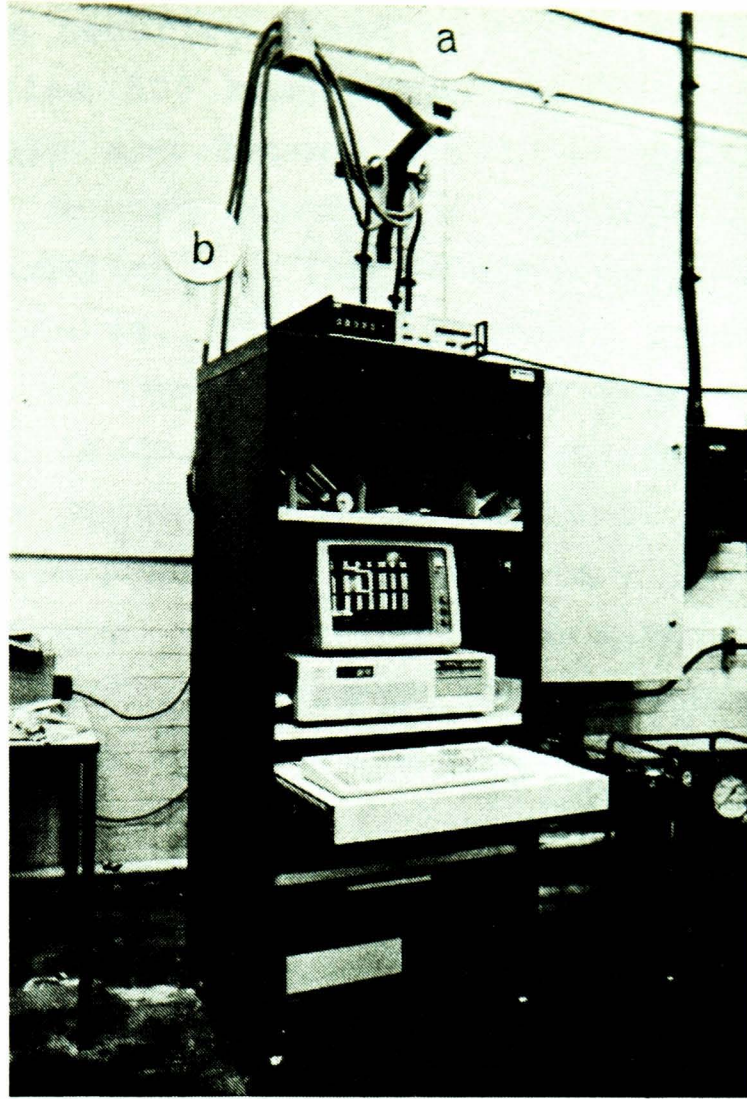
The computer, printer and workstation were assembled into a security stand comprising a system, see fig. 4.4. The necessary circuitry to connect the instrumentation to various sensing devices on the Conform machine were installed as follows.

Initially plans were drawn up and the necessary electrical items were purchased to complete the wiring installation. Various techniques for routing the leadwires from the sensing devices on the Conform machine to the series 500 base board were considered. This is because cross-talk and interference from mains power supply cables to the Conform machine and control panel must be avoided.

The necessary brackets, electrical connection panel and conduit were assembled, see fig 4.4. Screened leadwires were routed through the conduit, and the appropriate quick release (snap) connectors were fastened to the ends of the multi-core leadwires.

Three module cards were supplied with the series 500 base board to allow connection of the sensing devices to the base board via the module cards. The modules are a 12 bit analogue-to-digital (A/D) converter (AMM1) or the master module card, a thermocouple card (AIM3) and a strain gauge card (AIM6) located in slots 1, 3 and 5 respectively of the base board unit, see fig. 4.1.

With regard to the AMM1 module, three 2-core leadwires were tapped off the output terminals of three Lee-Integer signal converter and power units, which connect the two pressure transducers and the tachometer sensing devices, in turn, to the AMM1 module card. The power supply, signal conditioning, amplification and zero setting adjustments are provided by the Lee-integer units. The 2-core leadwires connect these devices via a standard DB25 connection on the connector panel on the



- a. swivel bracket
- b. flexible conduit
- c. thermocouple connections
- d. DB25 connections

Figure 4.4. The workstation

rear of the security stand to the A/D converter (AMM1) module in the series 500 baseboard, see fig 4.4 for details. The power supply and return from the sensing devices are all routed by 4-core leadwires through conduit between the terminal locations on the sensing devices and the Lee-integer units. However, flexible conduit piping was provided for connection of the output signals from the Lee-Integer units via 2-core leadwires to the security stand. The flexible conduit was secured to a large swivel bracket protruding from the wall with ample length given to allow free movement of the security stand. A wiring loom within the security stand provides connection between the connection panel on the back of the security stand and the AMM1 module.

The signal conditioning amplifier for the tachometer was modified to enable interfacing with AMM1 module. This is because the voltage output from the Lee-Integer unit was measured at 44 V when connected to the AMM1 module. A change in the impedance was required in order to reduce the voltage to an acceptable level for A/D conversion, i.e. below 10 V. The modification was accomplished by placing a dummy load in the circuit prior to the raw signal from the tachometer reaching the Lee-Integer unit. In addition, the output signal from the signal conditioning amplifier to the chart recorder was a negative output voltage. The design of the chart recorder enabled the instrument to accept a +ve or -ve signal from the Lee-Integer unit. Consequently, further modification of the tachometer circuit was achieved by introducing a common earth connection, as detailed in fig. 4.5.

Six Type 'K' thermocouple probes were connected to the AIM3 module card via 2-core leadwires to a terminal block situated on the shoe of the Conform machine. The six screened 2-core leadwires were routed to the terminal block through a 20 mm diameter bore conduit section, which is separate from the transducers and tachometer conduit. The screened leadwires are suitably labelled. At the other end, these leadwires were fed through flexible conduit to the back of the security stand. Two-pin thermocouple connectors are fastened to one

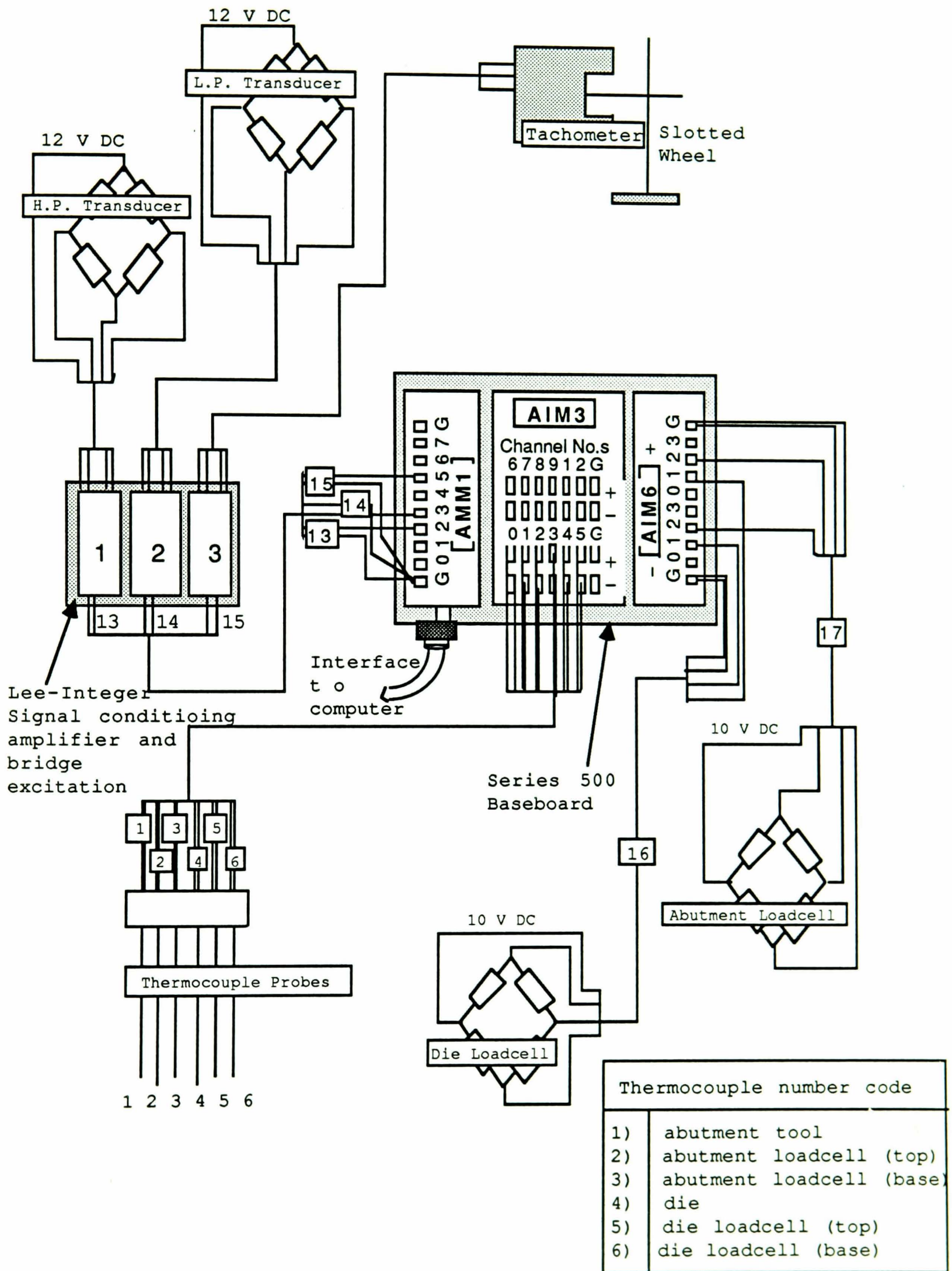


Figure 4.5 Main circuit diagram

end of each of the six 2-core leadwires. The wiring loom within the security stand then feeds the screened thermocouple leadwires to the AIM3 module in slot 3 of the base board unit. These signals are then directed to the AMM1 in slot 1 of the work station for analogue-to-digital conversion, see fig. 4.6.

The AIM3 module required modification in order to allow the use of thermocouple probes with this module. This is because differential connections, in contrast to single-ended, had been chosen to connect the thermocouple leadwires to the input terminals (or channels) 0 to 5, of the AIM3 module. Consequently, the accuracy of the signals processed in this way is increased.

Finally, two column loadcells were connected to the AIM6 module via two screened 4-core leadwires. The two screened 4-core leadwires are selected to provide the power supply (voltage excitation) to each loadcell and relay the output signal back to the AIM6 module in slot 5 of the base board unit. The AIM6 module provides the necessary voltage excitation to each sensor and, in addition, signal conditioning and amplification of the output signals before the signals are directed to the A/D converter. The bridge excitation is set to a 10 V stabilised DC supply and the gain is set to 50, see fig 4.5 for details.

Cable ties were appropriately positioned in order to prevent tangling of interface cables within the security stand. These cable ties were also used to keep mains power cables well away from interface cables and screened leadwires.

4.4 CALIBRATION OF MEASURING EQUIPMENT

In order to calibrate the sensing devices, it was necessary to use the work station and computer in conjunction with the calibration of the sensing devices. Therefore it was deemed necessary to incorporate a real-time digital display of the data from all the variables on the computer for calibration

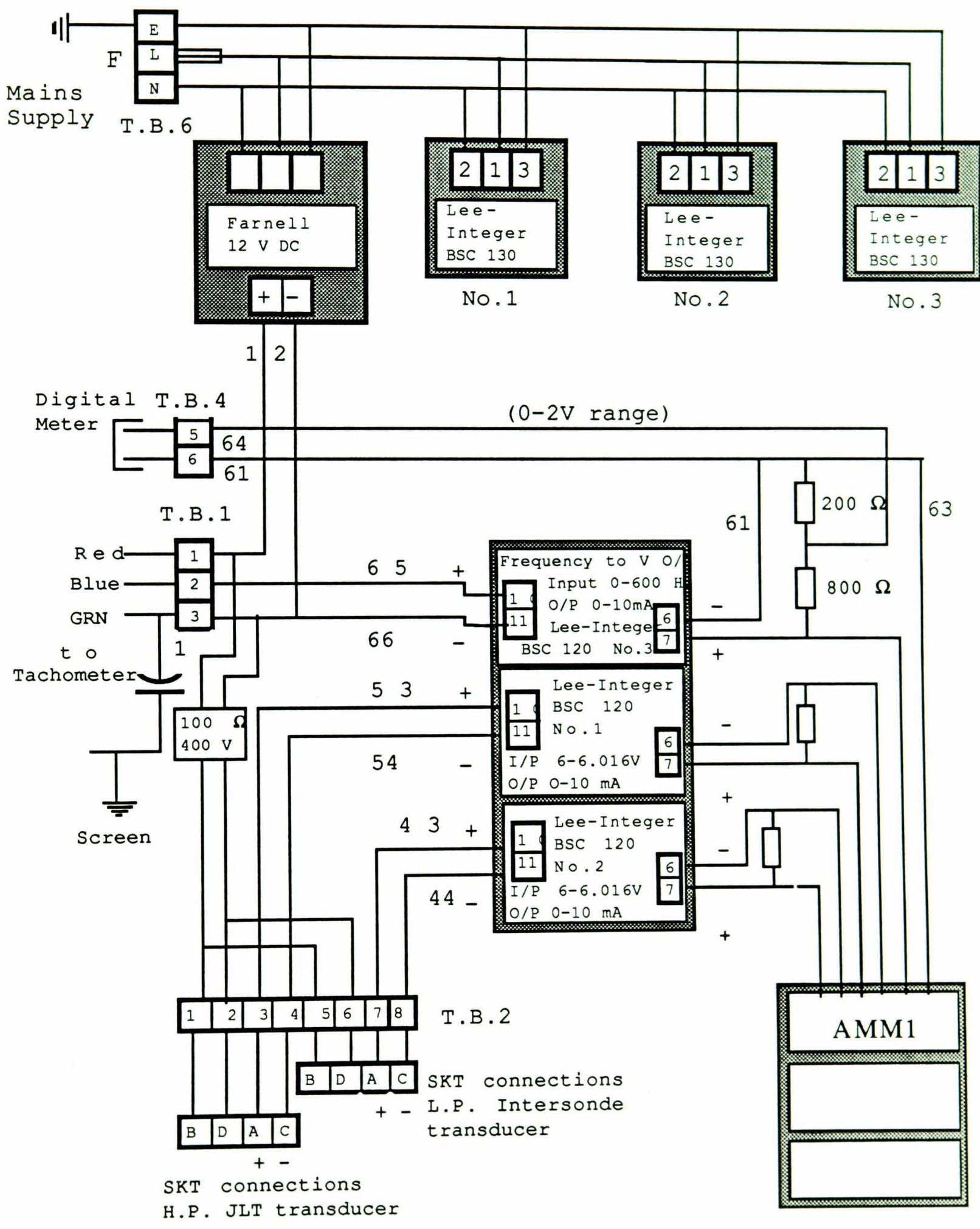


Figure 4.6 Circuit details

purposes. The data were displayed in units of volts and degrees celcius corresponding to the load and thermocouple devices respectively, see fig 4.7. This feature is incorporated at the start of the main test programme since it also provides a means of observing the data for the zero load condition. The small zero offset which normally accompanies the data at zero load was stored in the main test programme to be retrieved for the calibration conversion during the real-time data logging sequence. The thermocouple measurements at ambient temperature required a 30 min period for full stabilisation.

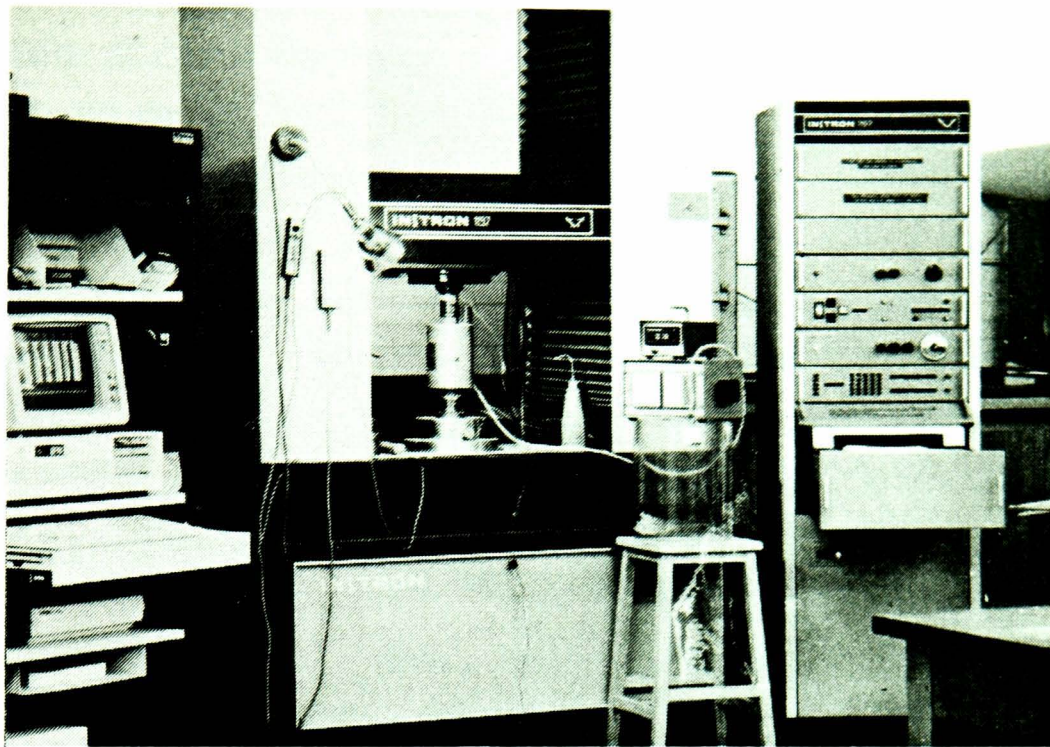
4.4.1 DIE LOADCELL

The calibration of the EN 24 and tungsten carbide loadcell required the repositioning of the computer stand adjacent to a 500 kN Instron testing machine, see fig 4.8 for details. The EN 24 die loadcell was initially set up in the testing machine with the appropriate connections to the AIM6 module card made via 4-core leadwire. The bridge excitation was set to 10 V DC on the software-driven configuration table and the gain set to 50. The output was in the range 5 - 80 mV corresponding to the load range 0 - 100 kN. Two potentiometer controls are provided for each of the four channels on the AIM6 module card to allow manual adjustment of the zero offset and gain. However, it was found that insufficient adjustment on the manual potentiometer control prevented the offset returning a zero value, consequently, the minimum offset remained at 5 mV for the zero load condition at 18 °C.

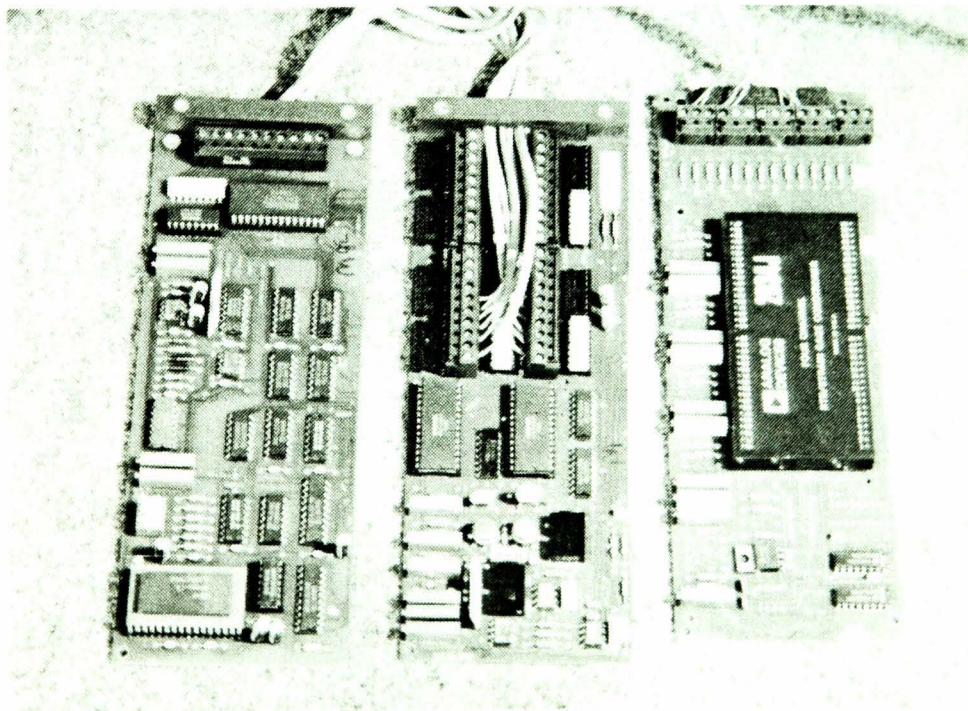
The calibration of the loadcell was initially carried out at ambient temperature. The loadcell was rotated at approximately 45° increments for the full 360° in order to observe the repeatability over the load range. The deviation in load was measured at + 0.8 mV corresponding to the full scale condition (repeatability accuracy = $0.6/(70-5) = + 0.9 \% \text{ F.S.}$). Lubrication was then placed on the upper and lower faces of the loadcell and the test repeated. A fractional



Figure 4.7. Showing how the data recorded from the measuring devices is displayed on the computer in real time, for calibration.



a



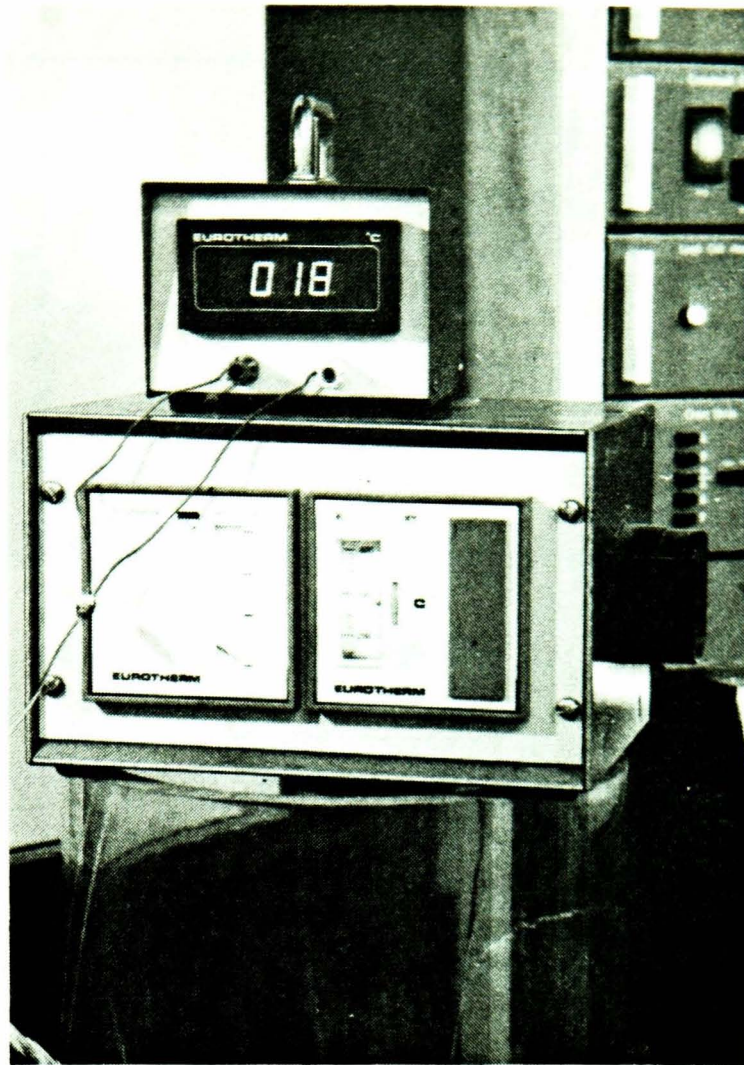
b

Figure 4.8. Showing a) the set-up for calibration of the high temperature loadcells
b) the connection of the sensing devices to the module cards in the work station.

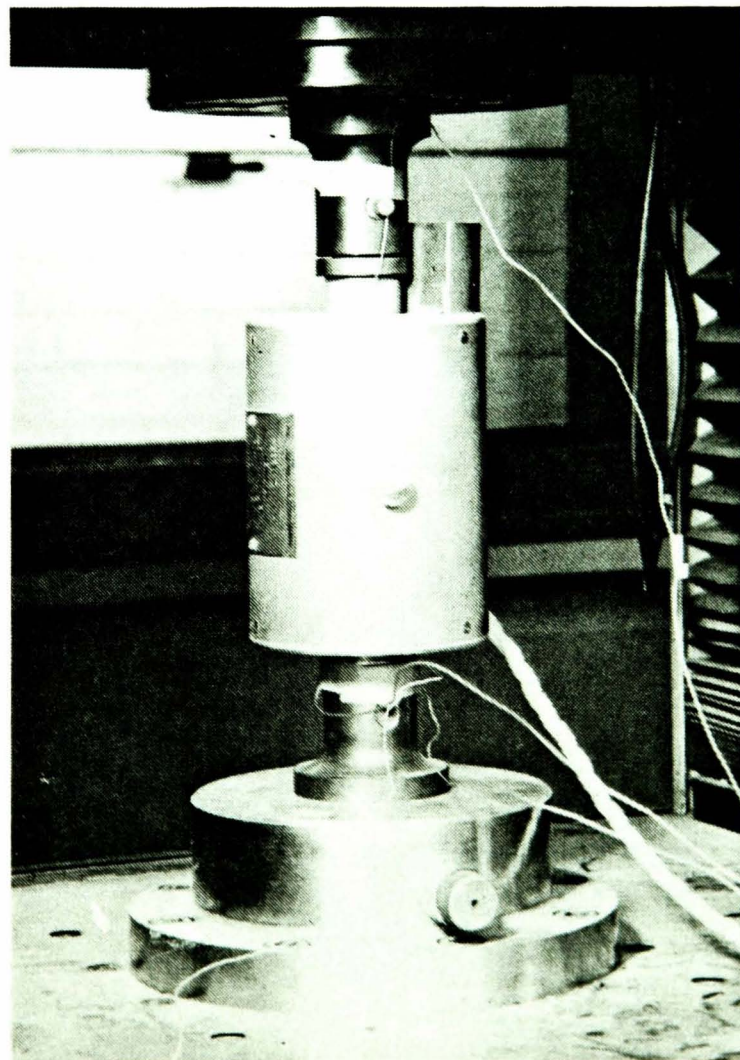
increase in repeatability was noted.

In order to calibrate the loadcell over the temperature range expected during machine operation, a small induction coil was used to provide the heat source. The leadwires from a k-type thermocouple probe were connected to a power supply, with the probe attached to the inside face of the coil. Two further probes were then attached to the upper and lower peripheral flange faces of the die loadcell with the leadwires attached to a multi-channel digital display, see fig 4.9. The upper compression pin was lowered into the coil which is at ambient temperature. The initial calibration was carried out at ambient temperature 18 °C. The temperature of the coil was increased to 50 °C and maintained at that temperature for approximately 60 min under the zero load condition. The calibration procedure was then repeated for the up scale and down scale condition. The temperature difference between the thermocouple probes located on the loadcell is of the order 2 °C. This temperature difference increased with increasing coil temperature to 4 °C for the maximum temperature 256 °C. Finally, the temperature of the coil was reduced to the ambient condition and the calibration procedure repeated.

It is observed from the graphs in figs 4.10a and 4.10b, that the variation in the zero drift and gradient indicated by the calibration relationships over the temperature range is small, of the order 2 % and 1 % respectively. This implies that the loadcell is fairly stable over the temperature range concerned. The temperature of the die loadcell during machine operation is greater than 200 °C for the range of reduction and speed. Therefore it was desirable to select the mean calibration relationship for temperatures in excess of 200 °C. The limitation of each test being the maximum temperature of the die loadcell which is 260 °C. The limiting factor is, in turn, the maximum temperature of the fine gauge 4-core Teflon leadwire attached to the bridge circuit of the loadcell being 260 °C. For this reason, the leadwire was attached to the bridge circuit near the base of the loadcell where the temperature differential across the upper and lower faces of



a



b

Figure 4.9. Showing a) the temperature controller b) the induction coil in which heat is transferred to the loadcell under close control.

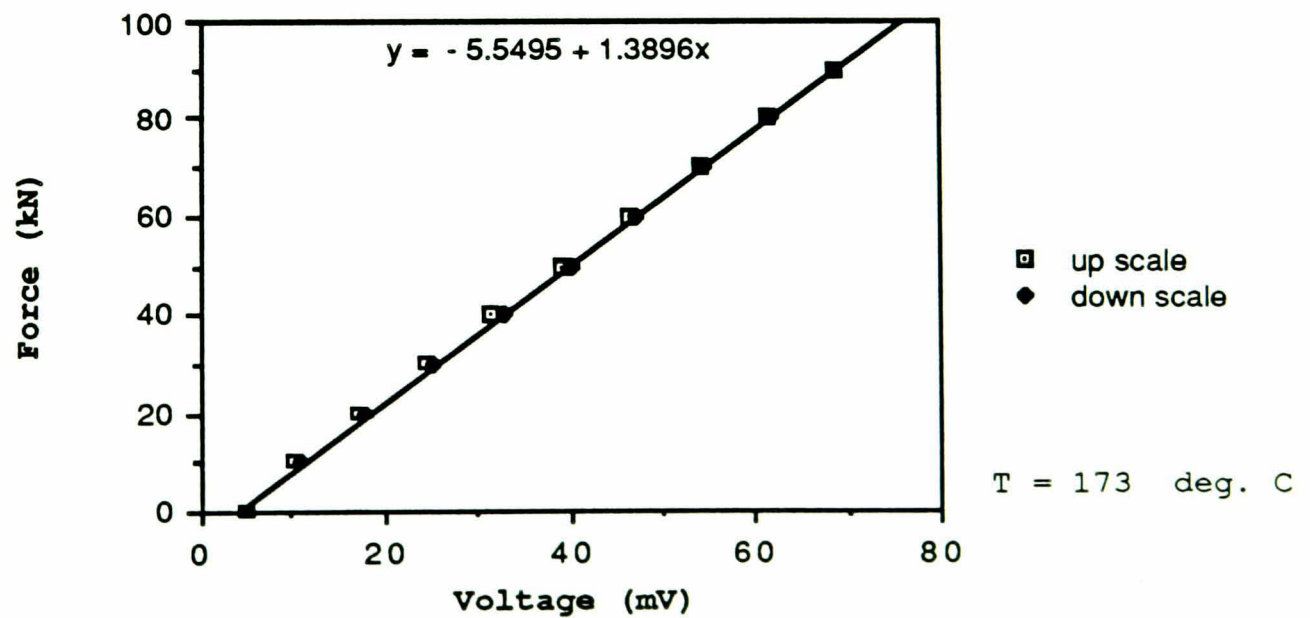
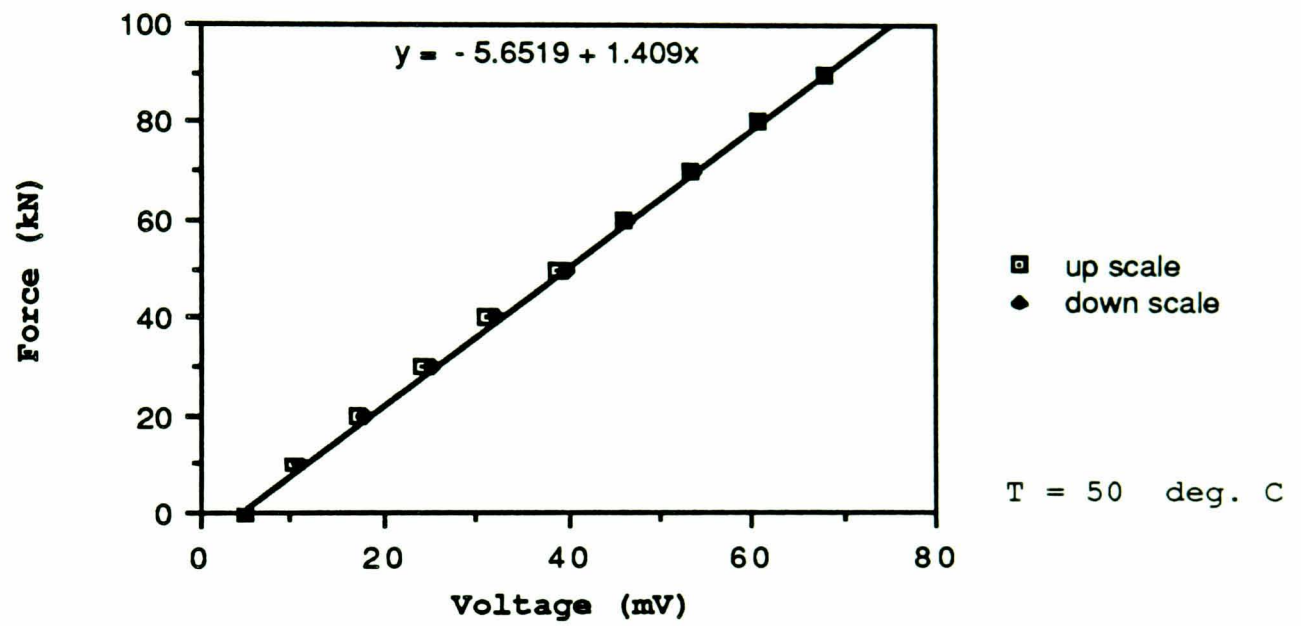
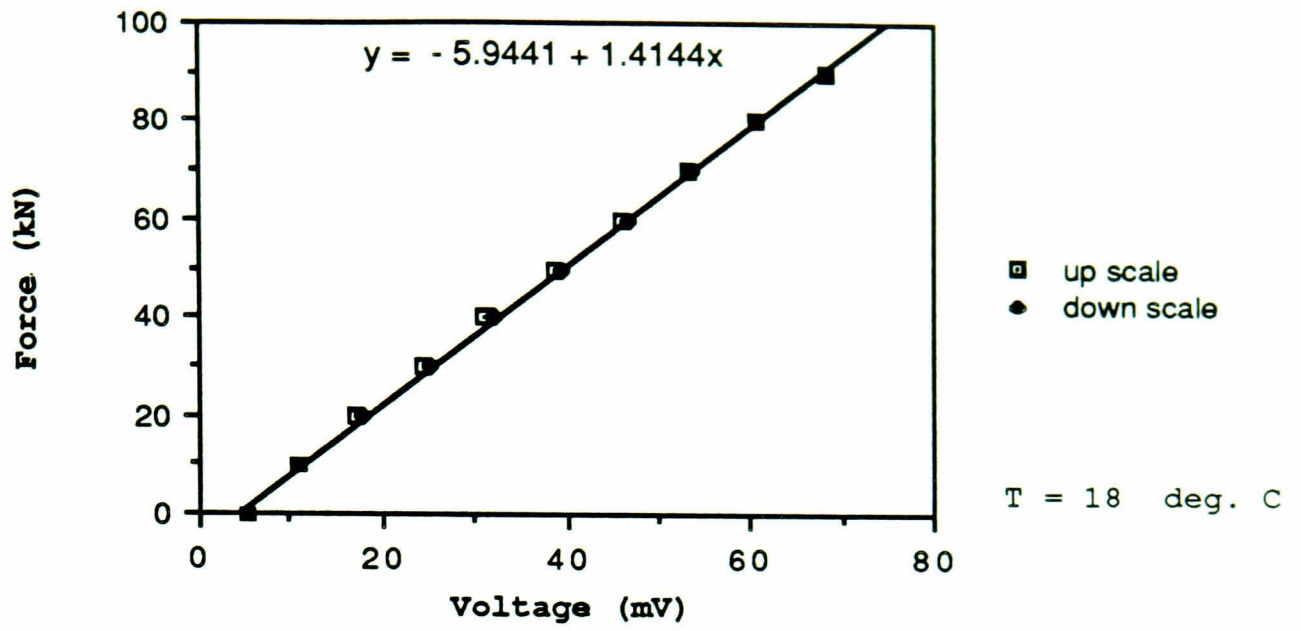


Figure 4.10a The graphs illustrate the relationship between die force and voltage output for varying operating temperatures 18, 50, 173 °C, for the first calibration of the EN 24 loadcell.

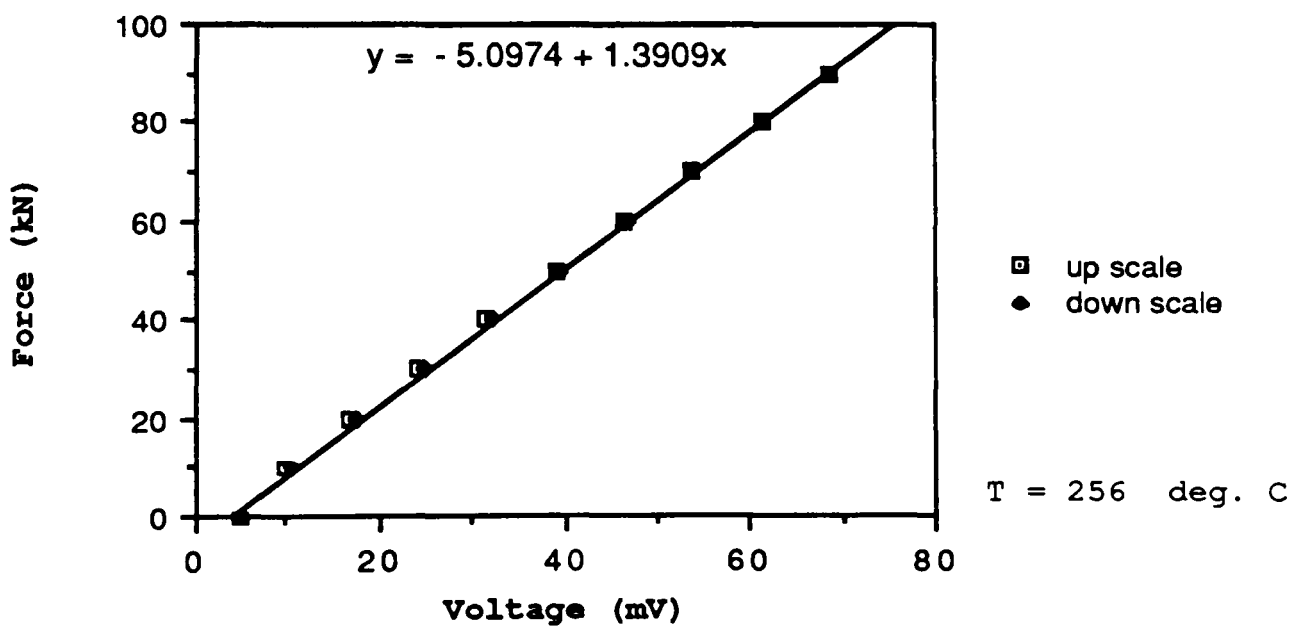
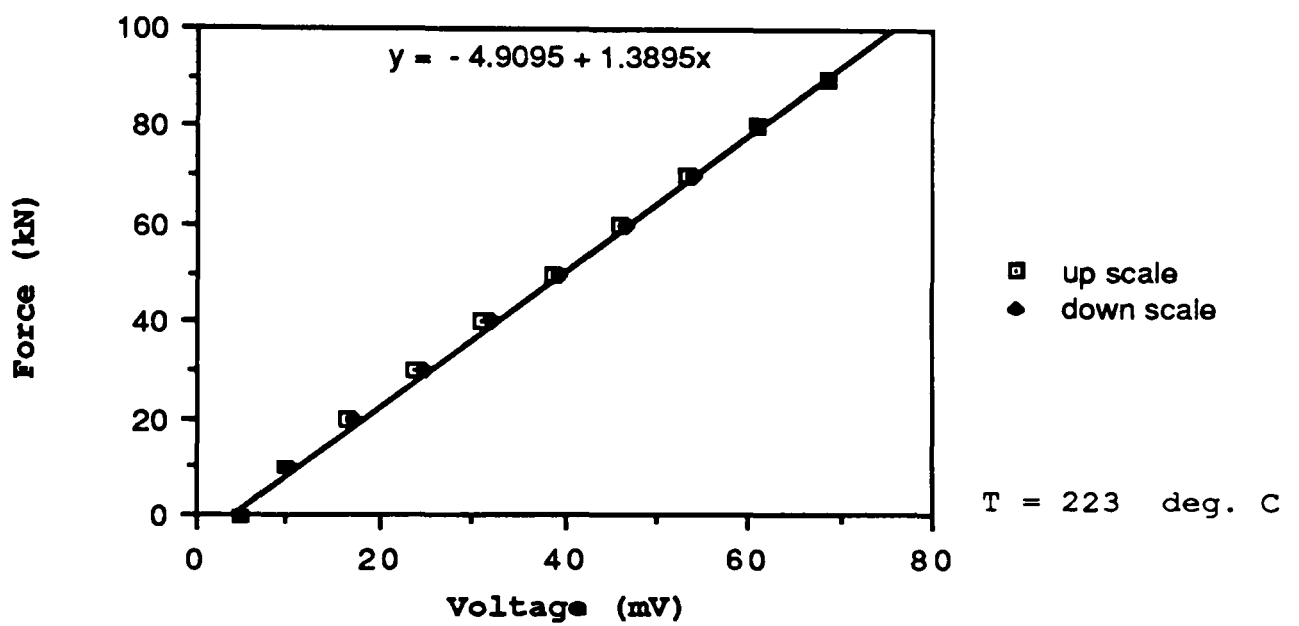
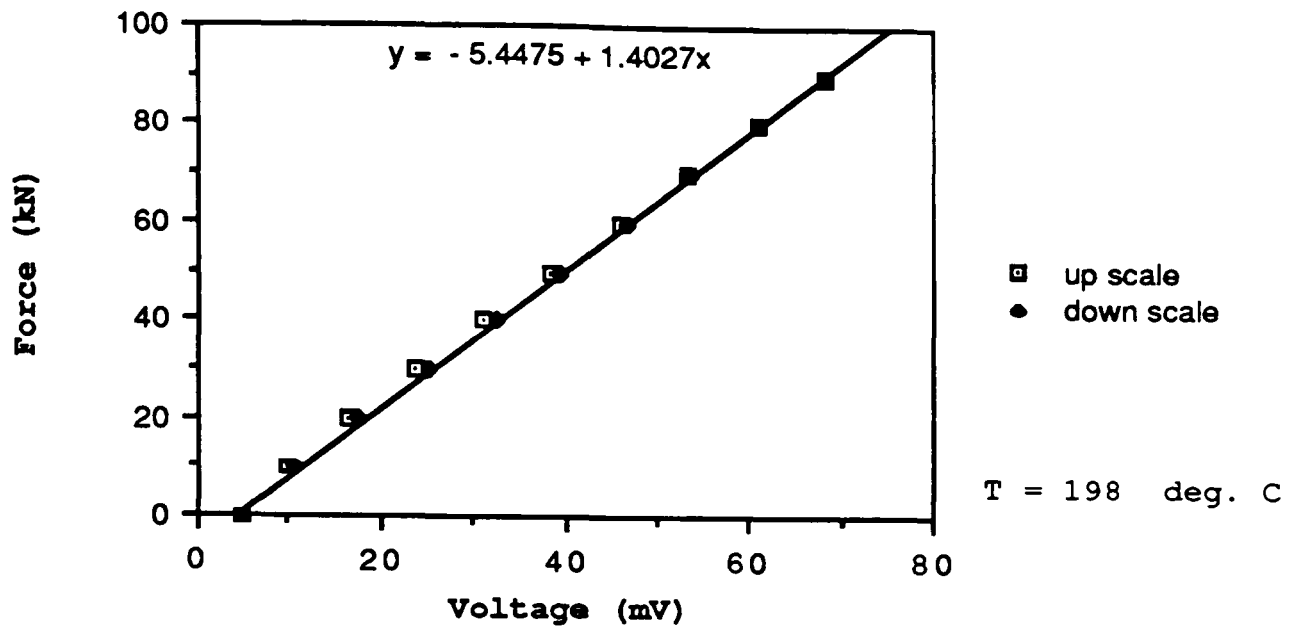


Figure 4.10b The graphs illustrate the relationship between die force and voltage output for varying operating temperatures 198, 223, 256 °C, for the first calibration of the EN 24 loadcell.

the loadcell during machine operation implies a lower temperature away from the heat source. The strain gauges can operate up to a maximum temperature of 315 °C. The protective coating for the strain gauge bridge circuit was selected to operate up to 260 °C. An alternative protective coating compound is available which can operate up to temperatures in excess of 310 °C. However, this could not be successfully applied by the manufacturers due to shrinkage during the curing stage, and subsequent damage to the strain gauges.

A second calibration was carried out at a later stage during the test programme in order to check the reliability of the first calibration relationships at high temperature. The agreement between the two calibration tests was good, with a measured deviation in accuracy of the order 1% full scale. This is considered to be within the limits of acceptable accuracy and repeatability of the loadcell and therefore the first calibration remained in use for test numbers 10e - 39e, see Section 6.

At a latter stage in the test programme, test number 40e, the die-loadcell broke down at the beginning of the test. The cause suggested by the manufacturers was fatigue due to the consistent high temperature operation at a high working strain. The fatigue life was estimated at less than 100 hrs.

A replacement EN 24 loadcell was manufactured, to the same specification as that previously described in order to repeat test no. 40e, and continue testing to no. 55e, see Section 6.

A similar calibration test procedure was applied to the tungsten carbide die loadcell. The loadcell was rotated at 45° increments for the full 360° in order to observe the repeatability, this was measured at ± 0.7 mV at full scale load (repeatability accuracy = $0.7/(60-15) = \pm 1.5$ % F.S.). The calibration curves are illustrated in figs 4.11a, 4.11b and 4.11c for the range of temperature 22 - 259 °C. It is observed from the graphs in these figures, that the variation

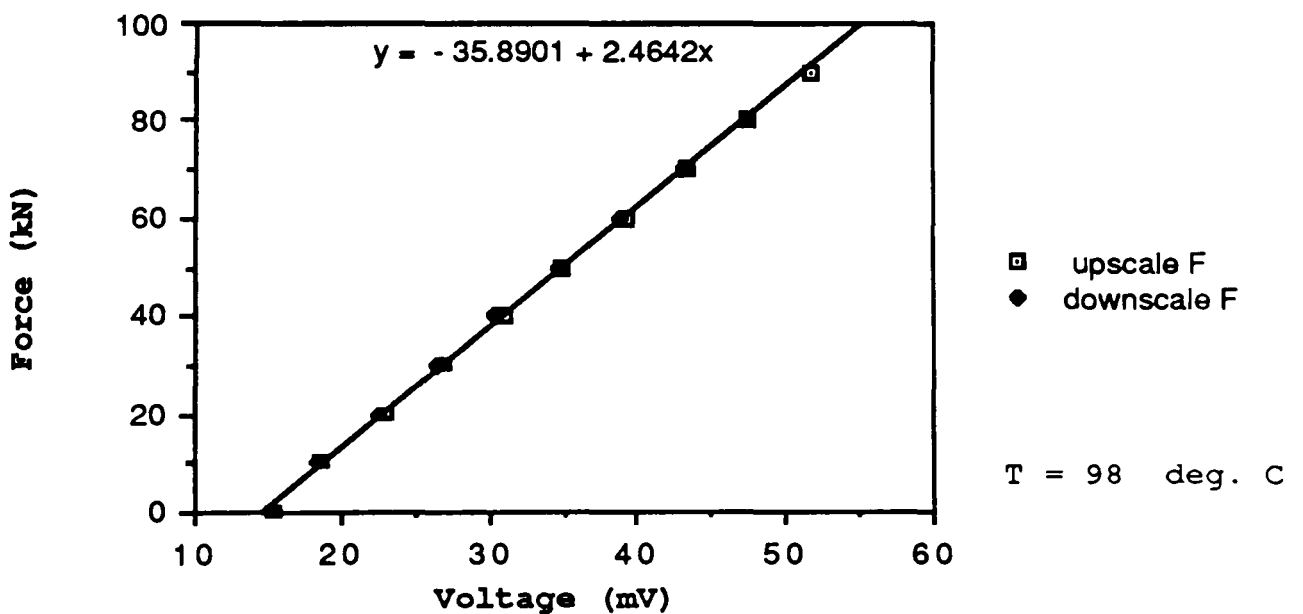
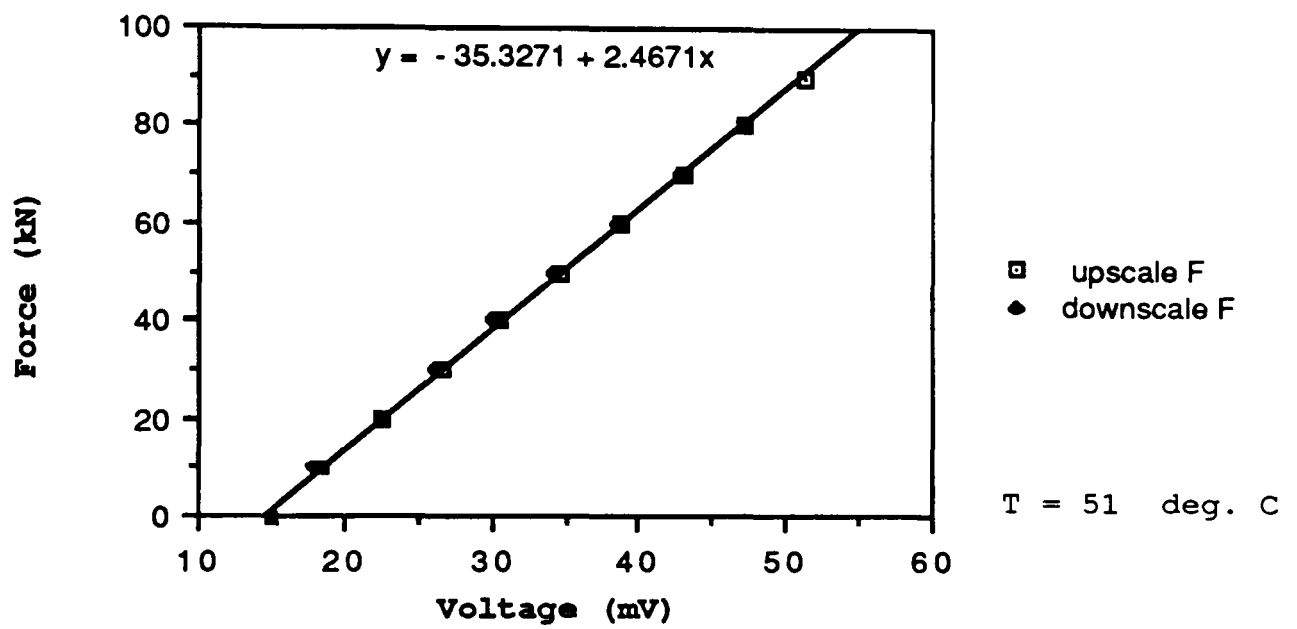
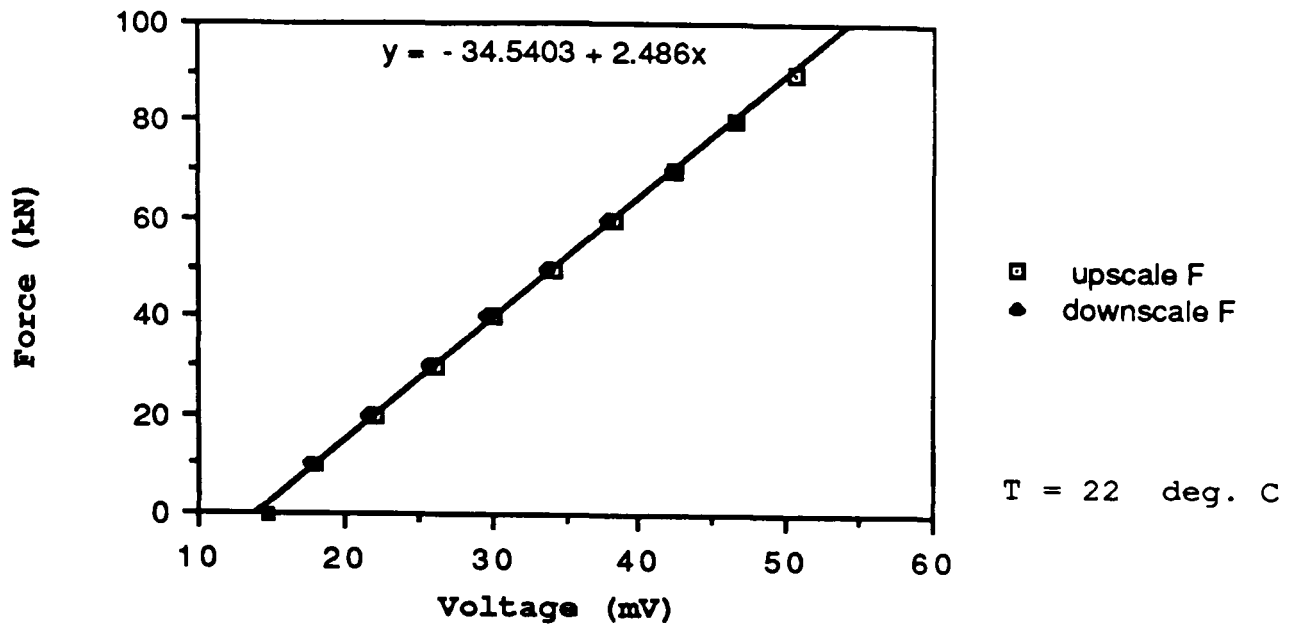


Figure 4.11a The graphs illustrate the relationship between die force and voltage output at varying operating temperatures 22, 51, 98 °C, for the first calibration of the tungsten carbide loacell.

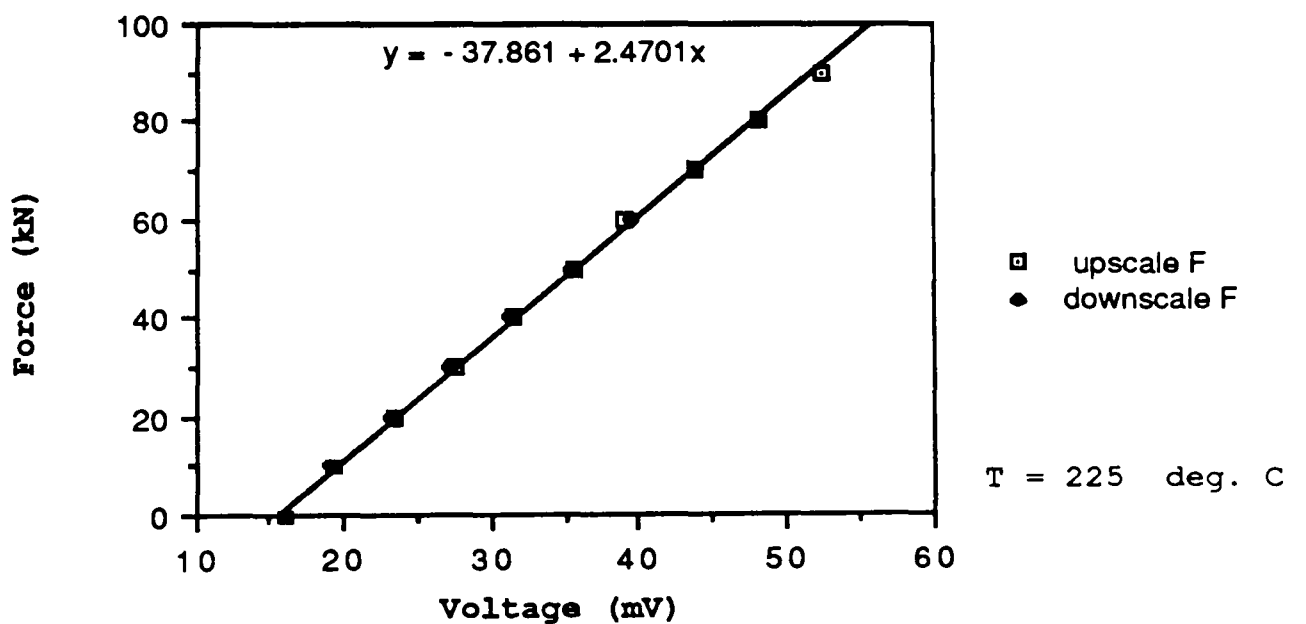
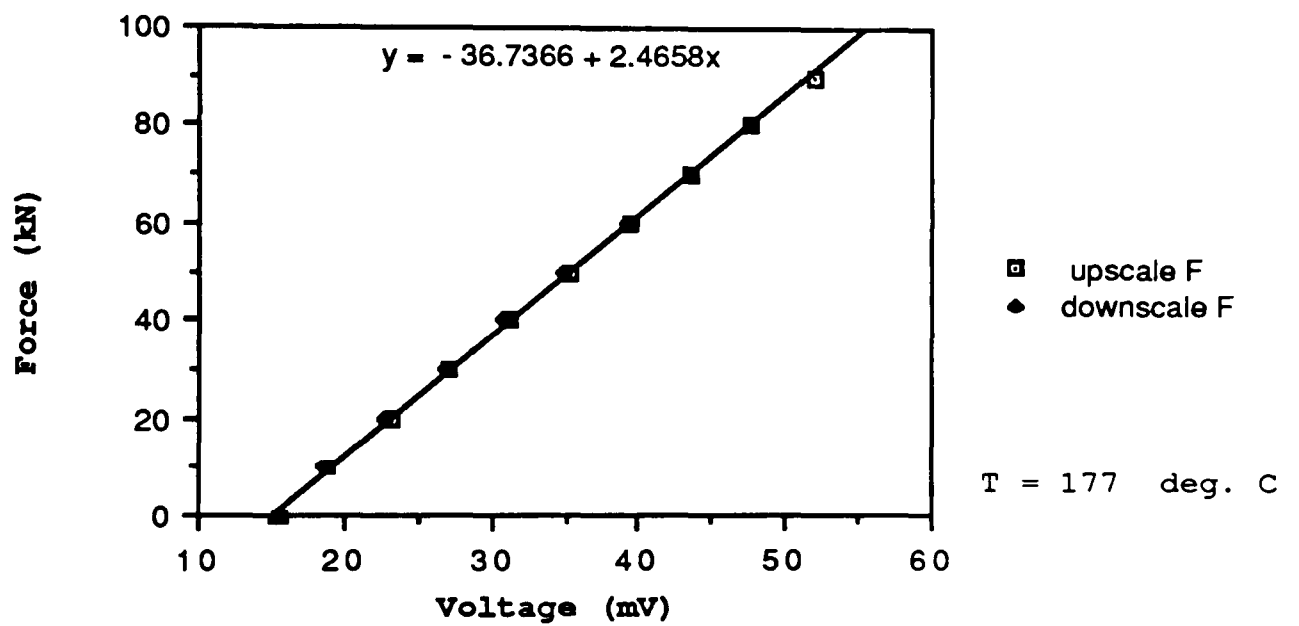
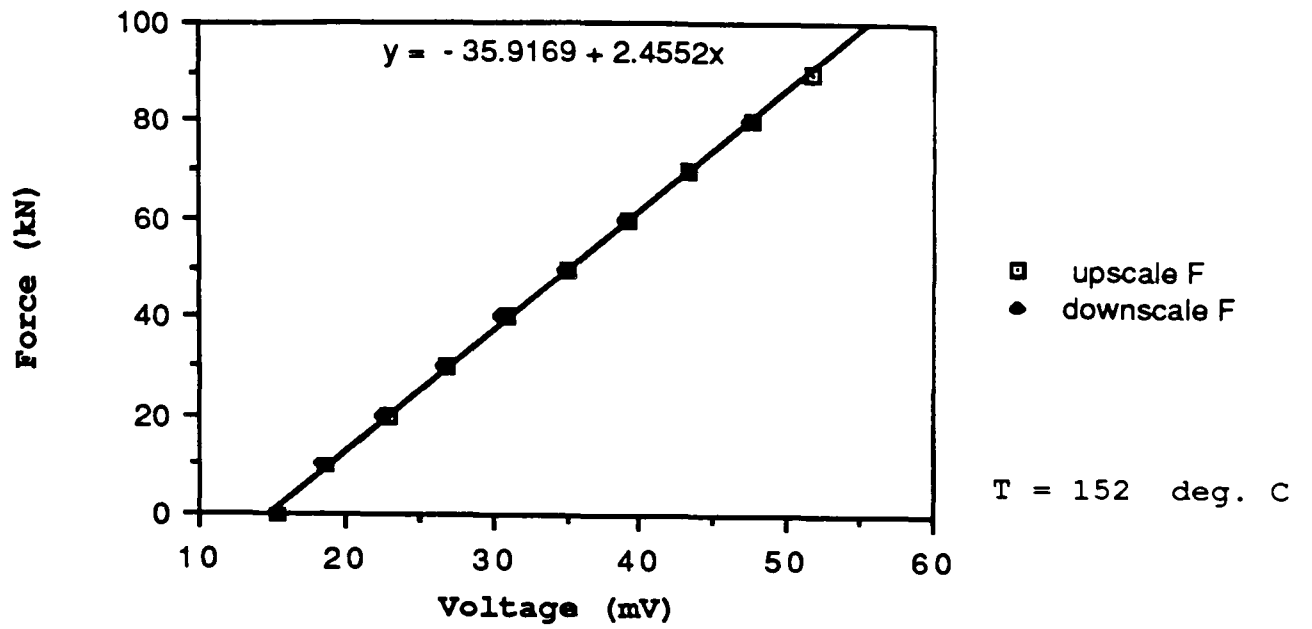


Figure 4.11b The graphs illustrate the relationship between die force and voltage output at varying operating temperatures 152, 177, 225 °C, for the first calibration of the tungsten carbide loacell.

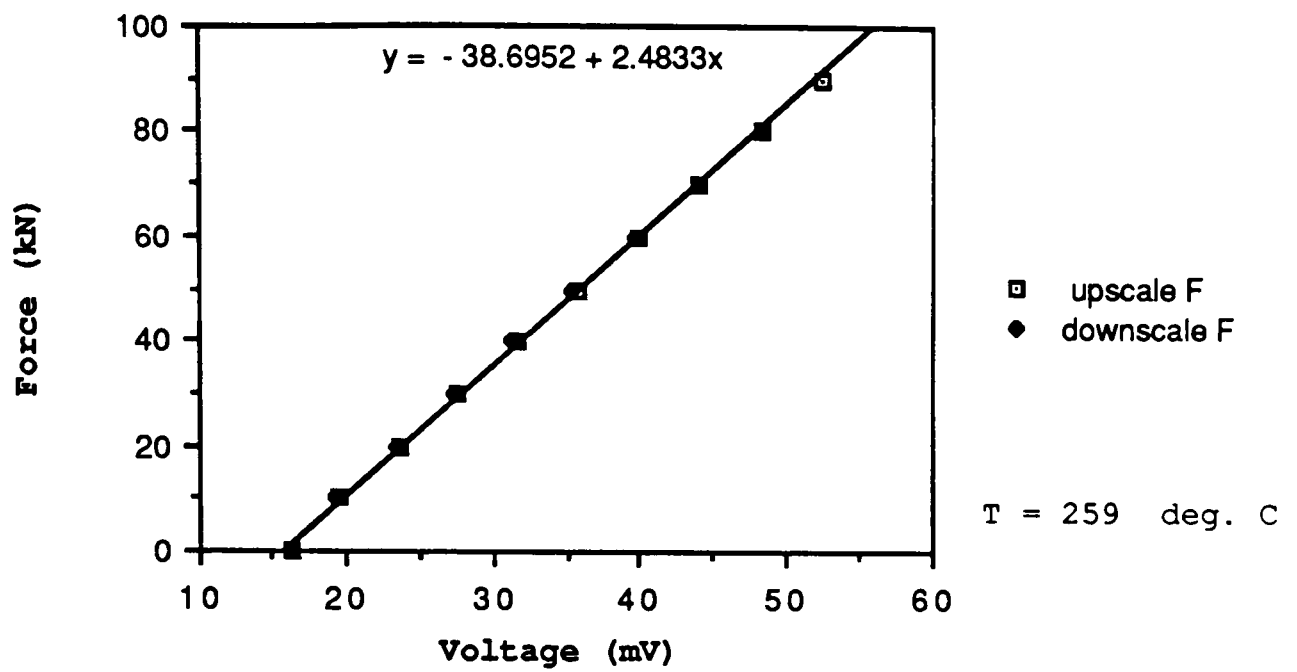


Figure 4.11c The graph illustrates the relationship between die force and voltage output at the operating temperature 259 °C, for the first calibration of the tungsten carbide loacell.

in the zero drift and gradient indicated by the calibration relationships over the temperature range is small of the order 8 % and 1 % respectively. It was desirable to select the mean calibration relationship for temperatures in excess of 200 °C. As with the EN 24 loadcell, the limitation of each test being the maximum temperature of the die loadcell which is 260 °C. Also, the zero value could not be selected below 14 mV for the zero load condition. For the load range 0 - 100 kN, the corresponding voltage output is 15 - 60 mV

4.4.2 ABUTMENT LOADCELL

The calibration of the abutment loadcell was initially carried out at ambient temperature. The loadcell was rotated at approximately 45° increments for the full 360° in order to observe the repeatability over the load range. The deviation in load was measured at ± 0.4 mV corresponding to the full scale condition (repeatability accuracy = $0.4/45 = \pm 0.9\%$ F.S.).

The graphs of the calibration curves for the range of temperatures 19 - 257 °C are illustrated in figs 4.12a and 4.12b. It is observed from the graphs that the variation in the zero drift and gradient indicated by the calibration relationships over the temperature range is small, of the order 5 % and 1 % respectively.

A second and third calibration was carried out at a later stage in the test programme at test numbers 10e and 39e respectively, in order to confirm the reproducibility of initial calibration relationships over the temperature range. The second calibration relationship remained within an acceptable degree of error of the order 1%. However, the third calibration was found to deviate by a greater margin corresponding to the zero drift as illustrated in fig 4.13a and 4.13b. The gradient however, remained in good agreement with the error less than 1%.

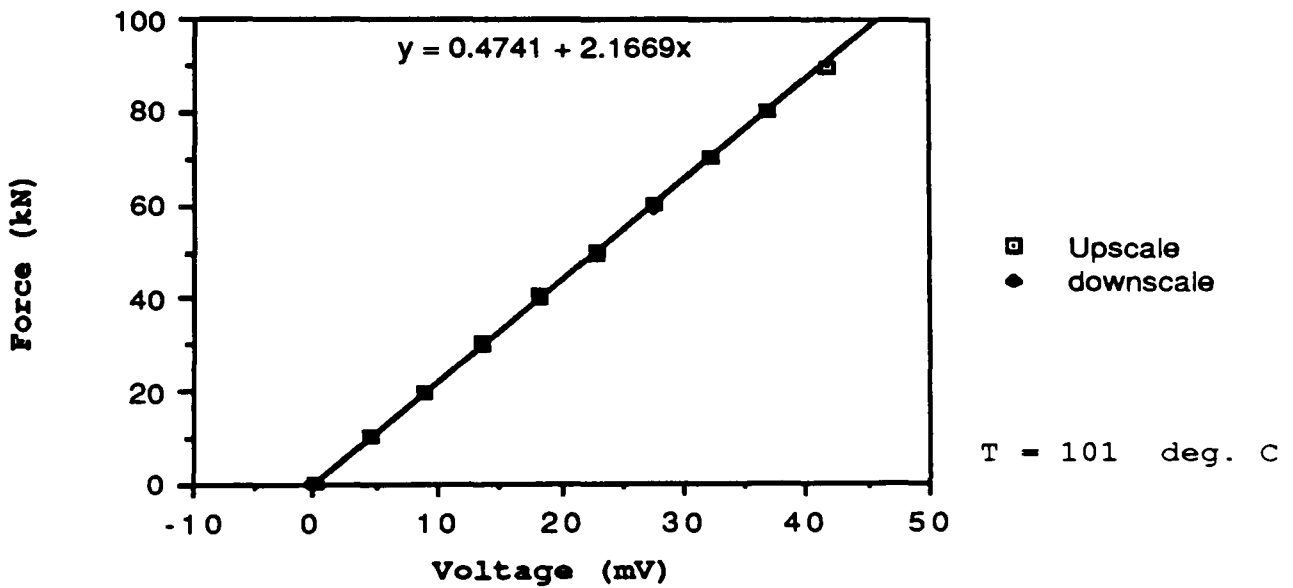
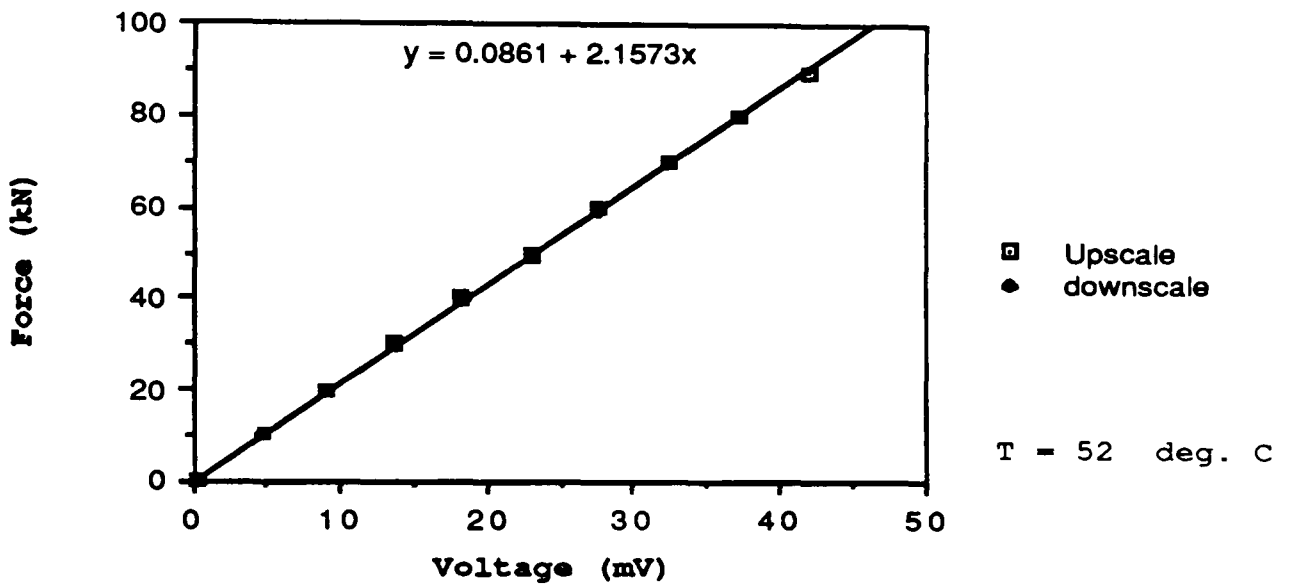
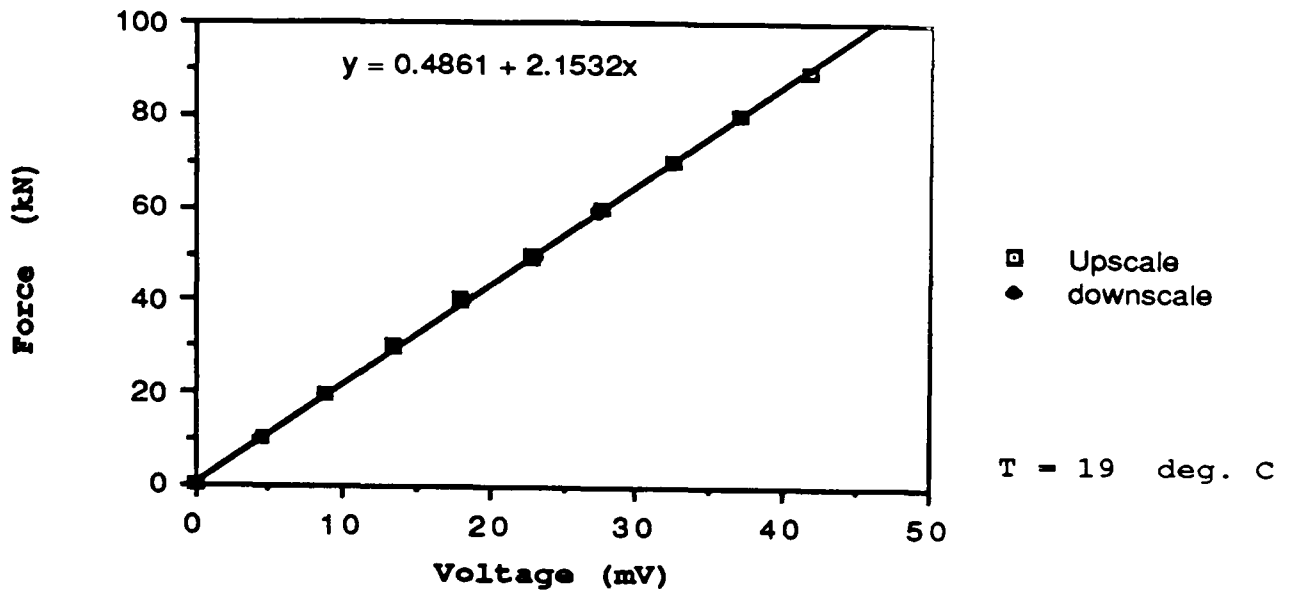


Figure 4.12a The graphs illustrate the relationship between abutment force and voltage output for varying operating temperatures 19, 52, 101 °C, for the first calibration of the tungsten carbide loadcell.

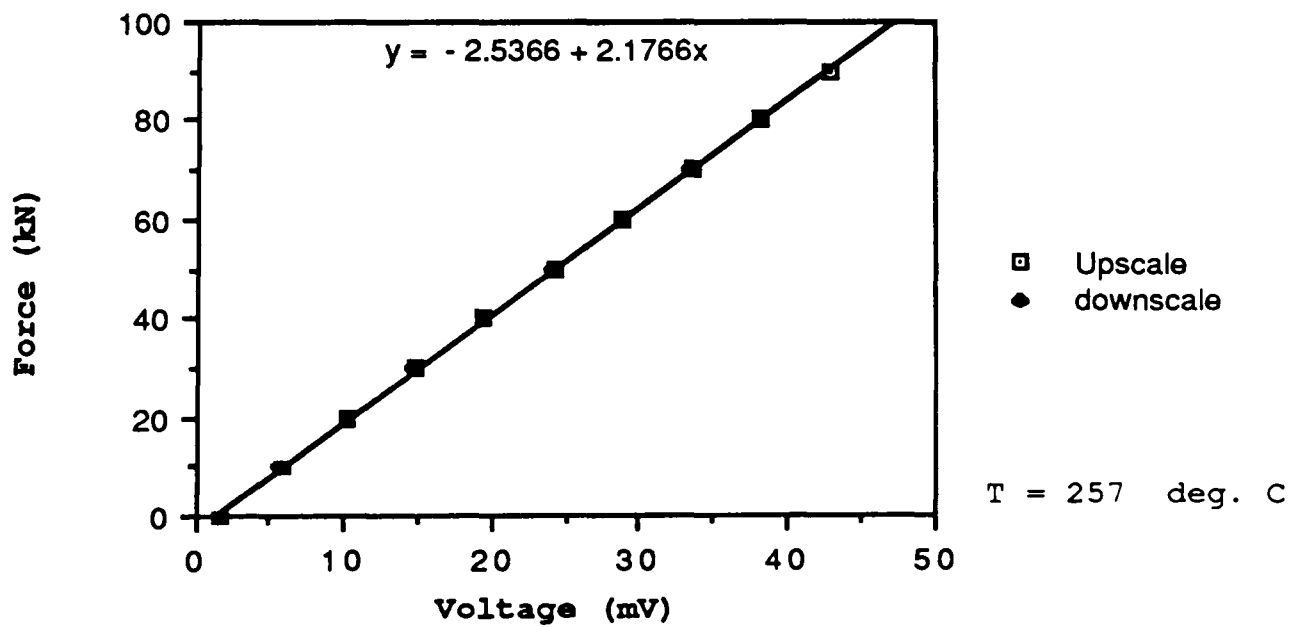
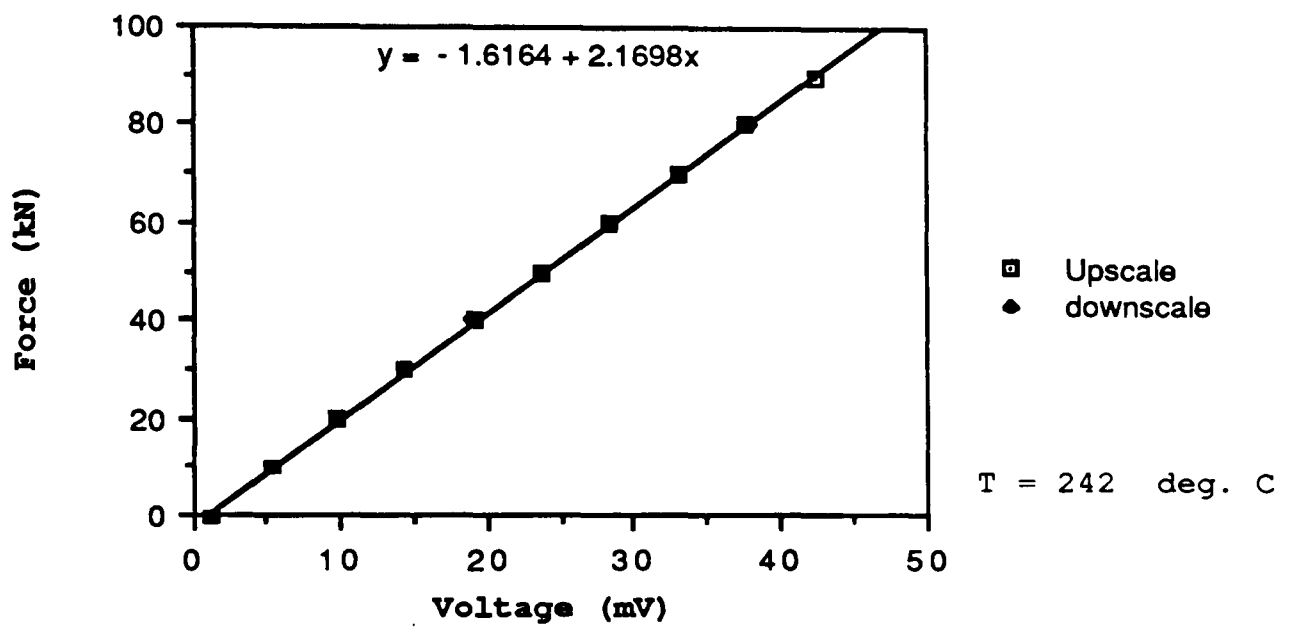
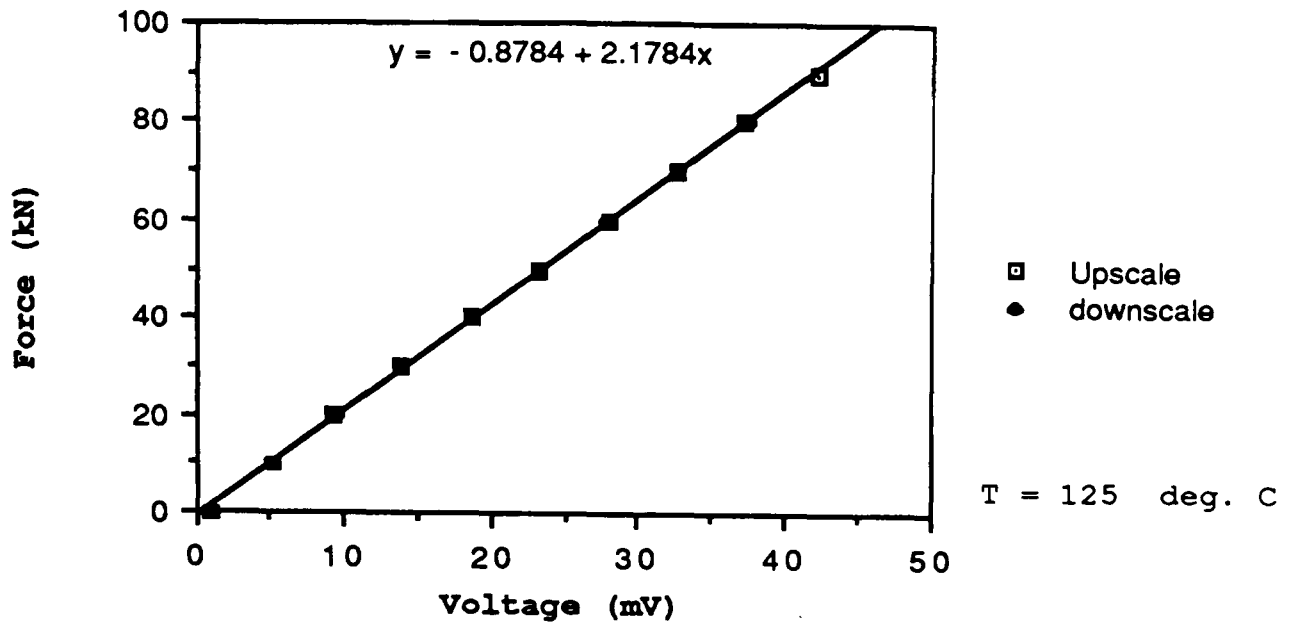


Figure 4.12b The graphs illustrate the relationship between abutment force and voltage output for varying operating temperatures 125, 242, 257 °C, for the first calibration of the tungsten carbide loadcell.

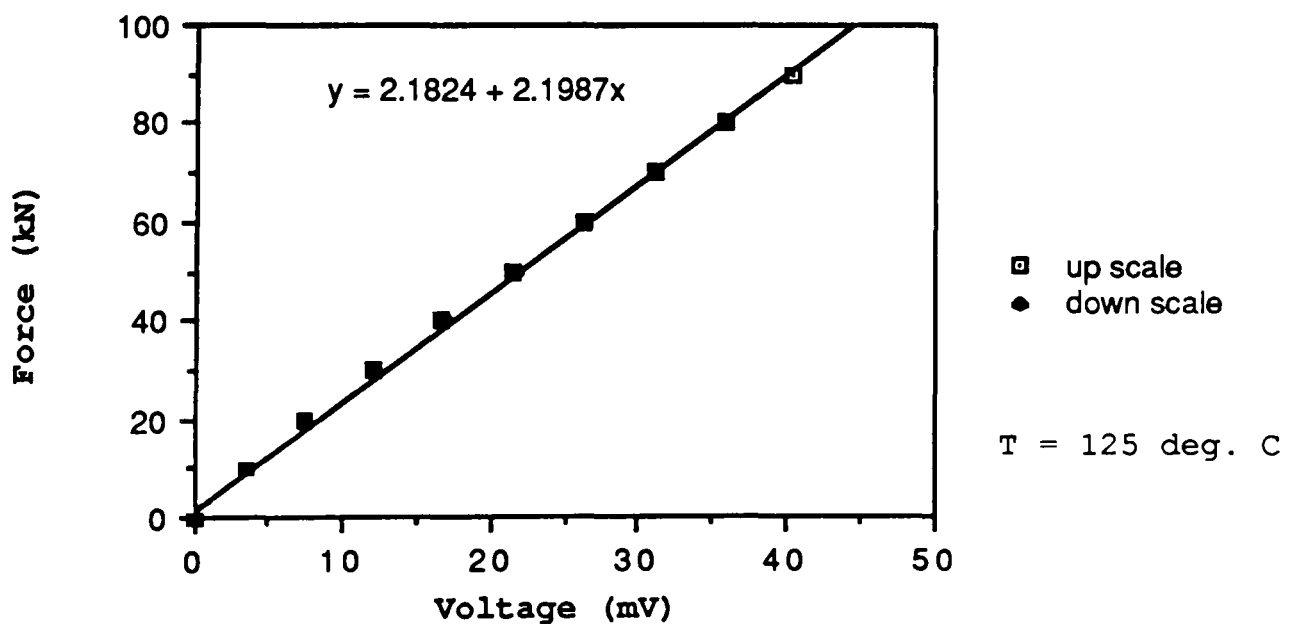
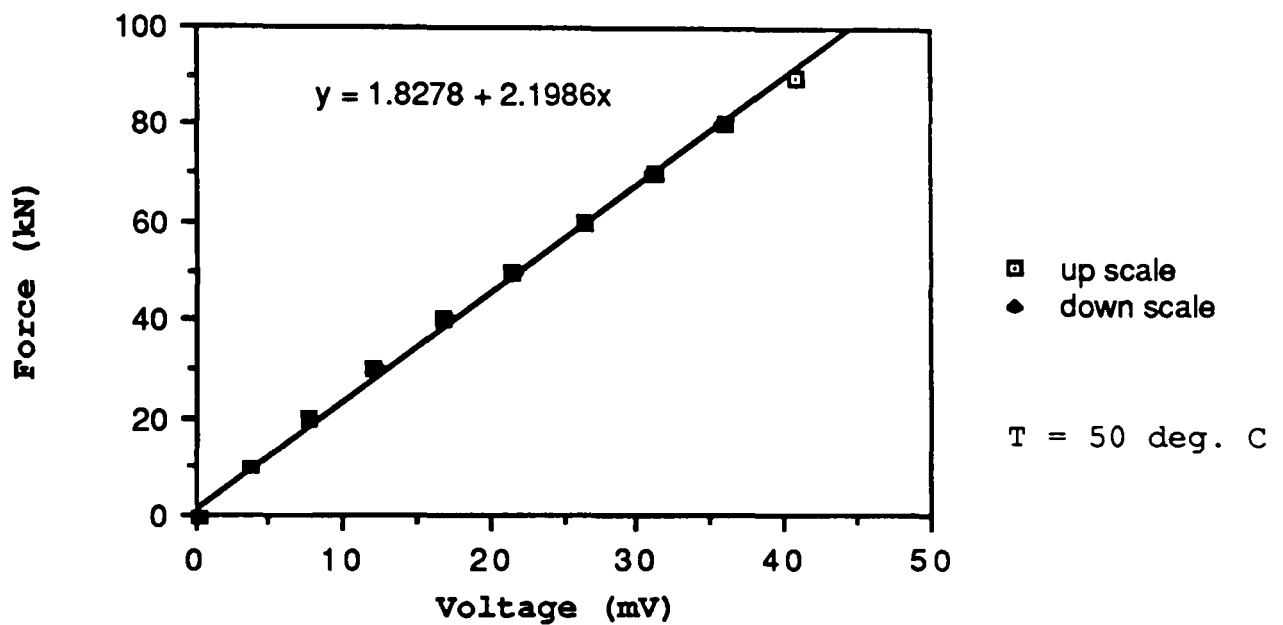
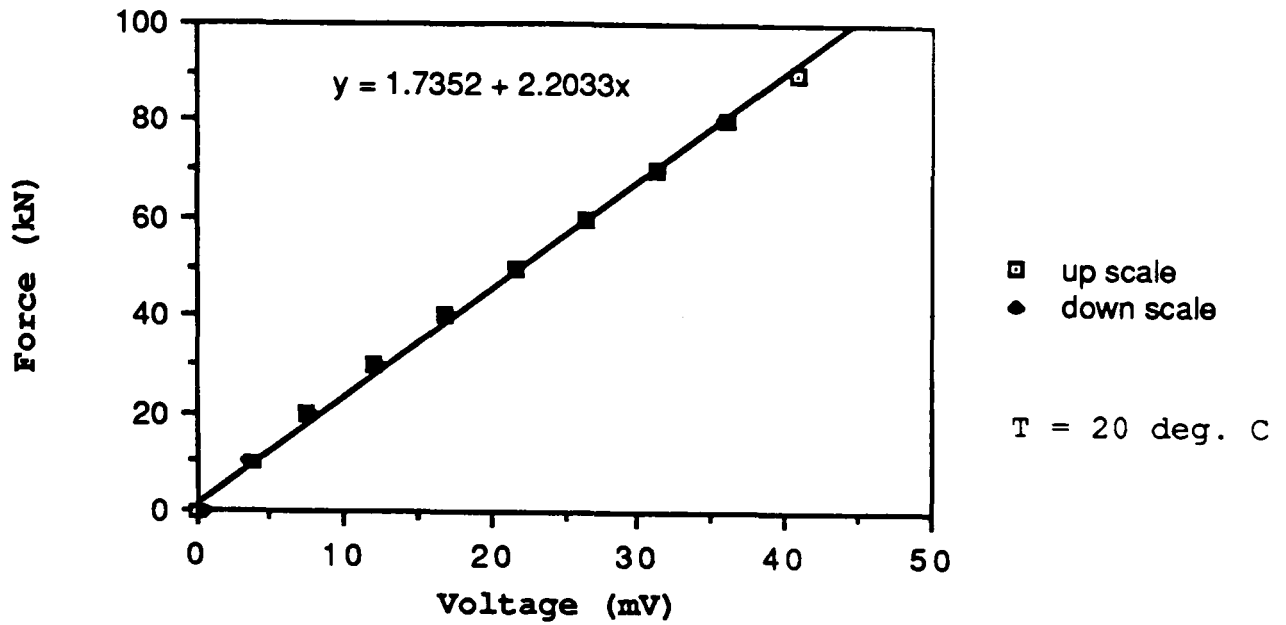


Figure 4.13a The graphs illustrate the relationship between abutment force and voltage output for varying operating temperatures 20, 50, 125 °C, for the third calibration of the tungsten carbide loadcell.

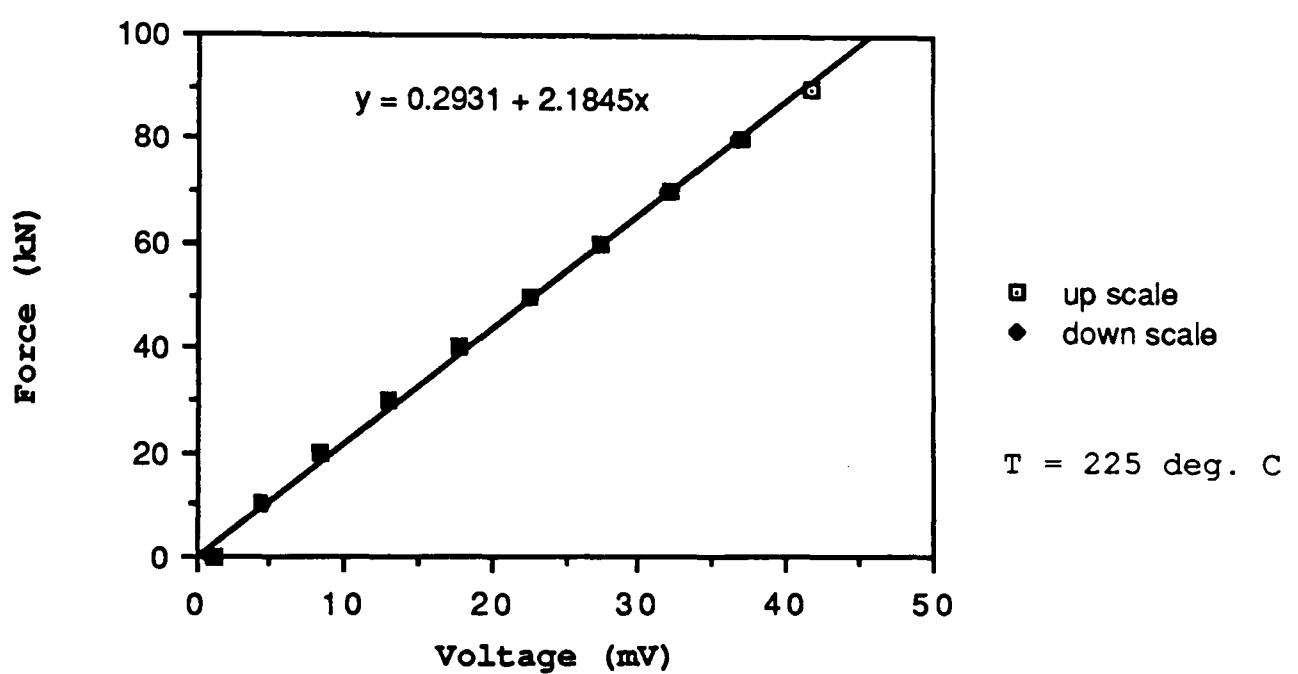
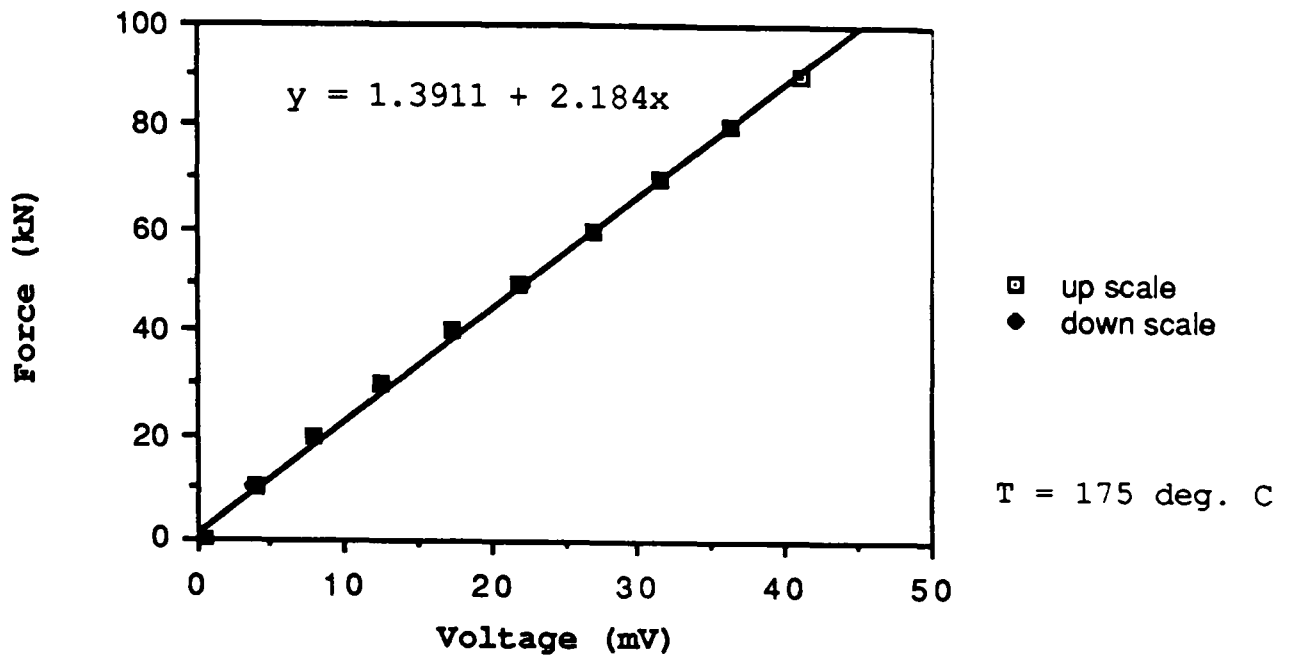


Figure 4.13b The graphs illustrate the relationship between abutment force and voltage output for varying operating temperatures 175 and 225 °C, for the third calibration of the abutment loadcell.

It should be noted that the maximum temperature attained by the abutment loadcell during machine operation is less than 150 °C.

4.4.3 PRESSURE TRANSDUCERS

The calibration of the pressure transducers was carried out on a Budenburg dead weight calibration test machine. The high pressure (H.P.) transducer, which is normally connected to the inlet pipe of the hydraulic motor, was reconnected to the test machine, whilst the electronic circuitry remained in tact. The loading range was 0 - 21 MPa (3000 lbf/in²) and the corresponding output was 0 - 10 V. The calibration curve for the H.P. transducer is given in fig 4.14.

The calibration curve for the low pressure transducer is given in fig 4.15. The torque curve was then determined from the differential pressure indicated on the graphical plot of the performance curves provided with the hydraulic motor from the manufacturers, see fig 4.16 for details.

4.4.4 TACHOMETER

The calibration equipment used was a portable tachometer which measures the relative surface speed of the rotating shaft with which the tachometer is in contact.

The calibration curve for the tachometer is given in fig 4.17. The speed range is 0 - 25 rev/min with a corresponding voltage output of 0 - 5 V.

4.4.5 THERMOCOUPLE PROBES

Calibration of the thermocouple probes was not necessary because the AIM3 module has a built-in cold junction reference source adjacent to the terminal block, to which each of the

thermocouple probes is attached by leadwires.

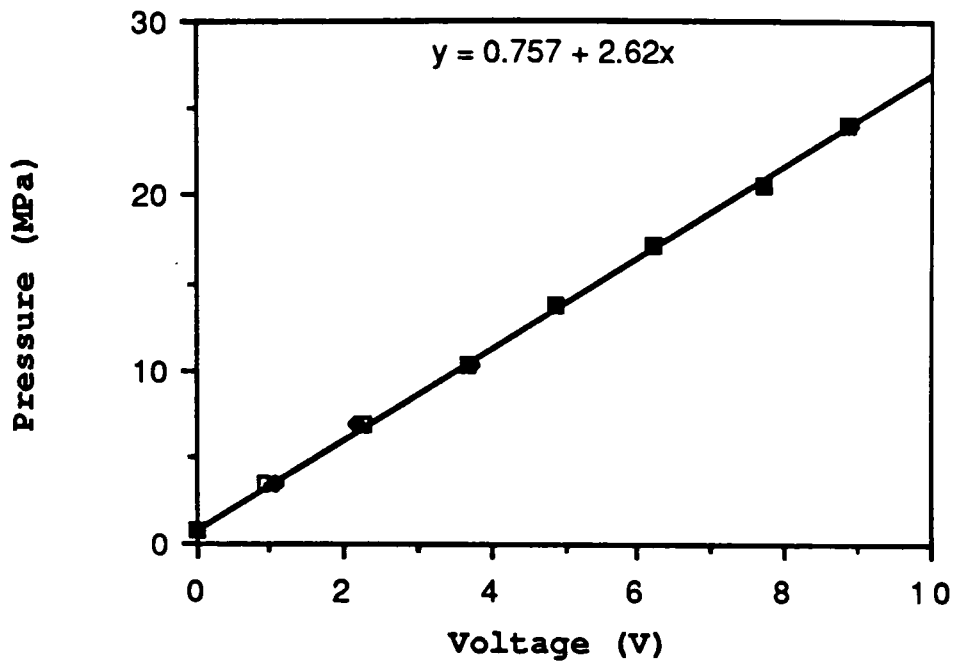


Figure 4.14 The graph illustrates the relationship between pressure and voltage output from the bridge circuit of the high pressure transducer.

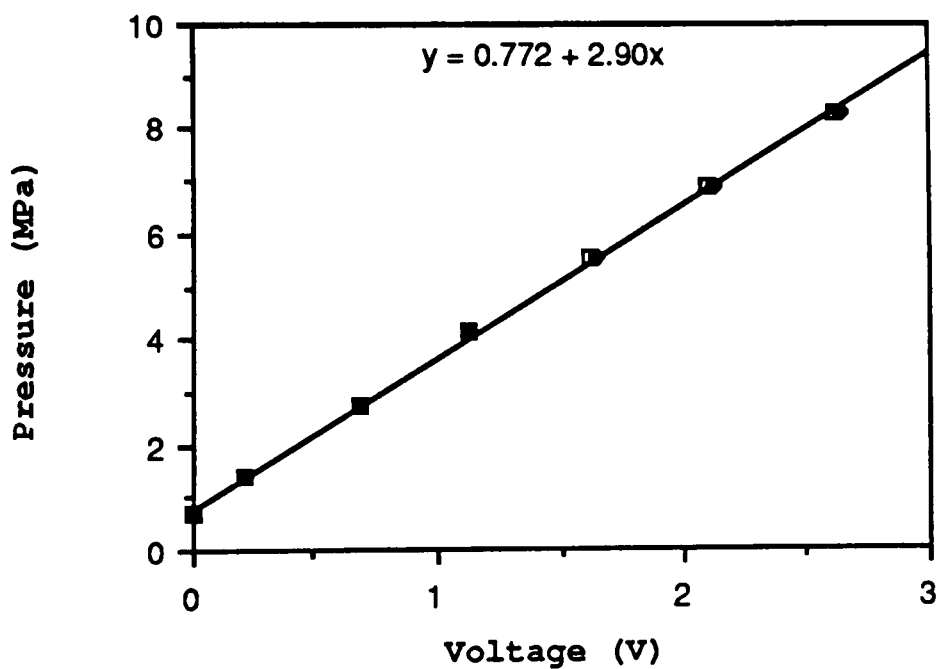


Figure 4.15 The graphs illustrate the relationship between pressure and voltage output from the bridge circuit of the low pressure transducer.

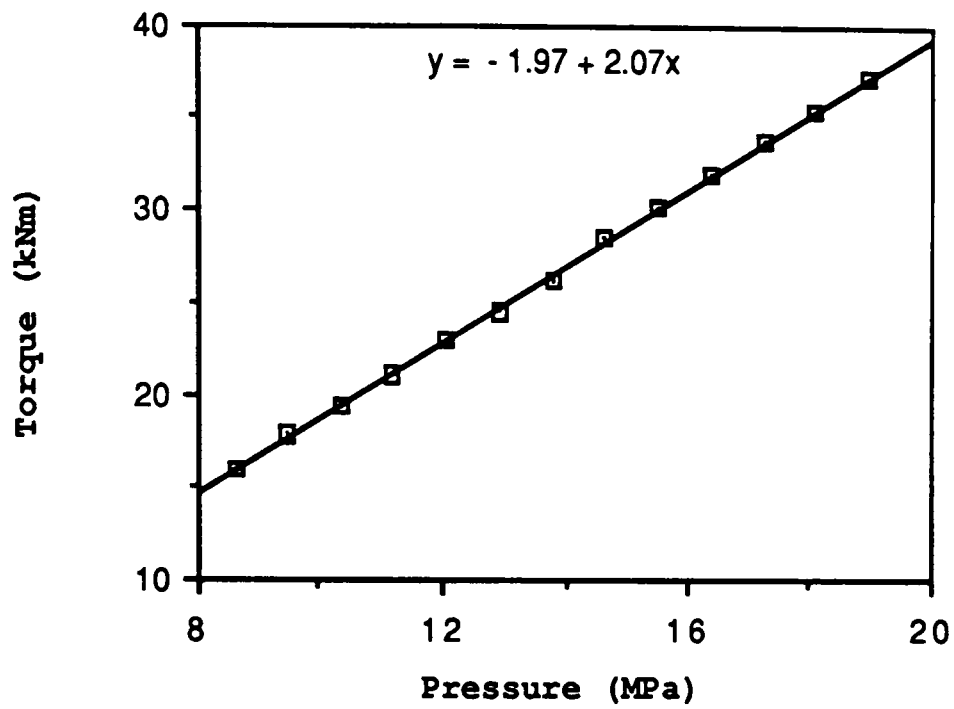


Figure 4.16 The graph illustrates the relationship between torque against pressure differential across the hydraulic motor (the graph may be used for the pressure range indicated and wheel speeds in the range 5 - 25 rev/min).

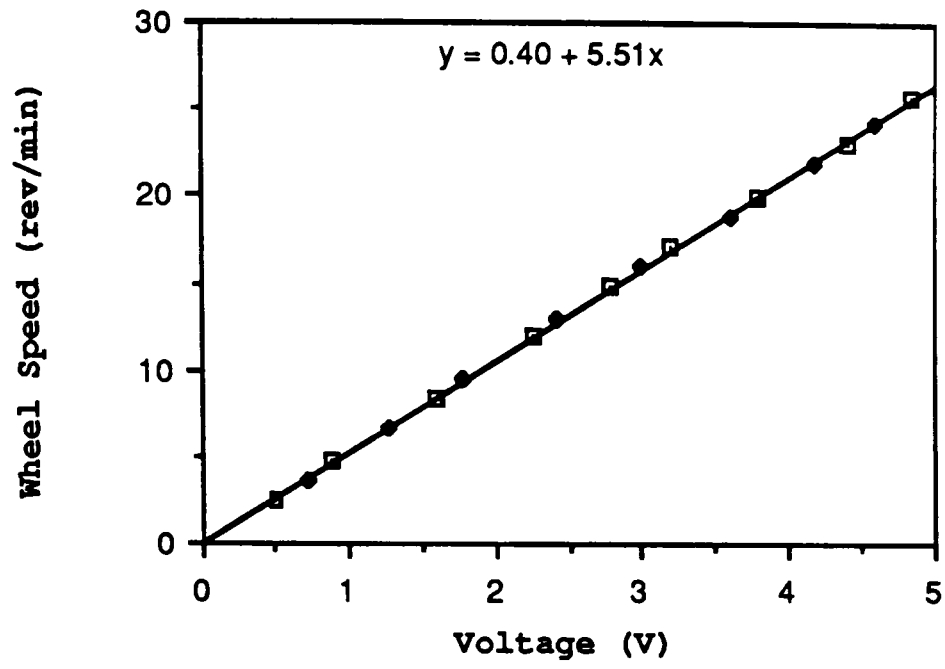


Figure 4.17 The graph illustrates the relationship between wheel speed and voltage output from the tachometer.

5.0 THEORETICAL ANALYSIS

The formulation of a reliable mathematical model will depend on the selection of the appropriate constitutive equations. These will be derived by considering the flow stress (stress state) of the feed metal, corresponding to a particular stage in the deformation zone. The flow stress is determined from knowledge of the level of strain, strain rate, temperature and feed metal under consideration. In addition, the assembly of the constitutive equations into a single expression which describes the rate of internal work of deformation (work done), will be derived using the minimum upper bound (or energy) theorem.

5.1 EXISTING THEORIES

There are presently four known theoretical models⁽¹⁾⁽¹⁷⁾⁽¹⁸⁾⁽²⁰⁾, which predict extrusion pressure in the Conform process. These models have each been derived by different analytical methods and can be described as generalised in their present form, since none predicts the variation in extrusion pressure corresponding to a change in the rate of deformation and temperature. Indeed, no research has been done on metal flow corresponding to the flow stress at a given station in the deformation zone.

The first analytical model was given by Green⁽¹⁾, and subsequently extended by Etherington⁽¹⁷⁾ and was derived in order to predict the maximum extrusion pressure for tangential and radial extrusion, using the upper bound energy method. The analytical model was based on many simplifying assumptions since it was essentially intended for use as basic design criteria for the design of the early Conform machine. The general equations given in the report⁽¹⁷⁾ provide details on the overall power requirements for the extrusion of commercial purity aluminium rod in the annealed and pre-strained conditions. It should be noted that the analytical model was

based on a rod feed input and output since the forces involved in the extrusion of particulate feed are significantly lower.

The second model was based on a theoretical and experimental investigation by Tirosh, Grossman and Gordon⁽¹⁸⁾. The analytical model has been based on an upper bound analysis and provides a measure of the pressing force (abutment force) for the tangential extrusion of lead. However, the use of their model for predicting the extrusion pressure of various metals is limited, since there is no mention of a constitutive equation for lead in the upper bound equation (i.e. the very nature of the Conform process introduces significant changes in temperature in the metal as it passes through the deformation zone). The use of lead as a model material in this programme has been considered unsuitable for practical reasons, although it has been successfully used to simulate hot steel in tube rolling processes⁽¹⁹⁾ under isothermal conditions.

In addition, the experimental apparatus used to simulate the action of the Conform process employed a variable speed D.C. motor, which allowed feed metal entry speed variations between 4.4 - 5.5 m/s. In general, commercial feed metal entry speed varies from 0.08 - 0.7 m/s.

The third model has been derived from a theoretical and experimental analysis by Russian authors⁽²⁰⁾.

Further to the above investigations there has been extensive research by other authors specialising in the metallurgical aspects of different metals processed on the Conform machine. This work will assist in formulating an analytical model based on assumptions derived from knowledge of the micro-structural changes which arise during deformation. At this stage however, it is not felt necessary to describe all papers relating to this subject but to make reference to the appropriate paper in the subsequent discussion.

5.2 ELEMENTS OF THE THEORY OF PLASTICITY

Some fundamental elements in relation to the theory of plasticity are presented first.

5.2.1 EQUATION FOR EFFECTIVE STRESS AND STRAIN

Many early researchers made comparisons of experimental test data derived from different mechanical testing methods, with the implicit assumption that, providing the correct methods of calculation were employed, the results of these tests should coincide⁽²¹⁾. It is now widely accepted that different modes of deformation will generate differing types of crystallographic anisotropy and, hence, the consequent divergence of test results.

It is usual therefore to determine a general expression for the complex state of stress or strain in terms of invariant functions of stress and strain. This implies that the same flow curve describing the relationship between the stress and strain can be obtained regardless of the experimental method for which the flow curve was initially determined.

The effective stress determined from the uniaxial tension (data obtained before the onset of necking) or compression test (data obtained before the onset of flow bulging) can be expressed as a uniaxial stress system i.e.,

$$\sigma = \sigma_L$$

The components of true strain can be expressed in the constant volume relationship,

$$\epsilon_L + \epsilon_R + \epsilon_C = 0$$

The expression for the effective strain expressed in relation to the uniaxial compression test i.e.,

$$\epsilon = \epsilon_L = 2\epsilon_c = 2\ln(d_f/d_1) \quad \text{--- (5.1)}$$

In general, the effective stress and effective strain can be expressed in terms of the true stress and true strain in relation to the data obtained from the compression and tension testing methods.

The total strain that the feed metal will undergo is determined by considering the geometry of the deformation zone, i.e. the strain history can be ascertained by considering the natural strain corresponding to geometrical changes in the deformation zone (discussed in more detail later).

5.2.2 DETERMINATION OF FRICTION CONDITIONS

The von Mises shear strain energy criterion has been employed in order to relate the maximum shear stress κ , to the principal stress (or effective stress) as follows,

$$\kappa = \sigma/\sqrt{3} \quad \text{--- (5.2)}$$

The friction conditions which exist between the tools and the feed metal in a deformation process where metal is plastically deformed has been widely studied(22) (23) (24) (25). The two expressions most commonly used in the theory of plasticity are the Coulomb friction and the constant friction factor.

The Coulomb friction is an expression used to determine the tangential stress, which is assumed to be proportional to the normal (or direct) pressure between the two bodies P i.e.,

$$\tau = \mu P$$

μ is the coefficient of friction and, is usually assumed to be constant for a given set of conditions.

The second type is commonly referred to as the constant shear stress factor where the shear yield stress of the feed metal being deformed is assumed constant irrespective of pressure i.e.,

$$\tau = mK \qquad \text{--- (5.3)}$$

m is the friction factor and, is assumed constant for a given set of conditions.

The value of the friction coefficient is small (typically $\mu < 0.1$ for the wire drawing process), however, the friction factor can hold a value in the range 0 to 1. Noting, that in the absence of friction, $m = \mu = 0$. For complete sticking between the tools and feed material, $m = 1$.

The feed metal employed is commercial purity aluminium. This has a tendency to stick to the steel tooling under the mechanical and thermal stresses developed in the deformation zone. Subsequently, the feed metal preferentially shears internally at a small distance from the actual feed metal and tooling interface. Therefore it is not unreasonable to assume that $m = 1$ and that this assumption holds true for the entire deformation zone. In other words, the maximum shear a metal can withstand according to the von Mises yield criterion is the combination of equations (5.2) and (5.3) as follows,

$$\tau = \sigma / \sqrt{3} \qquad \text{--- (5.4)}$$

noting, that $\tau = K$ since $m = 1$

noting, that $\tau = K$ since $m = 1$

In general, computations of friction losses based on the constant shear stress factor are made easier, since the friction factor shear stress is a constant dependent only on the material state of stress. However, the friction coefficient shear stress is determined from the normal pressure which exists between the feed metal and the tooling interface.

Although the friction factor has been assumed equal to unity, comparisons between experimental and theoretical data for the condition $0 < m < 1$, will be made under section 6.

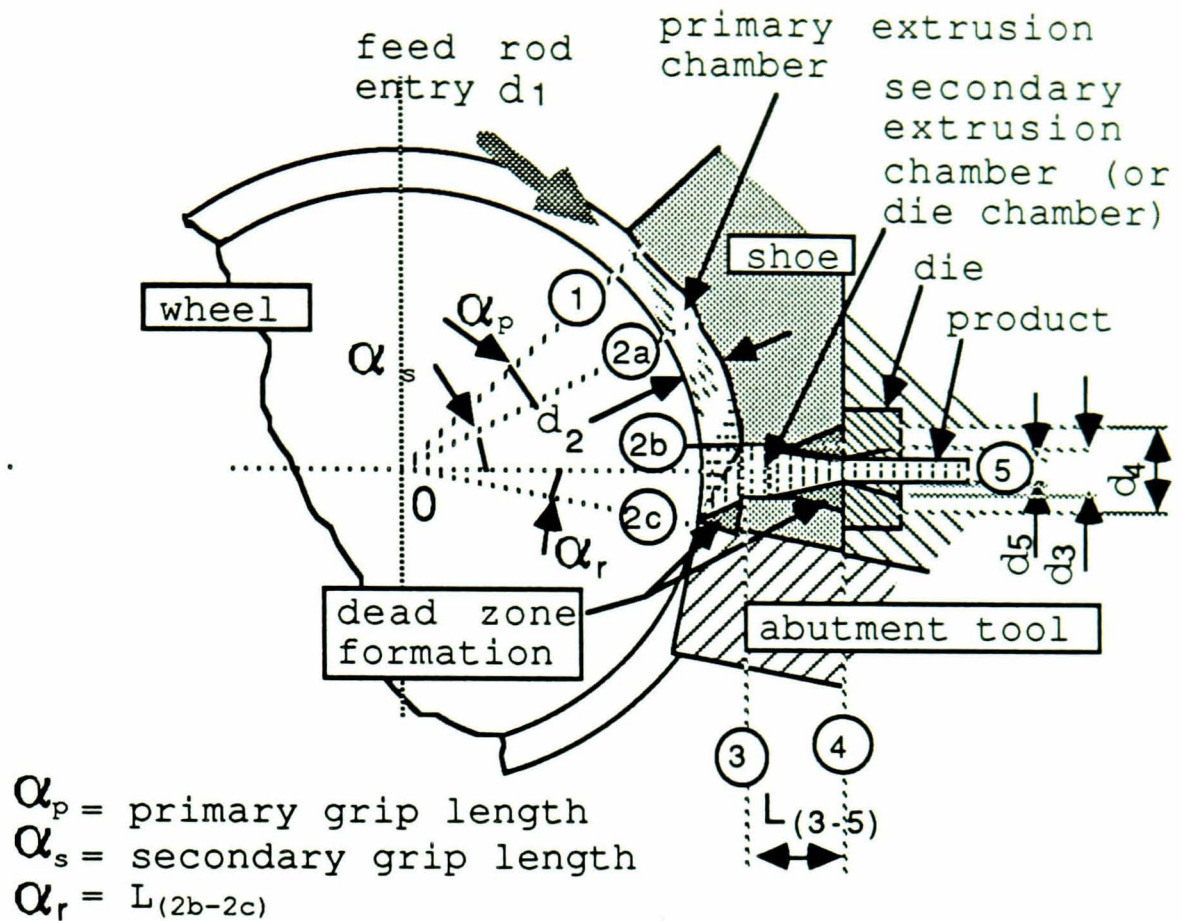
5.3 UPPER BOUND EXPRESSION FOR INTERNAL WORK OF DEFORMATION

The general equation for the upperbound theorem used by Hill⁽²⁶⁾ for the treatment of constrained plastic deformation is denoted by the following expression,

$$W_t = W_h + W_r + W_f \quad \text{--- (5.5)}$$

W_t is the total internal work done per unit volume per unit time for a given stage of deformation.

It is necessary to separate the deformation zone into two distinctly different parts see fig 5.0. Initially, the secondary extrusion chamber (or die chamber) which houses the die at stages 3 to 5 will be considered. The effect of the conical extrusion chamber in which the die is housed in the real process has been neglected for simplicity in the subsequent analysis (i.e. $d_3 = d_4 = 13.5$ mm).



note: The circled numbers refer to a particular stage in the deformation zone

Figure 5.0 The diagram illustrates the geometry of the deformation zone

Avitzur⁽²⁷⁾ has derived a generalised upper bound expression from equation (5.5) for the conventional direct extrusion process detailed as follows (see also appendix C1),

$$\begin{aligned}
 W_{t(3-5)} &= \int_3^5 \sigma_{(3-5)} f(\alpha_2) \delta \epsilon && \{W_h\} \\
 &+ 2K_{(3-5)} \left(\frac{\alpha_2}{\sin^2(\alpha_2)} - \cot(\alpha_2) \right) && \{W_R\} \\
 &+ 2K_{(3-5)} \cot(\alpha_2) \epsilon_c && \{W_f\}_d \\
 &+ 2\tau_{(3-5)} \left(\frac{2L_{(3-5)}}{d_3} - \left(1 - \frac{d_5}{d_3} \right) \cot(\alpha_2) \right) && \{W_f\}_c
 \end{aligned}$$

--- (5.6)

where, $\tau = mK$

The internal work of deformation in expression (5.6) represents the internal power consumed per unit volume per unit time (i.e. the ram or back pressure) for a given axisymmetric deformation process. The influence of the average effective strain $f(\alpha_2)$ as a function of the ideal strain, is expressed in terms of the die cone angle (or dead zone angle) and has been incorporated in the homogeneous work done term. In addition, the assumption of a spherical velocity field which bounds the planes of deformation is an implicit feature in the derivation of the redundant work done term (W_R).

The pressure developed on a flat-faced die is determined from knowledge of the geometry of the dead zone formation which arises from the internal shearing of the feed metal as it passes through the planes of deformation. In turn, the minimum upper bound can be derived by assuming that there exists a dead zone angle which will give the minimum work done⁽²⁷⁾, see also fig 5.1. The angle of the dead zone is therefore referred to as a pseudo-independent process parameter.

In order to determine the die pressure from knowledge of the optimum dead zone angle, the portion of equation (5.6) detailing the power consumed by friction at the container wall and feed metal interface is neglected, i.e. $m = 0$. The die pressure is then described as follows,

$$\begin{aligned}
 P_d = & \int_3^5 \sigma_{(3-5)} f(\alpha_2) \delta \epsilon \\
 & + 2K_{(3-5)} \left((\alpha_2 / \sin^2(\alpha_2)) - \cot(\alpha_2) \right) \\
 & + 2K_{(3-5)} \cot(\alpha_2) \epsilon_c \qquad \text{--- (5.7)}
 \end{aligned}$$

In order to determine the internal work done corresponding to the primary extrusion chamber at stages 1 to 3, a similar expression for (5.6) has been proposed. It is suggested that deformation in the primary region takes place at two localised regions, namely, the initial small strain required to change the shape of the feed metal to the chamber cross-section (stage 1 to 2a) and the larger strain required to effect a change in direction as feed metal leaves the primary chamber and enters the secondary die chamber at stage 2b to 3.

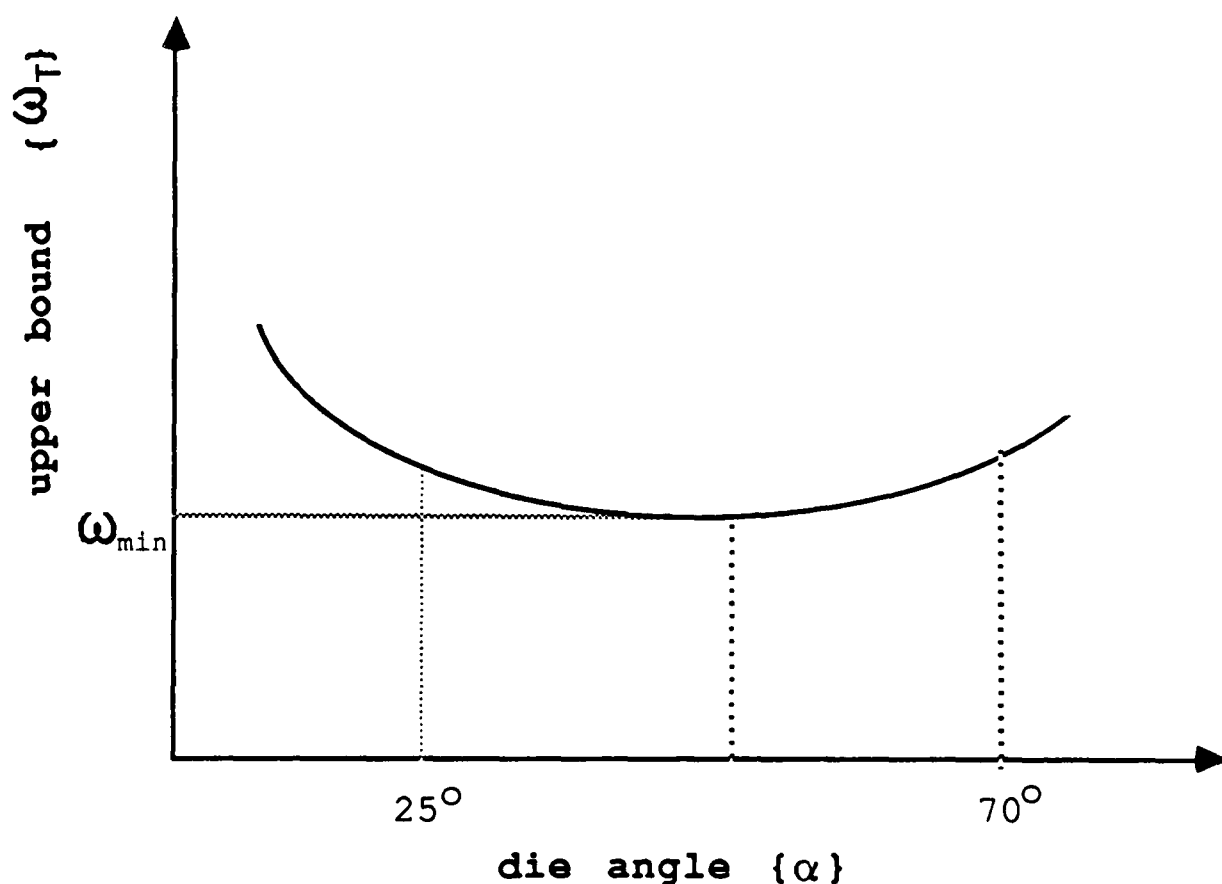


Figure 5.1 The diagram illustrates the change in the upper bound value for work done corresponding to die angle

The components of redundant and friction work in equation (5.6) will be neglected for stages 1 to 2a since they are considered to have a comparatively small effect on the overall power requirements. This is not the case, however, for stages 2b to 3 where the redundant and friction work components have a pronounced effect on the deformation loads.

The homogeneous work of deformation for stages 1 to 2a will suffice in order to determine the small pressure to initiate lateral yielding of the feed metal i.e.,

$$W_{h(1-2a)} = \int_1^{2a} \sigma_{(1-2a)} \delta \epsilon \quad \text{--- (5.8)}$$

Motomura⁽¹⁷⁾ has carried out a detailed micro-structural examination of the feed metal in the primary deformation zone, using a hardness survey and macro-etch which highlights regions of severe localised straining, see fig 5.2. The schematic diagram clearly indicates the planes of deformation bounded by stages 2b, 2c and 3. A modification of the upper bound expression after equation (5.6) has been proposed as follows (see appendix C2 for details),

$$\begin{aligned} W_{t(2b-3)} &= \int_{2b}^3 \sigma_{(2b-3)} \delta \epsilon && \{W_h\} \\ &+ 2K_{(2b-3)} (1.25 + (\alpha_1 / \sin^2(\alpha_1)) - \cot(\alpha_1)) && \{W_R\} \\ &+ 2K_{(2b-3)} \cot(\alpha_1) \epsilon_c && \{W_f\} \end{aligned} \quad \text{--- (5.9)}$$

It is apparent from fig 5.2 that a dead zone will exist between the orifice to the secondary extrusion chamber (i.e. stage 3) and the abutment tool face stage 2c. The angle of the dead zone formation is bounded by the the planes of deformation at stages 2b, 2c and 3. In other words, the feed metal experiences a change in direction at stage 2b (see appendix C2) and then another change in direction at stages 2c to 3.

The influence of the dead zone angle at stages 2b to 3 on the minimum upper bound will have only a small effect for dead

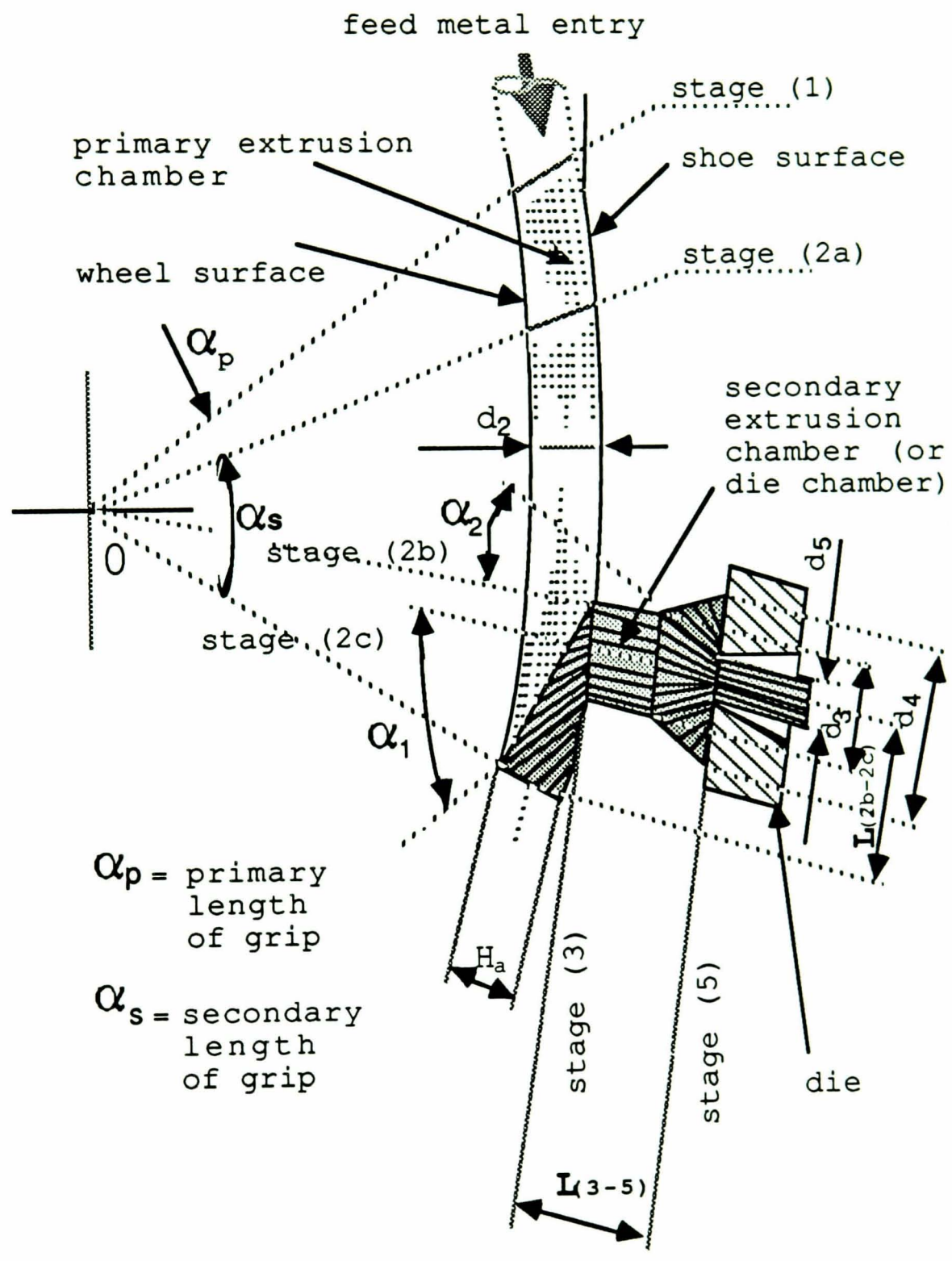


Figure 5.2 The diagram illustrates the plastic deformation zone in 2-D for radial extrusion

zone angles in the range $25^\circ < \alpha_1 < 70^\circ$, this will be discussed under section 5.10.

The total work of internal deformation is the combination of equations (5.6), (5.8) and (5.9) in the following form,

$$P_a = W_T = W_{t(1-2a)} + W_{t(2b-3)} + W_{t(3-5)} \quad \text{--- (5.10)}$$

5.4 CONSTITUTIVE EQUATIONS

The selection of an appropriate constitutive equation which describes the stress state (or flow stress) of the feed metal at a given stage in the deformation zone is considered important. The flow stress of the feed metal is determined from knowledge of the metallurgical structure of the feed metal, the strain, strain rate and temperature. The known value for the flow stress is then used in conjunction with the upper bound equations (5.6), (5.8) and (5.9) respectively in order to solve for extrusion (or abutment) pressure, equation (5.10).

There are different experimental methods by which to determine the effective stress, the choice largely depending on the process in which the constitutive equation is to be employed. For example, tension testing is limited to small strains, 0 - 0.03, and strain rates due to the onset of necking instability⁽²⁹⁾ and the consequent difficulties associated with material reorientation (i.e. a change from a uniaxial to a triaxial state of stress). Compression testing is limited to comparatively moderate strains, 0 - 0.7, and strain rates 0 - $10^2/s$ due to the onset of flow bulging. However, necking instability is not encountered in compression testing. In addition, the influence of friction which exists at the faces of contact on the test piece under compression may be minimised in order to maintain a more homogeneous deformation.

Torsion testing, on the other hand, can be used to determine the true stress at high strain, 0 - 8, and high strain rates, 0 - $10^3/s$. Other experimental methods are available⁽³⁰⁾ for example, the cam plastometer introduced by Orowan in 1950 was specifically intended to provide constant strain rate data in the range $10^1 - 10^2/s$. Also, the hydraulic forging press was used for tests on hot steel in the range $10^{-2} - 10^1/s$ by Lueg, Muller and Krause in 1957.

It is necessary at this stage to examine the levels of strain, strain rate and temperature that will be developed at a particular stage in the deformation zone. From this knowledge, it is then possible to select the appropriate experimental method (or existing data if available) to determine the equation of true stress for a given feed metal.

The magnitude of the effective strain developed in the primary extrusion chamber at stages 1 to 2a and 2b to 3 is of the order of 0 - 1.5, this is due to the geometrical changes (i.e. abutment penetration depth) in the feed metal as it is plastically deformed. Variations in die size in the secondary extrusion chamber (or die chamber) at stages 3 to 5 imply a further increase in strain in the range 0.5 - 5.

The strain rate will vary at each stage in the deformation zone. Smaller rates of strain will exist at stages 2b to 3 and comparatively larger strain rates exist at stages 3 to 5 i.e. 1/s - 500/s.

Knowledge gained from preliminary experimentation detailed under section (3.1.3), has shown that a temperature range 20 - 350 °C may exist in the feed metal in the primary extrusion chamber. The temperature rise depends on the magnitude of the internal work of deformation. The temperature increase in the die chamber is in the order of 50 - 250 °C.

It is clear that the plasticity curve relating the true stress to strain will vary corresponding to changes in strain rate

and temperature across the deformation zone, see fig 5.3.

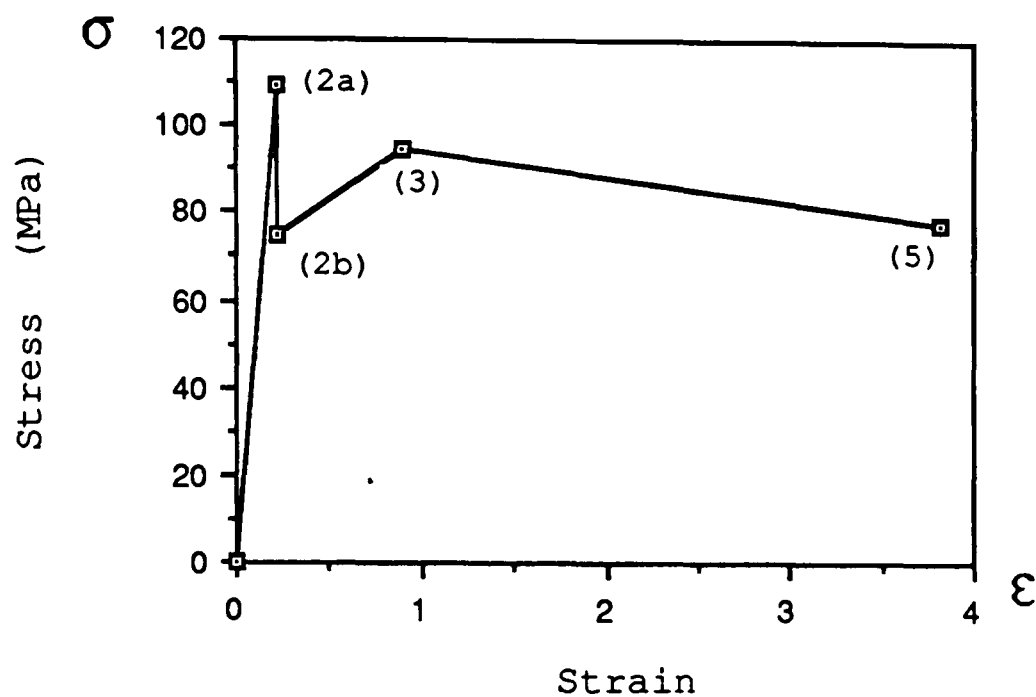


Figure 5.3, The graph shows a typical stress against strain curve across the deformation zone derived from analytical data.

In addition, the temperature changes from the ambient (or cold working) condition, to the high temperature (or hot working) condition. Effectively, the feed metal entering the deformation zone in the annealed or part pre-strained condition, will undergo further strain hardening, then a stage will be reached in the deformation zone where flow softening will offset further strain hardening. For this reason, it was considered necessary to experiment with various constitutive equations proposed by different researchers, selected on the basis of the feed metal subjected to a wide range of different processing parameters (feed metal specification is given under section 2.3).

5.4.1 THE CONSTITUTIVE EQUATION DERIVED FROM THE COMPRESSION TEST

The data from compression tests given by Alder and Philips (31) for commercially pure aluminium (spec. 99.5 % purity, in the annealed condition), has been selected in order to formulate an elementary form of the constitutive equation. A software package available for use on the Apple PC computer for plotting graphs, was employed to derive an expression for the state of stress as a function of homologous temperature, strain rate and strain as follows,

$$\sigma = A (1 - BT_H) \dot{\epsilon}^n \epsilon^m \quad \text{--- (5.11)}$$

where $m = C (10^{DT_H})$ and, $0.1 < \epsilon < 0.7$

and, $T_H = T/T_M$ where T_M is the melting point temperature for commercial purity aluminium.

(details of constant values are given in appendix C3).

Equation (5.11) is a variation of the elementary power law equation. The exponent (m) represents the strain rate sensitivity index which is a function of homologous temperature in the range of strain rates 1 - 40/s (limits of strain rate for the compression test in question). The exponent (n) represents the strain hardening index which is assumed to be a constant for the range of strain, 0 - 0.7 (limits of strain for compression test after Alder and Philips). The temperature is taken in the range of 18 - 550 °C. It is possible to extrapolate the stress state beyond the range of strain and strain rate, however, further errors may be introduced when flow softening becomes the predominant mechanism for deformation in this region.

It is therefore necessary to gain further knowledge of the combined effect of high strain and high strain rates on the

stress state in the feed metal. Samanta⁽³²⁾ has carried out experimental compression tests on commercially pure aluminium in the annealed condition for a strain range, 0.1 - 0.5, strain rate range 1 - 400/s and temperature 250 - 550 °C. The equation for stress follows after equation (5.11) in form (details of constant values are given in appendix C3). The limitation of the work by Samanta being the level of strain developed in the compression test.

Hockett⁽³³⁾ has also experimented with the compression test in order to determine the stress, corresponding to the strain, strain rate and temperature in compliance with Alder and Philips and, Samanta. In his paper, various known forms of the constitutive equations proposed by different researchers, are described for the purpose of determining the best fit equation to experimental data. The knowledge gained from these tests is not useful in making a further contribution to the test data derived by Alder and Philips and Samanta. However, useful comparisons between the experimental data of the three authors described above is given.

The derivation of a generalised model of the process will incorporate the use of commercial purity aluminium in the annealed and part pre-strained condition. It is therefore necessary to establish a constitutive equation that can describe the stress in the feed metal entering the deformation zone, in the part or full pre-strain condition as well as the annealed condition. Johnson⁽³⁴⁾ has developed such an equation which uses a variation of the power law equation detailed as follows,

$$\sigma = A (E + \epsilon)^n \quad \text{--- (5.12)}$$

and rearranging,

$$\sigma = AE^n \left(1 + \frac{\epsilon}{E}\right)^n \quad \text{--- (5.12a)}$$

where, E represents the level of pre-strain in the range 0 - 1 (i.e. E is a constant pertaining to the amount of prior cold work which the feed rod has received, details of various hardness conditions are given under appendix C3), and ϵ the variable strain. A similar expression has been proposed for equation (5.11) as follows,

$$\sigma = AE^n (1 - BT_H) \dot{\epsilon}^m (1 + \epsilon/E)^n \quad \text{--- (5.13)}$$

where, $m = C (10^{DT_H}) \quad \text{--- (5.13a)}$

5.4.2 THE CONSTITUTIVE EQUATION DERIVED FROM THE HOT TORSION TEST

To overcome the limitations of the compression test, the hot torsion test by Akeret⁽³⁵⁾ provides an alternative solution for higher levels of strain, 0.5 - 8, moderate strain rates 0 - 50/s and temperature in the range 350 - 580 °C. The hot torsion test was employed by Akeret in order to determine the mechanical behaviour of commercially pure aluminium in the recrystallised state. From these graphs, the hot torsion test data can be described by the following expression,

$$\sigma = A (1 - BT_H) \dot{\epsilon}^m \quad \text{--- (5.14)}$$

where $0.5 < \epsilon < 2.5$

the constant values are detailed in appendix C3. The strain rate sensitivity index (m) maintains a constant value in this case. The strain component is not included in equation (5.14) since the curves of stress against strain are very nearly constant in the range $0.5 < \epsilon < 2.5$ and then decrease with a further increase in strain. The rate of decrease in the flow stress curves beyond a strain of 2.5 becomes more pronounced

for higher rates of strain corresponding to lower temperatures.

5.4.3 FLOW SOFTENING

The information gained from the compression and hot torsion test data contributes to an understanding of the mechanism of deformation. It has been understood for many years in a metal which normally work hardens that the flow softening can occur at a particular combination of strain, strain rate and temperature. Dynamic recovery is the mechanism which accounts for flow softening observed in the conventional extrusion of aluminium⁽³⁶⁾.

Bearing in mind the rise in temperature of the feed metal is due to the heat generated by plastic deformation and friction, it is feasible to view the extrusion of pure aluminium as a thermally dominated process^{(37) (38)} even when the feed metal is at ambient temperature. Recovery is a thermally activated process and the temperature of initiation for a given metal is related to the melting temperature. Thus recovery may occur in a metal such as commercially pure aluminium at low temperature i.e. $T > 200$ °C.

The feed metal enters the deformation zone at ambient temperature and passes the die exit in the range 250 - 550 °C, depending on the magnitude and rate of plastic deformation imparted in the feed metal. The precise determination of the temperature at stage 3 is important because the extrapolation of data from the compression test equation (5.11), for example, will yield constant strain hardening from stages 1 to 3 and stages 3 to 5 irrespective of temperature.

It is convenient to use the expression most suited to describing the incremental strain, strain rate and temperature distribution across the deformation zone. The initial suggestion is equation (5.13) after the data of Alder and

Philips. Corrections can then be implemented to this equation for stages 3 to 5, based on the assumption that flow softening prevails at stage 3. This is not an unreasonable assumption since preliminary experimentation has shown that the minimum strain level at stage 3 is greater than 0.7 corresponding to a minimum temperature of 200 °C. Therefore, the flow curve associated with dynamic recovery can assume a value independent of further straining between stages 3 and 5 and, is dependent on temperature and strain rate only i.e.,

$$\sigma_5 = A (1 - BT_{H(5)}) \dot{\epsilon}^m (E + \epsilon_3)^n \quad \text{--- (5.15)}$$

It is noted, that the variable strain ϵ in equation 5.15 for stress at stage 5, will yield the level of strain reached at stage 3 independent of further straining in the die chamber.

However, strict caution should be observed when using the constitutive equation for the determination of the stress state as a function of temperature in the upper bound expression, in particular, the extrapolated values for stress based on high levels of strain and strain rate. This is because the temperature increase through adiabatic deformation is also determined from the upper bound expression (discussed in detail in section 5.6). Therefore, if errors are present in the derivation for the stress state from constitutive relationships, these could be magnified when determining the corresponding minimum upper bound values for work done.

5.5 EQUATION FOR STRAIN RATE

The strain rate varies pertaining to a particular stage in the deformation zone i.e. stages 2b to 3 and stages 3 to 5. The strain rate is brought about by the change in the particle velocity of the feed metal as it passes between the planes of

geometry bounds the limits of deformation (i.e. dead zone formation).

In general, the effect of increasing strain rate on the deformation load serves to increase the stress and consequently the load requirements. Also, the strain rate sensitivity index (m) becomes greater for elevated temperature deformation (see equation 5.13a).

In the real extrusion process, the strain rate varies across the transverse plane and the axial plane of deformation. Indeed, it is apparent that a severe localised strain rate distribution is centred around the die orifice⁽³⁶⁾. This feature is brought about by the changing dead zone angle corresponding to changes in stress in the feed metal as it passes between the planes of deformation. Avitzur has studied the changes in strain rate across the planes of deformation for the isothermal⁽²⁷⁾ and adiabatic⁽³⁹⁾ axisymmetric extrusion process for a linearly varying dead zone angle.

Concerning the mean strain rate distribution for the die chamber, the modified Feltam equation⁽⁴⁰⁾ provides an expression based on the time average mean strain rate which the feed metal takes to traverse the planes of deformation detailed as follows,

$$\dot{\epsilon}_{(3-5)} = 6\dot{V}_3 d_3^2 \epsilon_{(3-5)} \tan(\alpha_2) / (d_3^3 - d_5^3) \quad \text{--- (5.16)}$$

It is observed that the strain rate is a function of the pseudo-independent parameter i.e. the dead zone angle (α_2) and, the process variables strain and speed.

It is noted, that axial symmetry has been assumed for the die region stages 3 to 5 for the derivation of the Feltam equation in accordance with the upper bound equation (5.6) after Avitzur. The geometry of the primary extrusion chamber

however, is certainly not axisymmetric. The upper bound equation (5.9) for stages 2b to 3 after Avitur has been modified to accommodate the dead zone angle (α_1) which forms ahead of the abutment tool face in the primary extrusion chamber.

The determination of the strain rate at stages 2b to 3 in the primary extrusion chamber can be determined from knowledge gained from Motamora⁽¹⁷⁾. Observation of fig 5.2 clearly shows the planes of deformation in two dimensions. From the geometry of the planes of deformation bounded by stages 2b, 2c, 3 and the cross-sectional area, the time average mean strain rate can be derived as follows (appendix C4 gives a complete derivation),

$$\dot{\epsilon}_{(2b-3)} = 2\dot{V}_{2b} \epsilon_{(2b-3)} \tan(\alpha_1) / d_4 \quad \text{--- (5.17)}$$

The strain rate at stages 1 to 2a is small in comparison with equations (5.16) and (5.17), but assumed large enough to approximate the value $\dot{\epsilon}^m = 1$. Noting that the influence of the upper bound value for pressure at stages 1 to 2a has only a small effect on the overall power requirements, as mentioned previously.

5.6 EFFECT OF TEMPERATURE AND SPEED

When metals are deformed, the greater part of the internal work of deformation manifests itself as heat. In general, the temperature of the feed metal in the deformation zone depends on a) the initial temperature of the tooling chamber and feed metal, b) heat generation due to plastic deformation, c) heat generated by friction at the extrusion chamber and feed metal interface and, d) heat transfer between the deforming feed metal and the tooling chamber and surrounding environment.

Farren and Taylor⁽⁴¹⁾ have shown that for a heavily deformed metal between 90 and 99 % of the work done is converted into heat. It can therefore be shown that the temperature generated due to the plastic deformation per unit volume is,

$$\Delta T_i = \beta_1 W_t / \rho_f C_f J \quad \text{--- (5.18)}$$

In other words, the temperature increase due to plastic deformation is a function of the work done, the density and specific heat capacity of the feed metal. The constant β_1 is the fraction of deformation work which is converted into heat. The value $\beta_1 = 95 \%$ has been assumed.

The intention is to determine the temperature at each stage of plastic deformation corresponding to a change in strain, in order to predict a temperature profile in the feed metal across the deformation zone. To do this, it is necessary to determine the constitutive equation for stress state at each stage of deformation. It is then possible to determine the plastic work done at each stage of deformation. Clearly, an iterative solution to the upper bound equation (5.6) will be required, since the temperature is determined from the upper bound equation for work done and the constitutive equation requires knowledge of temperature.

The temperature increase in the primary extrusion chamber arises due to friction resistance at the stationary tooling segment, and moving feed metal interface. The expression given by Altan and Gegel⁽⁴²⁾ for the temperature increase due to friction is detailed as follows,

$$\Delta T_{(2a-2b)} = \tau_{m(2a-2b)} \dot{V}_1 A_a \delta t / \rho_f C_f V_f J \quad \text{--- (5.19)}$$

Where, $\tau_{m(2a-2b)} = (\sigma_{(2a)} + \sigma_{m(2b-3)}) / 2\sqrt{3}$ is the mean stress in

shear using the von Mises yield criterion and $m = 1$ as detailed under section (5.2.2).

The expression after equation (5.19) has been modified in order to determine the temperature increase in the feed metal in the primary extrusion chamber as follows (see appendix C5 for details),

$$\Delta T_{(2a-2b)} = \beta_2 \tau_{m(2a-2b)} L_{(2a-2c)} / \rho_f C_f d_2 J \quad \text{--- (5.20)}$$

It is noted, that part of the heat generated through friction is transferred to the feed metal and the remaining portion to the tooling (in particular the tooling segment) in the primary extrusion chamber.

The development of a simple mathematical expression which describes the heat lost to the container and die for a discrete billet in a conventional extrusion chamber has not been forthcoming. However, Singer and Al-Samarrai⁽⁴³⁾ have presented a simplified model, which is as follows.

When extrusion is initiated, the temperature of the feed metal (or billet) becomes higher than the container, as a result heat flows outwards from the deformation zone of the billet (assuming that the container temperature is at the same temperature of the pre-heated billet). The heat balance is complicated by the forward motion of the feed metal and by the fact that the container gradually heats up as extrusion proceeds.

The heat balance considered by Singer and Al-Samarrai has been based on many assumptions. In their paper, the emergent temperature of the product from the die orifice has been expressed as a function of the temperature generated through plastic deformation (i.e. the maximum temperature developed in the deforming feed metal before heat conduction takes place).

The emergent (or final) temperature corresponding to plastic deformation in the die chamber (i.e. stages 3 to 5), is determined by considering the heat lost to the container and die assembly in a short interval of time. The heat balance is described as follows,

$$\theta_f = \theta_i + \theta_c + \theta_d \quad \text{--- (5.21)}$$

evaluation of equation (5.21) after Singer and Al-Samarrai will yield,

$$T_f = T_i / \left(1 + \frac{\dot{\theta}_c k}{\rho_f^2 C_f^2 v^2 A_i} + \frac{\dot{\theta}_d}{\rho_f C_f v} \right) \quad \text{--- (5.22)}$$

The terms $\dot{\theta}_c$ and $\dot{\theta}_d$ in equation (5.21) refer to the rate of heat lost to the container (length of dead zone in die chamber) and die face respectively in the conventional extrusion chamber.

The rate of heat loss to the container $\dot{\theta}_c$ in equation (5.22) is derived by considering that perfect contact exists between the feed metal and the semi-infinite steel container surface. In addition, the interior surface of the steel container is assumed to be at the same temperature as the feed metal, which is uniform at any cross-section. It has been shown by Germant⁽⁴⁴⁾ that the rate of heat loss decreases with time of contact and he has presented an analytical model in the form of tabulated data. The variables in the model are the container diameter and time of contact. The tabulated data can be expressed by the following equation (see appendix C5 for details of constant values),

$$\dot{\theta}_c = (A + B d_i / d_d) t^c \quad \text{--- (5.23)}$$

The rate of heat loss to the die $\dot{\theta}_d$, is determined by considering that unidirectional heat flow exists between the cross-section area of the feed metal contacting a semi-infinite steel die. The time taken for plastic deformation between stages 3 to 5 is determined by algebraic manipulation of equation (5.16), i.e. dividing the strain by the time-averaged mean strain rate in this region. The expression for the rate of heat loss to the die after Germant is presented as follows.

$$\dot{\theta}_d = At^c \quad \text{--- (5.24)}$$

It should be noted that the derivation of equation (5.24) can also be obtained from a standard text book⁽⁴⁵⁾, where the rate of heat loss is determined from the assumption that nonsteady one-dimensional heat conduction exists over a semi-infinite body i.e.,

$$\dot{\theta} = k / (\lambda\pi t)^c \quad \text{--- (5.25)}$$

Equation (5.22) will hold for describing heat conduction at stages 2b to 3 into the tooling. The abutment mean diameter has been selected as the initial container (or chamber) diameter in equation (5.23). The time taken for deformation can be determined by dividing the strain by the strain rate, equation (5.17) at that stage.

A modification to equation (5.22) is proposed in order to provide an expression for the heat lost through conduction in the primary extrusion chamber at stages 2a to 2b. The heat loss to the die $\dot{\theta}_d$ is simply neglected, i.e., it is assumed that heat is conducted radially into the tooling chamber. However, further modification to the expression for $\dot{\theta}_c$ in

that frictional resistance which arises at the stationary tooling segment and feed metal interface is the only heat source in this region. In addition, further uncertainties are introduced because the primary extrusion chamber is not axisymmetric.

It is therefore suggested that the value β_2 in equation (5.20) is selected to account for the quantity of heat generated, in part to the feed metal, and the remainder to the tooling. It is also noted that the Conform process, unlike conventional extrusion, is a truly continuous operation. This implies that a steady state (or near steady state) operation will be attained under a given set of extrusion conditions. Consequently, if the tooling surrounding the primary and secondary extrusion chamber is perfectly insulated, thermal gradients which would otherwise stem from the extrusion chamber would be negligible, in accordance with the semi-infinite analytical expressions for heat conduction detailed in equations (5.23) and (5.24).

Initially, it was thought that the value for β_2 could assume a constant value. However, preliminary experimentation has shown that the cross-section geometry of the primary extrusion chamber (i.e. varying the abutment depth penetration) influences the heat developed by friction in the feed metal between stages 2a and 2b. This is because the frictional resistance at the tooling segment and feed metal interface is fixed by the geometry of the tooling segment, i.e. the width. It can then be assumed that the tooling will reach a near uniform temperature in the immediate vicinity surrounding the primary extrusion chamber under steady state conditions. As a result, more heat will be lost initially through heat transfer to the tooling under transient operating conditions, and subsequently when steady state operation prevails some heat will be given back to the deforming feed metal as it passes through the deformation zone. This implies that less heat will be lost to the tooling under steady state operation, noting that heat loss depends on the insulating capacity of

the tooling. The expression for β_2 has subsequently been derived from the interpretation of experimental data as follows (details of constant values are provided in appendix C5),

$$\beta_2 = A (d_i/SA)^c \quad \text{--- (5.26)}$$

Finally, the temperature distribution in the primary and die chambers i.e. stages 2a to 2b, 2b to 3 and 3 to 5, can be determined by the summation of the final temperatures pertaining to each stage in the deformation zone.

It is noted, that the emergent temperature of the product is assumed uniform throughout the cross section area. Indeed, the analytical expressions detailed above assume that the temperature at any stage in the deformation zone is constant throughout any cross-section. This is not the case in reality since the surface of the product exiting the die is likely to be at a higher temperature than the core. A temperature gradient will therefore exist across the product cross-section as it emerges from the landed region of the die. Also, because the primary extrusion chamber is not axisymmetric the temperature in the feed metal at the stationary tooling surface is likely to be much greater than at the root of the wheel groove.

5.7 WORK DONE DUE TO UNKNOWN EXTERNAL FORCES

The external driving force required to initiate extrusion is provided by the torque through the rotating wheel. The surface area per unit length (W) of the grooved wheel is greater than the surface area per unit length of the tooling segment (SA) in the primary extrusion chamber. Consequently, a forward thrust is imparted to the feed metal in the primary extrusion chamber effectively forcing the feed metal to impinge on the abutment tool and, in turn, forcing the feed

metal into the secondary extrusion chamber and, finally, through the die orifice.

The cross-sectional area of the primary extrusion chamber remains constant for the entire length in the present analysis (in other words, the cross-sectional area is not considered a variable in the subsequent investigation).

The length of the primary extrusion chamber is a function of the total internal work done per unit volume i.e., the greater the total internal work of deformation, the greater the length of the primary extrusion chamber required for a given W/SA ratio. However, the inter-relationship between W/SA and the internal work of deformation on the length of the primary extrusion chamber is more complex if friction and adiabatic heating are to be considered.

The primary extrusion chamber has been considered by other researchers^{(1) (17)} to be composed of two parts, namely the primary and secondary grip lengths, see fig 5.0. The influence of the primary grip length on the overall power requirements is small because the primary grip length is required only to initiate the small strain at stages 1 to 2a in order to allow the feed metal to take the shape of the chamber cross-section. The major contribution to the overall power requirements arises from the secondary grip length, therefore the primary extrusion chamber in this analysis is considered to be composed solely of the secondary grip length initiated at stage 2a. The external direct force on the abutment tool is derived by equating the external forces to the product of the total work of internal deformation and the abutment cross-sectional area as follows,

$$\begin{aligned}
 W_T A_a = & (\tau_{m(1-3)} L_{(2a-2c)} SA) \\
 & - (\tau_{m(1-3)} L_{(2b-2c)} W) \\
 & + (W_{t(1-2a)} A_a) \quad \text{--- (5.27)}
 \end{aligned}$$

Where, $\tau_{m(1-3)} = (\sigma_{(2a)} + \sigma_{m(2b-3)}) / 2\sqrt{3}$

rearranging equation (5.27) in terms of the length of the primary extrusion chamber as follows,

$$L_{(2a-2c)} = ((W_T - W_{t(1-2a)}) A_a) / \tau_{m(1-3)} (SA - W) \quad \text{--- (5.28)}$$

It is observed that the secondary length of grip is a function of the total work of internal deformation $W_T = P_a$.

5.7.1 ABUTMENT FORCE

The direct force acting on the abutment tool face, is determined by equation (5.27). However, the external work of deformation should include the friction which exists at the stationary dead metal zone at stages 2b to 3 and the moving wheel. This implies that the abutment tool will sense a larger force. In addition, friction will exist between the small landed region surrounding the abutment tool which protrudes into the wheel groove. The influence of the combined effect of friction on the abutment tool force can be determined as follows,

$$F_{f1} = 2/3 \left((d_3/2 + L_{(2b-2c)}) (SA - W) \right) \tau_{m(2b-3)} \quad \text{--- (5.29)}$$

where F_{f1} describes the effect of the dead zone friction and,

$$F_{f2} = L_a \tau_{m(2b-3)} SA \quad \text{--- (5.30)}$$

F_{f2} describes the effect of friction over the landed region of the abutment tool. The total external and internal work of deformation on the abutment tool is,

$$F_a = F_{f1} + F_{f2} + W_T A_a \quad \text{--- (5.31)}$$

where, F_a is the abutment tool force.

It is recalled that an oxide film develops on the surface of the feed metal coating (which in turn adheres to the surface of the wheel groove), in the primary extrusion chamber. The influence of the oxide film on the frictional forces which exist over the abutment tool surface will cause additional loading on the abutment tool. However, it is not considered necessary to develop a quantitative expression for the inclusion of oxide on the friction force in this analysis.

5.7.2 DIE FORCE

The die force is determined from the product of the die pressure and the cross-sectional area over which the dead zone acts in the secondary extrusion chamber i.e.,

$$F_d = P_d \pi / 4 (d_3^2 - d_5^2) \quad \text{--- (5.32)}$$

5.8 EFFECT OF METAL LEAKAGE

The necessity of control over the level of metal leakage (or flash) developed at the running clearance, is considered important in relation to minimising waste metal for the purposes of acceptable industrial production. However, preliminary experimentation has revealed, that, for the higher

levels of flash produced, a considerable reduction in temperature can be effected. This is quite understandable since, for a higher level of flash output, a proportional reduction in the rate of deformation in the die chamber will be realised.

It is noted that the pressure in the feed metal increases according to the expression (5.27). As this pressure increases, the proportion of flash developed also increases as the metal traverses through the primary extrusion chamber. Subsequently, it is expected that a non-linear relationship exists between the metal loss through flash and the rate of traverse of the feed metal through the primary extrusion chamber.

Since the level of flash developed in the industrial processes is small (usually $\zeta > 95\%$), the influence of the flash in terms of deformation loads is also small. However, under certain conditions, it is imperative to control the level of temperature attained in the feed metal in the deformation zone. In addition, it was soon realised from preliminary experimentation that, at high reduction ratios, difficulty was encountered when trying to minimise the level of flash output to below 27 % for the minimum abutment setting i.e. $H = 7$ mm.

Also, it is recalled that the operation of the die and abutment loadcell is restricted to a maximum temperature of 260 °C. It was established during preliminary experimentation that under high speed operation combined with high reduction ratios, that the temperature developed in the die loadcell would reach the limiting temperature of the die loadcell before the steady state operating condition prevailed, if the test was allowed to proceed under those conditions. To overcome this difficulty, the proportion of flash output was increased in order to allow the test to proceed under the extreme operating conditions.

It has therefore been considered necessary to provide a simple explanation of the relationship between deformation loads, temperature and flash output, in order to compare analytical and experimental data. The expression for the corresponding reduction in the average velocity of the feed metal at stage 2b is given as follows (see appendix C4 for derivation),

$$\dot{V}_{2b_f} = \zeta \dot{V}_{2b} = \zeta \dot{V}_{2a} \quad \text{--- (5.33)}$$

Noting, that $\dot{V}_{2b} = \dot{V}_{2a}$ since there is no change in cross-sectional area for the length of the primary extrusion chamber $L_{(2a-2c)}$.

The subsequent determination of the average velocity of the feed metal at stages 3 and 5 is determined by assuming constancy of volume, as no further metal loss through flash arises between stages 3 and 5.

5.9 TORQUE AND POWER REQUIREMENTS

An attempt has been made to derive an expression for the torque requirements based on the analytical knowledge gained from the determination of the abutment force. Further information, however, is required in relation to friction conditions which exist between the feed metal in the primary extrusion chamber and the tooling segment.

A coating of feed metal is deposited on the surface (or periphery) of the wheel adjacent to the primary extrusion chamber, where metal escapes as flash. The width of the feed metal coat is dependent on the pressure, i.e. higher abutment loads generate a greater amount of flash and, consequently, the spread (or width) of flash across the wheel periphery is also greater for the same pre-set running clearance. However, the thickness of the flash is greater for higher loads because

elastic distortions in the machinery become more pronounced, allowing wider running clearances to prevail.

If it is assumed, however, that a flash coating is deposited for the entire width of the tooling segment under transient conditions and remains rigid in that position (see under section 3.2.6), and also if the flash output is reduced to zero under subsequent steady state operation, the friction contact between the tooling segment and the coating on the wheel surface is then described by the following the expression,

$$F_{\text{wheel}} = \tau_{\text{wheel}} L_{(2a-2c)} W_{\text{flash}} \quad \text{--- (5.34)}$$

where, $\tau_{\text{wheel}} = mK_{\text{wheel}}$ and $0 < m < 1$.

However, it should be noted that, in the real process the scraper tool removes the oxide film on the surface of the feed metal coating in the wheel groove, therefore providing an escape route for continuous flash output.

Friction resistance also exists between the surface of the tooling segment and the moving feed metal in the primary extrusion chamber. This can be expressed as follows,

$$F_{\text{tool}} = \tau_{\text{tool}} L_{(2a-2c)} W \quad \text{--- (5.35)}$$

The torque required is determined from the summation of all the tangential forces multiplied by the radius of the wheel, i.e.,

$$T = (F_{\text{wheel}} + F_{\text{tool}} + F_{\text{abutment}})^{D/2} \quad \text{--- (5.36)}$$

5.10 SOLUTION TO UPPER BOUND EQUATIONS

It is clear that an iterative procedure is necessary in order to solve the upper bound equations for work done at the abutment and die. The work of internal deformation in the primary extrusion chamber is considered initially, where values for abutment pressure, die pressure and the mean stress at stages 2b to 3 are assumed as a first approximation (see fig 5.4 for details of the flow chart).

Initially, the process parameters are input to the computer program. The first subroutine in the program calculates the first solution to the upper bound equation (5.9) in the primary extrusion chamber. In order of calculation, the stress state at stages 1 to 2a is determined from equation (5.13) by assuming ambient temperature (or let $T_{H1}/T_M = 0$) and $\dot{\epsilon}^m = 1$ i.e.,

$$\sigma_{(2a)} = A (E + \epsilon_{(1-2a)})^n \quad \text{--- (5.36a)}$$

where, E = level of pre-strain

and, $\epsilon_{(1-2a)} = 2\epsilon_{c(1-2a)}$ strain at stage 1 to 2a

$$\epsilon_{(1-2a)} = 2 \ln (d_1/d_2) \quad \text{if } d_1 > d_2$$

or, $\epsilon_{(1-2a)} = 2 \ln (d_2/d_1) \quad \text{if } d_2 > d_1$

then, to determine the work done from equation (5.8), the integration of equation (5.8) is simple, since stress is a function of a single variable i.e. strain. Substitution of the above equation for $\sigma_{(2a)}$ (letting $E = 0$ for feed metal in the annealed condition) in the following will yield,

$$W_{h(1-2a)} = A (\epsilon_{(1-2a)}^{(n+1)}) / (n+1)$$

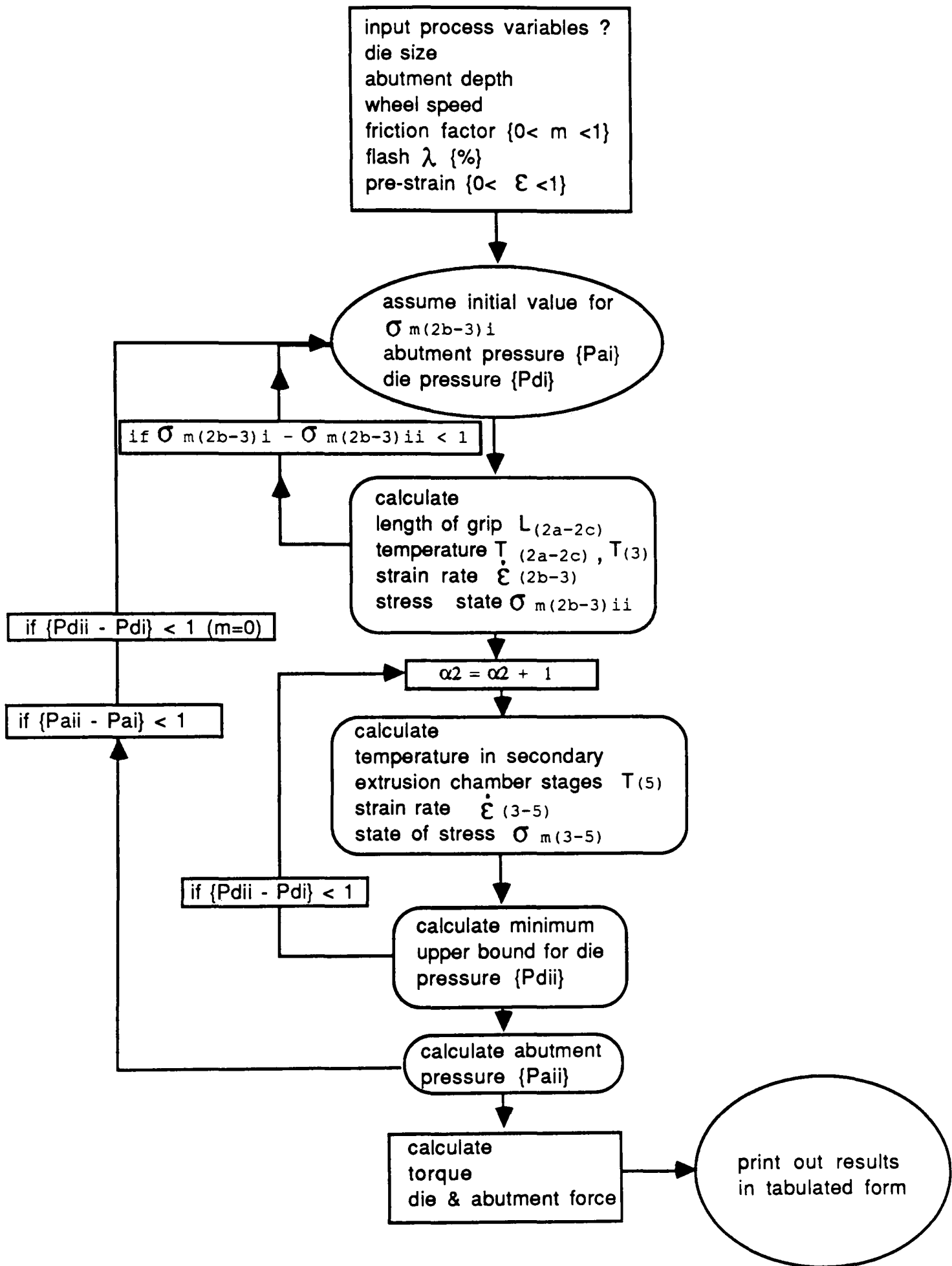


Figure 5.4. The diagram illustrates the flow chart for the Processing of analytical test results

Noting, that integration of the expression for $W_{h(1-2a)}$ with $E > 0$, will require algebraic manipulation of the equation for stress $\sigma_{(1-2a)}$ into a binomial series.

The temperature increase due to friction in the primary extrusion chamber i.e. stages 2a to 2b is computed using equation (5.20). Then, the stress at stage 2b is calculated using equation (5.13) and letting $\dot{\epsilon}^m = 1$, i.e.,

$$\sigma_{(2b)} = A (1 - BT_{H(2b)}) \epsilon_{(1-2a)}^n \quad \text{--- (5.36b)}$$

where, the level of strain at stage 2b remains unchanged from the stage 2a.

The stress at stage 3 is determined by considering the individual components of strain, strain rate and temperature at stage 3. Initially, the dead zone angle adjacent to the abutment tool face is determined using the following expression,

$$\alpha_1 = \tan^{-1} \left((L_{(2b-2c)} - d_3/2) / H \right) \quad \text{--- (5.37)}$$

and subsequently, the strain rate is computed using equation (5.17).

The actual temperature increase using equation (5.22) is determined from the work done and therefore indirectly from the strain. Noting, that strain rate and temperature are also functions of strain. This implies that there are four variables including the index (m) which are all dependent on strain within the integral for homogeneous deformation i.e.

$$\partial \mathcal{E} = f(\epsilon, \dot{\epsilon}, T_H, n)$$

It has been considered necessary therefore to modify equation (5.9) by using a mean value for stress in the term for homogeneous work done i.e.,

$$\begin{aligned}
 W_{t(2b-3)} &= \sigma_{m(2b-3)} \epsilon_{(2b-3)} && \{W_h\} \\
 &+ 2K_{m(2b-3)} \left(1.25 + \alpha_1 / \sin^2(\alpha_1) - \cot(\alpha_1) \right) && \{W_R\} \\
 &+ K_{m(2b-3)} \cot(\alpha_1) \epsilon_{(2b-3)} && \{W_f\}
 \end{aligned}$$

--- (5.38)

where, $\epsilon_{(2b-3)} = 2\epsilon_{c(2b-3)}$ strain at stage 2b to 3

and, $\epsilon_{(2b-3)} = 2\ln(d_3/d_2)$ if $d_3 > d_2$

$\epsilon_{(2b-3)} = 2\ln(d_2/d_3)$ if $d_2 > d_3$

Noting, that the stress $\sigma_{(3)}$ (equation 5.13), is determined independently of the work done at stage 3 by computing the strain rate, time taken (by dividing the strain $\epsilon_{(2b-3)}$ by the strain rate $\dot{\epsilon}_{(2b-3)}$) and the actual temperature increase using equation 5.22 i.e.,

$$T_{(3)} = T_{f(2b-3)} + T_{(2b)} \quad \text{--- (5.39)}$$

The homologous temperature $T_{H(3)} = T_{(3)}/T_M$ is then used in conjunction with equation (5.13). The corresponding total strain at stage 3 is determined incrementally from the strain history in the deformation zone as follows,

$$\epsilon_{(1-3)} = \sum_1^3 \epsilon$$

$$\text{or, } \epsilon_{(1-3)} = \epsilon_{(2b-3)} + \epsilon_{(1-2a)} + E \quad \text{--- (5.40)}$$

particular stage in the deformation zone and $\epsilon_{(1-3)}$ is then inserted in equation (5.13) as follows,

$$\sigma_{(3)} = A (1 - BT_{H(3)}) \dot{\epsilon}_{(3)}^m \epsilon_{(1-3)}^n \quad \text{--- (5.40a)}$$

Finally, a new value for the mean stress corresponding to stages 2b to 3 is computed using the following equation,

$$\sigma_{m(2b-3)} = (\sigma_{(2b)} + \sigma_{(3)}) / 2$$

The initial assumed value for the mean stress at stage 2b to 3 is compared with the new value, and the cycle is repeated until the two values for the stress converge to an acceptable level of accuracy. The total work of internal deformation at the abutment (stages 2b to 3) has been deferred for calculation under a third subroutine.

A second subroutine is set up to determine the internal work of deformation in the die chamber. Initially, the actual temperature at stage 5 using equation 5.22 is determined from the initial assumed value for work done in the die chamber. Then the increase in temperature at stage 5 is calculated as follows,

$$T_{(5)} = T_{f(3-5)} + T_{(3)} \quad \text{--- (5.41)}$$

and, the homologous temperature $T_{H(5)} = T_{(5)} / T_M$

The total strain at stages 3 to 5 is determined incrementally from the strain history in the deformation zone as follows,

$$\epsilon_{(1-5)} = \sum_1^5 \epsilon$$

noting that the level of strain in the die chamber will not influence the stress due to the onset of dynamic recovery at stage 3, then $\epsilon_{(3-5)} = 0$ in equation 5.42.

The main variable is the dead zone angle α_2 and it is noted that the upper bound equation 5.6, the stress $\sigma_{(5)}$, strain rate $\epsilon_{(3-5)}$ and $f(\alpha_2)$ are all functions of the dead zone angle where,

$$f(\alpha_2) = 1 + \alpha/16 + 5\alpha^2/36 + 2\alpha^3/19 \quad \text{--- (5.43)}$$

$f(\alpha_2)$ has been expressed as a 3rd order polynomial in terms of the data provided by Avitzur⁽²⁷⁾. It is noted, that $f(\alpha_2) \approx 1$ when $\alpha_2 < 45^\circ$.

These expressions are all suitably arranged within a for-next-loop in order to determine the minimum upper bound value for the internal work of deformation and, subsequently the corresponding dead zone angle. The stress equation (5.15) is calculated independently of the work done as follows,

$$\sigma_{(5)} = A (1 - BT_{H(5)}) \dot{\epsilon}_{(3-5)}^m \epsilon_{(1-3)}^n \quad \text{--- (5.44a)}$$

The homogeneous component of work done in equation (5.6) is then modified as follows,

$$\begin{aligned} W_{t(3-5)} &= \sigma_{m(3-5)} f(\alpha_2) \epsilon_{(3-5)} && \{W_h\} \\ &+ 2K_{m(3-5)} (\alpha_2/\sin^2(\alpha_2) - \cot(\alpha_2)) && \{W_R\} \\ &+ K_{m(3-5)} \cot(\alpha_2) \epsilon_{(3-5)} && \{W_f\}_d \\ &+ 2\tau_{m(3-5)} (2L_{(3-5)}/d_3 - (1 - d_5/d_3) \cot(\alpha_2)) && \{W_f\}_c \end{aligned}$$

where, $\sigma_{m(3-5)} = (\sigma_{(3)} + \sigma_{(5)}) / 2$

and, $\epsilon_{(3-5)} = 2\epsilon_{c(3-5)}$ strain at stages 3 to 5

$$\epsilon_{(3-5)} = 2\ln(d_3/d_5) \quad \text{if } d_3 > d_5$$

(note, that the equation 5.6 can be differentiated with respect to cone angle α_2 , where $\partial W / \partial \alpha_2 = 0$ for the turning point and the subsequent determination of cone angle corresponding to the minimum work done).

A third subroutine is set up to determine the total work of internal deformation (i.e. the abutment pressure), since the abutment pressure is determined from the summation of the work done in the die and primary extrusion chamber, see equation 5.10. The influence of the external frictional force is also computed using equation (5.30). The abutment pressure is then compared with the initial assumed value and the appropriate for-next-loop is provided in the program (i.e. the full cycle is repeated) for convergence to an acceptable level of accuracy. The work done at stages 3 to 5 is then compared with the initial value, and the cycle is again repeated for convergence until the desired level of accuracy is attained. Finally, the cycle is repeated in order to compare the last value of abutment pressure with the new, and also the last value of work done in the die chamber.

The die pressure is then determined using equation (5.40b) where friction is neglected at the container wall interface, i.e. $\{W\}_c = 0$. In other words, a single cycle in the program is repeated maintaining constant values for the previously determined values for internal work of deformation in the die chamber and primary extrusion chamber. Finally, the abutment force and die force are computed.

The data are presented in tabular form. The table includes

state corresponding to each stage in the deformation zone, the strain rates pertaining to each stage, grip length $L(2a-2b)$, abutment and die pressure, abutment and die force. The process variables are also presented.

The computation time for running a programme is dependent mainly on the power of the hardware and the programming language (software) used in the computation. The hardware used is an Apple MacPlus PC with 1 Mbyte of RAM and programmed in 'BASIC'. Therefore the computation time limited by the hardware and the software will be determined by the level of accuracy required, which is, in turn, determined by the acceptable difference between the two converging values concerned. In addition, the increment for the main variable α_2 (where $16^\circ < \alpha_2 < 90^\circ$ noting that the minimum value of $\alpha_2 = 16^\circ$ is determined by the geometry of the die chamber) will be selected by trial and error. This is because the computation time is considerably increased if smaller increments are selected. It is also expected that the turning point on the curve for the upper bound value against dead zone angle will give a flatter curve at the turning point, see fig 5.3. Consequently, it is considered inappropriate to select an increment value for $\alpha_2 < 1^\circ$. The software programme for the solution of the upper bound equations is detailed under appendix D6.

The procedure used to determine the minimum upper bound expression for the die chamber (i.e. by varying the dead zone angle α_2), should, in theory, be used to determine the minimum upper bound for the angle α_1 . However, the influence of the change in α_1 on the upper bound expression for work done is small in the range $25^\circ < \alpha_1 < 70^\circ$, see fig 5.1.

5.11 EQUATIONS USED FOR BASIC MACHINE DESIGN CRITERIA

The derivation of the analytical model detailed under sections 5.3 to 5.8 is considered complex, albeit a simplified analytical model in comparison with other modelling tools in particular, finite elements. However, in order to present a simplified model for basic machine design criteria it is necessary to modify the various equations detailed above into a user-friendly format, thereby enabling the tool and machine designer to select the appropriate material and component design to support a given load and temperature. In addition, since the analytical model has been complemented with experimental data, the value of the model in terms of industrial use should serve to provide a reliable model for machine design.

Initially, the dead zone angle variable α_2 in the die chamber can be selected from the equation after Sheppard⁽⁴⁶⁾ i.e.,

$$\alpha_2 = A + B \ln(\epsilon) \quad \text{--- (5.45)}$$

where, $A = 54.1$ and, $B = 3.45$

It is noted that the dead zone angle is a function of the strain ϵ and consequently, does not require iteration for the optimum dead zone angle.

Alternatively, the original Feltam equation (5.16) assumes a dead zone angle corresponding to 45° . In addition, the influence of the work done at stage 1 to 2a and the friction over the container wall ($\{W\}_c = 0$, if $d_4 \approx L_{(3-5)}$) in the die chamber is small and can therefore be neglected. The resulting upper bound expression for work done at the abutment (i.e. abutment pressure) is then reduced as follows,

$$\begin{aligned}
P_a = \sigma_{m(2b-3)} (1.15\epsilon_{(2b-3)} + 2.1) \\
+ \sigma_{m(3-5)} (1.15\epsilon_{(3-5)} + 0.66)
\end{aligned}
\quad \text{--- (5.46)}$$

The resulting expression for die pressure is,

$$P_d = \sigma_{m(3-5)} (1.15\epsilon_{(3-5)} + 0.66) \quad \text{--- (5.47)}$$

noting that, $f(\alpha_2) = 1$, when $\alpha_2 < 45^\circ$

The constitutive equations which describe the stress state corresponding to a particular stage in the deformation zone are inserted into the above equations. However, an iterative procedure is still required to solve for the temperature rise due to plastic deformation, friction and grip length at stages 2b to 3 and, 3 to 5, unless however, the temperature is determined from experimental data.

6.0 EXPERIMENTAL AND THEORETICAL TEST DATA LAYOUT

The details of a typical experimental set-up and procedure are given under section 3.4. The main variables under consideration are the die size, abutment depth setting and wheel speed. The dies used for these tests range from 1 to 9 mm diameter, the abutment depth settings used are 7, 8 and 9 mm, and wheel speeds range from 5 to 20 rev/min.

The test results are presented in a tabular form on pages 171 to 220. The tables are all headed with the geometric variables, which remain constant for each test i.e. die size, abutment depth setting. The wheel speed is increased during the course of each test, and is therefore listed in the tabulated section corresponding to deformation measurements.

The feed metal is commercial purity aluminium {spec: $99.3 \leq Al \leq 99.7$ }. The feed rod is supplied in the annealed and 50 % cold worked (i.e. 50 % cold work (4H) = half hard) condition. Test results are classified into two main categories i.e.,

6.1) Experimental data

6.1.1) Geometric constants and variables

6.1.2) Deformation

6.1.3) Loads and pressures

6.2) Theoretical data

6.2.1) Geometric variables

6.2.2) Deformation variables

6.2.3) Loads and pressures

The main variables in the following list are identified by the sign (†), and these are included in the tabulated data. The variables which are maintained constant in the present analysis are also identified and their corresponding values have been given in the following list.

6.1 EXPERIMENTAL DATA

Initially, the experimental test data are presented in terms of the deformation zone geometry i.e.,

6.1.1 GEOMETRIC CONSTANTS AND VARIABLES (MEASURED VALUES)

d_1 (mm) feed rod diameter = 9.6

d_2 (mm) mean diameter of primary extrusion chamber
(calculation based on measured value of abutment depth H and the exposed area A_a of the abutment tool appendix C5) (variable)

d_3 (mm) mean diameter of die chamber entry = 12.4

d_4 (mm) diameter of exposed die face = 13.5

d_5 (mm) diameter of product (\dagger)

$L_{(3-5)}$ (mm) length of die chamber = 14.0

$L_{(2b-2c)}$ (mm) arc length of primary chamber ahead of the die chamber = 18.0, see fig 5.0 for details.

$L_{(2a-2c)}$ (mm) arc length of primary chamber from entry to abutment tool face = 125 (135 mm inclusive of the tapered entry) (\dagger)

H (mm) abutment depth setting or penetration into wheel groove (\dagger)

R reduction ratio where, $R = 2 \ln(d_1/d_5)$ (\dagger)

shoe angle (deg) determines the clearance available for metal leakage (or flash) between the stationary tooling and the rotating wheel (\dagger)

C_a (mm) pre-set clearance between the abutment tool and die holder upper part (DHUP) (\dagger)

6.1.2 DEFORMATION (CALCULATIONS BASED ON MEASURED VALUES)

E (%) level of pre-strain (†)

$\epsilon_{(1-2a)} = 2\epsilon_{c(1-2a)}$ strain at stage 1 to 2a (†)

$$2\ln(d_1/d_2) \quad \text{if } d_1 > d_2$$

or, $2\ln(d_2/d_1)$ if $d_2 > d_1$

$\epsilon_{(2b-3)} = 2\epsilon_{c(2b-3)}$ strain at stage 2b to 3 (†)

$$2\ln(d_3/d_2) \quad \text{if } d_3 > d_2$$

$$2\ln(d_2/d_3) \quad \text{if } d_2 > d_3$$

$\epsilon_{(3-5)} = 2\epsilon_{c(3-5)}$ strain at stage 3 to 5 (†)

$$2\ln(d_3/d_5) \quad \text{if } d_3 > d_5$$

T_1 (°C) ambient temperature = 20 °C

T_d (°C) peripheral die temperature (†)

∂T_a (°C) temperature variation across abutment loadcell (†)

∂T_d (°C) temperature variation across die loadcell (†)

S (rev/min) wheel speed (†)

\dot{V}_1 (m/s) feed rod entry speed (†)

\dot{V}_{fl} (m/s) rate of flash removal by scraper tool (†)

\dot{V}_5 (m/s) exit speed of product from die (†)

Δ_f (kg) mass of product weighed after test (†)

Δ_i (kg) mass of feed stock weighed before test (†)

Δ_{fl} (kg) mass of flash weighed after test (†)

W_{fl} (mm) spread of flash across the peripheral wheel surface from the pre-set clearance between the stationary tooling and the rotating wheel (†)

6.1.3 LOADS AND PRESSURES (BASED ON MEASURED VALUES)

F_d (kN) die load (measured) (†)

F_a (kN) abutment load (measured) (†)

T (kNm) wheel torque (measured) (†)

P_d (MPa) die pressure (calculated from measured value using equation 5.32) (†)

P_{Ta} (MPa) abutment pressure (calculated from measured value using equation 5.31) (†)

6.2 THEORETICAL DATA (BASED ON CALCULATED VALUES)

The geometry of the deformation zone is defined under 1.1, however, an assumption is made in relation to the geometry at stage 3 in the theoretical analysis, i.e., $d_3 = d_4 = 13.5$ mm.

6.2.1 GEOMETRIC VARIABLES

$L_{(1a-2c)}$ (mm) length of primary extrusion chamber (equation 5.28) (†)

α_1 (deg) angle of dead zone at stages 2b to 3 (determined by iteration for minimum upper bound (equation 5.37) (†)

α_2 (deg) angle of dead zone at stages 3 to 5 (equation 5.44) (†)

W_{fl} (mm) spread of flash across wheel surface (see appendix E4) (†)

t_{fl} (mm) clearance available for metal leakage (or flash) between the stationary tooling in the shoe and rotating wheel (†)

6.2.2 DEFORMATION VARIABLES (CALCULATED VALUES)

- E (%) level of pre-strain (†)
- $\sigma_{(2a)}$ state of stress at stages 2a (equation 5.36a) (†)
- $\sigma_{(2b)}$ state of stress at stages 2b (equation 5.36b) (†)
- $\sigma_{(3)}$ state of stress at stages 3 (equation 5.40a) (†)
- $\sigma_{(5)}$ state of stress at stages 5 (equation 5.43a) (†)
- $\dot{\epsilon}_{(2b-3)}$ strain rate in primary extrusion chamber i.e. stages 2b to 3 (equation 5.16) (†)
- $\dot{\epsilon}_{(3-5)}$ strain rate in die chamber i.e. stages 3 to 5 (equation 5.17) (†)
- \dot{V}_1 (m/s) feed rod entry speed (†)
- \dot{V}_{f1} (m/s) rate of flash removal by scraper tool $\approx V_1$
- \dot{V}_5 (m/s) exit speed of product from die (†)
- T_{2b}, T_{2c} ($^{\circ}\text{C}$) temperature increase due to friction in primary extrusion chamber (equation 5.20) (†)
- T_3 ($^{\circ}\text{C}$) temperature increase due to plastic deformation at stage 3 (equation 5.22) (†)
- T_5 ($^{\circ}\text{C}$) temperature increase due to plastic deformation at stage 5 (equation 5.22) (†)
- $\dot{\Delta}_f / \dot{\Delta}_i$ mass flow rate of product per unit mass flow rate of feed rod (†)

6.2.3 LOADS AND PRESSURES (CALCULATED VALUES)

- F_d (kN) die load (equation 5.32) (†)
- F_a (kN) abutment load (equation 5.31) (†)
- T (kNm) torque (equation 5.36) (†)
- P_d (MPa) die pressure (equation 5.44) (†)
- P_a (MPa) abutment pressure (equation 5.38) (†)

(6.3)

EXPERIMENTAL TABULATED DATA

EXPERIMENTAL TEST DATA

Test No	1e			2e	
d_5 (mm)	6			3	
H_a (mm)	8			8	
R	2.4			10.2	
Shoe angle	75°			75°	
C_a (mm)	0.4/0.6			0.4/0.6	
E (%)	0			0	
$\epsilon_{(1-2a)}$	0.06			0.06	
$\epsilon_{(2b-3)}$	0.74			0.74	
$\epsilon_{(3-5)}$	1.55			3.00	
T_1 (°C)	16			17	
T_d (°C)	340	373		484	408
δT_a (°C)	6	5		5	6
δT_d (°C)	17	21		18	23
S (rev/min)	5.2	7.8		5.0	7.8
\dot{V}_1 (m/s)	-			-	
\dot{V}_5 (m/s)	-			-	
Δ_f (kg)	-			-	
Δ_i (kg)	-			-	
Δ_{fl} (kg)	-			-	
W_{fl} (mm)	-			-	
F_d (kN)	24	22		-	-
F_a (kN)	65	61		73	75
T (kNm)	-	-		-	-
P_d (MPa)	269	247		-	-
P_{Ta} (MPa)	947	889		1064	1093

EXPERIMENTAL TEST DATA

Test No	3e		4e
d_5 (mm)	2		4
H_a (mm)	8		8
R	23.0		5.8
Shoe angle	75°		75°
C_a (mm)	0.4/0.6		0.4/0.6
E (%)	0		0
$\epsilon_{(1-2a)}$	0.06		0.06
$\epsilon_{(2b-3)}$	0.74		0.74
$\epsilon_{(3-5)}$	3.82		2.43
T_1 ($^\circ\text{C}$)	18		18
T_d ($^\circ\text{C}$)	387	409	369
δT_a ($^\circ\text{C}$)	3	4	4
δT_d ($^\circ\text{C}$)	17	-	18
S (rev/min)	5.0	7.7	5.0
\dot{V}_1 (m/s)	-		-
\dot{V}_5 (m/s)	-		-
Δ_f (kg)	-		-
Δ_i (kg)	-		-
Δ_{fl} (kg)	-		-
W_{fl} (mm)	-		-
F_d (kN)	-	-	-
F_a (kN)	78	76	67
T (kNm)	24	21	24
P_d (MPa)	-	-	-
P_{Ta} (MPa)	1137	1108	977

EXPERIMENTAL TEST DATA

Test No	5e		6e		
d_5 (mm)	5		7		
H_a (mm)	8		8		
R	3.7		1.9		
Shoe angle	75°		75°		
C_a (mm)	0.4/0.6		0.4/0.6		
E (%)	0		0		
$\epsilon_{(1-2a)}$	0.06		0.06		
$\epsilon_{(2b-3)}$	0.74		0.74		
$\epsilon_{(3-5)}$	1.98		1.31		
T_1 (°C)	18		19		
T_d (°C)	35		361	367	386
δT_a (°C)	2		5	9	8
δT_d (°C)	-		17	19	22
S (rev/min)	5.0		5.1	10.6	16.0
\dot{V}_1 (m/s)	-		0.087	0.173	0.280
\dot{V}_5 (m/s)	-		0.114	0.241	0.368
Δ_f (kg)	-		38.5	-	-
Δ_i (kg)	-		44.7		
Δ_{f1} (kg)	-		-		
W_{f1} (mm)	-		-		
F_d (kN)	-		-	-	-
F_a (kN)	58		54	53	52
T (kNm)	23		-	-	-
P_d (MPa)	-		-	-	-
P_{Ta} (MPa)	845		787	773	758

EXPERIMENTAL TEST DATA

Test No	7e			
d_5 (mm)	8			
H_a (mm)	8			
R	1.4			
Shoe angle	75°			
C_a (mm)	0.4/0.6			
E (%)	0			
$\epsilon_{(1-2a)}$	0.06			
$\epsilon_{(2b-3)}$	0.74			
$\epsilon_{(3-5)}$	1.04			
T_1 (°C)	18			
T_d (°C)	333	362	381	395
δT_a (°C)	6	9	9	10
δT_d (°C)	19	21	22	25
S (rev/min)	5.1	7.8	10.7	16.2
\dot{V}_1 (m/s)	0.091	0.135	0.158	0.269
\dot{V}_5 (m/s)	0.107	0.147	0.183	0.292
Δ_f (kg)	35.6	-	-	-
Δ_i (kg)	39.0			
Δ_{f1} (kg)	-			
W_{f1} (mm)	-			
F_d (kN)	-			
F_a (kN)	47	49	48	47
T (kNm)	22	21	19	19
P_d (MPa)	-			
P_{Ta} (MPa)	685	714	700	685

EXPERIMENTAL TEST DATA

Test No	10e			11e		
d_5 (mm)	2			3		
H_a (mm)	8			8		
R	23.0			10.2		
Shoe angle	75°			75°		
C_a (mm)	0.4/0.6			0.4/0.6		
E (%)	0			0		
$\epsilon_{(1-2a)}$	0.06			0.06		
$\epsilon_{(2b-3)}$	0.74			0.74		
$\epsilon_{(3-5)}$	3.82			3.00		
T_1 (°C)	20			17		
T_d (°C)	349	388	414	378	404	
δT_a (°C)	4	5	5	3	3	
δT_d (°C)	42	46	49	42	46	
S (rev/min)	5.1	7.8	10.6	5.1	7.8	
\dot{V}_1 (m/s)	0.095	0.142	-	0.095	0.140	
\dot{V}_5 (m/s)	1.220	1.930	-	0.439	0.787	
Δ_f (kg)	13.6			17.8		
Δ_i (kg)	23.6			27.3		
Δ_{fl} (kg)	10.3			-		
W_{fl} (mm)	-			-		
F_d (kN)	59	57	56	50	46	
F_a (kN)	75	76	78	64	63	
T (kNm)	25	22	21	25	22	
P_d (MPa)	421	407	400	368	338	
P_{Ta} (MPa)	1093	1108	1137	933	918	

EXPERIMENTAL TEST DATA

Test No	12e				13e			
d_5 (mm)	3				4			
H_a (mm)	8				8			
R	10.2				5.7			
Shoe angle	80°				75°			
C_a (mm)	0.4/0.6				0.4/0.6			
E (%)	0				0			
$\epsilon_{(1-2a)}$	0.06				0.06			
$\epsilon_{(2b-3)}$	0.74				0.74			
$\epsilon_{(3-5)}$	3.00				2.43			
T_1 ($^\circ\text{C}$)	17				18			
T_d ($^\circ\text{C}$)	382	416	454	485	332	364	398	449
δT_a ($^\circ\text{C}$)	3	4	4	4	4	5	6	7
δT_d ($^\circ\text{C}$)	46	48	50	54	45	50	51	52
S (rev/min)	5.0	7.7	13.3	18.8	5.1	7.8	13.3	18.9
\dot{V}_1 (m/s)	0.096	0.140	0.229	0.318	0.089	0.138	0.225	0.318
\dot{V}_5 (m/s)	0.559	1.016	1.676	2.362	0.138	0.483	0.914	1.500
Δ_f (kg)	-				40.2			
Δ_i (kg)	35.7				50.0			
Δ_{fl} (kg)	10.0				10.1			
W_{fl} (mm)	-				-			
F_d (kN)	47	44	43	45	37	34	35	33
F_a (kN)	62	61	61	59	69	70	64	67
T (kNm)	25	23	21	20	25	22	20	19
P_d (MPa)	346	324	316	331	282	259	267	252
P_{Ta} (MPa)	904	889	889	860	1006	1020	933	977

EXPERIMENTAL TEST DATA

Test No	14e				15e			
d_5 (mm)	5				2			
H_a (mm)	8				8			
R	3.7				23.0			
Shoe angle	75°				75°			
C_a (mm)	0.4/0.6				0.4/0.6			
E (%)	0				0			
$\epsilon_{(1-2a)}$	0.06				0.06			
$\epsilon_{(2b-3)}$	0.74				0.74			
$\epsilon_{(3-5)}$	1.98				3.82			
T_1 ($^\circ\text{C}$)	19				18			
T_d ($^\circ\text{C}$)	316	352	389	421	348	378	424	
δT_a ($^\circ\text{C}$)	2	2	3	4	3	4	4	
δT_d ($^\circ\text{C}$)	35	40	42	44	40	44	47	
S (rev/min)	5.0	7.8	13.4	18.8	5.1	7.9	13.3	
\dot{V}_1 (m/s)	0.087	0.138	0.234	0.310	0.092	0.138	0.229	
\dot{V}_5 (m/s)	0.223	0.343	0.689	0.970	0.914	1.372	2.210	
Δ_f (kg)	24.0				13.6			
Δ_i (kg)	29.0				26.0			
Δ_{f1} (kg)	5.5				12.7			
W_{f1} (mm)	-				26	26.5	27	
F_d (kN)	35	32	30	31	61	59	56	
F_a (kN)	62	62	61	61	73	71	74	
T (kNm)	24	22	20	19	25	22	20	
P_d (MPa)	282	258	242	250	436	421	400	
P_{Ta} (MPa)	904	904	889	889	1064	1035	1079	

EXPERIMENTAL TEST DATA

Test No	16e				17e			
d_5 (mm)	6				5			
H_a (mm)	8				8			
R	2.6				3.7			
Shoe angle	75°				75°			
C_a (mm)	0.4/0.6				0.4/0.6			
E (%)	0				0			
$\epsilon_{(1-2a)}$	0.06				0.06			
$\epsilon_{(2b-3)}$	0.74				0.74			
$\epsilon_{(3-5)}$	1.62				1.98			
T_1 ($^\circ\text{C}$)	17				19			
T_d ($^\circ\text{C}$)	326	359	397	424	315	347	376	412
δT_a ($^\circ\text{C}$)	2	3	4	4	2	3	4	4
δT_d ($^\circ\text{C}$)	37	42	45	47	40	44	46	48
S (rev/min)	5.1	7.9	13.4	18.9	5.1	7.8	13.4	19.0
\dot{V}_1 (m/s)	0.091	0.138	0.225	0.325	0.091	0.138	0.221	0.325
\dot{V}_5 (m/s)	0.140	0.216	0.381	0.559	0.165	0.259	0.438	0.622
Δ_f (kg)	37.0				17.4			
Δ_i (kg)	48.9				28.3			
Δ_{fl} (kg)	11.8				10.7			
W_{fl} (mm)	19	19	19	19	21	21	22	22
F_d (kN)	31	28	25	24	35	32	32	32
F_a (kN)	54	52	54	52	65	63	66	67
T (kNm)	23	21	20	19	23	20	19	18
P_d (MPa)	270	243	217	209	282	258	258	258
P_{Ta} (MPa)	787	758	787	758	947	918	962	977

EXPERIMENTAL TEST DATA

Test No	18e				19e			
d_5 (mm)	3				2			
Ha (mm)	7				7			
R	10.2				23.0			
Shoe angle	80°				80°			
C_a (mm)	0.4				0.4			
E (%)	0				0			
$\epsilon_{(1-2a)}$	0.2				0.22			
$\epsilon_{(2b-3)}$	0.90				0.90			
$\epsilon_{(3-5)}$	3.00				3.82			
T_1 ($^\circ\text{C}$)	19				17			
T_d ($^\circ\text{C}$)	379	407	438	468	342	382	411	446
δT_a ($^\circ\text{C}$)	2	1	3	2	10	6	5	6
δT_d ($^\circ\text{C}$)	41	42	45	47	41	44	48	50
S (rev/min)	5.1	7.9	13.3	18.8	5.2	7.8	13.4	18.8
\dot{V}_1 (m/s)	0.091	0.138	0.220	0.305	0.095	0.138	0.216	0.305
\dot{V}_5 (m/s)	0.320	0.559	1.054	1.499	0.584	0.978	1.803	2.667
Δ_f (kg)	12.7				9.1			
Δ_i (kg)	25.3				22.8			
Δ_{f1} (kg)	12.8				13.6			
W_{f1} (mm)	20				24			
F_d (kN)	62	60	57	57	75	74	72	70
F_a (kN)	56	55	55	56	63	61	60	62
T (kNm)	24	21	20	19	24	22	20	19
P_d (MPa)	456	441	419	419	536	529	514	500
P_{Ta} (MPa)	949	932	932	949	1068	1034	1017	1051

EXPERIMENTAL TEST DATA

Test No	20e				21e			
d_5 (mm)	4				5			
H_a (mm)	7				7			
R	5.8				3.7			
Shoe angle	80°				80°			
C_a (mm)	0.4				0.4			
E (%)	0				0			
$\epsilon_{(1-2a)}$	0.22				0.22			
$\epsilon_{(2b-3)}$	0.90				0.90			
$\epsilon_{(3-5)}$	2.43				1.98			
T_1 ($^\circ\text{C}$)	18				19			
T_d ($^\circ\text{C}$)	324	351	394	426	317	342	381	409
δT_a ($^\circ\text{C}$)	2	2	3	3	2	3	3	4
δT_d ($^\circ\text{C}$)	43	44	48	51	40	43	46	48
S (rev/min)	5.1	7.8	13.3	18.9	5.0	7.8	13.3	18.9
\dot{V}_1 (m/s)	0.091	0.138	0.225	0.305	0.087	0.138	0.225	0.305
\dot{V}_5 (m/s)	0.206	0.368	0.635	0.978	0.145	0.241	0.419	0.648
Δ_f (kg)	13.0				15.9			
Δ_i (kg)	23.9				26.7			
Δ_{f1} (kg)	10				10.8			
W_{f1} (mm)	20				21	20	19	
F_d (kN)	49	46	46	46	35	34	32	31
F_a (kN)	57	56	58	61	52	52	52	53
T (kNm)	23	21	20	19	22	20	19	18
P_d (MPa)	374	351	351	351	282	274	258	250
P_{Ta} (MPa)	966	949	983	1034	881	881	881	898

EXPERIMENTAL TEST DATA

Test No	22e				23e			
d_5 (mm)	6				3			
H_a (mm)	7				9			
R	2.6				10.2			
Shoe angle	80°				80°			
C_a (mm)	0.4				0.4			
E (%)	0				0			
$\epsilon_{(1-2a)}$	0.22				0.06			
$\epsilon_{(2b-3)}$	0.90				0.62			
$\epsilon_{(3-5)}$	1.62				3.00			
T_1 (°C)	18				19			
T_d (°C)	315	341	376	402	382	407	437	461
δT_a (°C)	2	3	4	4	3	4	4	5
δT_d (°C)	40	42	45	48	43	45	48	50
S (rev/min)	5.1	7.9	13.4	18.9	5.1	7.9	13.4	18.8
\dot{V}_1 (m/s)	0.091	0.138	0.230	0.315	0.091	0.138	0.230	0.318
\dot{V}_5 (m/s)	0.109	0.182	0.323	0.457	0.597	0.889	1.511	2.108
Δ_f (kg)	18.3				19.6			
Δ_i (kg)	28.7				26.1			
Δ_{f1} (kg)	10.5				6.4			
W_{f1} (mm)	18	19	19	-	19	19	19.5	20
F_d (kN)	31	28	27	25	52	48	47	47
F_a (kN)	53	51	51	51	83	82	81	82
T (kNm)	23	20	18	18	25	23	21	21
P_d (MPa)	270	243	235	217	382	353	346	346
P_{Ta} (MPa)	898	864	864	864	1061	1049	1036	1049

EXPERIMENTAL TEST DATA

Test No	24e				25e			
d_5 (mm)	6				2			
Ha (mm)	9				9			
R	2.6				23.0			
Shoe angle	85°				85°			
C_a (mm)	0.7				0.7			
E (%)	0				0			
$\epsilon_{(1-2a)}$	0.06				0.06			
$\epsilon_{(2b-3)}$	0.62				0.62			
$\epsilon_{(3-5)}$	1.62				1.98			
T_1 (°C)	19				17			
T_d (°C)	319	347	379	412	352	384	431	452
δT_a (°C)	3	4	5	5	4	4	5	7
δT_d (°C)	40	41	43	46	43	44	46	49
S (rev/min)	5.1	7.8	13.3	19.0	5.1	7.9	13.4	18.9
\dot{V}_1 (m/s)	0.091	0.135	0.206	0.325	0.091	0.138	-	-
\dot{V}_5 (m/s)	0.173	0.269	0.456	0.508	0.092	1.740		
Δ_f (kg)	26.5				15.8			
Δ_i (kg)	29.0				23.0			
Δ_{fl} (kg)	2.7				7.0			
W_{fl} (mm)	11	11	12	-	18	18.5		
F_d (kN)	30	27	24	25	74	70	77	75
F_a (kN)	80	79	74	73	91	88	92	91
T (kNm)	24	22	19	19	26	24	23	21
P_d (MPa)	261	235	209	217	529	300	550	536
P_{Ta} (MPa)	1023	1010	946	934	1164	1125	1176	1164

EXPERIMENTAL TEST DATA

Test No	26e				27e			
d_5 (mm)	4				5			
H_a (mm)	9				9			
R	5.8				3.7			
Shoe angle	85°				85°			
C_a (mm)	0.7				0.7			
E (%)	0				0			
$\epsilon_{(1-2a)}$	0.06				0.06			
$\epsilon_{(2b-3)}$	0.74				0.74			
$\epsilon_{(3-5)}$	1.62				1.98			
T_1 (°C)	19				18			
T_d (°C)	329	354	389	426	323	347	389	415
δT_a (°C)	3	3	4	5	3	4	4	5
δT_d (°C)	40	41	45	46	40	42	45	47
S (rev/min)	5.1	7.8	13.3	18.9	5.1	7.8	13.4	18.9
\dot{V}_1 (m/s)	0.091	0.138	0.206	-	0.091	0.138	0.224	0.320
\dot{V}_5 (m/s)	0.394	0.597	0.067	-	0.229	0.389	0.673	0.965
Δ_f (kg)	24.8				25.9			
Δ_i (kg)	27.5				27.6			
Δ_{fl} (kg)	2.7				1.7			
W_{fl} (mm)	12	11	-	-	11	9	10	-
F_d (kN)	39	38	36	38	32	31	30	31
F_a (kN)	72	73	75	74	69	72	68	69
T (kNm)	24	22	20	19	23	21	20	19
P_d (MPa)	298	290	275	290	258	250	242	250
P_{Ta} (MPa)	921	934	959	946	882	921	870	882

EXPERIMENTAL TEST DATA

Test No	30e			31e		
d_5 (mm)	9			9		
H_a (mm)	9			9		
R	5.8			3.7		
Shoe angle	90°			90°		
C_a (mm)	0.5			0.5		
E (%)	50			50		
$\epsilon_{(1-2a)}$	0.06			0.06		
$\epsilon_{(2b-3)}$	0.62			0.62		
$\epsilon_{(3-5)}$	0.81			1.62		
T_1 ($^\circ\text{C}$)	18			18		
T_d ($^\circ\text{C}$)	334	361	391	349	366	
δT_a ($^\circ\text{C}$)	4	4	3	4	4	
δT_d ($^\circ\text{C}$)	44	47	49	48	49	
S (rev/min)	5.1	7.8	13.3	5.1	7.9	
\dot{V}_1 (m/s)	0.091	0.135	0.229	0.091	0.138	
\dot{V}_5 (m/s)	0.090	0.137	0.230	0.203	0.305	
Δ_f (kg)	13.3			10.1		
Δ_i (kg)	13.5			10.2		
Δ_{fl} (kg)	0.2			-		
W_{fl} (mm)	-			-		
F_d (kN)	13	11	12	23	22	
F_a (kN)	69	65	65	74	71	
T (kNm)	23	21	20	30	24	
P_d (MPa)	163	138	138	200	191	
P_{Ta} (MPa)	882	831	831	946	908	

EXPERIMENTAL TEST DATA

Test No	32e			33e		
d_5 (mm)	2			9		
H_a (mm)	9			8		
R	23.0			1.1		
Shoe angle	90°			90°		
C_a (mm)	0.6			0.6		
E (%)	50			50		
$\epsilon_{(1-2a)}$	0.06			0.06		
$\epsilon_{(2b-3)}$	0.62			0.62		
$\epsilon_{(3-5)}$	3.82			0.81		
T_1 ($^\circ\text{C}$)	18			17		
T_d ($^\circ\text{C}$)	398	419		366	412	
δT_a ($^\circ\text{C}$)	4	6		2	3	
δT_d ($^\circ\text{C}$)	52	54		49	53	
S (rev/min)	5.1	7.8		5.2	7.9	
\dot{V}_1 (m/s)	0.091	0.135		0.095	0.138	
\dot{V}_5 (m/s)	0.194	1.816		0.087	0.126	
Δ_f (kg)	7.2			10.1		
Δ_i (kg)	8.6			10.2		
Δ_{f1} (kg)	1.3			0.1		
W_{f1} (mm)	21			-		
F_d (kN)	61	60		14	12	
F_a (kN)	85	86		60	61	
T (kNm)	31	26		29	26	
P_d (MPa)	436	429		175	150	
P_{Ta} (MPa)	1087	1100		875	889	

EXPERIMENTAL TEST DATA

Test No	34e			35e		
d_5 (mm)	6			2		
H_a (mm)	8			8		
R	2.6			23.0		
Shoe angle	90°			90°		
C_a (mm)	0.5			0.5		
E (%)	50			50		
$\epsilon_{(1-2a)}$	0.06			0.06		
$\epsilon_{(2b-3)}$	0.74			0.74		
$\epsilon_{(3-5)}$	1.62			3.82		
T_1 ($^\circ\text{C}$)	19			18		
T_d ($^\circ\text{C}$)	388	438	478	406	449	
δT_a ($^\circ\text{C}$)	4	5	6	9	-	
δT_d ($^\circ\text{C}$)	51	54	58	48	51	
S (rev/min)	5.2	7.9	13.4	5.1	7.9	
\dot{V}_1 (m/s)	0.095	0.138	-	0.091	0.138	
\dot{V}_5 (m/s)	0.178	0.267	-	0.965	1.537	
Δ_f (kg)	9.4			6.6		
Δ_i (kg)	9.7			9.1		
Δ_{fl} (kg)	0.2			2.4		
W_{fl} (mm)	-			24		
F_d (kN)	22	21	46	68	64	
F_a (kN)	62	63	65	78	79	
T (kNm)	31	26	24	34	30	
P_d (MPa)	191	183	200	591	557	
P_{Ta} (MPa)	904	918	948	1137	1152	

EXPERIMENTAL TEST DATA

Test No	36e			37e	
d_5 (mm)	9			2	
H_a (mm)	8			7	
R	1.1			23.0	
Shoe angle	90°			90°	
C_a (mm)	0.5			0.4	
E (%)	50			50	
$\epsilon_{(1-2a)}$	0.06			0.22	
$\epsilon_{(2b-3)}$	0.74			0.90	
$\epsilon_{(3-5)}$	0.81			3.82	
T_1 ($^\circ\text{C}$)	20			21	
T_d ($^\circ\text{C}$)	355	389	428	429	
δT_a ($^\circ\text{C}$)	5	6	6	4	
δT_d ($^\circ\text{C}$)	43	45	46	42	
S (rev/min)	5.1	7.8	13.5	5.1	
\dot{V}_1 (m/s)	-	0.138	0.229	0.091	
\dot{V}_5 (m/s)	-	0.125	0.208	0.660	
Δ_f (kg)	9.9			3.1	
Δ_i (kg)	10.3			4.3	
Δ_{fl} (kg)	0.3			1.1	
W_{fl} (mm)	-			12	
F_d (kN)	31	29	27	68	
F_a (kN)	65	67	69	60	
T (kNm)	31	28	25	32	
P_d (MPa)	387	362	338	486	
P_{Ta} (MPa)	904	918	1006	1017	

EXPERIMENTAL TEST DATA

Test No	38e		39e			
d_5 (mm)	6		9			
H_a (mm)	7		7			
R	2.6		1.1			
Shoe angle	90°		90°			
C_a (mm)	0.4		0.4			
E (%)	50		50			
$\epsilon_{(1-2a)}$	0.22		0.22			
$\epsilon_{(2b-3)}$	0.90		0.90			
$\epsilon_{(3-5)}$	1.62		0.81			
T_1 (°C)	22		22			
T_d (°C)	395		389	432	398	
δT_a (°C)	2		3	3	4	
δT_d (°C)	41		42	45	40	
S (rev/min)	5.2		5.2	7.8	5.2	
\dot{V}_1 (m/s)	0.095		0.095	0.120	-	
\dot{V}_5 (m/s)	0.140		0.075	1.110	-	
Δ_f (kg)	3.0		9.1			
Δ_i (kg)	3.7		10.3			
Δ_{fl} (kg)	0.6		1.0			
W_{fl} (mm)	-		10			
F_d (kN)	20		13	15	16	
F_a (kN)	58		62	62	59	
T (kNm)	30		32	27	30	
P_d (MPa)	174		163	187	200	
ρ_{fa} (MPa)	983		1051	1051	1000	

EXPERIMENTAL TEST DATA

Test No	40e				41e			
d_5 (mm)	9				6			
H_a (mm)	8				8			
R	1.14				2.6			
Shoe angle	90°				90°			
C_a (mm)	0.4				0.4			
E (%)	0				0			
$\epsilon_{(1-2a)}$	0.06				0.06			
$\epsilon_{(2b-3)}$	0.74				0.74			
$\epsilon_{(3-5)}$	0.81				1.62			
T_1 ($^\circ\text{C}$)	17				18			
T_d ($^\circ\text{C}$)	358	388	438	370	360	392	440	368
δT_a ($^\circ\text{C}$)	1	2	1	1	5	6	6	4
δT_d ($^\circ\text{C}$)	40	42	44	40	40	39	42	35
S (rev/min)	5.1	7.8	13.4	5.1	5.0	7.8	13.3	5.0
\dot{V}_1 (m/s)	0.089	0.137	0.233	-	0.087	0.137	0.231	
\dot{V}_5 (m/s)	0.084	0.119	0.213		0.180	0.270	0.472	
Δ_f (kg)	23.4				11.9			
Δ_i (kg)	24.3				12.8			
Δ_{f1} (kg)	0.6				0.9			
W_{f1} (mm)	10				8	8	8	
F_d (kN)	67	13	14	12	22	20	21	22
F_a (kN)	62	66	68	59	72	70	73	68
T (kNm)	28	25	23	26	28	23	21	25
P_d (MPa)	175	163	175	150	191	174	183	191
P_{Ta} (MPa)	977	962	991	860	1050	1020	1064	991

EXPERIMENTAL TEST DATA

Test No	42e			43e		
d_5 (mm)	4			4		
H_a (mm)	8			8		
R	5.8			5.8		
Shoe angle	90°			90°		
C_a (mm)	0.4			0.4		
E (%)	0			0		
$\epsilon_{(1-2a)}$	0.06			0.06		
$\epsilon_{(2b-3)}$	0.74			0.74		
$\epsilon_{(3-5)}$	2.43			2.43		
T_1 ($^\circ\text{C}$)	17			18		
T_d ($^\circ\text{C}$)	400	440		397	428	
δT_a ($^\circ\text{C}$)	3	5		3	3	
δT_d ($^\circ\text{C}$)	32	34		34	36	
S (rev/min)	5.1	7.9		5.1	7.9	
\dot{V}_1 (m/s)	0.089			0.090	0.130	
\dot{V}_5 (m/s)	0.31			0.360	0.510	
Δ_f (kg)	7.9			9.3		
Δ_i (kg)	10.3			11.1		
Δ_{fl} (kg)	2.5			1.8		
W_{fl} (mm)	30			16		
F_d (kN)	-	-		47	45	
F_a (kN)	76	76		82	85	
T (kNm)	-	-		29	24	
P_d (MPa)	-	-		359	344	
P_{Ta} (MPa)	1108	1108		1195	1239	

EXPERIMENTAL TEST DATA

Test No	44e			45e			
d_5 (mm)	2			9			
H_a (mm)	8			7			
R	23.0			1.1			
Shoe angle	90°			90°			
C_a (mm)	0.4			0.4			
E (%)	0			0			
$\epsilon_{(1-2a)}$	0.06			0.22			
$\epsilon_{(2b-3)}$	0.74			0.90			
$\epsilon_{(3-5)}$	3.82			0.81			
T_1 ($^\circ\text{C}$)	17			18			
T_d ($^\circ\text{C}$)	405	445		368	428	380	
δT_a ($^\circ\text{C}$)	4	5		2	3	2	
δT_d ($^\circ\text{C}$)	30	31		33	35	32	
S (rev/min)	5.1	7.9		5.1	7.9	5.0	
\dot{V}_1 (m/s)	0.082	0.131		0.082	0.130	-	
\dot{V}_5 (m/s)	0.911	1.371		0.072	0.103	-	
Δ_f (kg)	6.3			-			
Δ_i (kg)	8.6			9.8			
Δ_{f1} (kg)	2.1			1.6			
W_{f1} (mm)	40	-		11			
F_d (kN)	65	66		13	15	13	
F_a (kN)	84	86		52	57	49	
T (kNm)	32	28		30	27	26	
P_d (MPa)	458	465		163	188	163	
P_{Ta} (MPa)	1224	1254		881	966	831	

EXPERIMENTAL TEST DATA

Test No	46e			47e	
d_5 (mm)	4			2	
H_a (mm)	7			7	
R	5.8			23.0	
Shoe angle	90°			90°	
C_a (mm)	0.3			0.3	
E (%)	0			0	
$\epsilon_{(1-2a)}$	0.22			0.22	
$\epsilon_{(2b-3)}$	0.90			0.90	
$\epsilon_{(3-5)}$	2.43			3.82	
T_1 ($^\circ\text{C}$)	18			18	
T_d ($^\circ\text{C}$)	408	443	413	430	
δT_a ($^\circ\text{C}$)	2	6	1	3	
δT_d ($^\circ\text{C}$)	36	38	36	40	
S (rev/min)	5.1	7.9	5.1	5.1	
\dot{V}_1 (m/s)	0.084	0.138		-	
\dot{V}_5 (m/s)	0.281			-	
Δ_f (kg)	6.2			2.8	
Δ_i (kg)	-			4	
Δ_{f1} (kg)	2			1.1	
W_{f1} (mm)	18			15	
F_d (kN)	35	34	34	69	
F_a (kN)	64	66	65	64	
T (kNm)	30	27	30	33	
P_d (MPa)	267	260	260	493	
P_{Ta} (MPa)	1085	1119	1034	1085	

EXPERIMENTAL TEST DATA

Test No	48e			49e		
d_5 (mm)	6			9		
H_a (mm)	7			9		
R	2.6			1.1		
Shoe angle	90°			90°		
C_a (mm)	0.3			0.5		
E (%)	0			0		
$\epsilon_{(1-2a)}$	0.22			0.06		
$\epsilon_{(2b-3)}$	0.90			0.62		
$\epsilon_{(3-5)}$	1.62			0.81		
T_1 ($^\circ\text{C}$)	18			18		
T_d ($^\circ\text{C}$)	370	411	379	319	341	326
δT_a ($^\circ\text{C}$)	2	1	1	1	1	1
δT_d ($^\circ\text{C}$)	38	38	34	37	37	35
S (rev/min)	5.2	7.9	5.0	5.1	7.9	5.1
\dot{V}_1 (m/s)	0.081	-	-	0.086	-	-
\dot{V}_5 (m/s)	0.137	-	-	0.081	-	-
Δ_f (kg)	10			13.9		
Δ_i (kg)	12.3			-		
Δ_{fl} (kg)	2			0.4		
W_{fl} (mm)	10			6		
F_d (kN)	22	24	26	15	12	13
F_a (kN)	48	49	45	78	76	74
T (kNm)	29	26	28	23	20	23
P_d (MPa)	191	209	226	188	150	163
P_{Ta} (MPa)	814	831	763	997	972	946

EXPERIMENTAL TEST DATA

Test No	50e			51e		
d_5 (mm)	6			4		
H_a (mm)	7			9		
R	2.6			5.8		
Shoe angle	90°			90°		
C_a (mm)	0.5			0.5		
E (%)	0			0		
$\epsilon_{(1-2a)}$	0.22			0.06		
$\epsilon_{(2b-3)}$	0.62			0.62		
$\epsilon_{(3-5)}$	1.62			2.43		
T_1 (°C)	19			17		
T_d (°C)	319	341	326	325	355	3 31
δT_a (°C)	1	1	1	2	3	2
δT_d (°C)	37	37	35	36	37	33
S (rev/min)	5.1	7.9	5.1	5.1	7.9	5.1
\dot{V}_1 (m/s)	0.086	0.140		0.086	0.137	
\dot{V}_5 (m/s)	0.178	0.274		0.343	0.635	
Δ_f (kg)	9.8			9.3		
Δ_i (kg)	-			10.7		
Δ_{f1} (kg)	0.5			1.3		
W_{f1} (mm)	8			13		
F_d (kN)	35	37	37	43	40	39
F_a (kN)	82	84	81	89	89	85
T (kNm)	24	23	25	25	22	23
P_d (MPa)	304	322	322	328	305	298
P_{Ta} (MPa)	1049	1074	1036	1138	1138	1087

EXPERIMENTAL TEST DATA

Test No	52e			53e		
d_5 (mm)	2			4		
H_a (mm)	9			9		
R	23.0			5.8		
Shoe angle	90°			90°		
C_a (mm)	0.5			0.5		
E (%)	0			0		
$\epsilon_{(1-2a)}$	0.06			0.06		
$\epsilon_{(2b-3)}$	0.62			0.62		
$\epsilon_{(3-5)}$	3.82			2.43		
T_1 ($^\circ\text{C}$)	18			19		
T_d ($^\circ\text{C}$)	345	375		332	356	
δT_a ($^\circ\text{C}$)	4	5		4	4	
δT_d ($^\circ\text{C}$)	31	33		34	35	
S (rev/min)	5.1	8.0		5.1	7.9	
\dot{V}_1 (m/s)	0.086			0.089		
\dot{V}_5 (m/s)	1.020			0.381		
Δ_f (kg)	7.7			6.2		
Δ_i (kg)	10.2			9.8		
Δ_{fl} (kg)	2.5			0.9		
W_{fl} (mm)	18			15		
F_d (kN)	72	70		45	41	
F_a (kN)	101	103		94	92	
T (kNm)	28	25		26	24	
P_d (MPa)	514	500		343	313	
P_{Ta} (MPa)	1292	1317		1202	1176	

EXPERIMENTAL TEST DATA

Test No	54e		55e	
d_5 (mm)	4		1	
H_a (mm)	9		9	
R	5.8		92	
Shoe angle	90°		90°	
C_a (mm)	0		0.5	
E (%)	0		0	
$\epsilon_{(1-2a)}$	0.06		0.06	
$\epsilon_{(2b-3)}$	0.62		0.62	
$\epsilon_{(3-5)}$	2.43		5.21	
T_1 ($^\circ\text{C}$)	18		20	
T_d ($^\circ\text{C}$)	328		395	
δT_a ($^\circ\text{C}$)	4		5	
δT_d ($^\circ\text{C}$)	31		37	
S (rev/min)	5.1		5.1	
\dot{V}_1 (m/s)	-		-	
\dot{V}_5 (m/s)	-		-	
Δ_f (kg)	4.8		2.1	
Δ_i (kg)	-		-	
Δ_{f1} (kg)	0.7		0.4	
W_{f1} (mm)	13		40	
F_d (kN)	42		106	
F_a (kN)	96		107	
T (kNm)	26		30	
P_d (MPa)	321		746	
P_{Ta} (MPa)	1228		1368	

(6.4)

THEORETICAL TABULATED DATA

ANALYTICAL TEST DATA

Test No.	1a				2a		3a	
d ₅	2				2		2	
H	7				7		7	
R	23.0				23.0		23.0	
A _a	59				59		59	
E	0	0	0	0	0	0	50	50
L _(2a-2c)	92	91	90	89	95	92	89	91
α ₁	58.1	58.1	58.1	58.1	58.1	58.1	58.1	58.1
α ₂	52	52	52	52	52	52	52	52
T _{2b}	196	193	191	192	200	195	200	204
T ₃	297	301	305	309	293	298	307	304
T ₅	440	464	481	490	418	449	450	430
S	5	7.9	13.4	20	5	7.9	5.0	5.0
v̇ ₁	0.087	0.138	0.235	0.350	0.087	0.138	0.087	0.087
v̇ ₅	2.020	3.193	5.416	8.083	1.475	2.33	2.020	1.515
Δ _f /Δ _i	1	1	1	1	0.73	0.73	1	0.75
σ _{1a}	109	109	109	109	109	109	116	116
σ _{2b}	75	76	76	76	74	75	87	86
σ ₃	95	96	97	98	94	95	95	95
σ ₅	78	76	75	74	81	77	78	80
ε̇ _(2b-3)	22	35	60	90	16	26	22	17
ε̇ ₍₃₋₅₎	96	152	259	386	70	111	96	72
w _{f1}	0	0	0	0	10.6	10.6	0	9.8
t _{f1}	0	0	0	0	1.84	1.84	0	1.84
F _d	69.5	67.5	66.1	65.8	71.8	68.8	69.0	71.2
F _a	64.8	64.0	63.7	63.7	63.7	64.5	66.7	67.7
T	20.2	19.8	19.8	19.8	24.9	24.2	24.2	25.0
P _d	496	480	473	471	513	490	493	509
P _a	925	909	902	901	944	919	944	962
P _{Ta}	1099	1085	1080	1080	1117	1094	1131	1147

ANALYTICAL TEST DATA

Test No.	4a				5a		6a	
d_5	2				2		2	
H	8				8		8	
R	23.0				23.0		23.0	
A_a	68.6				68.6		68.6	
E	0	0	0	0	0	0	50	50
$L_{(2a-2c)}$	113	110	109	109	115	112	95	97
α_1	54.6	54.6	54.6	54.6	54.6	54.6	54.6	54.6
α_2	52	52	52	52	52	52	52	52
T_{2b}	158	155	155	154	160	157	163	165
T_3	245	249	254	256	241	247	263	259
T_5	400	426	445	455	379	411	417	396
S	5	7.9	13.4	20	5	7.9	5.0	5.0
\dot{V}_1	0.087	0.138	0.235	0.350	0.087	0.138	0.087	0.087
\dot{V}_5	2.020	3.193	5.416	8.083	1.535	2.426	2.020	1.535
Δ_f/Δ_i	1	1	1	1	0.76	0.76	1	0.74
σ_{1a}	80	80	80	80	80	80	104	104
σ_{2b}	61	61	61	61	60	61	86	85
σ_3	99	100	101	102	99	100	100	100
σ_5	85	82	81	81	87	84	84	86
$\dot{\epsilon}_{(2b-3)}$	14	22	37	56	10	17	14	10
$\dot{\epsilon}_{(3-5)}$	96	152	259	386	73	116	96	73
w_{f1}	0	0	0	0	9.4	9.4	0	9.4
t_{f1}	0	0	0	0	1.84	1.84	0	1.84
F_d	75.0	72.9	72.0	72.2	77.2	74.0	74.6	76.7
F_a	75.9	74.8	75.5	74.7	77.0	75.4	80.2	81.3
T	21.9	21.6	21.5	21.6	27.0	26.2	23.4	27.6
P_d	537	522	515	515	550	530	532	547
P_a	940	923	917	919	957	932	976	994
P_{Ta}	1106	1091	1086	1089	1123	1099	1169	1186

ANALYTICAL TEST DATA

Test No.	7a				8a		9a	
d_5	2				2		2	
H	9				9		9	
R	23.0				23.0		23.0	
A_a	78.2				78.2		78.2	
E	0	0	0	0	0	0	50	50
$L_{(2a-2c)}$	105	102	101	101	107	103	92	93
α_1	51.3	51.3	51.3	51.3	51.3	51.3	51.3	51.3
α_2	52	52	52	52	52	52	52	52
T_{2b}	131	129	128	128	133	130	135	137
T_3	216	222	226	229	212	219	233	230
T_5	377	405	426	435	355	390	395	379
S	5	7.9	13.4	20	5	7.9	5	5
\dot{v}_1	0.087	0.138	0.235	0.350	0.087	0.138	0.087	0.087
\dot{v}_5	2.020	3.193	5.416	8.083	1.535	2.426	2.020	1.657
Δ_f/Δ_i	1	1	1	1	0.76	0.76	1	0.84
σ_{1a}	87	87	87	87	87	87	107	107
σ_{2b}	71	71	71	71	70	71	94	93
σ_3	102	102	103	104	102	102	103	103
σ_5	88	85	84	84	90	86	88	90
$\dot{\epsilon}_{(2b-3)}$	9	14	24	36	6	10	9	7
$\dot{\epsilon}_{(3-5)}$	96	152	259	386	73	116	96	79
w_{f1}	0	0	0	0	9.4	9.4	0	9.4
t_{f1}	0	0	0	0	1.84	1.84	0	1.84
F_d	77.9	75.8	74.9	74.7	79.8	76.8	73.3	79.9
F_a	89.6	88.3	87.7	88.0	90.9	89.0	94.9	95.9
T	24.3	24.0	23.8	23.9	29.3	28.5	25.8	29.2
P_d	556	541	534	534	570	549	559	570
P_a	965	947	940	942	982	957	1007	1021
P_{Ta}	1146	1129	1122	1125	1163	1138	1214	1277

ANALYTICAL TEST DATA

Test No.	10a				11a		12a	
d_5	3				3		3	
H	7				7		7	
R	10.2				10.2		10.2	
A_a	59				59		59	
E	0	0	0	0	0	0	50	50
$L_{(2a-2c)}$	87	85	84	84	88	86	83	85
α_1	58.1	58.1	58.1	58.1	58.1	58.1	58.1	58.1
α_2	48	48	44	44	48	48	48	48
T_{2b}	187	184	183	183	189	185	191	194
T_3	289	294	300	302	286	292	301	297
T_5	415	441	458	467	398	426	426	409
S	5	7.9	13.4	20	5	7.9	5	5
\dot{v}_1	0.087	0.138	0.235	0.350	0.087	0.138	0.087	0.087
\dot{v}_5	0.898	1.419	2.407	3.592	0.691	1.092	0.098	0.691
Δ_f/Δ_i	1	1	1	1	0.77	0.77	1	0.77
σ_{1a}	109	109	109	109	109	109	116	116
σ_{2b}	77	78	78	78	76	77	89	88
σ_3	97	98	99	100	97	97	97	97
σ_5	83	80	79	80	85	82	83	85
$\dot{\epsilon}_{(2b-3)}$	22	35	60	90	17	27	22	17
$\dot{\epsilon}_{(3-5)}$	66	91	155	231	51	80	66	51
w_{f1}	0	0	0	0	12.4	12.4	0	12.4
t_{f1}	0	0	0	0	1.33	1.33	0	1.84
F_d	59.2	59.0	57.8	58.1	60.7	58.2	58.9	60.5
F_a	62.1	61.3	61.1	61.3	62.8	61.8	64.0	64.8
T	19.3	19.1	19.0	19.0	24.3	23.7	19.9	24.8
P_d	435	432	426	427	445	429	433	444
P_a	874	860	855	858	886	868	894	907
P_{Ta}	1053	1040	1036	1040	1064	1047	1085	1098

ANALYTICAL TEST DATA

Test No.	13a				14a		15a	
d_5	2				2		2	
H	8				8		8	
R	23.0				23.0		23.0	
A_a	68.6				68.6		68.6	
E	0	0	0	0	0	0	50	50
$L_{(2a-2c)}$	104	103	102	102	105	103	88	89
α_1	54.5	54.5	54.5	54.5	54.5	54.5	54.5	54.5
α_2	48	48	48	48	48	48	48	48
T_{2b}	149	147	147	147	150	148	154	156
T_3	237	242	248	251	234	240	256	253
T_5	373	397	416	425	358	387	391	376
S	5	7.9	13.4	20	5	7.9	5	5
\dot{v}_1	0.087	0.138	0.235	0.350	0.087	0.138	0.087	0.087
\dot{v}_5	0.898	1.419	2.407	3.592	0.727	1.149	0.898	0.727
Δ_f/Δ_i	1	1	1	1	0.81	0.81	1	0.81
σ_{1a}	80	80	80	80	80	80	104	104
σ_{2b}	62	62	62	62	62	62	88	87
σ_3	101	102	103	104	101	102	101	101
σ_5	89	87	86	86	90	88	88	90
$\dot{\epsilon}_{(2b-3)}$	14	22	37	56	11	18	14	11
$\dot{\epsilon}_{(3-5)}$	66	105	178	266	53	85	66	53
w_{f1}	0	0	0	0	10.3	10.3	0	10.3
t_{f1}	0	0	0	0	1.33	1.33	0	1.33
F_d	63.6	62.3	61.5	61.5	64.7	62.8	63.1	64.3
F_a	71.9	71.0	70.8	71.2	72.5	71.3	76.3	77.0
T	20.7	20.5	20.4	20.5	25.7	25.0	22.0	26.4
P_d	467	456	452	453	474	460	463	472
P_a	878	866	862	865	887	870	916	927
P_{Ta}	1048	1036	1033	1038	1057	1040	1113	1123

ANALYTICAL TEST DATA

Test No.	16a				17a		18a	
d ₅	3				3		3	
H	9				9		9	
R	10.2				10.2		10.2	
A _a	78.2				78.2		78.2	
E	0	0	0	0	0	0	50	50
L _(2a-2c)	96	95	94	94	97	95	85	86
Q ₁	51.3	51.3	51.3	51.3	51.3	51.3	51.3	51.3
Q ₂	48	48	48	48	48	48	48	48
T _{2b}	123	122	122	122	124	122	128	130
T ₃	210	216	221	224	208	214	228	219
T ₅	350	376	394	404	335	366	368	350
S	5	7.9	13.4	20	5	7.9	5	5
v̇ ₁	0.087	0.138	0.235	0.350	0.087	0.138	0.087	0.087
v̇ ₅	0.898	1.419	2.407	3.592	0.736	1.163	0.898	0.736
Δ _f /Δ _i	1	1	1	1	0.82	0.82	1	0.82
σ _{1a}	87	87	87	87	87	87	107	107
σ _{2b}	72	72	72	72	72	72	95	95
σ ₃	103	103	104	105	103	103	105	106
σ ₅	91	89	89	89	93	90	92	95
ε̇ _(2b-3)	9	14	24	36	7	11	9	7
ε̇ ₍₃₋₅₎	66	105	178	266	54	86	66	54
w _{f1}	0	0	0	0	9.7	9.7	0	9.7
t _{f1}	0	0	0	0	1.33	1.33	0	1.33
F _d	65.5	64.2	63.3	63.5	66.3	64.6	66.0	68.0
F _a	84.4	83.3	83.2	83.4	85.1	83.7	89.8	91.6
T	22.9	22.6	22.5	22.6	27.5	26.8	24.3	28.8
P _d	481	882	879	881	906	887	939	961
P _a	940	923	917	919	957	932	976	994
P _{Ta}	1080	1066	1064	1067	1089	1071	1149	1172

ANALYTICAL TEST DATA

Test No.	19a				20a		21a	
d_5	4				4		4	
H	7				7		7	
R	5.8				5.8		5.8	
A_a	59				59		59	
E	0	0	0	0	0	0	50	50
$L_{(2a-2c)}$	81	80	80	80	82	80	78	79
α_1	58.1	58.1	58.1	58.1	58.1	58.1	58.1	58.1
α_2	40	40	40	40	40	40	40	40
T_{2b}	179	177	177	177	179	177	184	185
T_3	283	289	295	298	281	287	296	293
T_5	397	420	436	445	389	413	409	401
S	5	7.9	13.4	20	5	7.9	5	5
\dot{V}_1	0.087	0.138	0.235	0.350	0.087	0.138	0.087	0.087
\dot{V}_5	0.505	0.798	1.354	2.020	0.439	0.694	0.505	0.439
Δ_f/Δ_i	1	1	1	1	0.87	0.87	1	0.87
σ_{1a}	109	109	109	109	109	109	116	116
σ_{2b}	79	79	79	79	78	79	91	90
σ_3	99	99	100	101	98	99	99	99
σ_5	86	84	83	84	87	85	86	87
$\dot{\epsilon}_{(2b-3)}$	22	35	60	90	19	31	22	19
$\dot{\epsilon}_{(3-5)}$	41	65	110	165	35	56	41	35
w_{f1}	0	0	0	0	8.8	8.8	0	8.8
t_{f1}	0	0	0	0	1.05	1.05	0	1.05
F_d	51.5	50.3	50.0	49.8	52.1	50.5	51.3	51.9
F_a	59.7	59.2	59.1	59.3	60.0	59.3	61.6	61.9
T	18.5	18.3	18.3	18.4	21.9	21.5	19.2	22.4
P_d	481	882	879	881	906	887	939	961
P_a	395	385	382	383	399	388	393	397
P_{Ta}	1013	1003	1002	1006	1018	1006	1045	1050

ANALYTICAL TEST DATA

Test No.	22a				23a		24a	
d_5	4				4		4	
H	9				9		9	
R	5.8				5.8		5.8	
A_a	68.6				68.6		68.6	
E	0	0	0	0	0	0	50	50
$L_{(2a-2c)}$	97	96	95	95	98	96	83	83
α_1	54.5	54.5	54.5	54.5	54.5	54.5	54.5	54.5
α_2	40	40	40	40	40	40	40	40
T_{2b}	142	141	140	141	143	141	147	148
T_3	231	237	242	245	229	235	251	248
T_5	354	377	394	404	343	369	372	361
S	5	7.9	13.4	20	5	7.9	5	5
\dot{v}_1	0.087	0.138	0.235	0.350	0.087	0.138	0.087	0.087
\dot{v}_5	0.505	0.798	1.354	2.020	0.424	0.670	0.798	0.424
$\Delta f / \Delta_i$	1	1	1	1	0.84	0.84	1	0.84
σ_{1a}	80	80	80	80	80	80	104	104
σ_{2b}	63	63	63	63	63	63	89	89
σ_3	103	103	104	105	103	103	103	103
σ_5	91	90	89	90	93	90	91	92
$\dot{\epsilon}_{(2b-3)}$	14	22	37	56	11	18	14	11
$\dot{\epsilon}_{(3-5)}$	41	65	110	165	34	54	41	34
w_{f1}	0	0	0	0	10.9	10.9	0	10.9
t_{f1}	0	0	0	0	1.05	1.05	0	1.05
F_d	55.3	53.9	53.4	53.6	55.9	54.2	54.7	55.5
F_a	68.5	67.8	67.8	68.0	68.9	68.0	73.1	73.6
T	19.7	19.5	19.5	19.5	24.7	24.0	21.0	25.4
P_d	422	413	411	412	427	416	419	425
P_a	826	816	814	817	833	819	866	873
P_{Ta}	998	989	988	992	1005	992	1066	1073

ANALYTICAL TEST DATA

Test No.	25a				26a		27a	
d_5	4				4		4	
H	9				9		9	
R	5.8				5.8		5.8	
A_a	78.2				78.2		78.2	
E	0	0	0	0	0	0	50	50
$L_{(2a-2c)}$	90	88	88	88	91	89	79	80
α_1	51.3	51.3	51.3	51.3	51.3	51.3	51.3	51.3
α_2	40	40	40	40	44	40	40	40
T_{2b}	117	116	116	116	118	116	122	123
T_3	206	212	217	220	203	210	223	220
T_5	331	355	373	383	319	349	350	340
S	5	7.9	13.4	20	5	7.9	5	5
\dot{v}_1	0.087	0.138	0.235	0.350	0.087	0.138	0.087	0.087
\dot{v}_5	0.505	0.798	1.354	2.020	0.439	0.694	0.505	0.439
Δ_f/Δ_i	1	1	1	1	0.87	0.87	1	0.87
σ_{1a}	87	87	87	87	87	87	107	107
σ_{2b}	73	73	73	73	73	73	96	96
σ_3	104	104	105	106	104	104	106	106
σ_5	94	92	91	92	95	92	95	96
$\dot{\epsilon}_{(2b-3)}$	9	14	24	36	7	12	9	7
$\dot{\epsilon}_{(3-5)}$	41	65	110	165	41	56	41	35
w_{f1}	0	0	0	0	8.8	8.8	0	8.8
t_{f1}	0	0	0	0	1.05	1.05	0	1.05
F_d	56.6	55.4	54.9	55.1	56.0	55.6	57.3	57.8
F_a	80.2	79.4	79.2	79.4	80.8	79.6	85.8	86.2
T	21.7	21.5	21.4	21.5	25.7	25.0	23.2	26.8
P_d	433	424	421	422	427	426	437	442
P_a	840	829	826	829	848	832	884	891
P_{Ta}	1026	1016	1013	1016	1034	1018	1097	1103

ANALYTICAL TEST DATA

Test No.	28a				29a		30a	
d_5	5				5		5	
H	7				7		7	
R	3.7				3.7		3.7	
A_a	59				59		59	
E	0	0	0	0	0	0	50	50
$L_{(2a-2c)}$	77	77	76	76	78	76	75	75
α_1	58.1	58.1	58.1	58.1	58.1	58.1	58.1	58.1
α_2	36	36	36	36	36	36	36	36
T_{2b}	172	171	171	171	173	171	177	178
T_3	278	285	290	294	276	283	291	288
T_5	380	401	418	426	372	396	392	384
S	5	7.9	13.4	20	5	7.9	5	5
\dot{V}_1	0.087	0.138	0.235	0.350	0.087	0.138	0.087	0.087
\dot{V}_5	0.323	0.510	0.86	1.293	0.281	0.444	0.323	0.281
Δ_f/Δ_i	1	1	1	1	0.87	0.87	1	0.87
σ_{1a}	109	109	109	109	109	109	116	116
σ_{2b}	80	80	80	80	80	80	92	92
σ_3	100	100	101	102	10	100	100	100
σ_5	89	87	87	87	90	87	88	89
$\dot{\epsilon}_{(2b-3)}$	22	35	60	90	19	31	22	19
$\dot{\epsilon}_{(3-5)}$	29	47	80	119	26	41	29	26
w_{f1}	0	0	0	0	10.6	10.6	0	10.6
t_{f1}	0	0	0	0	0.88	0.88	0	0.88
F_d	43.6	42.7	42.4	42.5	44.0	42.9	49.5	43.9
F_a	57.8	57.3	57.3	57.6	58.0	57.4	59.7	60.0
T	17.9	17.7	17.7	17.8	21.8	21.3	18.5	22.3
P_d	354	346	344	345	357	348	352	356
t_a	795	786	785	788	799	788	815	821
P_{Ta}	980	972	972	976	984	973	1013	101

ANALYTICAL TEST DATA

Test No.	31a				32a		33a	
d_5	5				5		5	
H	8				8		8	
R	3.7				3.7		3.7	
A_a	68.6				68.6		68.6	
E	0	0	0	0	0	0	50	50
$L_{(2a-2c)}$	92	91	90	90	92	91	78	79
α_1	54.5	54.5	54.5	54.5	54.5	54.5	54.5	54.5
α_2	36	36	36	36	36	36	36	36
T_{2b}	136	135	135	135	137	135	142	142
T_3	227	233	238	241	225	232	247	245
T_5	336	358	374	383	328	352	355	349
S	5	7.9	13.4	20	5	7.9	5	5
\dot{V}_1	0.087	0.138	0.235	0.350	0.087	0.138	0.087	0.087
\dot{V}_5	0.323	0.510	0.866	1.293	0.284	0.449	0.323	0.294
Δ_f/Δ_i	1	1	1	1	0.88	0.88	1	0.91
σ_{1a}	80	80	80	80	80	80	104	104
σ_{2b}	64	64	64	64	64	64	90	90
σ_3	104	104	105	106	104	104	104	104
σ_5	94	92	92	93	95	93	94	94
$\dot{\epsilon}_{(2b-3)}$	14	22	37	56	112	19	14	12
$\dot{\epsilon}_{(3-5)}$	29	47	80	119	26	41	29	27
w_{f1}	0	0	0	0	9.8	9.8	0	7.3
t_{f1}	0	0	0	0	0.88	0.88	0	0.88
F_d	46.4	45.6	45.2	45.4	47.0	45.7	46.1	46.5
F_a	65.8	65.1	65.2	65.5	66.0	65.3	70.4	70.6
T	18.9	18.7	18.7	18.8	23.2	22.6	20.2	23.1
P_d	376	369	367	369	379	370	374	376
P_a	784	775	775	778	778	777	825	828
P_{Ta}	959	950	951	955	963	952	1027	1030

ANALYTICAL TEST DATA

Test No.	34a				35a		36a	
d_5	5				5		5	
H	9				9		9	
R	3.7				3.7		3.7	
A_a	78.2				78.2		78.2	
E	0	0	0	0	0	0	50	50
$L_{(2a-2c)}$	84	83	83	83	85	83	75	76
α_1	51.3	51.3	51.3	51.3	51.3	51.3	51.3	51.3
α_2	36	36	36	36	36	36	36	36
T_{2b}	113	111	111	112	113	112	117	118
T_3	201	208	213	216	200	207	219	218
T_5	313	336	353	361	309	332	331	328
S	5	7.9	13.4	20	5	7.9	5	5
\dot{v}_1	0.087	0.138	0.235	0.350	0.087	0.138	0.087	0.087
\dot{v}_5	0.323	0.510	1.866	2.293	0.300	0.475	0.323	0.307
Δ_f/Δ_i	1	1	1	1	0.93	0.93	1	0.95
σ_{1a}	87	87	87	87	87	87	107	107
σ_{2b}	73	74	74	74	73	74	97	97
σ_3	105	105	106	107	105	105	107	107
σ_5	96	94	94	94	96	95	97	97
$\dot{\epsilon}_{(2b-3)}$	9	14	24	36	8	13	9	8
$\dot{\epsilon}_{(3-5)}$	29	47	80	119	27	44	29	28
w_{f1}	0	0	0	0	5.7	5.7	0	4
t_{f1}	0	0	0	0	0.88	0.88	0	0.88
F_d	47.6	46.7	46.4	46.5	48.0	46.8	48.0	48.2
F_a	76.8	76.1	76.0	76.2	77.0	76.2	82.4	82.6
T	20.7	20.5	20.5	20.5	23.2	22.7	22.2	23.8
P_d	385	378	376	377	387	379	389	390
P_a	795	786	783	786	797	787	839	390
P_{Ta}	983	974	972	975	985	975	1054	1056

ANALYTICAL TEST DATA

Test No.	37a				38a		39a	
d_5	6				7		7	
H	7				7		7	
R	2.6				2.6		2.6	
A_a	59				59		59	
E	0	0	0	0	0	0	50	50
$L_{(2a-2c)}$	74	72	72	72	74	73	71	71
α_1	58.1	58.1	58.1	58.1	58.1	58.1	58.1	58.1
α_2	28	28	28	28	28	28	28	28
T_{2b}	166	166	164	165	167	165	171	171
T_3	273	280	285	290	272	278	286	284
T_5	369	389	406	414	363	384	381	375
S	5	7.9	13.4	20	5	7.9	5	5
\dot{v}_1	0.087	0.138	0.235	0.350	0.087	0.138	0.087	0.087
\dot{v}_5	0.244	0.354	0.601	0.898	0.199	0.315	0.224	0.202
Δ_f/Δ_i	1	1	1	1	0.89	0.89	1	0.90
σ_{1a}	109	109	109	109	109	109	116	116
σ_{2b}	81	81	81	81	81	81	94	94
σ_3	109	102	103	104	101	102	102	102
σ_5	91	89	89	89	91	89	91	91
$\dot{\epsilon}_{(2b-3)}$	22	35	60	90	20	31	22	20
$\dot{\epsilon}_{(3-5)}$	21	29	49	74	16	26	21	16
w_{fL}	0	0	0	0	10.4	10.4	0	9.4
t_{f1}	0	0	0	0	0.76	0.76	0	0.76
F_d	38.0	37.3	37.1	37.0	38.5	37.3	37.7	38.0
F_a	55.9	55.6	55.6	55.7	56.0	55.6	58.0	58.1
T	17.2	17.1	17.1	17.2	20.9	20.5	17.9	21.2
P_d	331	325	323	324	333	326	330	333
P_a	761	754	753	755	763	755	783	786
P_{Ta}	948	942	942	945	950	943	983	986

ANALYTICAL TEST DATA

Test No.	40a				41a		42a	
d_5	6				6		6	
H	8				8		8	
R	2.6				2.6		2.6	
A_a	68.6				68.6		68.6	
E	0	0	0	0	0	0	50	50
$L_{(2a-2c)}$	87	86	86	85	87	86	75	75
α_1	54.6	54.6	54.6	54.6	54.6	54.6	54.6	54.6
α_2	32	32	32	28	32	32	32	32
T_{2b}	131	130	130	130	131	130	137	137
T_3	223	229	234	237	222	228	243	242
T_5	319	340	356	370	315	337	339	336
S	5	7.9	13.4	20	5	7.9	5	5
\dot{v}_1	0.087	0.138	0.235	0.350	0.087	0.138	0.087	0.087
\dot{v}_5	0.224	0.354	0.601	0.898	0.208	0.329	0.224	0.215
Δ_f/Δ_i	1	1	1	1	0.93	0.93	1	0.96
σ_{1a}	80	80	80	80	80	80	104	104
σ_{2b}	65	65	65	65	65	65	91	91
σ_3	105	105	106	107	105	105	105	105
σ_5	96	96	95	94	97	95	96	96
$\dot{\epsilon}_{(2b-3)}$	14	22	37	56	13	20	14	13
$\dot{\epsilon}_{(3-5)}$	21	34	58	74	20	32	21	21
w_{fL}	0	0	0	0	6.6	6.6	0	3.7
t_{fL}	0	0	0	0	0.76	0.76	0	0.76
F_d	38.5	37.8	37.6	39.5	38.6	37.9	38.2	38.3
F_a	63.4	62.9	62.9	62.9	63.5	62.9	68.1	68.2
T	18.1	18.0	18.0	18.0	21.0	20.6	19.5	20.9
P_d	336	331	329	345	337	331	334	335
P_a	747	740	740	740	749	741	789	790
P_{Ta}	924	917	918	918	926	918	993	994

ANALYTICAL TEST DATA

Test No.	43a				44a		45a	
d ₅	6				6		6	
H	9				9		9	
R	2.6				2.6		2.6	
A _a	78.2				78.2		78.2	
E	0	0	0	0	0	0	50	50
L _(2a-2c)	87	86	86	85	87	86	75	75
α ₁	51.3	51.3	51.3	51.3	51.3	51.3	51.3	51.3
α ₂	32	32	32	32	32	32	32	32
T _{2b}	108	108	107	108	109	108	113	113
T ₃	198	205	210	213	197	204	216	215
T ₅	297	318	334	343	294	316	315	313
S	5	7.9	13.4	20	5	7.9	5	5
\dot{v}_1	0.087	0.138	0.235	0.350	0.087	0.138	0.087	0.087
\dot{v}_5	0.224	0.354	0.601	0.898	0.213	0.337	0.224	0.217
Δ _f /Δ _i	1	1	1	1	0.95	0.95	1	0.97
σ _{1a}	87	87	87	87	87	87	107	107
σ _{2b}	74	74	74	74	74	74	98	98
σ ₃	106	106	107	108	106	106	108	108
σ ₅	98	97	96	97	98	97	99	99
$\dot{\epsilon}_{(2b-3)}$	9	14	24	36	8	13	9	8
$\dot{\epsilon}_{(3-5)}$	25	34	58	87	20	32	21	21
w _{fL}	0	0	0	0	4.7	4.7	0	2.8
t _{f1}	0	0	0	0	0.76	0.76	0	0.76
F _d	39.3	38.6	38.4	38.7	39.4	38.7	39.7	39.8
F _a	73.9	73.2	73.2	73.5	74.0	73.3	79.4	79.6
T	19.9	19.7	19.7	19.8	21.8	21.5	21.4	22.5
P _d	343	338	336	337	344	338	347	348
P _a	755	748	746	749	757	748	800	801
P _{Ta}	945	937	936	940	946	936	1016	1018

ANALYTICAL TEST DATA

Test No.	46a				47a		48a	
d_5	7				7		7	
H	7				7		7	
R	1.9				1.9		1.9	
A_a	59				59		59	
E	0	0	0	0	0	0	50	50
$L_{(2a-2c)}$	70	70	69	69	70	70	68	68
α_1	58.1	58.1	58.1	58.1	58.1	58.1	58.1	58.1
α_2	24	24	32	24	24	24	24	24
T_{2b}	160	159	159	160	160	159	166	166
T_3	269	275	281	285	268	275	282	281
T_5	355	375	391	398	352	373	367	365
S	5	7.9	13.4	20	5	7.9	5	5
\dot{v}_1	0.087	0.138	0.235	0.350	0.087	0.138	0.087	0.087
\dot{v}_5	0.164	0.260	0.442	0.659	0.156	0.247	0.164	0.156
$\Delta f / \Delta_i$	1	1	1	1	0.95	0.95	1	0.95
σ_{1a}	109	109	109	109	109	109	116	116
σ_{2b}	82	82	82	82	82	82	95	95
σ_3	102	103	104	105	102	103	103	103
σ_5	93	91	91	92	93	92	93	93
$\dot{\epsilon}_{(2b-3)}$	22	35	60	90	21	34	22	21
$\dot{\epsilon}_{(3-5)}$	13	21	35	53	12	20	13	12
w_{fL}	0	0	0	0	5.3	5.3	0	5.3
t_{f1}	0	0	0	0	0.67	0.67	0	0.67
F_d	31.4	31.0	30.8	30.7	31.4	31.0	31.2	31.3
F_a	54.4	54.0	54.1	54.3	54.4	54.0	56.4	56.5
T	16.7	16.6	16.6	16.7	18.6	18.3	17.4	19.2
P_d	300	294	293	294	301	295	299	300
P_a	732	726	726	728	733	726	753	755
P_{Ta}	922	916	917	920	922	916	956	958

ANALYTICAL TEST DATA

Test No.	49a				50a		51a	
d_5	7				7		7	
H	8				8		8	
R	1.9				1.9		1.9	
A_a	68.6				68.6		68.6	
E	0	0	0	0	0	0	50	50
$L_{(2a-2c)}$	82	82	81	81	83	82	71	71
α_1	54.5	54.5	54.5	54.5	54.5	54.5	54.5	54.5
α_2	24	24	24	24	24	24	24	24
T_{2b}	126	125	125	126	126	125	132	132
T_3	219	225	231	234	218	225	239	239
T_5	310	330	346	354	307	328	329	327
S	5	7.9	13.4	20.3	5	7.9	5	5
\dot{v}_1	0.087	0.138	0.235	0.350	0.087	0.138	0.087	0.087
\dot{v}_5	0.164	0.260	0.442	0.659	0.156	0.747	0.164	0.156
Δ_f/Δ_i	1	1	1	1	0.95	0.95	1	0.97
σ_{1a}	80	80	80	80	80	80	104	104
σ_{2b}	65	65	65	65	65	65	92	92
σ_3	106	106	107	108	106	106	106	106
σ_5	98	96	96	96	98	96	97	98
$\dot{\epsilon}_{(2b-3)}$	14	22	37	56	13	21	14	13
$\dot{\epsilon}_{(3-5)}$	13	21	35	53	12	20	13	12
w_{fL}	0	0	0	0	5.3	5.3	0	5.3
t_{f1}	0	0	0	0	0.67	0.67	0	0.67
F_d	33.2	32.6	32.4	32.6	33.2	32.6	32.9	33.1
F_a	61.0	60.5	60.5	60.8	61.0	60.6	65.8	66.0
T	17.4	17.3	17.3	17.4	19.6	19.3	18.8	20.1
P_d	317	312	310	312	318	312	315	317
P_a	711	705	704	707	712	705	753	755
P_{Ta}	889	883	883	887	890	884	960	964

ANALYTICAL TEST DATA

Test No.	52a				53a		54a	
d_5	7				7		7	
H	9				9		9	
R	1.9				1.9		1.9	
A_a	78.2				78.2		78.2	
E	0	0	0	0	0	0	50	50
$L_{(2a-2c)}$	75	75	74	74	75	74	75	68
α_1	51.3	51.3	51.3	51.3	51.3	51.3	51.3	51.3
α_2	24	24	24	24	24	24	24	24
T_{2b}	104	104	104	104	105	104	109	109
T_3	195	202	207	210	194	201	213	212
T_5	288	308	324	332	285	306	306	304
S	5	7.9	13.4	20	5	7.9	5	5
\dot{v}_1	0.087	0.138	0.235	0.350	0.087	0.138	0.087	0.087
\dot{v}_5	0.164	0.260	0.442	0.659	0.156	0.247	0.164	0.156
Δ_f/Δ_i	1	1	1	1	0.95	0.95	1	0.95
σ_{1a}	87	87	87	87	87	87	107	107
σ_{2b}	75	75	75	75	75	75	99	99
σ_3	107	107	108	108	107	107	107	109
σ_5	9	97	96	97	98	97	99	99
$\dot{\epsilon}_{(2b-3)}$	9	14	24	36	8	13	9	8
$\dot{\epsilon}_{(3-5)}$	13	21	35	53	12	20	13	12
w_{fL}	0	0	0	0	5.3	5.3	0	5.3
t_{f1}	0	0	0	0	0.67	0.67	0	0.67
F_d	33.8	33.2	33.1	33.2	33.9	33.3	34.1	34.2
F_a	71.0	70.4	70.4	70.6	71.1	70.4	76.6	76.7
T	19.1	18.9	18.9	18.9	21.2	20.8	20.6	22.5
P_d	324	318	316	317	324	318	327	328
P_a	717	710	709	711	718	710	762	763
P_{Ta}	908	901	900	903	909	901	980	981

ANALYTICAL TEST DATA

Test No.	55a				56a		57a	
d_5	8				8		8	
H	7				7		7	
R	1.4				1.4		1.4	
A_a	59				59		59	
E	0	0	0	0	0	0	50	50
$L_{(2a-2c)}$	67	66	66	66	67	66	65	65
α_1	58.1	58.1	58.1	58.1	58.1	58.1	58.1	58.1
α_2	20	20	20	20	20	20	20	20
T_{2b}	156	155	155	155	156	155	161	161
T_3	266	273	279	282	265	272	278	278
T_5	343	362	376	384	339	360	355	352
S	5	7.9	13.4	20	5	7.9	5	5
\dot{v}_1	0.087	0.138	0.235	0.350	0.087	0.138	0.087	0.087
\dot{v}_5	0.126	0.199	0.338	0.505	0.119	0.189	0.126	0.119
Δ_f/Δ_i	1	1	1	1	0.95	0.95	1	0.95
σ_{1a}	109	109	109	109	109	109	116	116
σ_{2b}	83	83	83	83	83	83	96	96
σ_3	103	104	105	106	103	104	104	104
σ_5	95	93	93	94	95	93	95	95
$\dot{\epsilon}_{(2b-3)}$	22	35	60	90	21	34	22	21
$\dot{\epsilon}_{(3-5)}$	9	14	25	37	9	14	9	9
w_{FL}	0	0	0	0	5.9	5.9	0	5.9
t_{f1}	0	0	0	0	0.6	0.6	0	0.6
F_d	25.1	24.6	24.5	34.6	25.1	24.6	25.0	25.1
F_a	52.8	52.5	52.6	52.8	52.9	52.5	55.0	55.0
T	16.2	16.1	16.1	16.2	18.2	18.0	16.9	18.9
P_d	271	266	265	266	272	267	270	271
P_a	704	699	695	702	706	699	727	728
P_{Ta}	896	891	892	896	897	891	932	933

ANALYTICAL TEST DATA

Test No.	58a				59a		60a	
d_5	8				8		8	
H	8				8		8	
R	1.4				1.4		1.4	
A_a	68.6				68.6		68.6	
E	0	0	0	0	0	0	50	50
$L_{(2a-2c)}$	78	78	77	78	78	78	67	68
α_1	54.5	54.5	54.5	54.5	54.5	54.5	54.5	54.5
α_2	20	20	20	20	20	20	20	20
T_{2b}	122	121	121	122	122	121	128	128
T_3	216	222	227	231	215	221	236	235
T_5	297	317	331	339	294	315	317	315
S	5	7.9	13.4	20	5	7.9	5	5
\dot{v}_1	0.087	0.138	0.235	0.350	0.087	0.138	0.087	0.087
\dot{v}_5	0.126	0.199	0.338	0.505	0.119	0.189	0.126	0.119
$\Delta f / \Delta_i$	1	1	1	1	0.95	0.95	1	0.95
σ_{1a}	80	80	80	80	80	80	104	104
σ_{2b}	66	66	66	66	66	66	93	93
σ_3	107	107	108	109	107	107	107	107
σ_5	99	98	98	99	100	98	99	99
$\dot{\epsilon}_{(2b-3)}$	14	22	37	56	13	21	14	13
$\dot{\epsilon}_{(3-5)}$	9	14	25	37	9	14	9	9
w_{fL}	0	0	0	0	5.9	5.9	0	5.9
t_{f1}	0	0	0	0	0.6	0.6	0	0.6
F_d	26.7	26.2	26.0	26.2	26.7	26.2	26.5	26.6
F_a	59.0	58.6	58.7	58.9	59.0	58.6	63.8	63.9
T	16.2	16.7	16.7	16.8	19.2	18.9	18.2	20.3
P_d	286	282	281	282	287	282	284	285
P_a	680	674	675	677	681	675	723	724
P_{Ta}	860	855	856	859	861	855	931	932

ANALYTICAL TEST DATA

Test No.	61a				62a		63a	
d_5	8				8		8	
H	9				9		9	
R	1.4				1.4		1.4	
A_a	78.2				78.2		78.2	
E	0	0	0	0	0	0	50	50
$L_{(2a-2c)}$	71	71	70	70	71	71	65	65
α_1	51.3	51.3	51.3	51.3	51.3	51.3	51.3	51.3
α_2	20	20	20	20	20	20	20	20
T_{2b}	101	100	100	100	101	100	106	106
T_3	192	199	204	207	191	198	210	209
T_5	275	295	310	318	272	293	294	291
S	5	7.9	13.4	20	5	7.9	5	5
\dot{v}_1	0.087	0.138	0.235	0.350	0.087	0.138	0.087	0.087
\dot{v}_5	0.126	0.199	0.338	0.505	0.119	0.189	0.126	0.119
Δ_f/Δ_i	1	1	1	1	0.95	0.95	1	0.95
σ_{1a}	87	87	87	87	87	87	107	107
σ_{2b}	75	75	75	75	75	75	100	100
σ_3	108	108	108	109	108	108	109	109
σ_5	101	99	99	100	101	100	102	102
$\dot{\epsilon}_{(2b-3)}$	9	14	24	36	8	13	9	8
$\dot{\epsilon}_{(3-5)}$	9	14	25	37	9	14	9	9
w_{fL}	0	0	0	0	5.9	5.9	0	5.9
t_{f1}	0	0	0	0	0.6	0.6	0	0.6
F_d	27.2	26.7	26.6	26.7	27.3	26.7	27.5	27.6
F_a	68.5	68.0	68.0	68.2	68.6	68.1	74.2	74.3
T	18.4	18.2	18.2	18.3	20.6	20.3	19.9	22.0
P_d	292	287	285	286	293	287	292	296
P_a	684	678	677	679	686	678	729	731
P_{Ta}	876	870	870	873	878	871	949	950

ANALYTICAL TEST DATA

Test No.	64a				65a		66a	
d_5	9				9		9	
H	7				7		7	
R	1.1				1.1		1.1	
A_a	59				59		59	
E	0	0	0	0	0	0	50	50
$L_{(2a-2c)}$	64	64	64	63	64	64	62	62
α_1	58.1	58.1	58.1	58.1	58.1	58.1	58.1	58.1
α_2	16	16	16	16	16	16	16	16
T_{2b}	151	150	150	151	151	150	156	156
T_3	262	269	275	279	261	268	275	274
T_5	331	349	364	372	328	348	344	341
S	5	7.9	13.4	20	5	7.9	5	5
\dot{v}_1	0.087	0.138	0.235	0.350	0.087	0.138	0.087	0.087
\dot{v}_5	0.099	0.157	0.237	0.399	0.094	0.149	0.099	0.094
Δ_f/Δ_i	1	1	1	1	0.95	0.95	1	0.95
σ_{1a}	109	109	109	109	109	109	116	116
σ_{2b}	84	84	84	84	84	84	97	97
σ_3	104	105	106	107	104	105	105	105
σ_5	96	95	95	96	97	95	96	97
$\dot{\epsilon}_{(2b-3)}$	22	35	60	90	21	34	22	21
$\dot{\epsilon}_{(3-5)}$	6	10	17	26	6	9	6	6
w_{fL}	0	0	0	0	6.5	6.5	0	6.5
t_{f1}	0	0	0	0	0.55	0.55	0	0.55
F_d	19.5	19.2	19.2	19.3	19.6	19.3	19.5	19.5
F_a	51.4	51.2	51.2	51.5	51.5	51.2	53.6	53.7
T	15.8	15.7	15.7	15.8	17.9	17.7	16.5	18.6
P_d	245	241	240	241	246	241	245	245
P_a	679	674	674	677	690	674	702	703
P_{Ta}	872	868	869	873	873	868	909	910

ANALYTICAL TEST DATA

Test No.	67a				68a		69a	
d_5	9				9		9	
H	8				8		8	
R	1.1				1.1		1.1	
A_a	68.6				68.6		68.6	
E	0	0	0	0	0	0	50	50
$L_{(2a-2c)}$	75	74	74	74	75	74	64	65
α_1	54.5	54.5	54.5	54.5	54.5	54.4	54.4	54.5
α_2	16	16	16	16	16	16	16	16
T_{2b}	118	118	118	118	118	118	124	124
T_3	212	219	224	228	211	218	234	233
T_5	285	304	318	326	282	302	305	302
S	5	7.9	13.4	20	5	7.9	5	5
\dot{v}_1	0.087	0.138	0.235	0.350	0.087	0.138	0.087	0.087
\dot{v}_5	0.099	0.157	0.267	0.399	0.094	0.149	0.099	0.094
Δ_f/Δ_i	1	1	1	1	0.95	0.95	1	0.95
σ_{1a}	80	80	80	80	80	80	104	104
σ_{2b}	67	67	67	67	67	67	94	94
σ_3	108	108	109	109	108	108	108	108
σ_5	101	100	100	100	101	100	101	101
$\dot{\epsilon}_{(2b-3)}$	14	22	37	56	13	21	14	13
$\dot{\epsilon}_{(3-5)}$	6	10	17	26	6	9	6	6
w_{fL}	0	0	0	0	6.5	6.5	0	6.5
t_{f1}	0	0	0	0	0.55	0.55	0	0.55
F_d	20.6	20.3	20.2	20.3	20.6	20.3	20.3	20.4
F_a	57.1	56.8	56.8	57.0	57.2	56.8	62.0	62.1
T	16.2	16.1	16.1	16.2	18.8	18.5	17.7	19.9
P_d	259	255	254	255	259	255	257	258
P_a	651	646	646	649	653	646	685	696
P_{Ta}	833	828	828	832	834	828	904	905

ANALYTICAL TEST DATA

Test No.	70a				71a		72a	
d_5	9				9		9	
H	9				9		9	
R	1.1				1.1		1.1	
A_a	78.2				78.2		78.2	
E	0	0	0	0	0	0	50	50
$L_{(2a-2c)}$	68	67	67	67	68	67	62	62
α_1	51.3	51.3	51.3	51.3	51.3	51.3	51.3	51.3
α_2	16	16	16	16	16	16	16	16
T_{2b}	98	97	97	97	98	97	103	103
T_3	190	196	202	205	189	196	208	207
T_5	263	283	294	304	260	281	282	279
S	5	7.9	13.4	20	5	7.9	5	5
\dot{v}_1	0.087	0.138	0.235	0.350	0.087	0.138	0.087	0.087
\dot{v}_5	0.099	0.157	0.267	0.399	0.094	0.149	0.099	0.094
Δ_f/Δ_i	1	1	1	1	0.95	0.95	1	0.95
σ_{1a}	87	87	87	87	87	87	107	107
σ_{2b}	76	76	76	76	76	76	101	101
σ_3	108	108	109	110	108	108	101	101
σ_5	102	101	101	101	103	101	104	104
$\dot{\epsilon}_{(2b-3)}$	9	14	24	36	8	13	9	8
$\dot{\epsilon}_{(3-5)}$	6	10	9	26	6	9	6	6
w_{fL}	0	0	0	0	6.5	6.5	0	6.5
t_{f1}	0	0	0	0	0.55	0.55	0	0.55
F_d	20.8	20.6	20.5	20.6	20.9	20.6	21.0	21.1
F_a	847	65.7	65.7	66.0	66.3	65.8	71.9	72.0
T	17.7	17.6	17.6	17.6	20.1	19.8	19.3	21.5
P_d	263	259	258	259	264	259	266	267
P_a	654	648	647	650	655	648	699	700
P_{Ta}	847	841	841	844	848	842	920	921

7 DISCUSSION OF RESULTS

The subsequent discussion is focussed on the tabulated and graphical results detailed under section 6. It is considered necessary to separate these results under the appropriate subheadings in order to provide a clear understanding of the mechanics of deformation.

7.1 ABUTMENT FORCE

It is recalled under section (3.2.8) that there will be experimental error due to the ingress of feed metal into the clearance between the DHUP and the abutment tool holder, and its subsequent effect on the abutment tool force measurement. In other words, the load sensed by the abutment tool will vary depending on the magnitude of the pre-set clearance made available before each test. The graph of abutment force against pre-set clearance fig. 7.0 clearly illustrates the relationship for a typical reduction and abutment depth setting. It is observed that there is a small variation in force corresponding to a significant change in pre-set clearance in the range 0 - 1.0 mm. It should be noted that the DHUP was clamped tightly up against the abutment tool holder for pre-set clearance in the zero condition.

An explanation for this phenomenon is that thermal expansion of the tooling segment is sufficient to cause a high degree of interference between the grip segment and its seat in the shoe. This is because there is good tight fit between the grip segment and the shoe at ambient temperature. The temperature of the grip segment was measured by a thermocouple probe to be above 300 °C, corresponding to minimum reduction and speed at steady state conditions. Therefore it is considered that the tangential force was not sufficient to overcome the normal force generated by the interference fit, and as a consequence, placed no additional loading on the abutment tool.

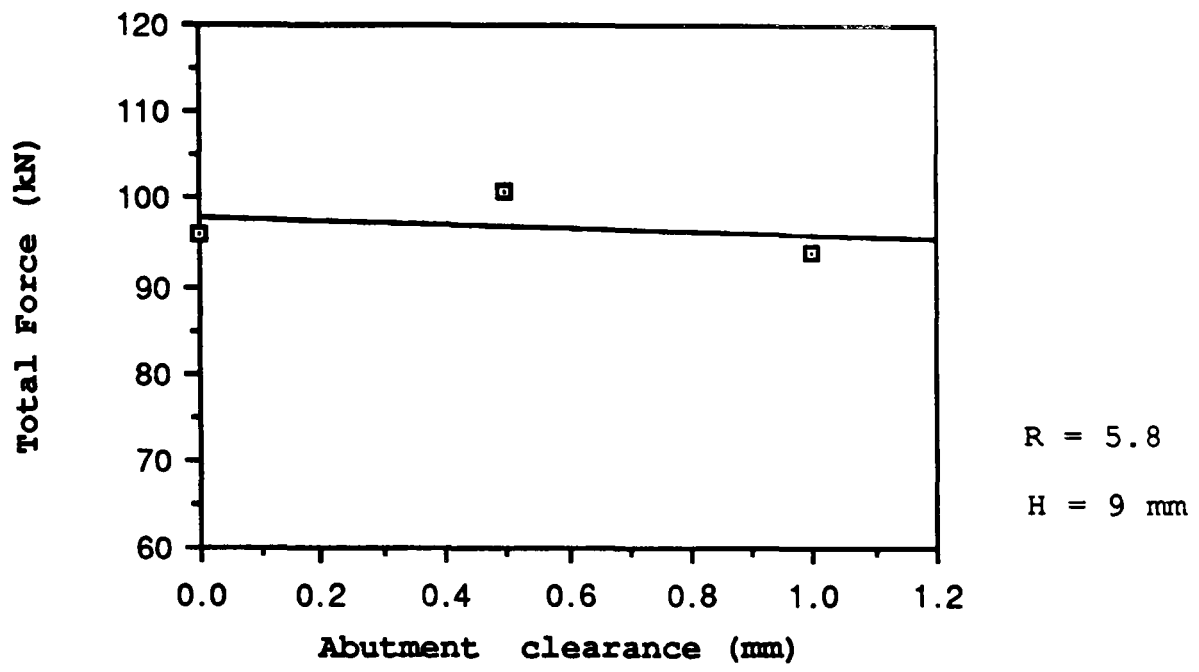


Figure 7.0 The graph illustrates the relationship between abutment force and abutment clearance for constant reduction ratio and abutment depth using the annealed feed stock.

It was also confirmed, after each test, during tool removal that only a small amount of feed metal had penetrated into the pre-set clearance in the range 4 to 10 mm, depending on the magnitude of reduction and pre-set clearance. This is because the dead zone wedged between the abutment tool and the die chamber prevented continuous extrusion into the pre-set clearance under normal operating conditions.

It is recognised that different tests for the same experimental conditions i.e. extrusion ratio, abutment depth setting and wheel speed, generated different amounts of flash per unit time as indicated in the tabulated data. In particular, the preliminary tests 1e - 7e and 10e - 27e generated a greater quantity of flash per unit time compared with tests 30e - 39e and 40e - 55e. The reduction in flash may be attributed to the removal of the scraper tool profile which is located in the wheel groove, and pre-set for different abutment depth settings. Also, the stationary tooling was maintained in close proximity to the moving wheel while ensuring that no contact was made other than through metal leakage (i.e. flash). To make suitable comparisons between experimental and analytical data, it was therefore considered necessary to use the analytical data which accounts for the levels of flash generated under experimental test conditions as indicated in the tabulated data where appropriate. However, the analytical data accounts only for the lower levels of flash generated per unit time as detailed under the later tests 30e - 39e and 40e - 55e. Therefore it is expected that a higher force will be sensed by the abutment tool for the early tests 1e - 7e and 10e - 27e.

Also, it is recognised that the experimental results were obtained under near steady state conditions. The transient operation of the machine was monitored on the computer VDU, by observing the reduction in torque and the increase in die temperature simultaneously, and the respective loadcell temperature and temperature difference. When an acceptable steady state machine operation prevailed (normally a period of

7 - 10 minutes), a further period of 2 - 5 minutes where the machine was allowed to proceed under the respective steady state conditions prior to effecting a further increase or decrease in wheel speed. The above procedure was repeated for the change in wheel speed.

The total time period of transient operation varied according to the reduction and, moreover, the level of increase or decrease in wheel speed. However, it was considered necessary to vary the wheel speed within each test because of the limitation on feed stock supply. In addition, after preliminary testing under constant wheel speed and extensive machine operating time (a period of 15 - 25 minutes), it was established that the variation in loadcell force and torque had a minimum effect on the steady state operation after a period of 7 - 10 minutes.

The graph of abutment force against reduction is illustrated in fig 7.1. The graphs show the correlation between experimental and theoretical load for different reductions and constant abutment depth setting and wheel speed using annealed feed stock. Observation of each graph for constant abutment depth indicates that the theoretical and experimental data are in fair agreement. The trend of the curves shows that, higher loads are expected for increasing reduction. Clearly, the trend of the curves illustrated in fig 7.1 follows a logarithmic relationship of the form,

$$Y = \ln X + C$$

where, C is the intercept on the force axis and X is the variable determined by the reduction ratio.

The scatter is attributable to accumulated experimental error. For example, the loadcell will generate more errors if used under a wider range of operating conditions such as varying temperature (i.e. non-isothermal conditions), temperature differential across loadcell faces, offset loading and the housing constraints imposed on the loadcell spring element

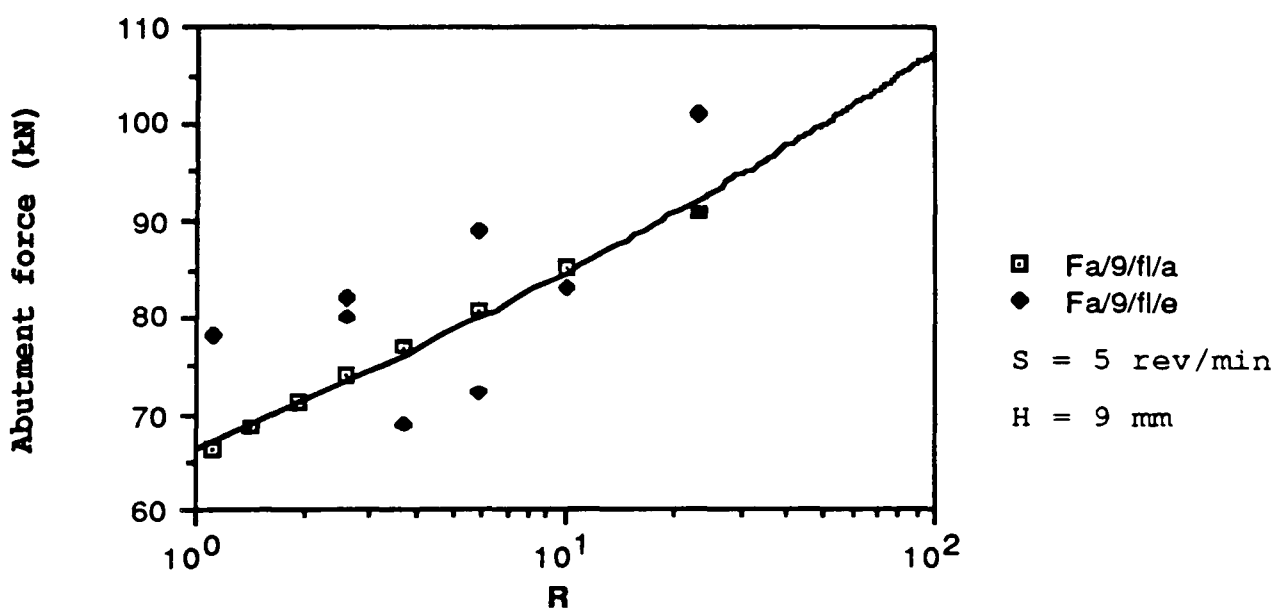
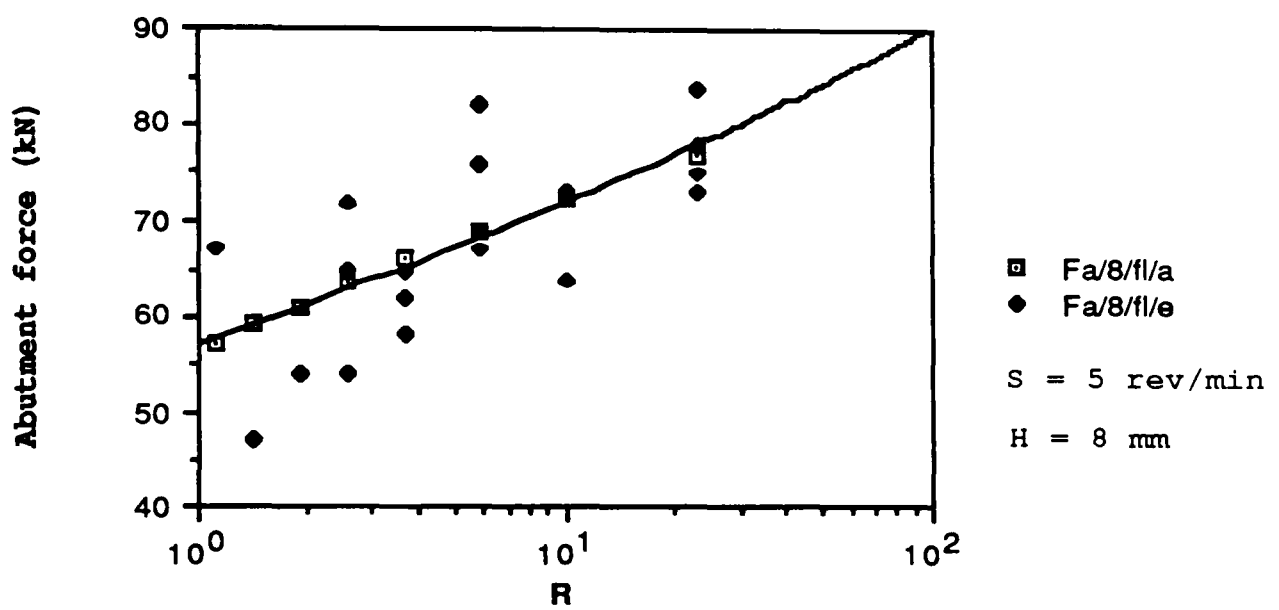
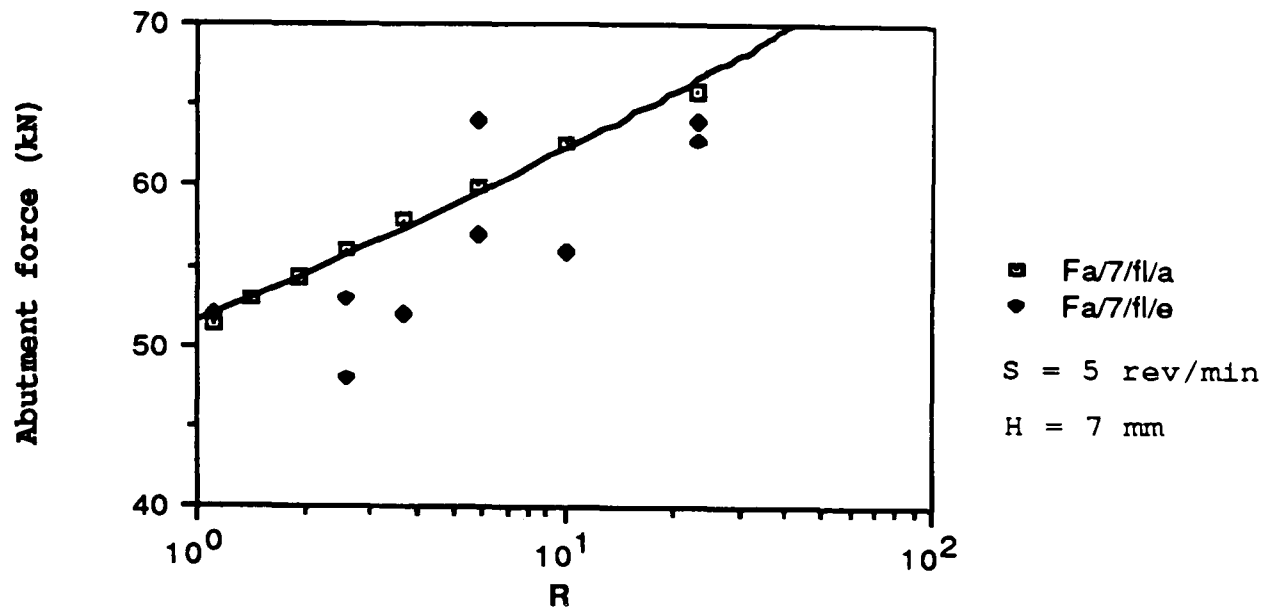


Figure 7.1 The graphs show the relationship between theoretical and experimental test data for abutment force against reduction ratio corresponding to various abutment depths 7, 8, 9 mm and constant wheel speed, using the annealed feed stock.

under normal testing conditions in contrast to the set up for calibration.

It is noted that only a small temperature differential exists between the upper and lower faces of the abutment loadcell compared with the die loadcell (or average 5 °C). The abutment loadcell spring element was manufactured from tungsten carbide which has a much higher thermal conductivity than the medium carbon steel equivalent. It is note-worthy that the miniature strain gauges cemented on the gauge length measured less than 1/4 of the total gauge length. Therefore the temperature differential across the strain gauges was less than 1/4 of the total temperature differential across the loadcell spring element i.e. 1 °C.

The graph of abutment force against reduction, fig 7.2, shows the analytical expressions for different abutment depth settings and constant wheel speed on the same plot. The trend of the curves shows that an increase in load accompanies an increase in abutment depth setting (or increasing abutment area). The trend of the graphs clearly follows a well defined logarithmic relationship as illustrated by the curve fit to the data.

The graph of abutment force against reduction ratio for the cold worked feed stock is shown in fig 7.3. The analytical and experimental results are generally in reasonable agreement, however it is noted that the limited experimental results for the cold worked feed stock cannot be considered as a major case for discussion.

However, comparisons can be drawn between the experimental and analytical data for the abutment force and pressure against reduction for the cold worked and annealed feed stock, illustrated in fig 7.4 and fig 7.5. The experimental data of fig 7.4 indicates that no clear correlation exists, due to the insufficient number of data points pertaining to the cold worked feed stock. It is noted, however, that the data points for the cold worked feed stock remain within the band width of

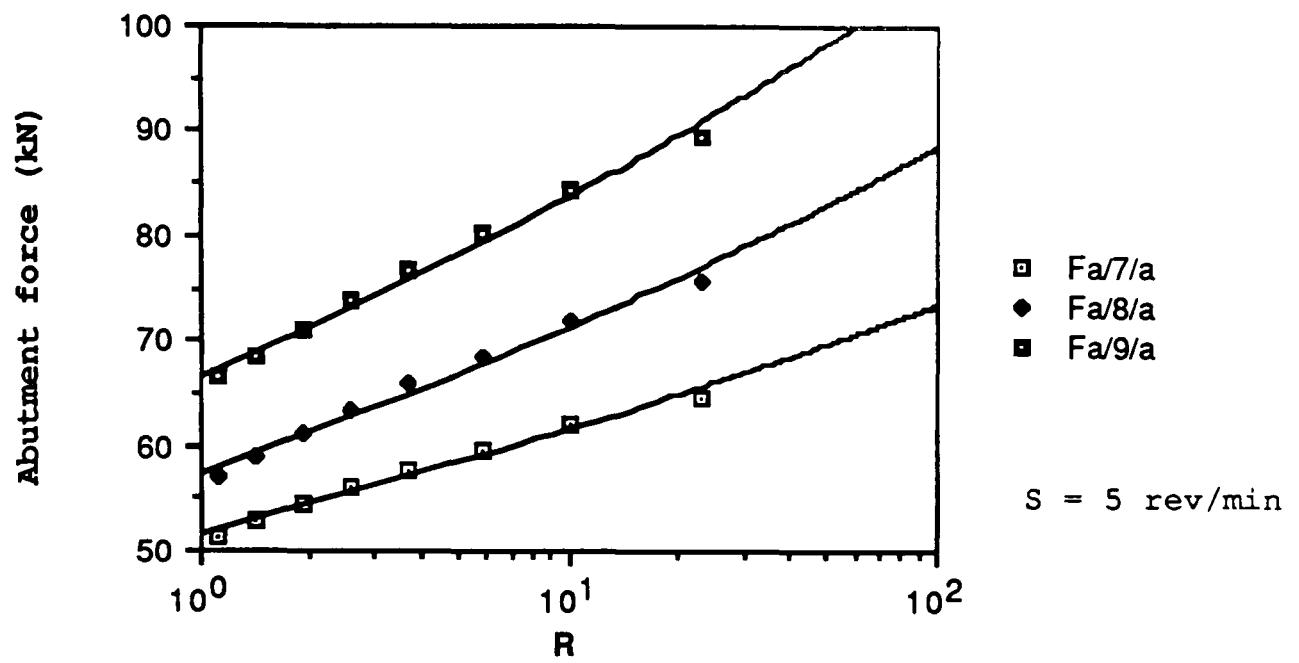


Figure 7.2 The graph illustrates the theoretical relationship between abutment force against reduction ratio with varying abutment depths 7, 8, 9 mm and constant wheel speed, using the annealed feed stock.

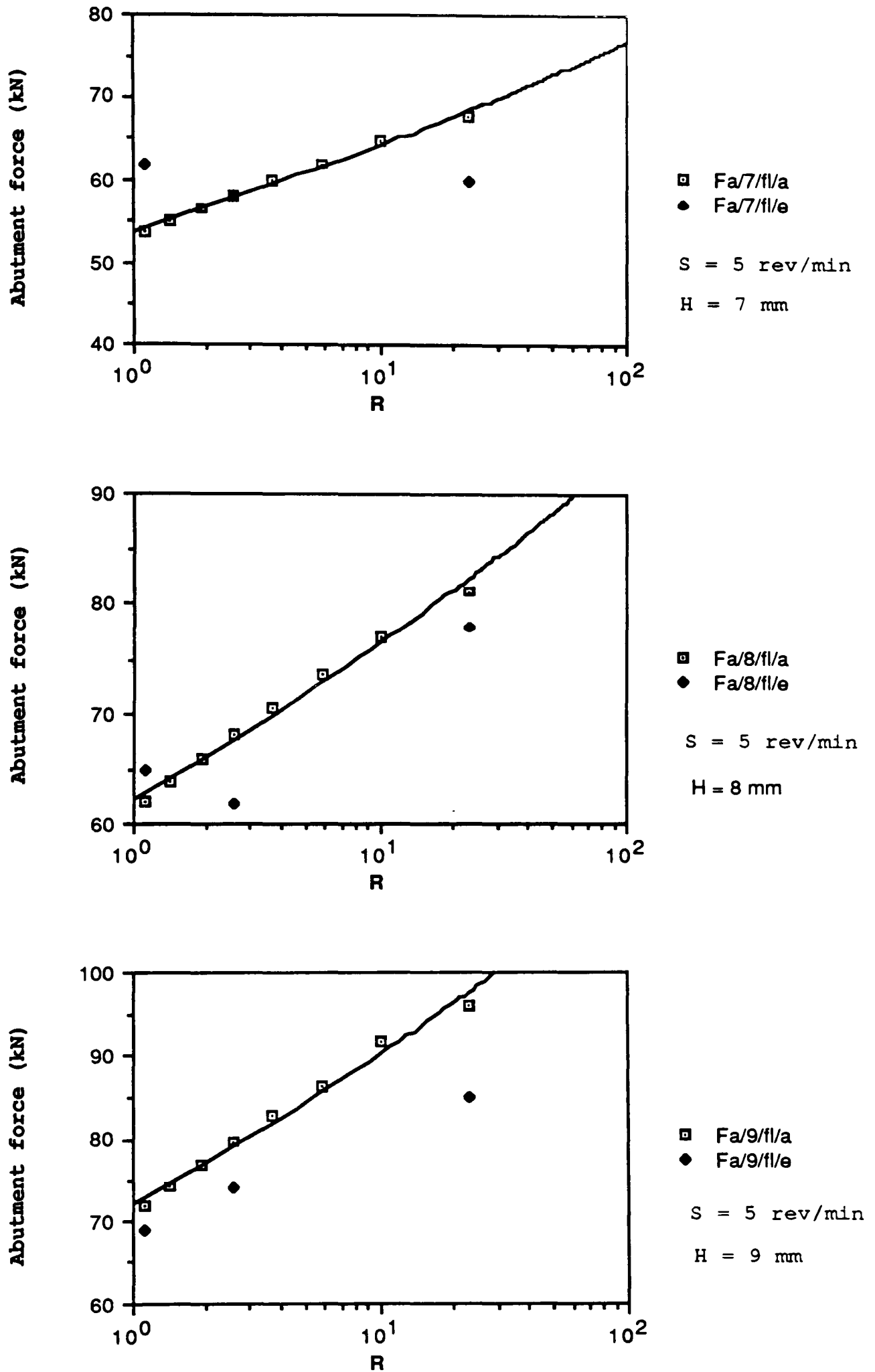


Figure 7.3 The graphs show the relationship between theoretical and experimental test data for abutment force against reduction ratio corresponding to various abutment depths 7, 8, 9 mm and constant wheel speed, using the cold worked feed stock.

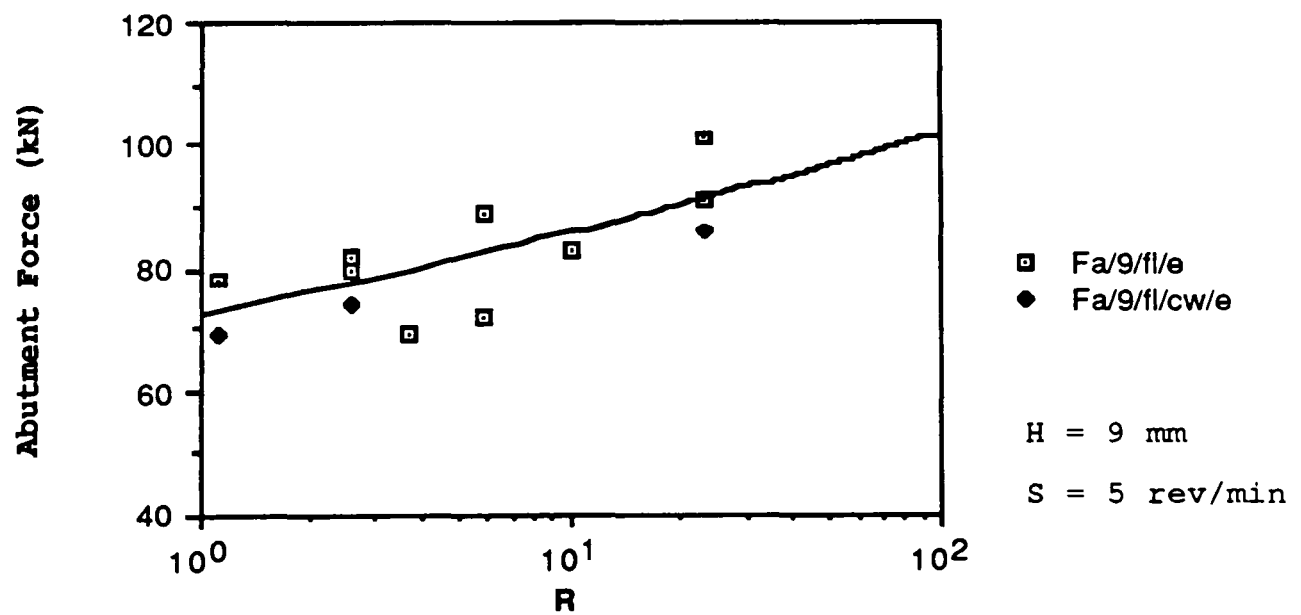
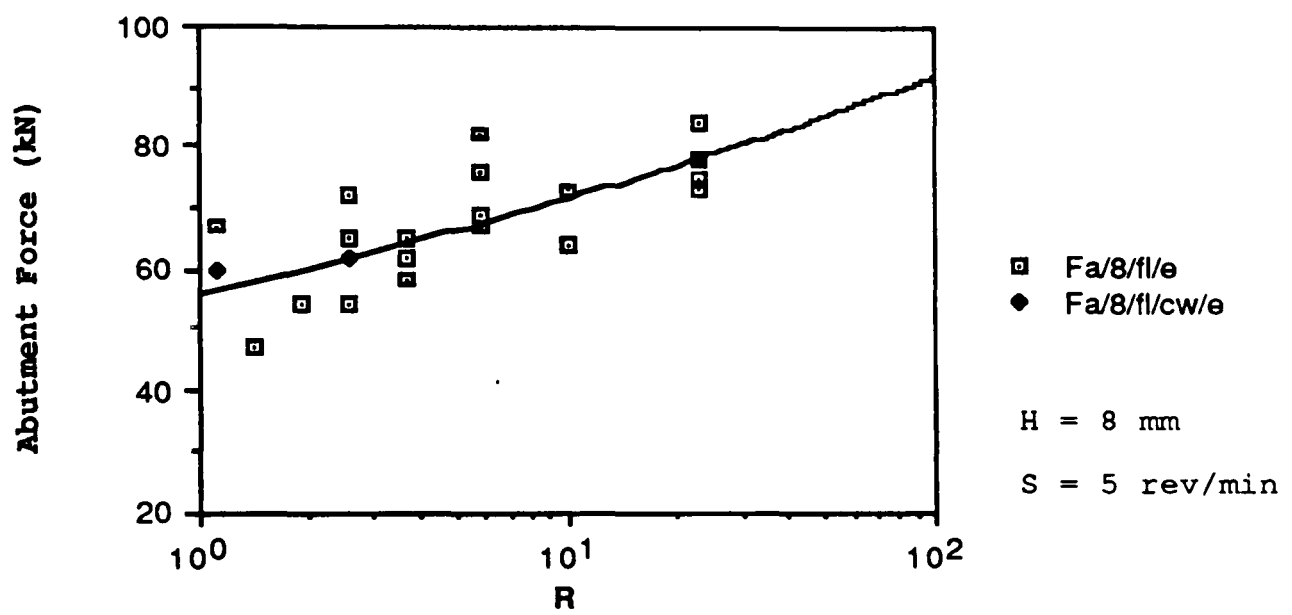
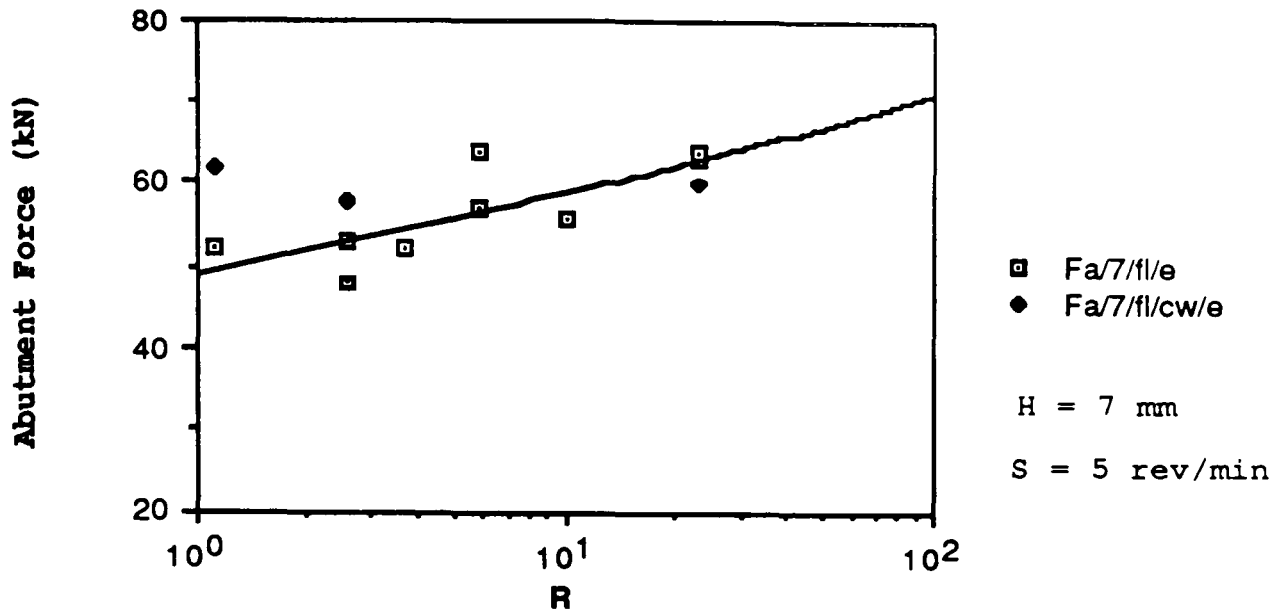


Figure 7.4 The graphs illustrate the experimental relationship between abutment force and reduction ratio for the cold-worked and annealed feed stock with varying abutment depths 7, 8, 9 mm and constant wheel speed.

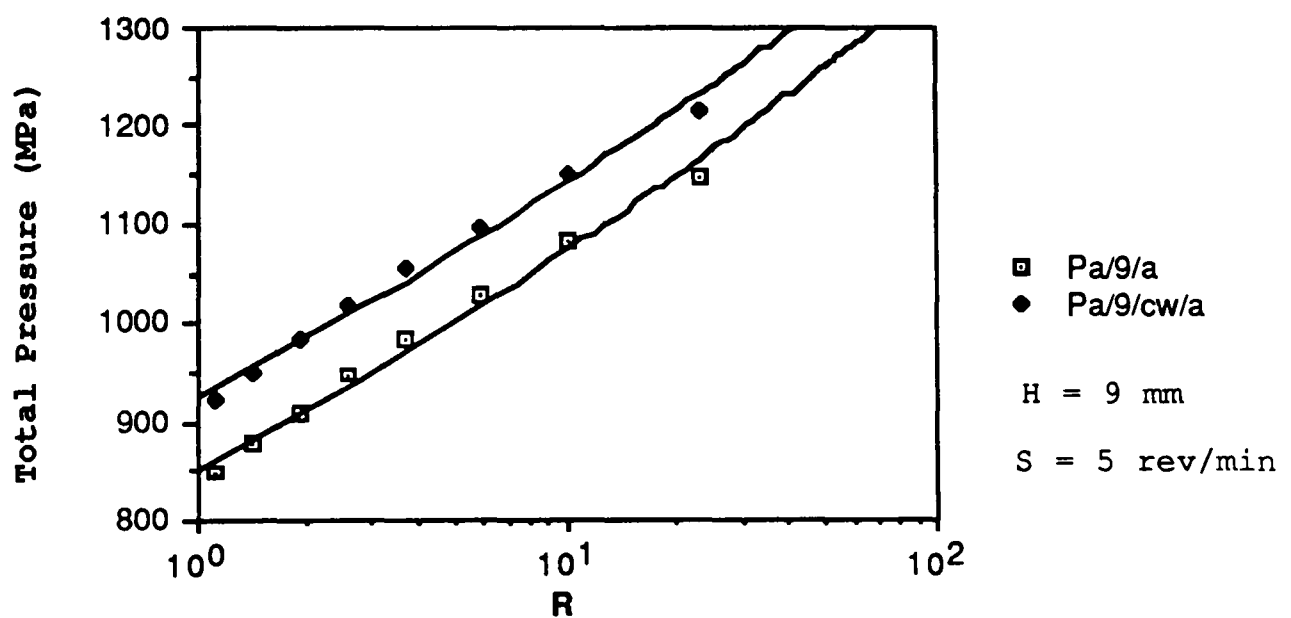
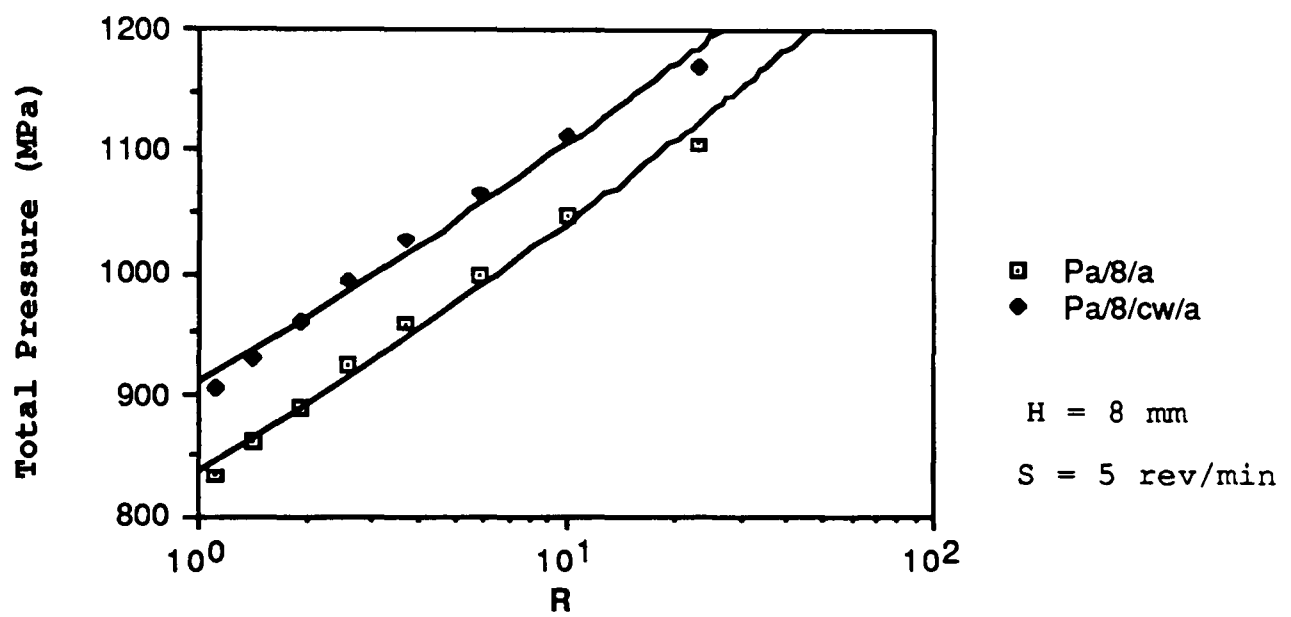
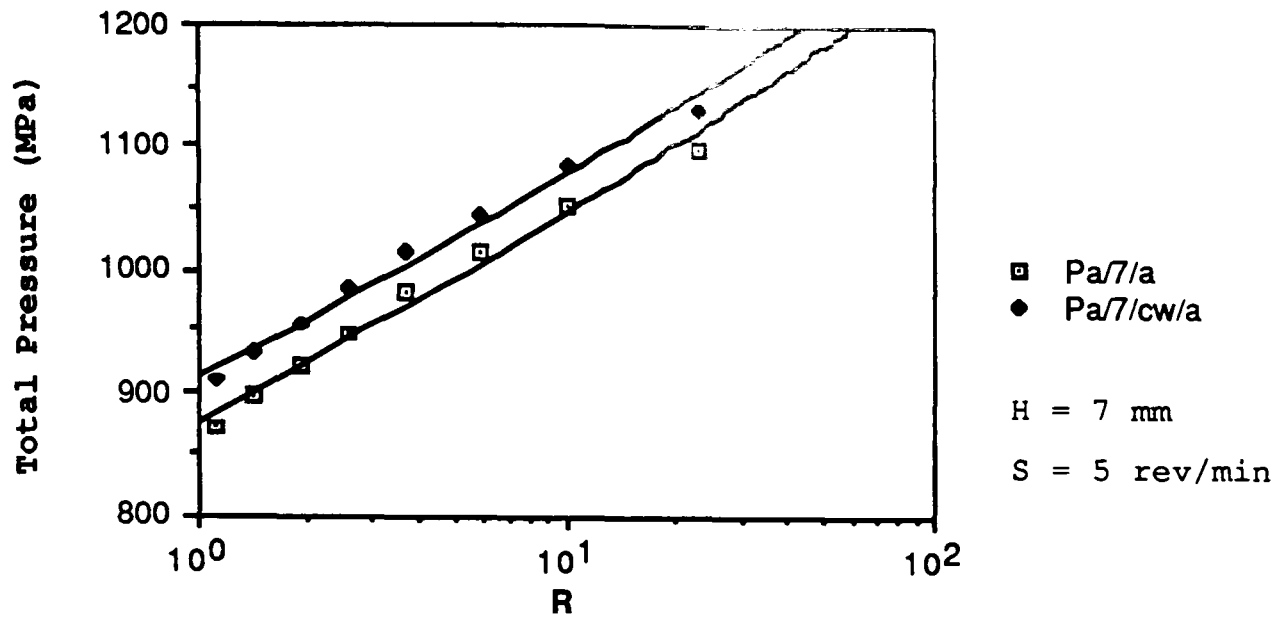


Figure 7.5 The graphs illustrate the theoretical relationship between abutment pressure and reduction ratio for the cold-worked and annealed feed stock with varying abutment depths 7, 8, 9 mm and constant wheel speed.

scatter for the annealed feed stock. Reference to fig 7.5 clearly indicates that the trend of the analytical curves of total abutment pressure for the cold worked and annealed feed stock can be described by a logarithmic relationship of the form

$$Y = \ln X + C$$

where, C is the intercept on the pressure axis and X is the variable determined by the reduction ratio. It is noted that the curves have the same gradient and are only distinguished by the constant C corresponding to each abutment depth setting.

The variation of abutment force with wheel speed is illustrated in a typical plot given in fig 7.6 for constant reduction and abutment depth. The graph shows the relationship between analytical and experimental test data. It is noted from the analytical curve that a small reduction in force accompanies an increase in wheel speed. This implies that for an increase in wheel speed a slight reduction in force is attributable to a corresponding reduction in flow stress. However, with regard to the experimental curve, the scatter is considered to be within the band width of experimental error and cannot be used to complement the slight reduction in force as indicated by the analytical curve. In addition, reference to the tabulated experimental data indicates that there is not necessarily a significant reduction in force corresponding to an increase in wheel speed across the broad range of reductions and abutment depth settings. Indeed, it is apparent that a small increase is observed in a number of cases, and all are considered to remain within the band width of experimental error. However, the tabulated analytical data indicates that a small reduction in force accompanies an increase in wheel speed for the range of reductions and abutment depth settings.

Finally, figs 7.7 and 7.8 illustrate the analytical relationship between total abutment pressure and reduction

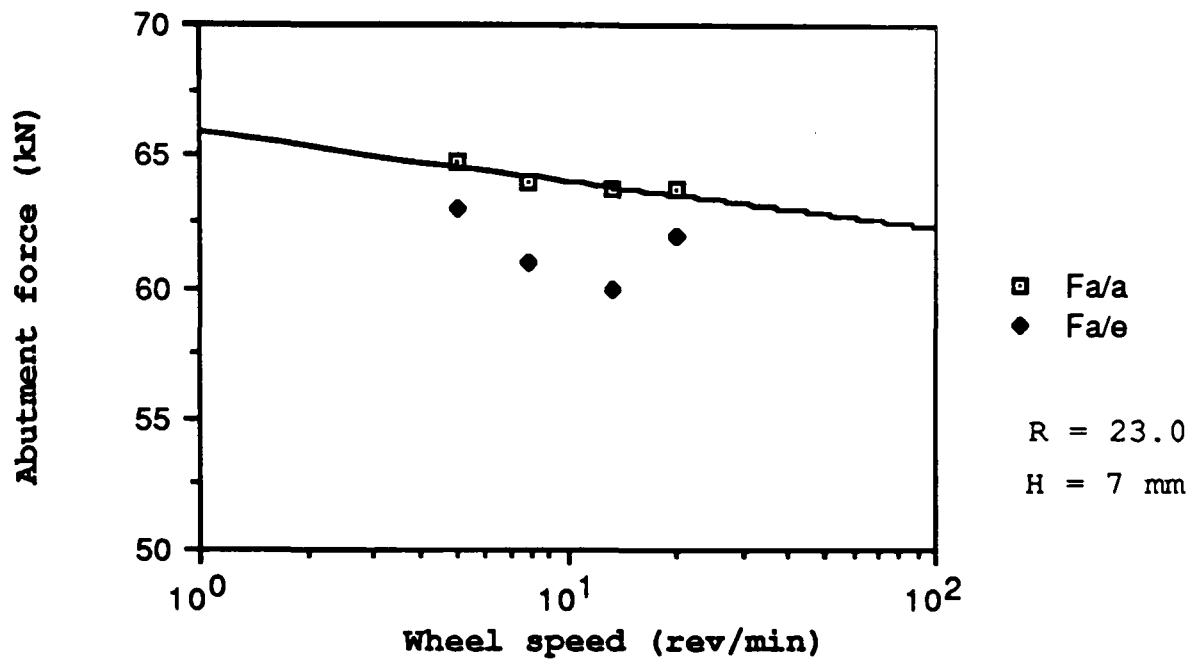


Figure 7.6 The graph illustrates the relationship between abutment force and wheel speed for constant reduction ratio and abutment depth using the annealed feed stock.

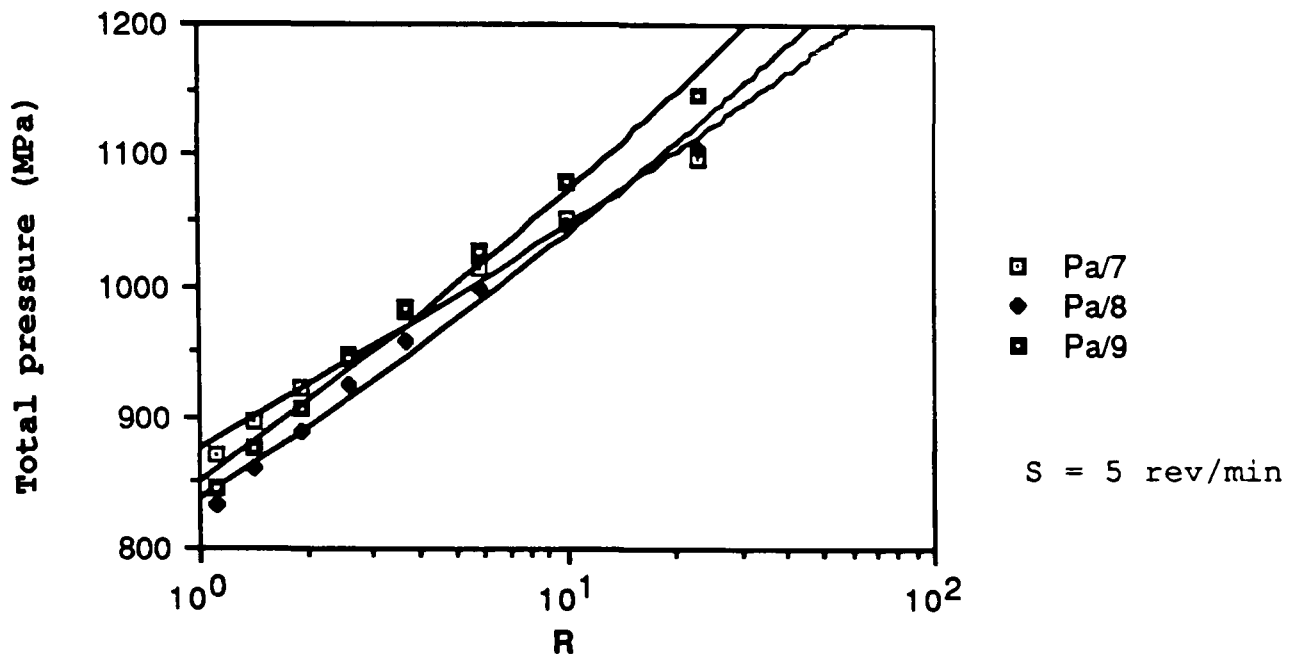


Figure 7.7 The graph illustrates the theoretical relationship between total abutment pressure (including friction) against reduction ratio for various abutment depths 7, 8, 9 mm and constant wheel speed, using the annealed feed stock.

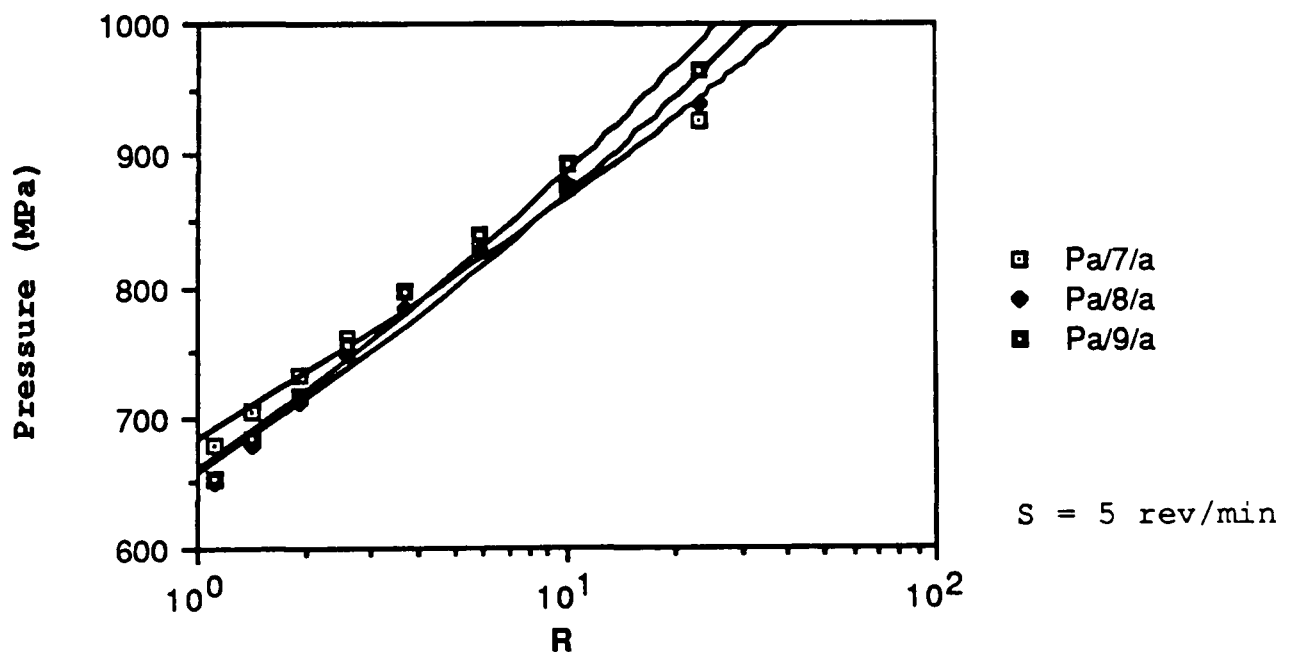


Figure 7.8 The graphs illustrate the theoretical relationship between (abutment) pressure against reduction ratio for various abutment depths 7, 8, 9 mm and constant wheel speed, using the annealed feed stock.

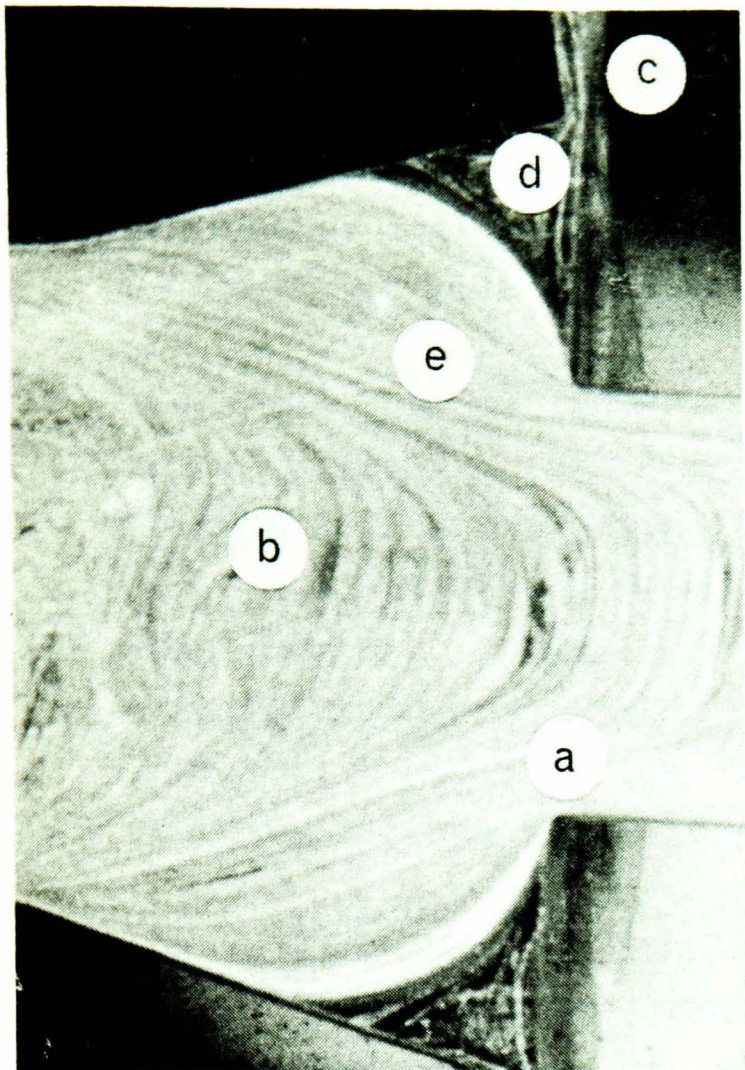
ratio for various abutment depths and constant wheel speed. The term 'total pressure' implies the total direct load per unit area including the influence of abutment tool and dead zone friction. It is apparent from the graphs that no significant variation in pressure is observed.

It is noted that the level of strain developed in the feed metal in the primary extrusion chamber is greater for the abutment depth setting 7 mm compared with abutment depth settings 8 and 9 mm. The energy expended, however, in deforming the feed metal is not necessarily greater for the higher strain condition, since the work done is determined by the product of the stress state and corresponding strain increment. The stress state is, in turn, determined from knowledge of the temperature, strain rate and strain. It is suggested therefore that a significant temperature increase is responsible for reducing the flow stress and subsequently balancing the energy equation as indicated in figs 7.7 and 7.8. The influence of temperature will be discussed in more detail under section 7.3.

7.2 DIE FORCE

The ingress of feed metal into the clearance between the die chamber in the DHUP and the die will generate some experimental error. This is because sufficient clearance was made available between the die and the die chamber in order to allow free radial and axial movement of the die under high temperature in the die chamber. Therefore flash entering this clearance will prevent free movement of the die and subsequently influence the load sensed by the die loadcell.

It was determined after the completion of each test and subsequent tool removal that different amounts of flash had entered into the die clearance, and this was primarily dependent on the reduction ratio. Figure 7.9 shows typical prints of various discards which were carefully removed from the die chamber on completion of each test. The wafer thin



- a. die orifice
- b. die chamber
- c. flash
- d. dead zone
- e. flow lines

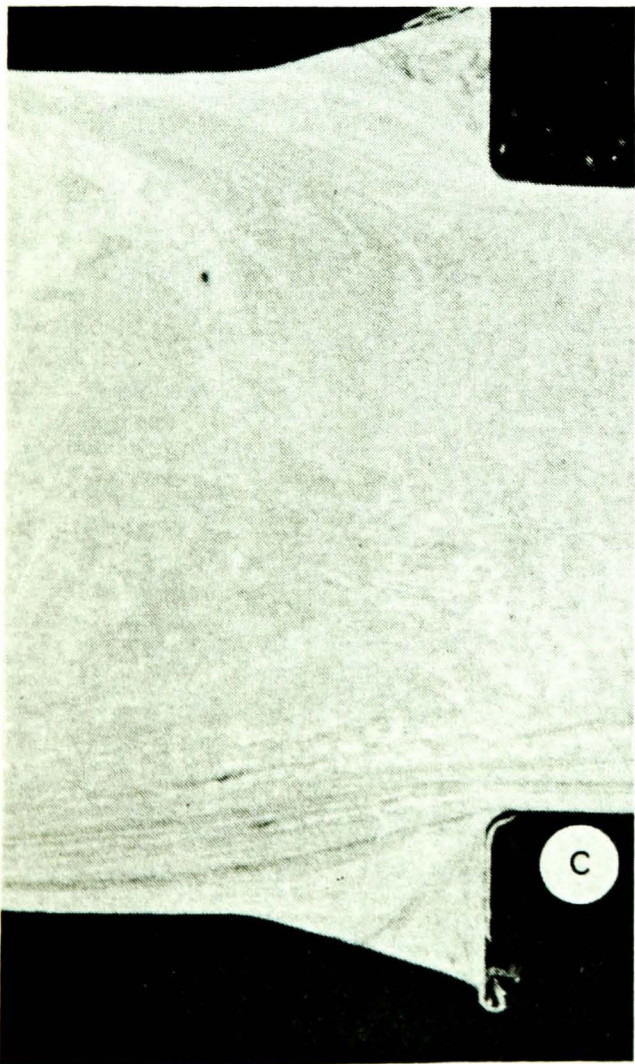
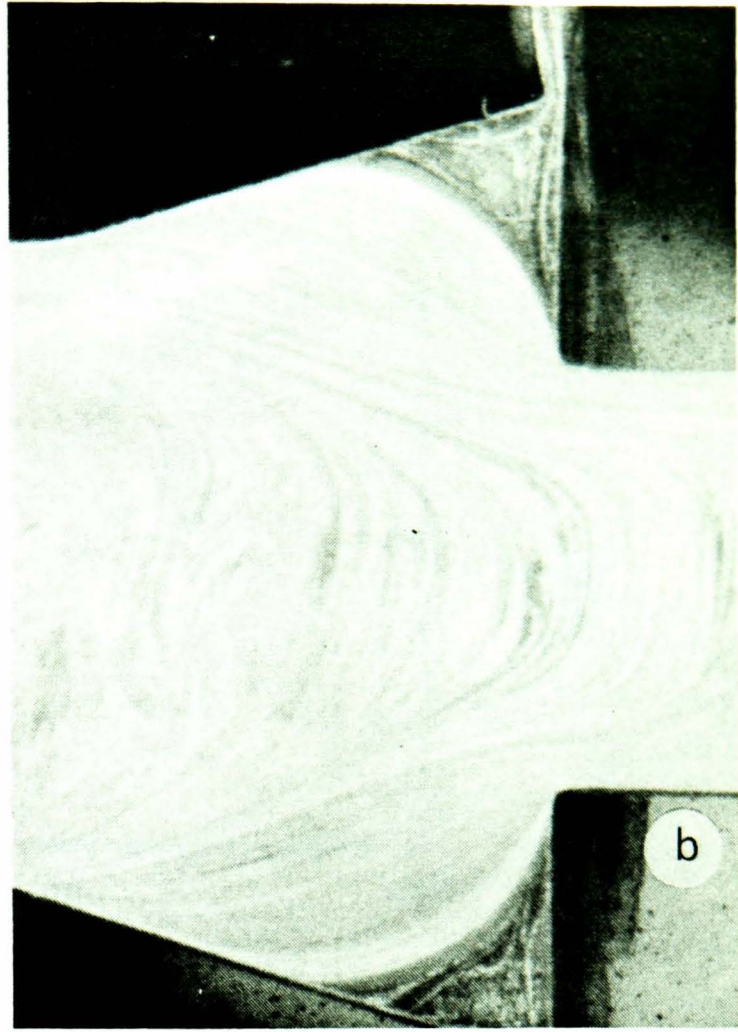
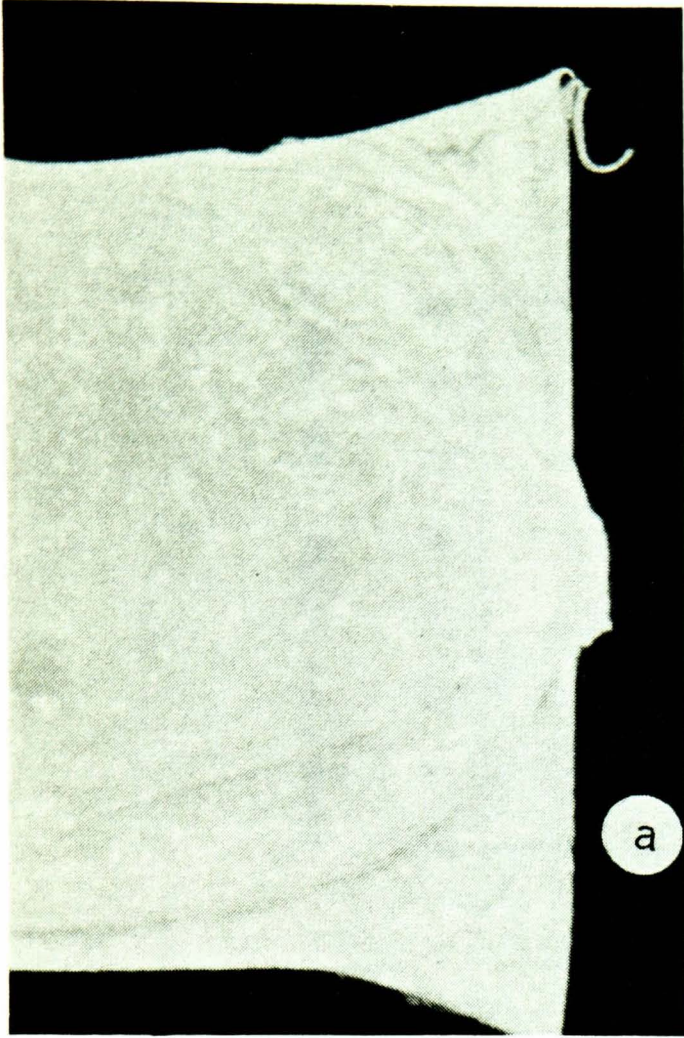
Figure 7.9. Photographs of various macro-etched discards which have been removed from the die chamber on completion of each test.

portion of flash is clearly indicated at the outer part of the die face. It was noted however, that even under extreme pressures i.e. high reduction, the flash was prevented from extruding into the radial clearance because of the influence of the dead zone formation in the die chamber.

The figs 7.9 and 7.10 provide a clear indication of the dead zone formation in the die chamber. The discards were sectioned and macro-etched in order to study the flow lines, this also allowed a measurement of the dead zone angle in the die chamber. However, it is clear from the macro-etched samples that no straight line exists between the planes of deformation i.e. from the start of the dead zone to the entrance of the die orifice.

An explanation to this phenomenon is that the stress state which is determined from knowledge of the temperature, strain rate and strain is constantly changing with plastic deformation. Indeed, the temperature and strain rate in the feed metal become extremely localised immediately surrounding the entrance to the die orifice. The analytical determination of the dead zone is expressed by the upper bound equation 5.44, and by varying α_2 to obtain the minimum value or, alternatively, differentiating equation 5.44 with respect to α_2 and equating to zero to give α_2 . It is noted that the dead zone angle is determined from the mean difference between the value of stress state at stage 3 and 5, and no consideration is given therefore to the intermediate (or changing) stress state based on a small increment of plastic strain.

Comparison between the predicted and experimental measurements of dead zone angle is given in fig. 7.11. The correlation between the predicted and experimental data shows that the agreement is reasonable, considering the simplicity of the analytical expression used to determine the dead zone angle as described previously. It is observed from the graph that the trend of the curves can be described by a logarithmic relationship. The predicted and experimental data have the same gradient and are distinguishable only by the constant.



- a. reduction ratio; 23
(die orifice; 2 mm dia.)
- b. reduction ratio; 2.6
(die orifice; 6 mm dia.)
- c. reduction ratio; 1.1
(die orifice; 9 mm dia.)

Figure 7.10. Photographs of various macro-etched discards which have been removed from the die chamber on completion of each test.

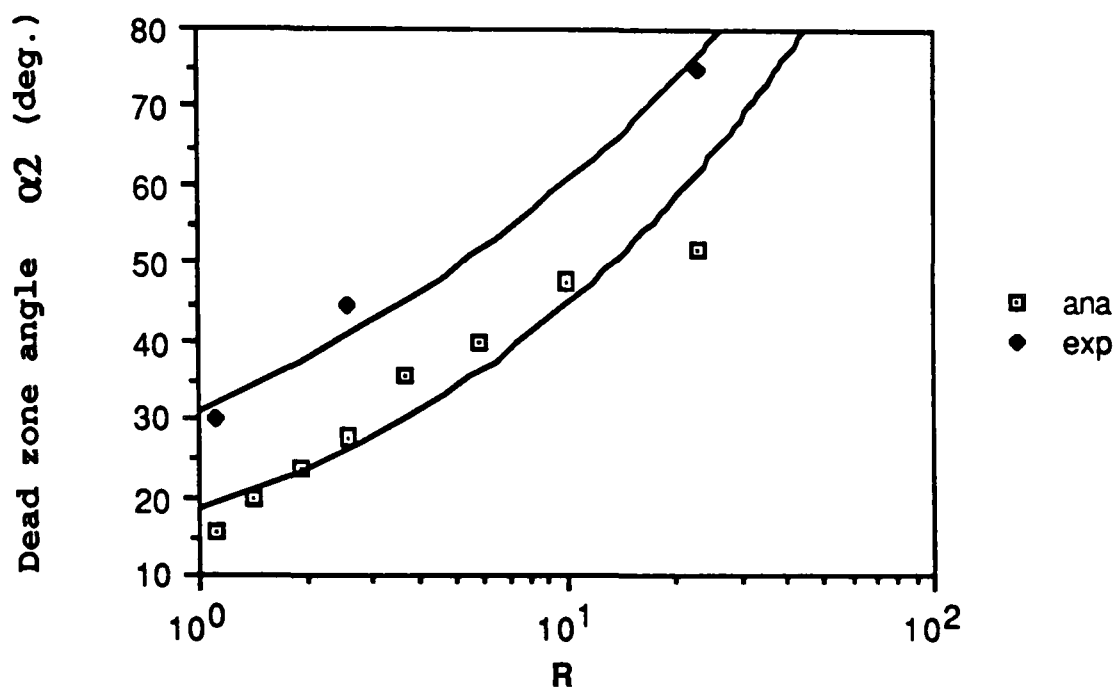


Figure 7.11 The graph illustrates the analytical and experimental relationship between dead zone angle and reduction.

A better correlation between the predicted and experimental data was obtained by assuming a friction factor 'm' in the range 0.5 - 0.8 in the analytical equations. This was possible by simply inserting the appropriate values for m when the computer program prompted the user to specify and input a value for m at the start of a program run. Reduction of the friction factor had the effect of increasing the dead zone angle in the analytical data and subsequently a better correlation with the predicted and experimental measurements taken from the prints of the macro-etched samples was observed. Correspondingly, a small reduction in load and temperature was noted for the lower value of friction factor used in the theoretical analysis in the order of 10% for the friction factor $m = 0.5$.

It is noted from the analytical data that a significant temperature differential existed across the faces of the EN 24 die loadcell during steady state condition. The thermocouple probes were positioned on the peripheral surface of the upper and lower flanges in order to measure this temperature difference, the average value of which was measured at 43 °C. However, the miniature strain gauges cemented on the gauge length of the loadcell spring element measured less than 1/5 of the gauge length of the loadcell. This implies that the temperature difference across the strain gauges measured less than 7 °C, compared to the 1 °C temperature differential across the strain gauges on the tungsten carbide loadcell. The influence of this temperature difference across the die loadcell on experimental error is difficult to assess numerically. However, it is clear that the error due to temperature difference is likely to be greater for the die loadcell than the abutment loadcell in this respect.

It should also be mentioned that the die and die loadcell were enclosed within a tool housing in the shoe during normal machine operation, which consequently imposed constraints on the freedom of movement of these components under the set up described in section (3.1.2), whereas the abutment tool holder was free to move within the wheel groove, and

subsequently over a hardened spherical button located on the upper face of the abutment loadcell. Observations on the comparative accuracy and performance of the two loadcells which is primarily determined by the tooling set-up around the respective loadcells, suggests that the die load measurements will, in general, provide better reliability than the data obtained from the abutment loadcell.

The graphs of die force against reduction, fig 7.12, show the correlation between experimental and theoretical load for different reductions and constant abutment depth setting and wheel speed using the annealed feed stock. Observation of each graph for constant abutment depth indicates that the theoretical and experimental data are in good agreement. It is noted that the experimental data obtained from the die loadcell is in better agreement with the analytical data than the load measurements obtained from the abutment loadcell. In addition, the band width of experimental error is smaller for the die loadcell than for the abutment loadcell data. The trend of the curves shows that for increasing reduction, higher loads are expected. It is also noted that the upper bound curve for die force remains higher than the curve corresponding to the experimental data. Therefore, implicit in the 'minimum upper bound' prediction of work done, the deviation of the theoretical and experimental curves for the range of reduction is considered to be minimum within the band width of experimental error (or scatter).

The analytical data is described by curves using a logarithmic relationship. It is observed, that this relationship deviates marginally from the analytical data at high and low reduction, and at an intermediate stage of reduction for all abutment depth settings.

The graph of die force against reduction ratio for the cold worked feed stock is illustrated in fig 7.13. The predicted and experimental results are in good agreement, however it is noted that the few experimental results for the cold worked feed stock are not to be considered as a major topic for

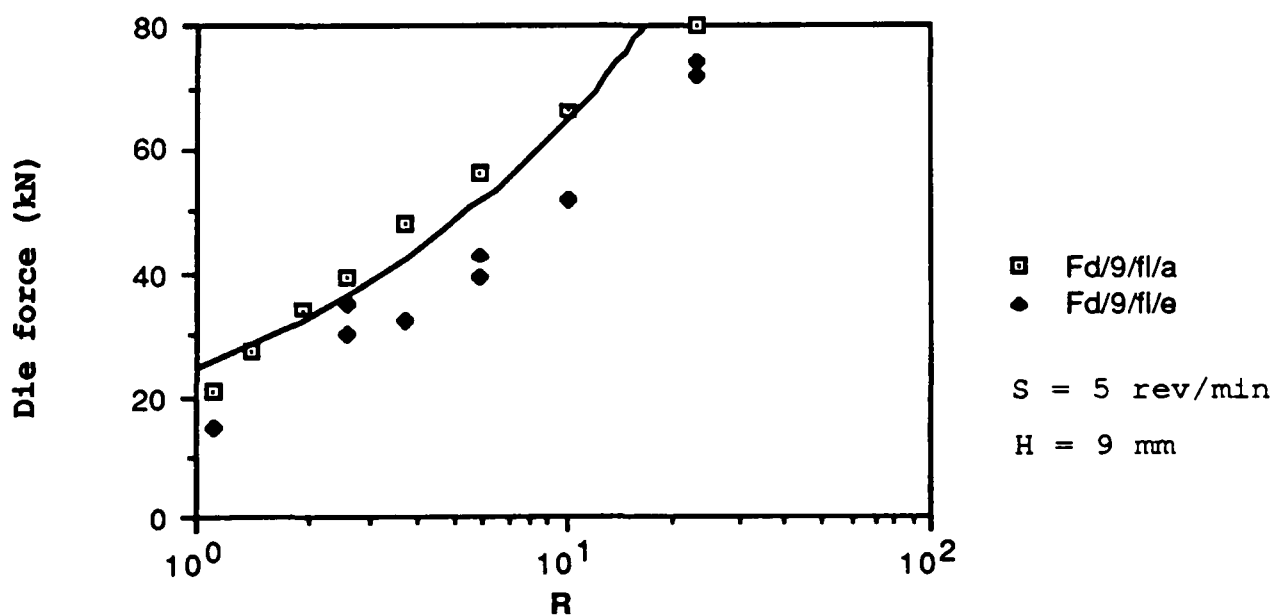
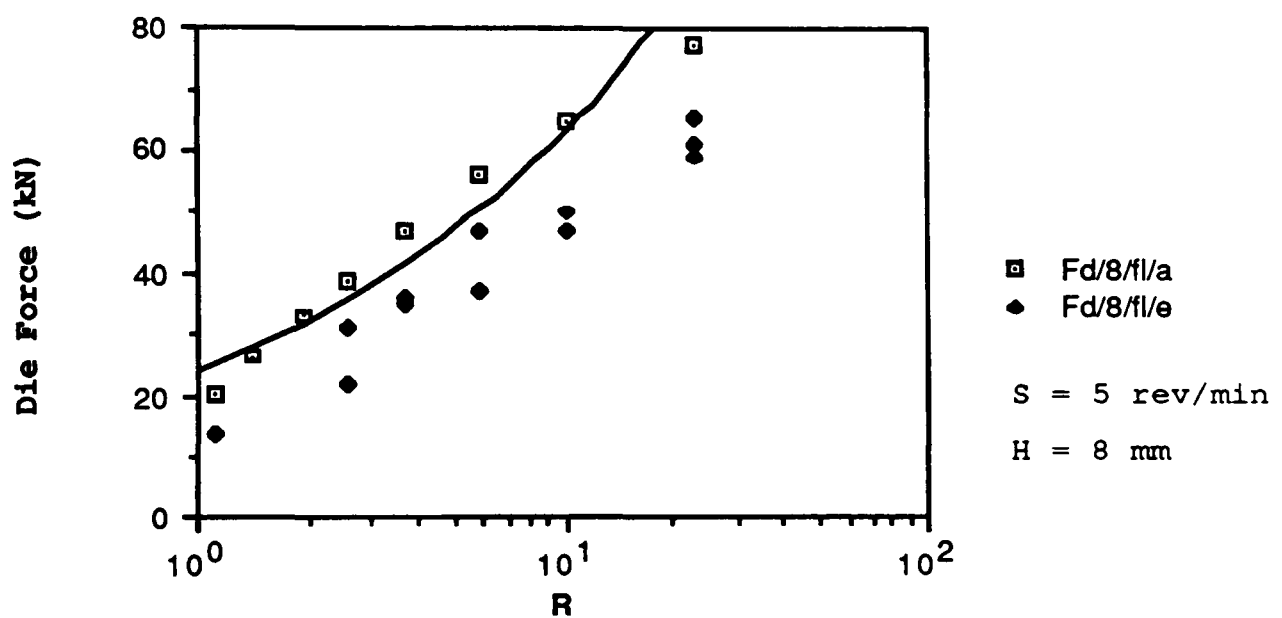
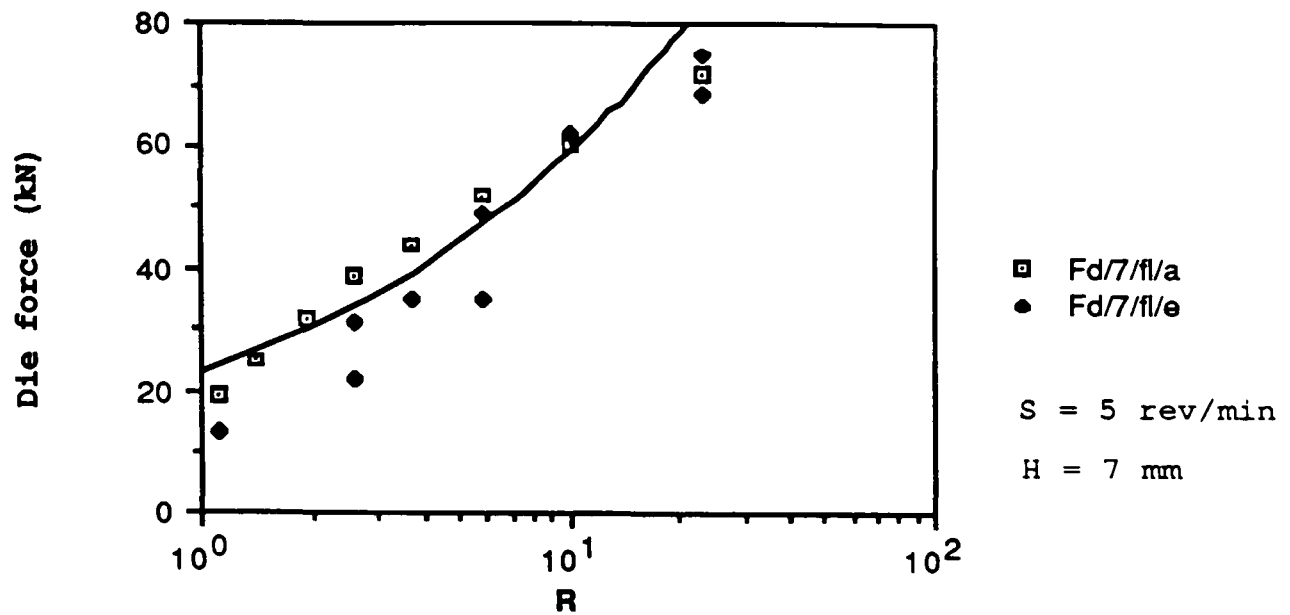


Figure 7.12 The graphs show the relationship between theoretical and experimental test data for die force against reduction ratio corresponding to various abutment depths 7, 8, 9 mm and constant wheel speed, using the annealed feed stock.

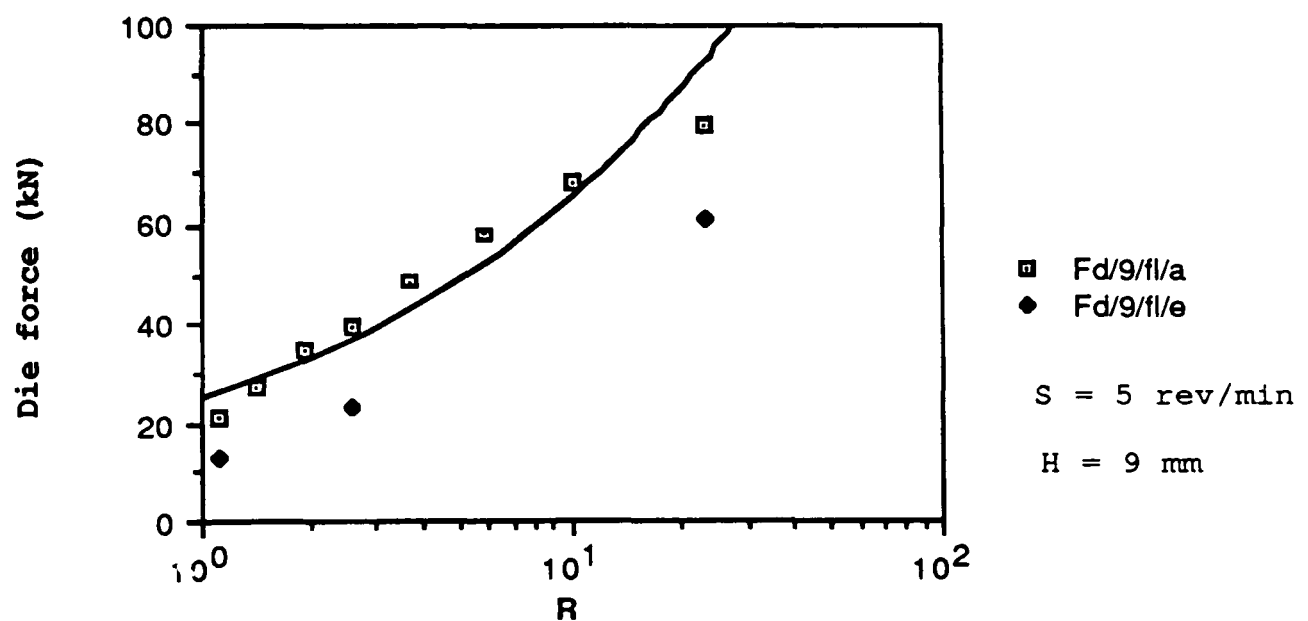
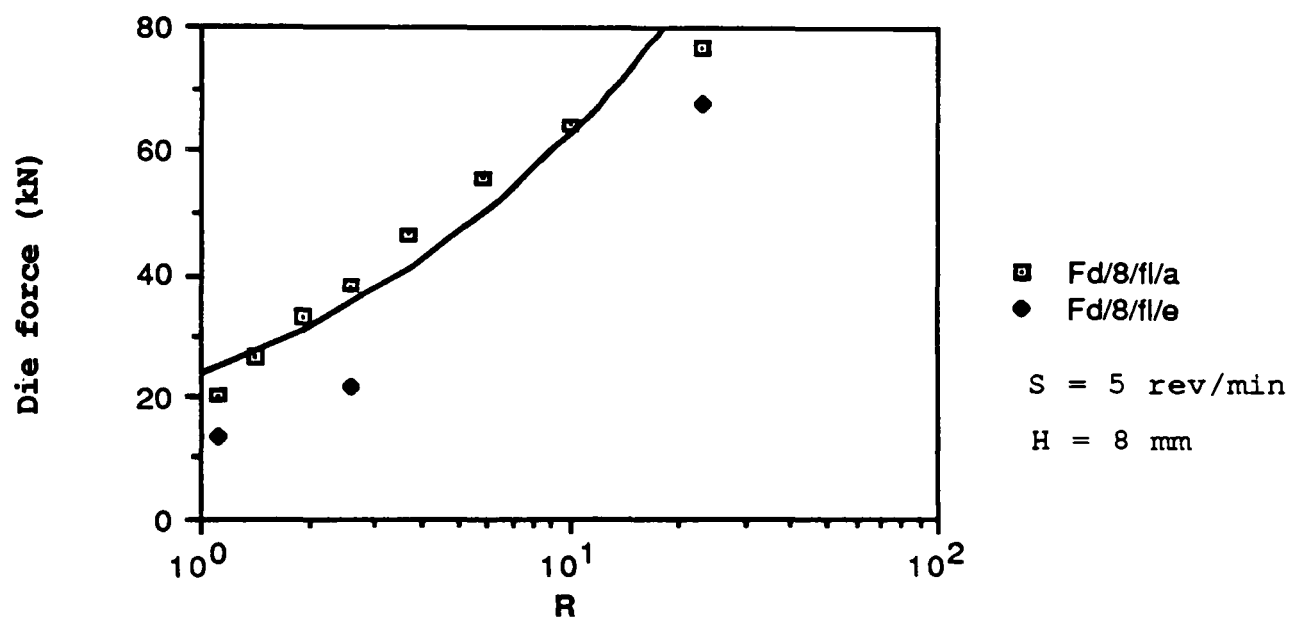
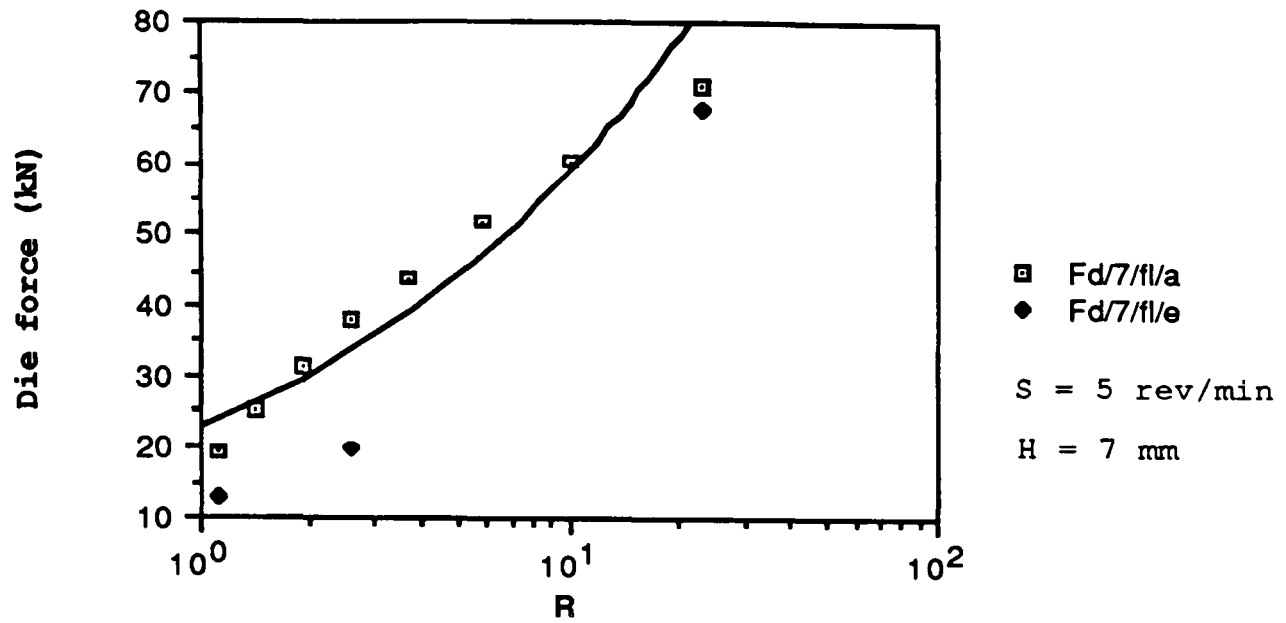


Figure 7.13 The graphs show the relationship between theoretical and experimental test data for die force against reduction ratio corresponding to various abutment depths 7, 8, 9 mm and constant wheel speed, using the cold worked feed stock.

discussion, as mentioned under abutment force in the foregoing section.

Comparisons between the experimental data from die force against reduction for the cold worked and annealed feed stock are illustrated in fig 7.14 for constant abutment depth setting and wheel speed condition. The graph indicates that a good correlation exists between the experimental and theoretical data in view of the limited amount of data pertaining to the cold worked feed stock. It is noted, however, that the cold worked data points remain below the data points obtained from the annealed feed stock, suggesting that the temperature increase in the cold worked feed stock in the primary extrusion chamber is greater than for the annealed feed stock subsequently, a reduction in the flow stress in the die chamber is observed.

The variation of die force with wheel speed is illustrated in a typical plot shown in fig 7.15 for constant reduction ratio and abutment depth setting. The graph indicates the relationship between analytical and experimental test data. It is noted from the analytical curve that a small reduction in force accompanies an increase in wheel speed. This implies that for an increase in wheel speed a slight reduction in flow stress is attributable to the corresponding reduction in force. From the experimental curve, the scatter is considered to be within the band width of experimental error and complements the reduction in force as indicated by the analytical curve. In addition, reference to the tabulated experimental data shows that there is, in all but a few cases, a slight reduction in force corresponding to an increase in wheel speed across the broad range of reduction and abutment depth settings. The tabulated analytical data suggests that a small reduction in force accompanies an increase in wheel speed for the range of reduction and abutment depth settings.

Finally, fig 7.16 illustrates the analytical relationship between die pressure and reduction ratio for various abutment depth setting and constant wheel speed. It is observed from

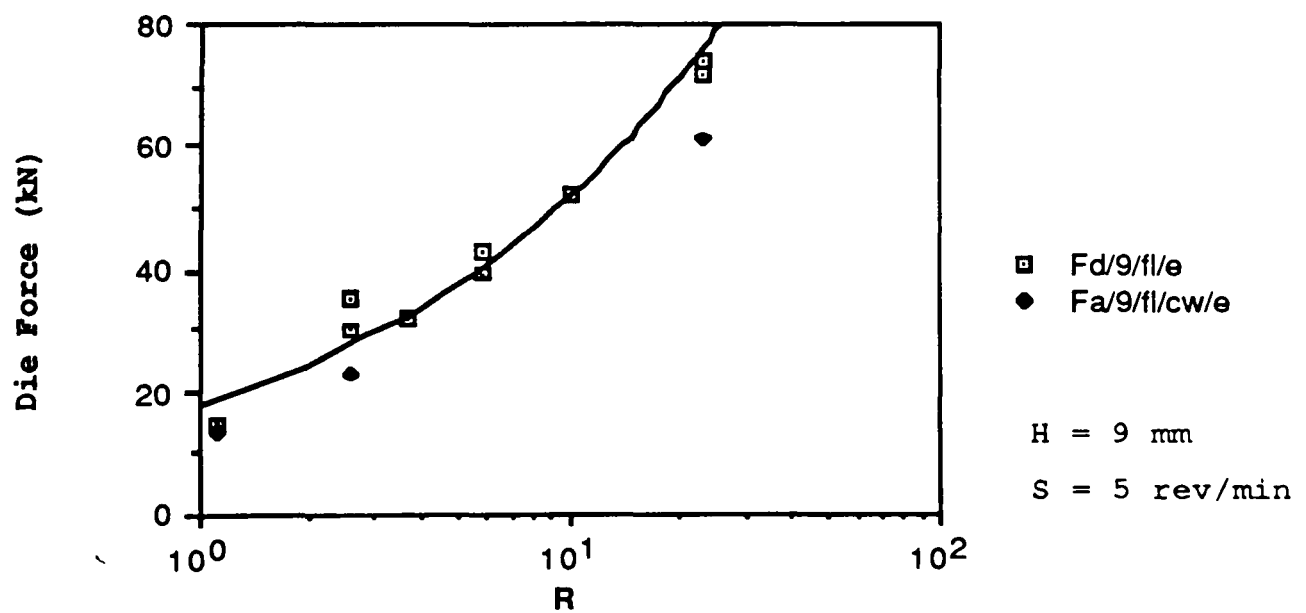
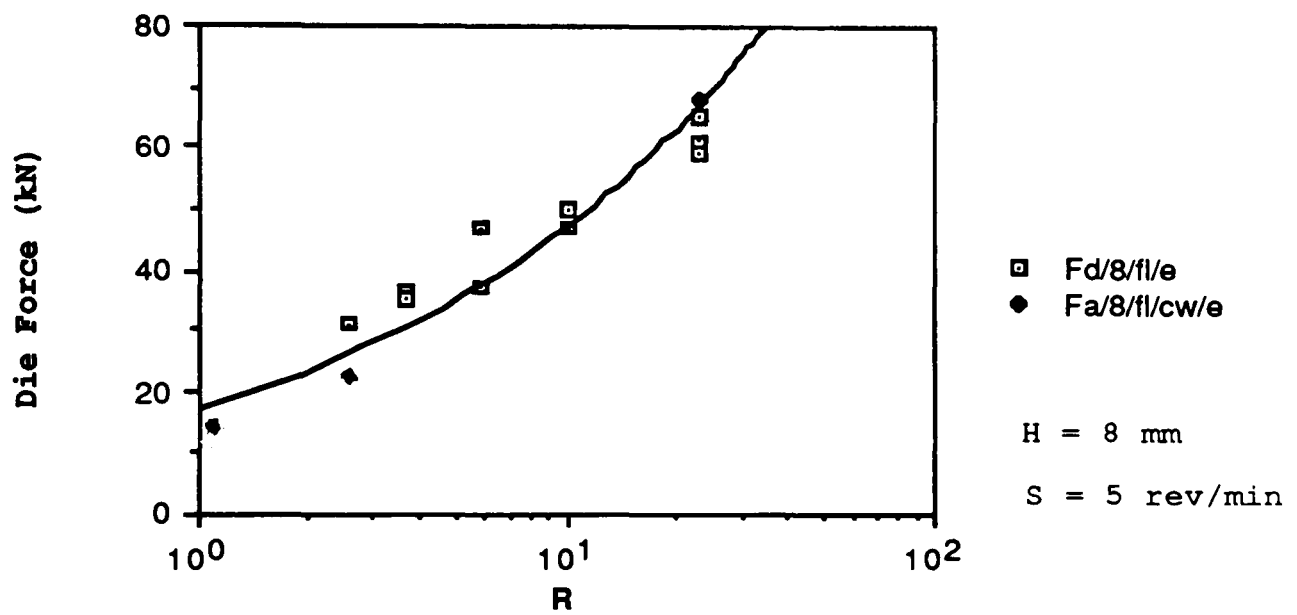
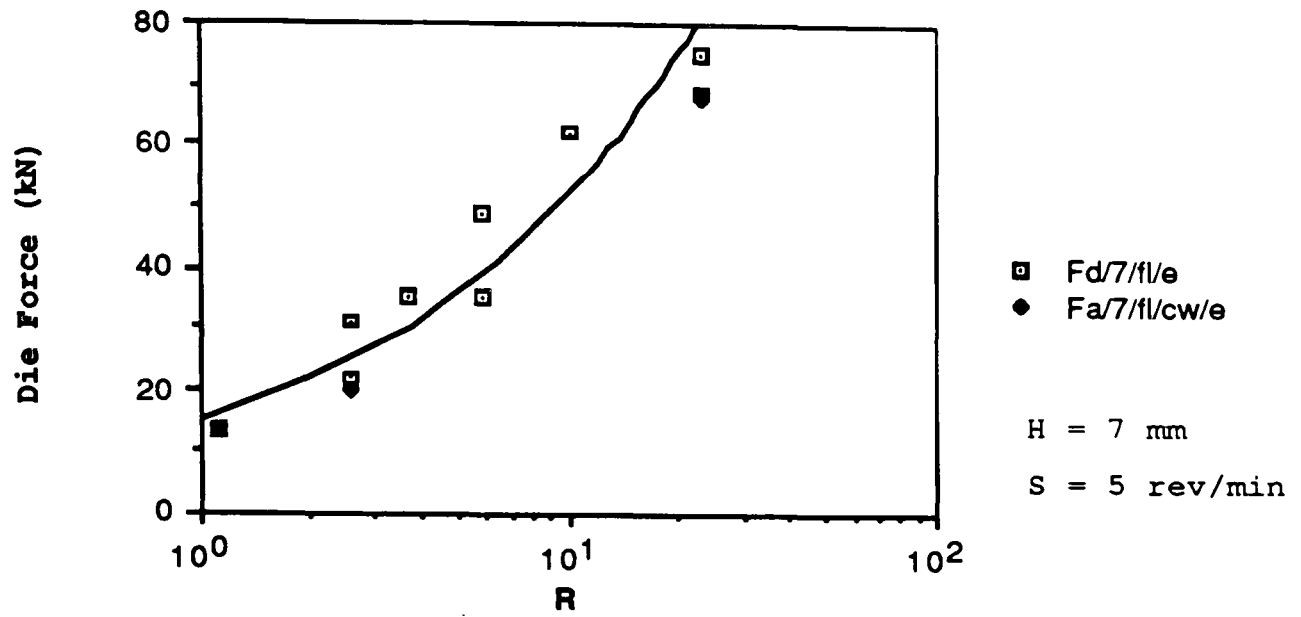


Figure 7.14 The graphs illustrate the experimental relationship between die force and reduction ratio for the cold-worked and annealed feed stock with varying abutment depths 7, 8, 9 mm and constant wheel speed.

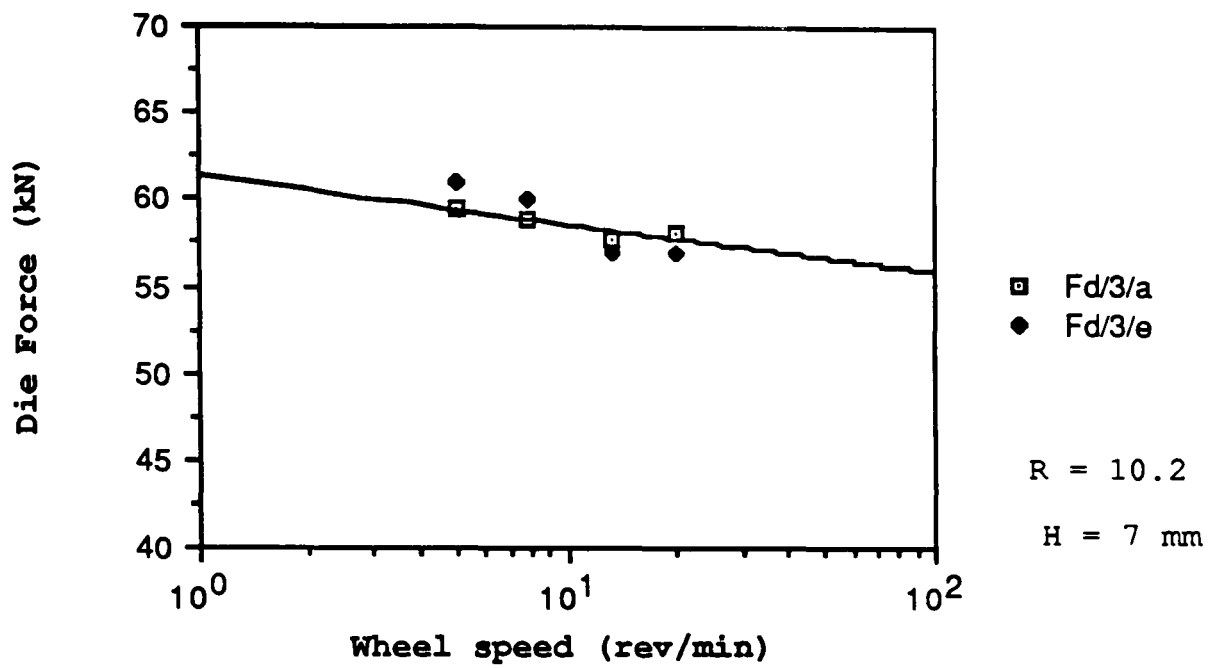


Figure 7.15 The graph illustrates the relationship between die force and wheel speed for constant reduction ratio and abutment depth setting using the annealed feed stock.

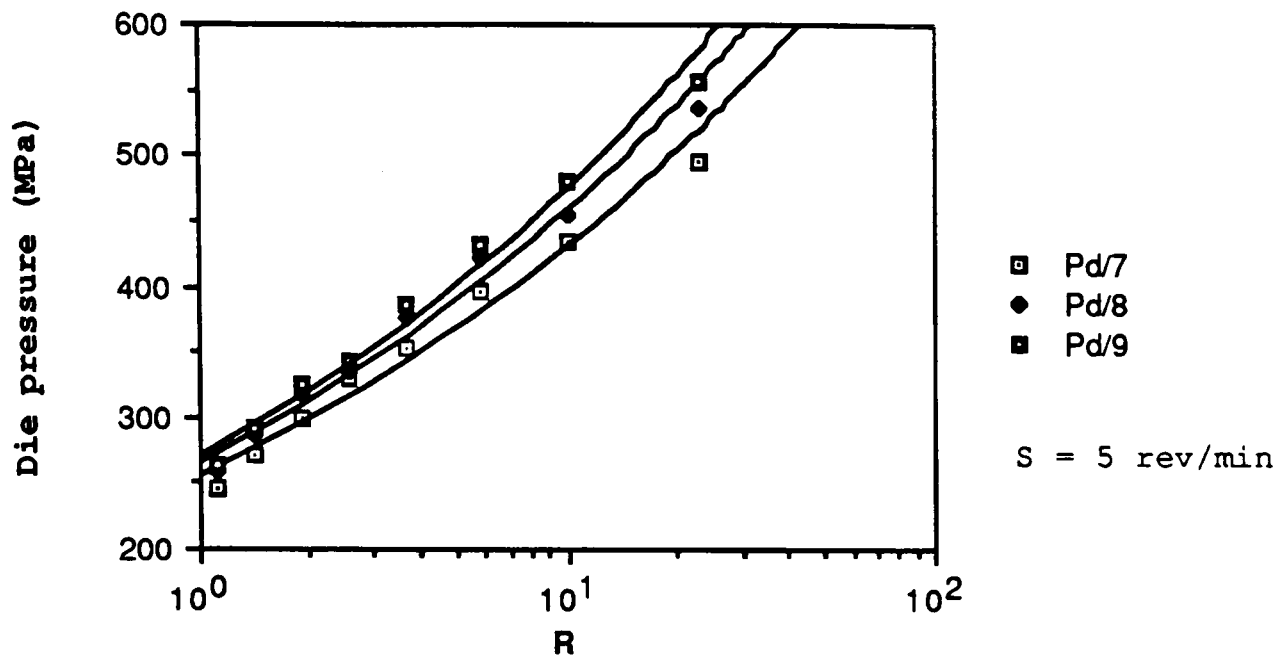


Figure 7.16 The graph illustrates the theoretical relationship between die pressure against reduction ratio for various abutment depths 7, 8, 9 mm and constant wheel speed, using the annealed feed stock.

the graph that an increase in die force is attributable to an increase in abutment depth. It has been suggested under section 7.1 that the temperature developed in the feed metal in the primary extrusion chamber is greater for the lower abutment depth setting, 7 mm, compared with abutment depth settings 8 and 9 mm. This has the consequent effect of reducing the flow stress in the die chamber corresponding to the lower abutment setting of 7 mm (the influence of temperature is discussed in the following section).

7.3) DIE TEMPERATURE

The die temperature is measured by securing a thermocouple probe to the periphery of the die. The temperature measured by the probe is not an exact measure of the temperature of the product emerging from the die, since thermal gradients will exist across the face and length (i.e. radial and longitudinal directions respectively) of the die. In addition, the temperature is not uniform across the transverse plane of the feed metal emerging from the die, since friction and redundant deformation will generate non-uniform temperature gradients across the transverse plane of the feed metal in the deformation zone as it approaches the die orifice. This variation of temperature has not been studied by considering the individual components of friction and redundant work done in the present analysis.

The theoretical analysis assumes a uniform temperature increase across the transverse plane, derived from the upper bound equations in section 5.6. The temperature measured by a probe positioned on the die will indicate the temperature after heat transfer (or conduction) through friction between the moving feed metal and the die interface. A complex theoretical analysis is required in order to determine the relationship between the feed metal friction temperature and peripheral die temperature and is not within the scope of this investigation. However, the variation between reduction and wheel speed on temperature can be used for comparative

purposes.

It is noted that different reductions require variations in the die orifice size and the consequent variation in the die wall thickness. Implicit in this set up is the variation in the length of conduction from the feed metal and die interface to the thermocouple probe positioned on the die surface. Since the conduction length is shorter for the smaller reduction (larger die orifice size) compared with the higher reduction, it is expected that a significant temperature deviation between experimental and theoretical data will result at one end of the reduction scale.

The temperature measured by the thermocouple probe on the die surface also provides an indication of whether transient or steady state operating conditions prevail. However, it is necessary to ensure that a constant temperature condition was maintained in order to provide consistent and reliable data for comparative purposes between varying reductions and wheel speeds. Consequently, it is important to ensure that the probe is located in the same position on the peripheral surface of the die, and contact between the die and probe was maintained for all tests.

The graph of temperature against reduction is illustrated in fig 7.17. The graphs show the correlation between experimental die temperature and theoretical product temperature for different reductions, and constant abutment depth and wheel speed using the annealed feed stock. The trend of the curves show that for increasing reduction higher temperatures are expected. The graph clearly indicates that the trend of the analytical curves can be expressed by a logarithmic relationship.

The influence on temperature by using the cold worked feed stock is illustrated in fig 7.18. The graphs show the experimental and theoretical relationship between the peripheral die temperature and the product exit temperature respectively against reduction ratio for different abutment

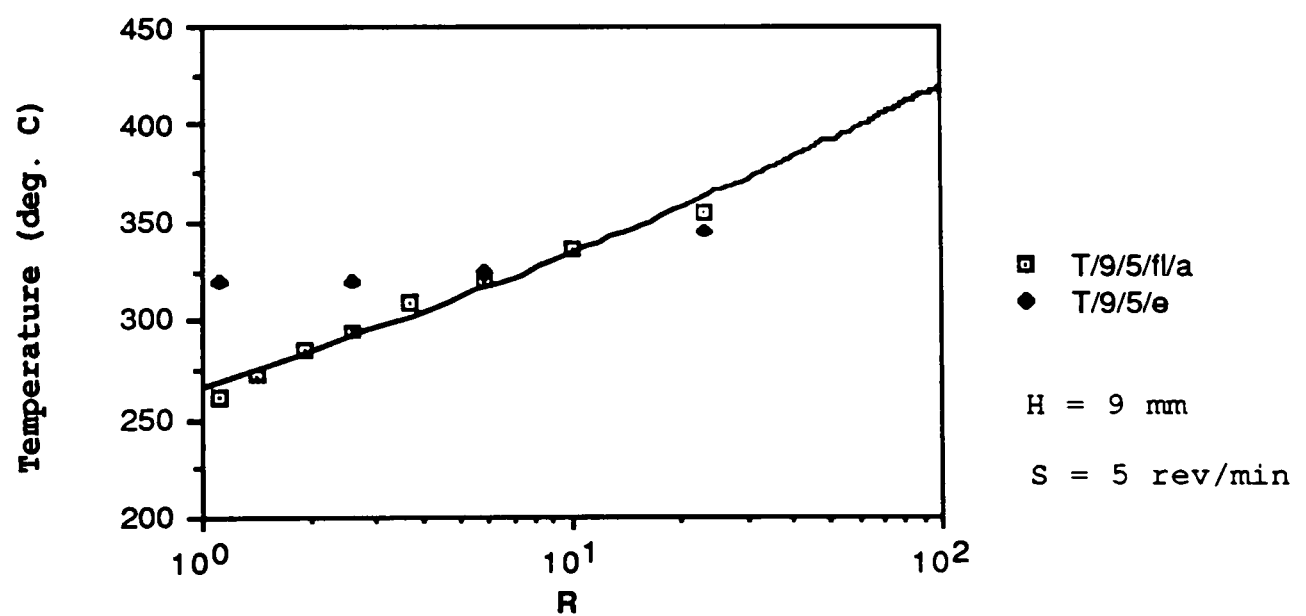
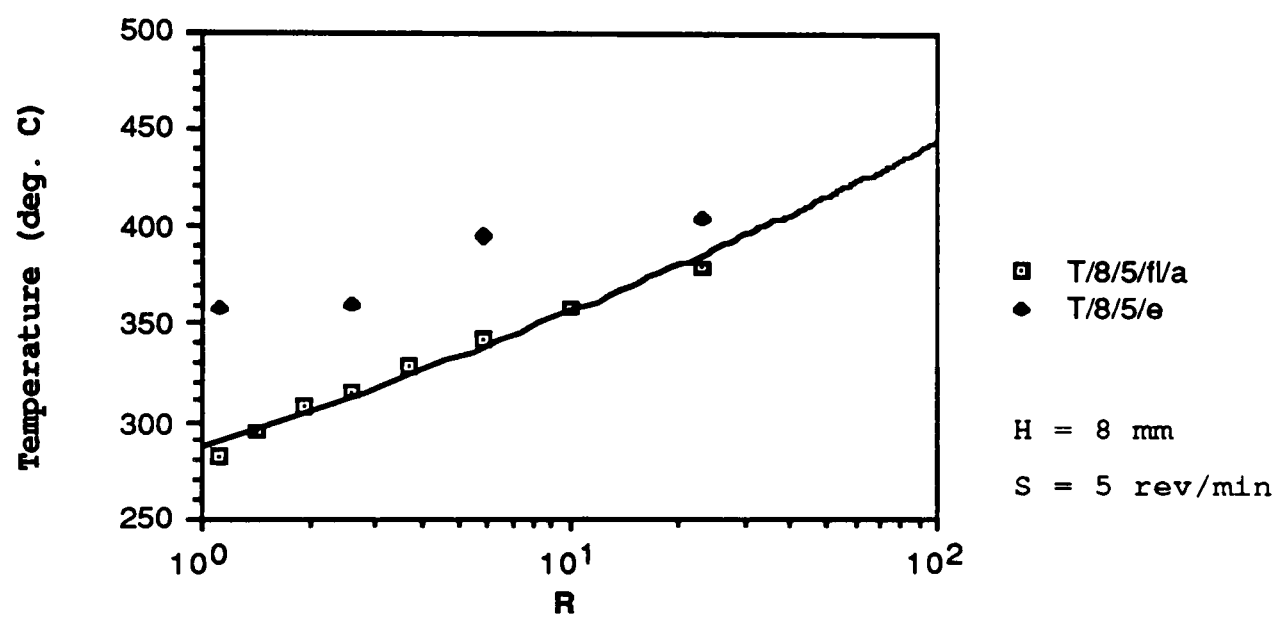
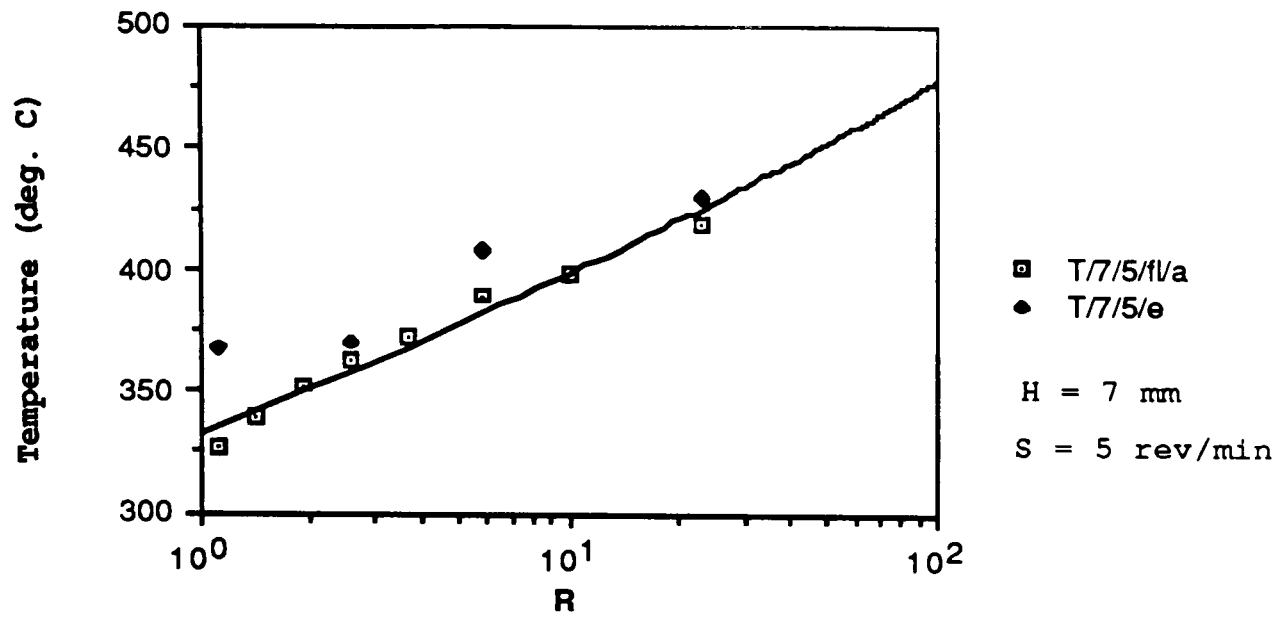


Figure 7.17 The graphs show the experimental and theoretical relationship between the peripheral die temperature and exit temperature respectively, and reduction ratio for different abutment depths 7, 8, 9 mm and constant wheel speed, using the annealed feed stock.

depths, while maintaining constant speed. As before, the trend of the curves show that for increasing reduction higher temperatures are expected.

Observation of figs 7.17 and 7.18 indicates that the theoretical and experimental data are in reasonable agreement. It is noted, however, that a greater deviation exists between the analytical and experimental data at lower reduction (max. error = 50 °C) common to the different abutment depth settings 7, 8 and 9 mm. This can be explained by the influence of the increase in friction contact area and reduced conduction length for the larger die orifice, indicating that more heat is dissipated at the die peripheral surface compared with the smaller die orifice. It also implies that the temperature measured by the die probe is a more accurate and reliable measurement of friction generated heat for small reductions (noting that this is not a measurement of the mean temperature of the product emerging from the die). Therefore, since the die temperature at elevated reduction is in close agreement with the analytical data, the friction temperature is likely to be much greater than the temperature recorded by the probe.

To illustrate the analytical relationship between product exit temperature and reduction ratio for the cold worked and annealed feed stock with varying abutment depth settings and constant wheel speed, reference is made to fig 7.19. The graph clearly demonstrates that a higher temperature is generated in deforming the cold worked feed metal. This complements the analytical data pertaining to the total pressure against reduction ratio, see fig 7.5, where the pressure required to deform the feed metal is higher for the cold worked feed stock.

However, it should be mentioned that an inherent limitation of the theoretical analysis under consideration is the precise determination of the stress state at high strain, and the subsequent onset of flow softening at the appropriate level of strain and temperature. This is because the stress state at high strain was determined from interpolated experimental

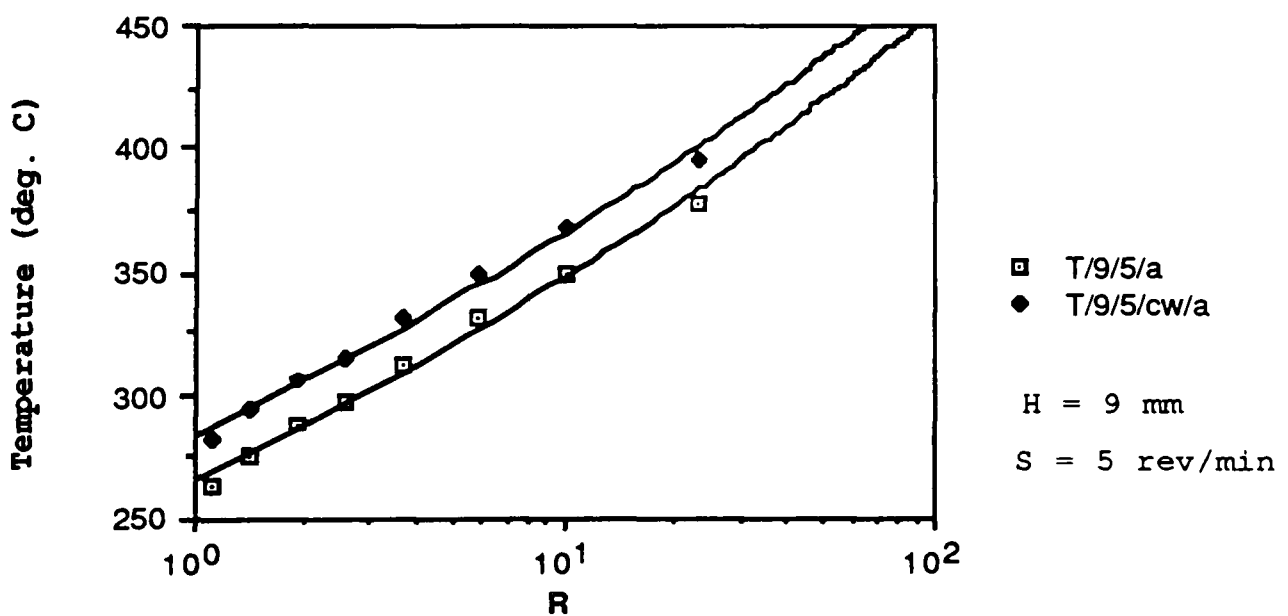
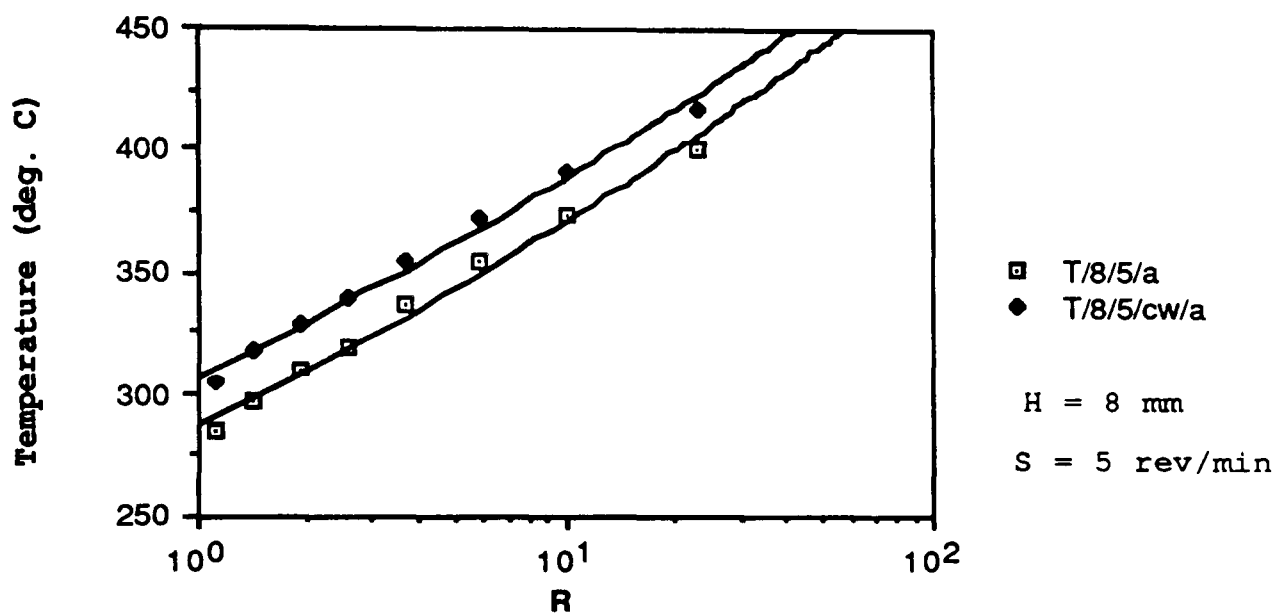
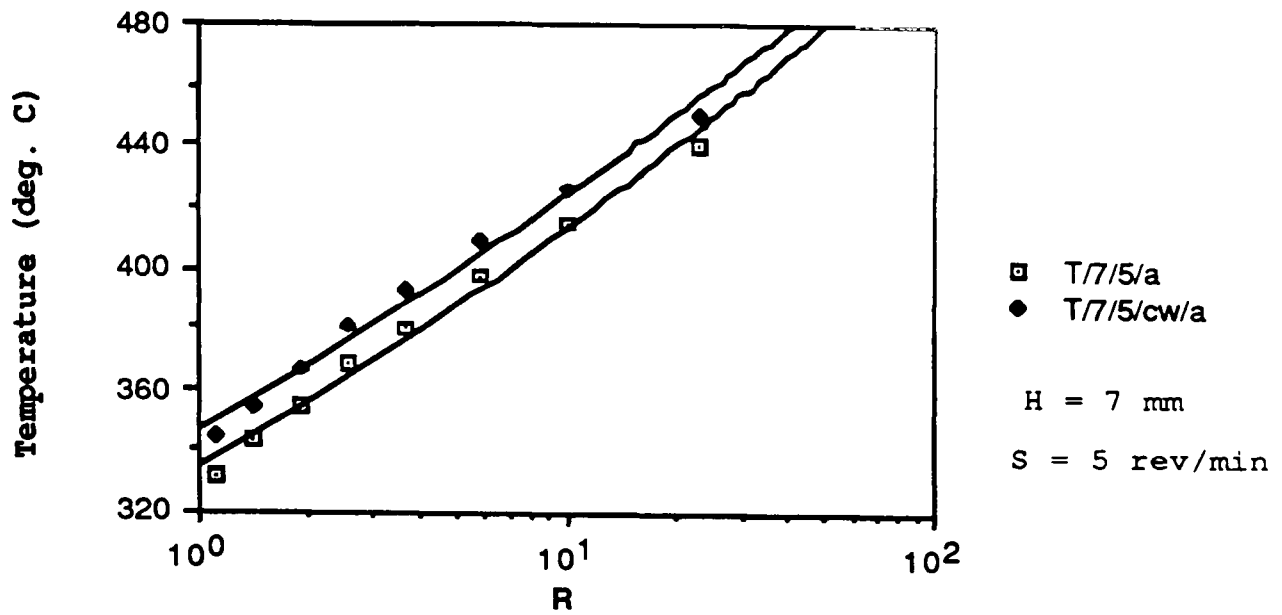


Figure 7.19 The graphs illustrate the theoretical relationship between exit temperature against reduction ratio for the cold-worked and annealed feed stock, with varying abutment depths 7, 8, 9 mm and constant wheel speed.

data. It was therefore assumed that flow softening would prevail as the feed metal entered the die chamber at stage 3, regardless of the level of the pre-straining influence in the primary extrusion chamber pertaining to the different abutment depth settings. Since the cold worked feed stock has undergone a high degree of pre-strain, it is reasonable to assume that the onset of flow softening will be initiated at some prior stage compared with the annealed feed stock. Consequently, it is suggested that the load and temperature requirements would reduce accordingly.

In addition, the determination of load and temperature at high strain rate was based on interpolated data. It is noted that an increase in strain rate accompanied an increase in wheel speed, it is suggested therefore that a greater margin of error should be allowed when considering the reliability of the analytical data at high wheel speed.

The graph of die temperature against reduction illustrated in fig 7.20 shows the experimental relationship for different abutment depths and constant wheel speed. The trend of the curves indicates that an increase in the peripheral die temperature accompanies a decrease in abutment depth setting. This implies that the temperature generated in the deformation zone is greater corresponding to the higher level of strain developed in the feed metal for the smaller abutment depth setting, 7 mm. Reference to fig 7.21 illustrates the theoretical relationship between product temperature and reduction ratio. The correlation between the two graphs, figs 7.20 and 7.21, shows that there is reasonable agreement between the trend of the curves for the different abutment depth settings. However, it is noted that the curve pertaining to the abutment depth setting, 8 mm is closer to the curve for the setting, 9 mm in relation to the analytical data given in fig 7.21. Whereas the abutment depth 8 mm is closer to the 7 mm abutment depth setting for the experimental data given in fig 7.20.

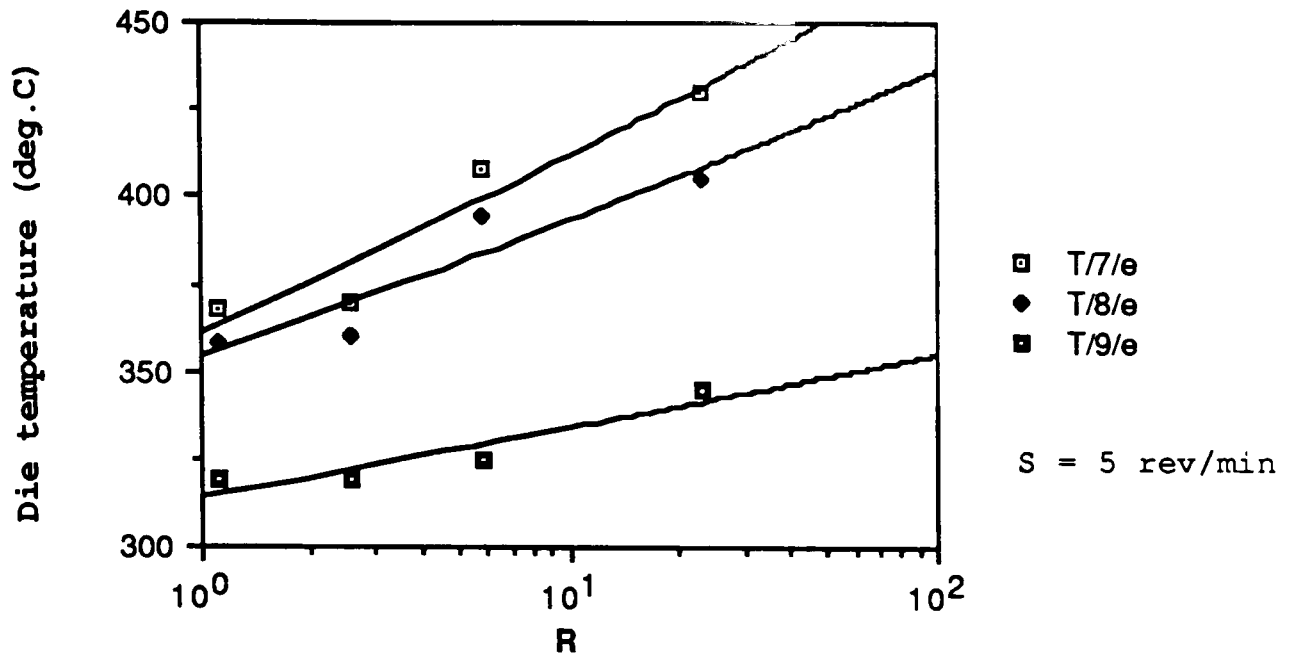


Figure 7.20 The graph shows the experimental relationship between the peripheral die temperature and reduction ratio for three different abutment depths 7, 8, 9 mm and constant wheel speed using the annealed feed stock.

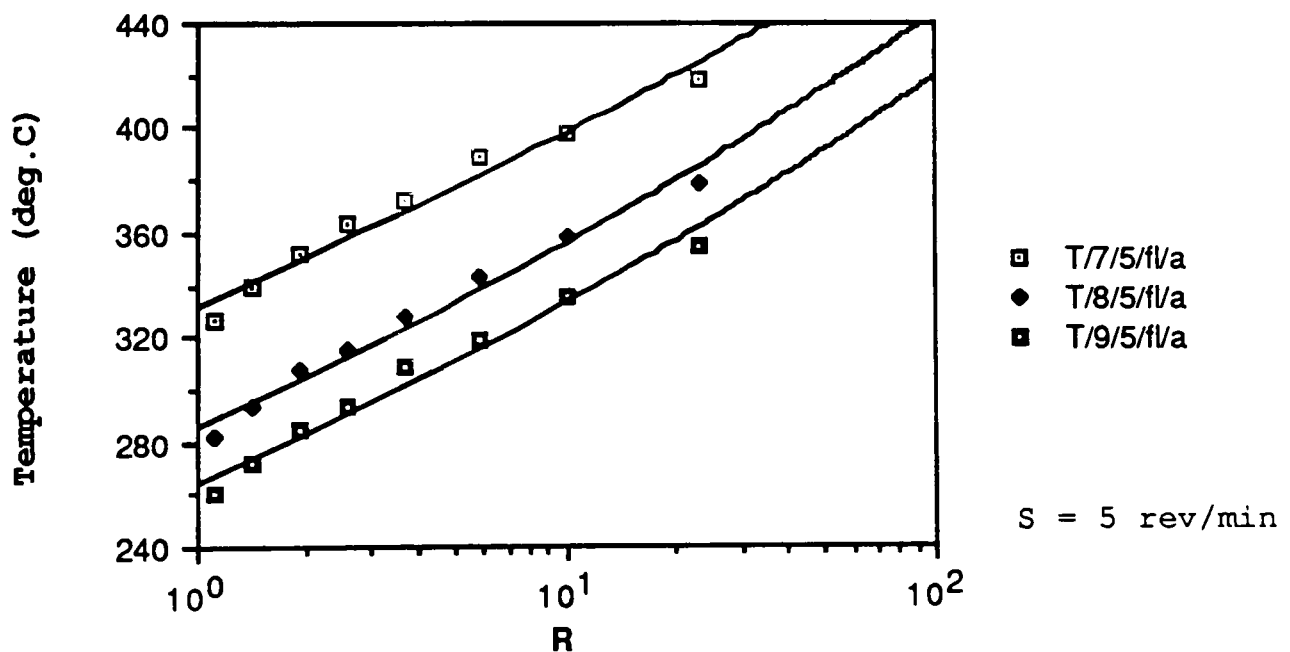


Figure 7.21 The graph shows the theoretical relationship between the product temperature against reduction ratio for different abutment depth settings 7, 8, 9 mm and constant wheel speed, using the annealed feed stock.

It is recalled under section 5.3 that the work done per unit volume is defined by the product of the stress state and corresponding strain increment. Reference to figs 7.7 and 7.8 shows that the total pressure against reduction for different abutment depth settings are in fair agreement. Therefore fig 7.20 confirms that more energy manifests itself as heat within the feed metal for the lower abutment depth setting 7 mm compared with settings, 8 and 9 mm. The theoretical explanation is that the adiabatic heat which transpires from the work done is a function of the temperature which, amongst other variables, determines the stress state and subsequently the work done corresponding to an increment of plastic strain.

Attention is drawn to fig 7.22 which shows the experimental relationship between peripheral die temperature and reduction ratio for different wheel speeds and constant abutment depth, using the annealed feed stock. The graph clearly indicates that, for an increase in wheel speed, a resulting increase in temperature can be expected. Confidence in these results is expressed due to the consistent increase in temperature and minimum scatter across the broad range of reduction and wheel speed.

The analytical relationship between the product exit temperature and wheel speed is illustrated in fig 7.23 for different reductions and constant abutment depth. The graphs show that, for an increase in reduction, a higher temperature is expected. In addition, a temperature increase accompanies an increase in wheel speed.

The graphs given in fig 7.24 show the relationship between product exit temperature and wheel speed for various abutment depth settings and constant reductions. It is clear that for a reduction in abutment depth setting, a corresponding increase in temperature will prevail. It is noted that band width for the different abutment depth settings reduces as the reduction ratio increases.

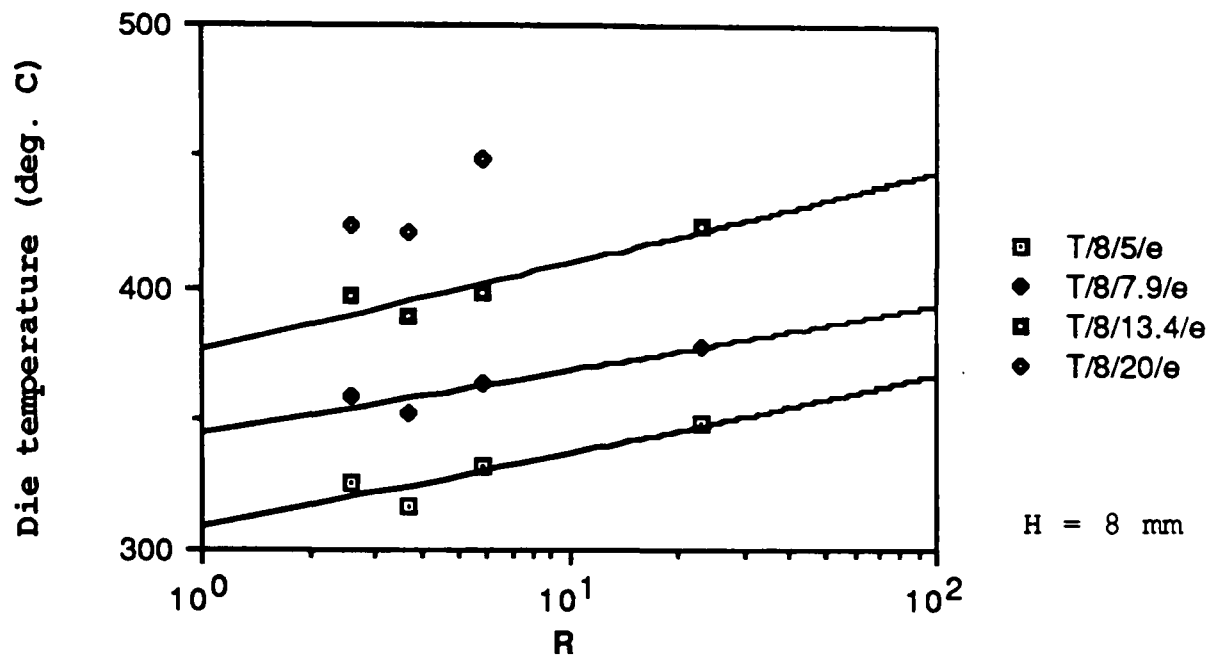


Figure 7.22 The graph shows the experimental relationship between the peripheral die temperature and reduction ratio for different wheel speeds 5, 7.9, 13.4, 20 rev/min and constant abutment depth 8 mm, using the annealed feed stock.

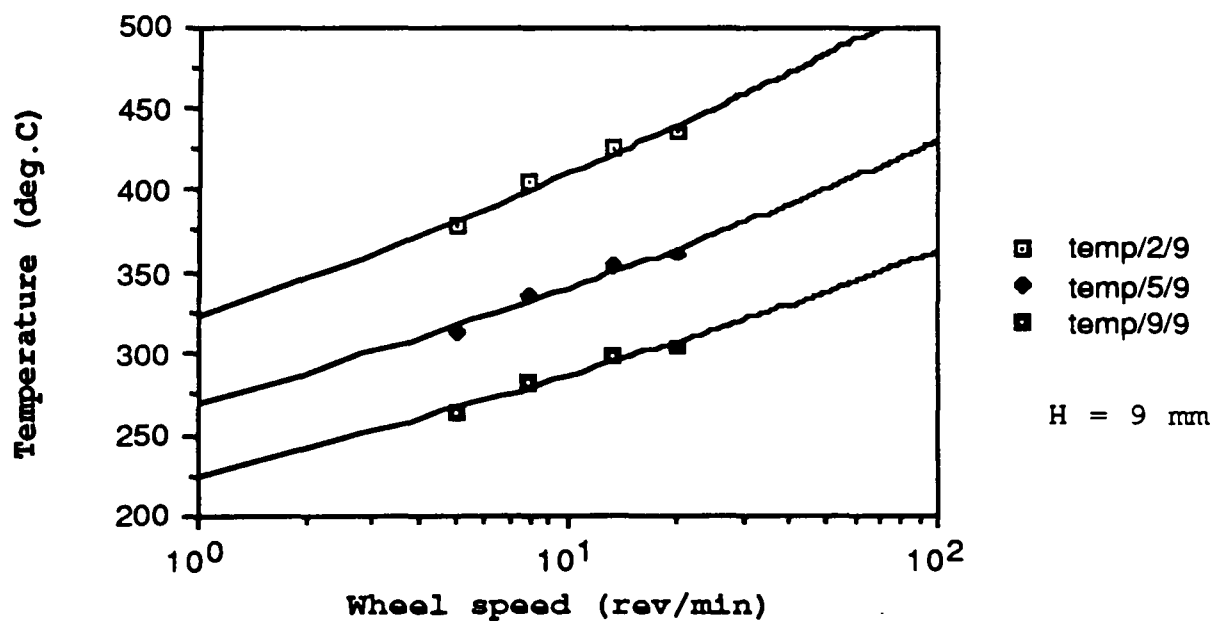
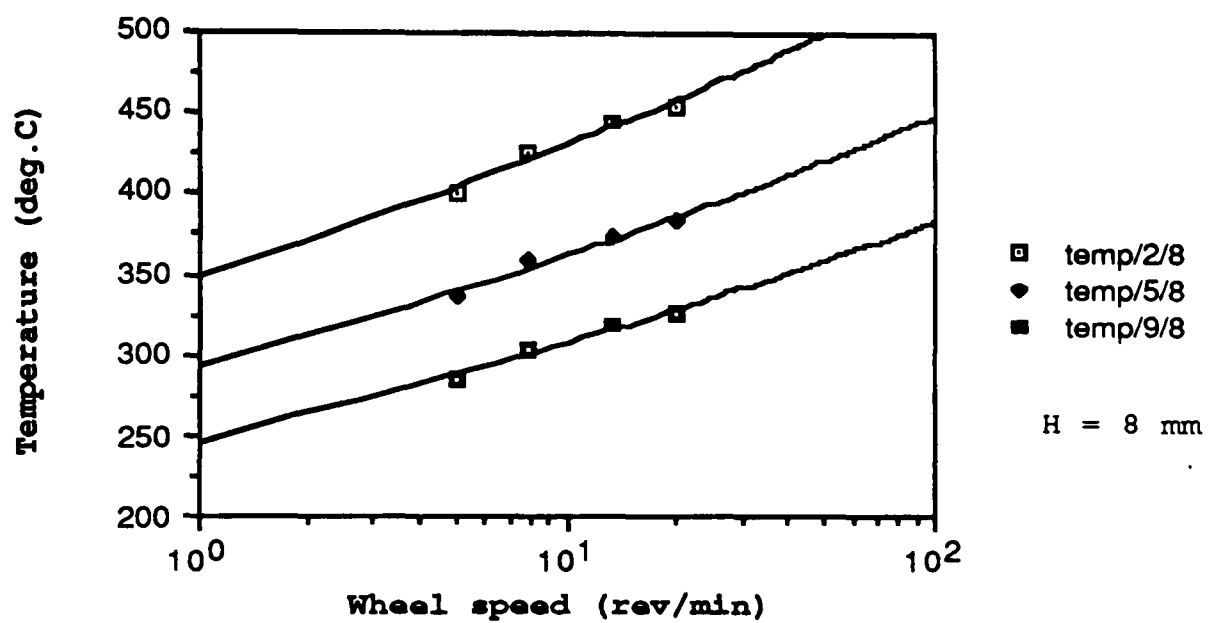
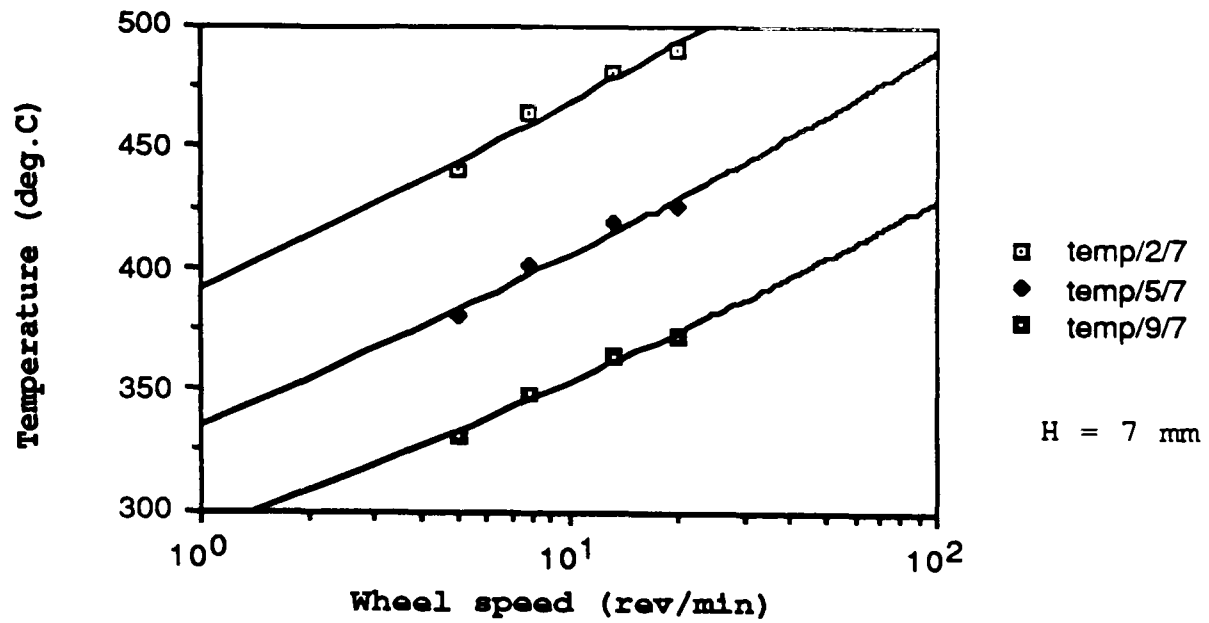


Figure 7.23 The graphs show the analytical relationship between the exit temperature and wheel speed for three different die sizes 2, 5, 9 ($R = 23.0, 3.7, 1.1$) and constant abutment depths 7, 8, 9 mm using the annealed feed stock.

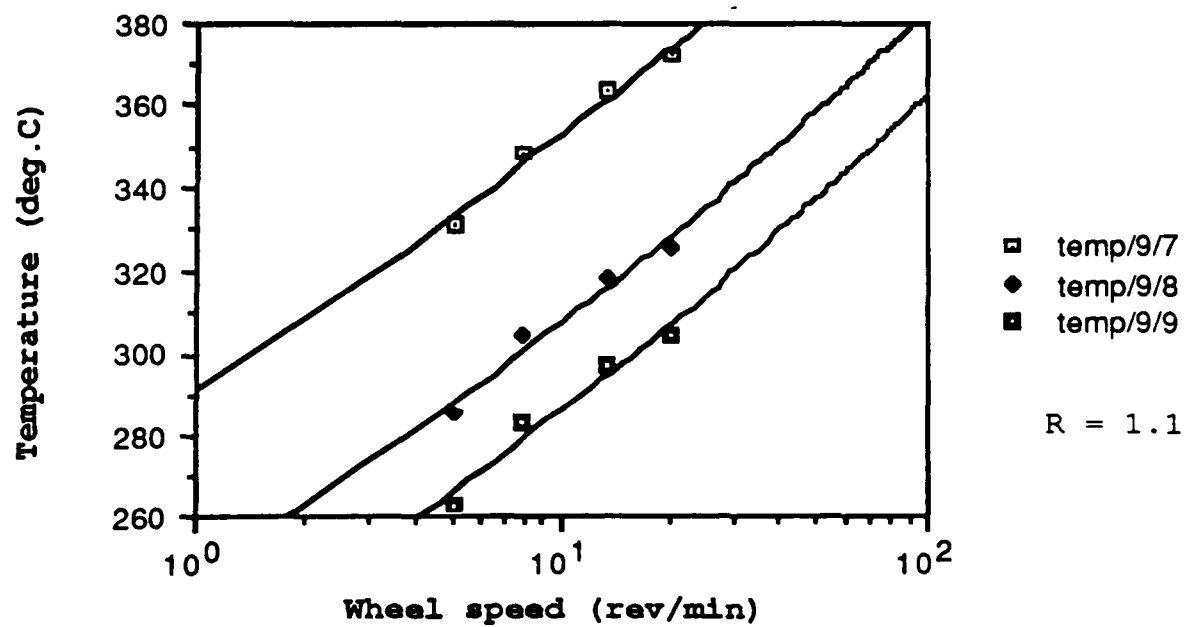
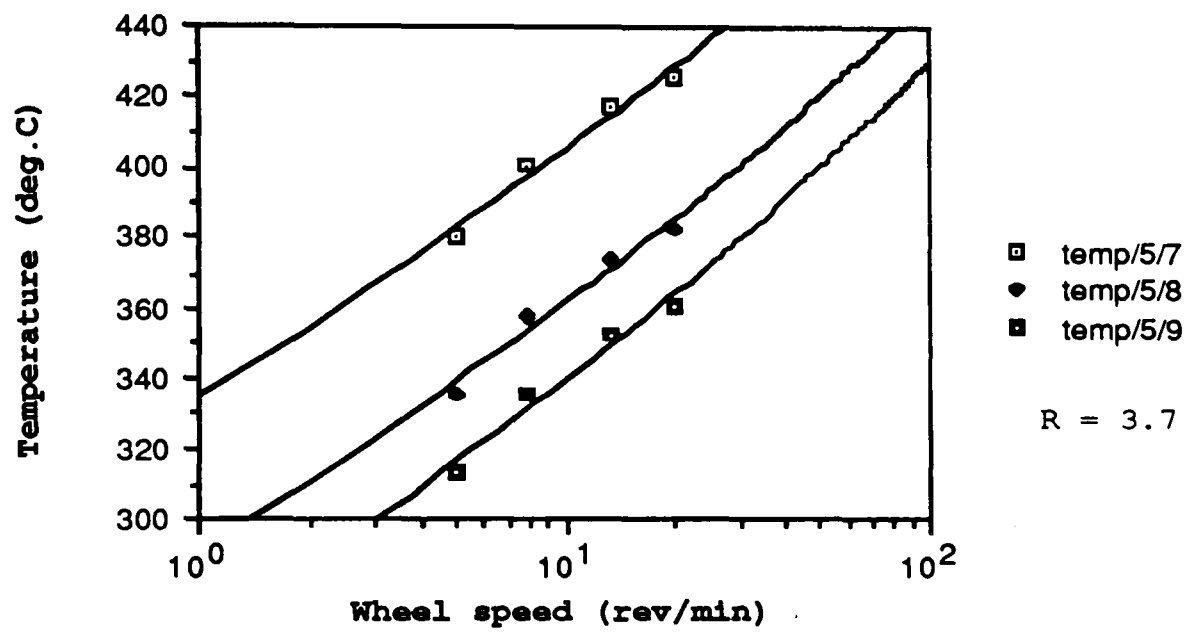
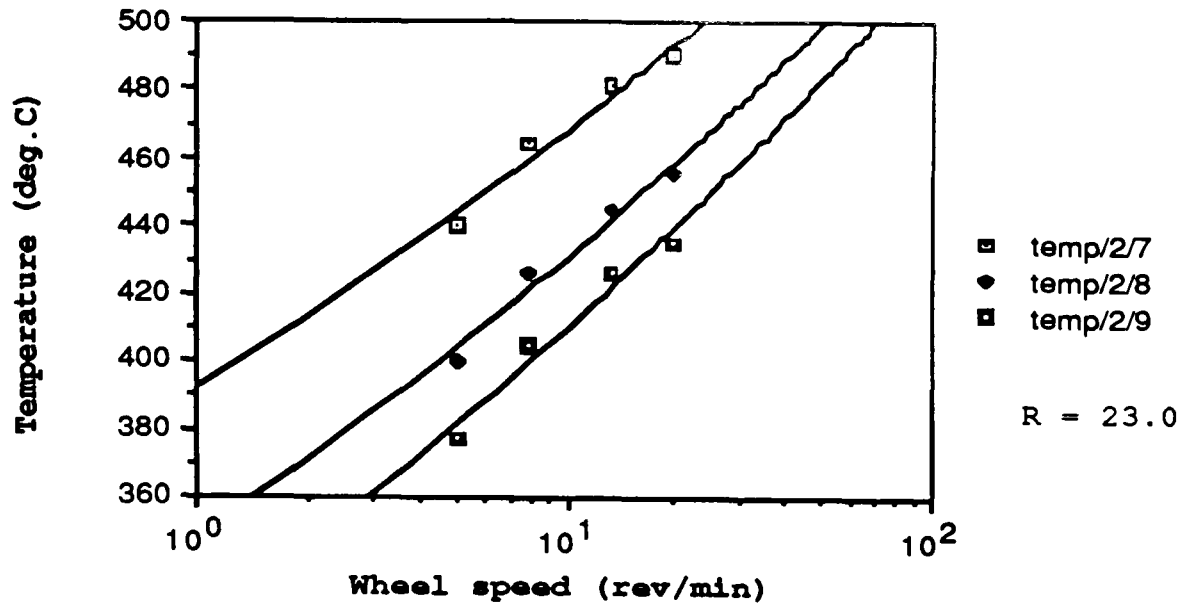


Figure 7.24 The graphs show the analytical relationship between the exit temperature and wheel speed for various abutment depths 7,8,9 mm and three constant die sizes 2, 5, 9 ($R = 23.0, 3.7, 1.1$ respectively) using the annealed feed stock.

7.4 TORQUE MEASUREMENT

The measurement of torque was determined by monitoring the differential pressure across the hydraulic motor corresponding to a particular wheel speed. A graph of the performance characteristics of the hydraulic motor under a wide range of operating conditions is supplied by the manufacturers. This was useful because it allowed the torque and power to be determined from the knowledge of two variables which, in this case, are the pressure differential from inlet and outlet of the motor and wheel speed.

The performance graph was interpreted by marking square grids, equally-spaced, in order to provide details of the torque measurement corresponding to a particular wheel speed. It was observed that the curves of pressure were constant in the range of wheel speeds 5 - 25 rev/min. Therefore it was possible to provide a calibrated relationship between torque and differential pressure at a known wheel speed. This allowed a direct reading of torque from the computer screen.

The hydraulic motor has been in service for a period of 10 - 15 years. Depending on the level of service it was considered that the performance curves provided by the manufacturers for the new hydraulic motor will be subject to some error of the order of $< 10\%$. However, accurate measurement of torque is not considered to be a priority, and it was primarily employed to indicate the transient or steady state operating condition. In addition, a useful measurement is the relationship between wheel speed and torque. It is noted from the experimental data that a decrease in torque accompanied an increase in wheel speed and temperature. This is useful in assessing the reliability of the experimental data obtained from the abutment and die loadcell.

It may be recalled from the theoretical analysis in section 5.9 that the torque provides a measure of the total energy expended in deformation. Therefore, from equation 5.36, it is clear that the torque provides the energy balance by equating

the product of the total tangential forces and wheel radius to the torque. From this equation, it is possible to make quantitative assessment of the reliability of the experimental data within the margin of experimental error and to compare the accuracy of the analytical and experimental data.

Observation of fig 7.25 illustrates the experimental and theoretical relationship between torque and reduction for constant abutment depth settings 7, 8 and 9 mm and wheel speed. It is noted that the curve pertaining to the analytical data is not smooth for the range of reduction, because the appropriate flash level has been incorporated in the theory corresponding to that which is generated in the experimental tests 40e - 55e. The correlation between the experimental and theoretical data, fig 7.25, shows that there is reasonable agreement between the data points on each graph.

However, it is noted that for increasing reduction an apparent convergence between experimental and theoretical data is observed. In addition, the experimental data remains higher than the predicted data for the lower range of reductions. Moreover, the graphs clearly indicate that a definable relationship exists between the experimental and predicted data with the appropriate allowance made for the generation of flash.

The experimental and theoretical relationship between torque and wheel speed and constant reduction and abutment depth setting is illustrated in fig 7.26. The graph clearly shows that the correlation between the experimental and theoretical data is reasonable. The trend of the curves indicates that a reduction in torque accompanies an increase in wheel speed, and this holds true for the range of reductions. However, it is recalled from fig 7.25 that the experimental curve for the lower reductions will remain above the theoretical curve. Also, it is noted that a greater reduction in torque accompanies an increase in wheel speed corresponding to the experimental data compared with the analytical data.

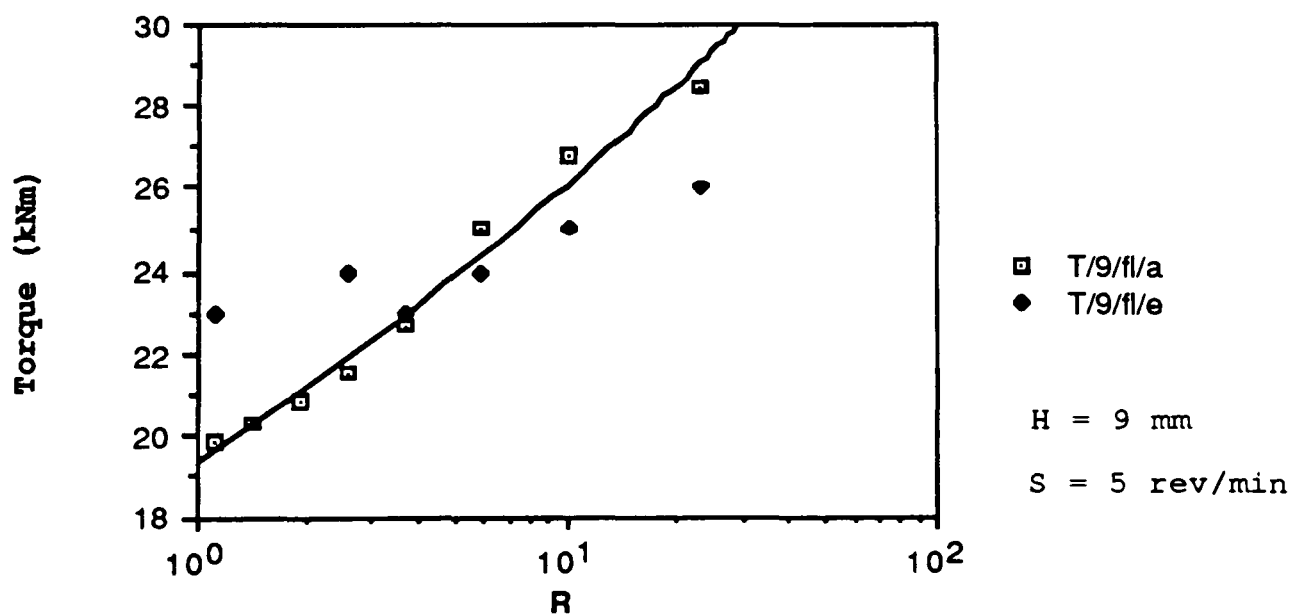
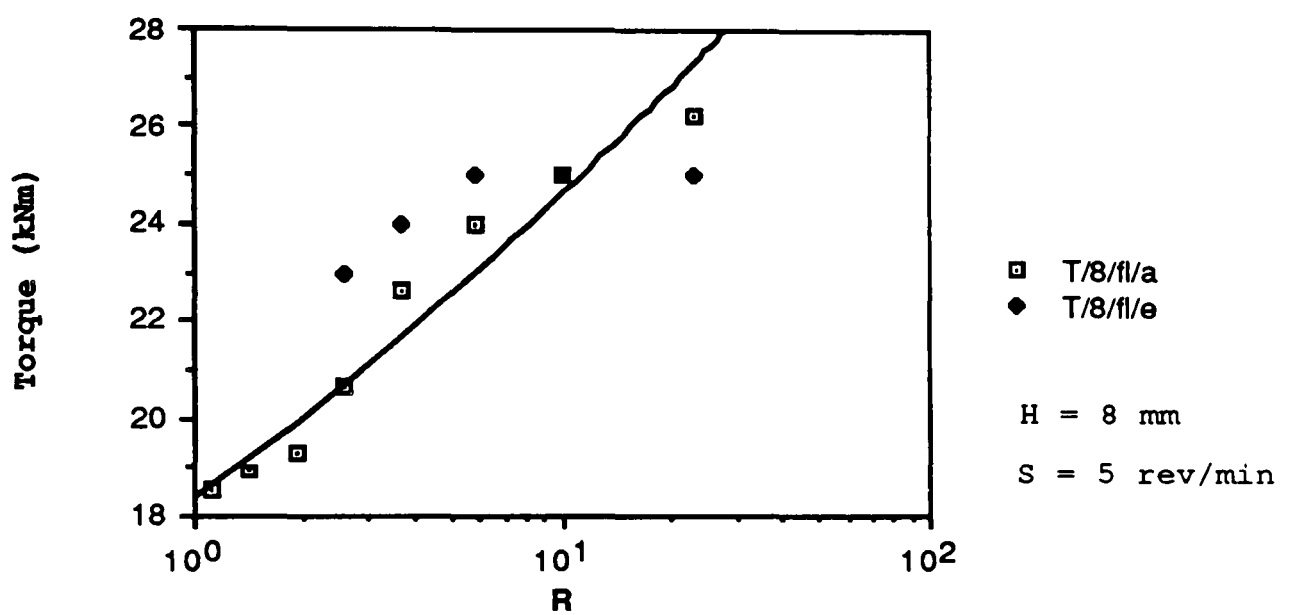
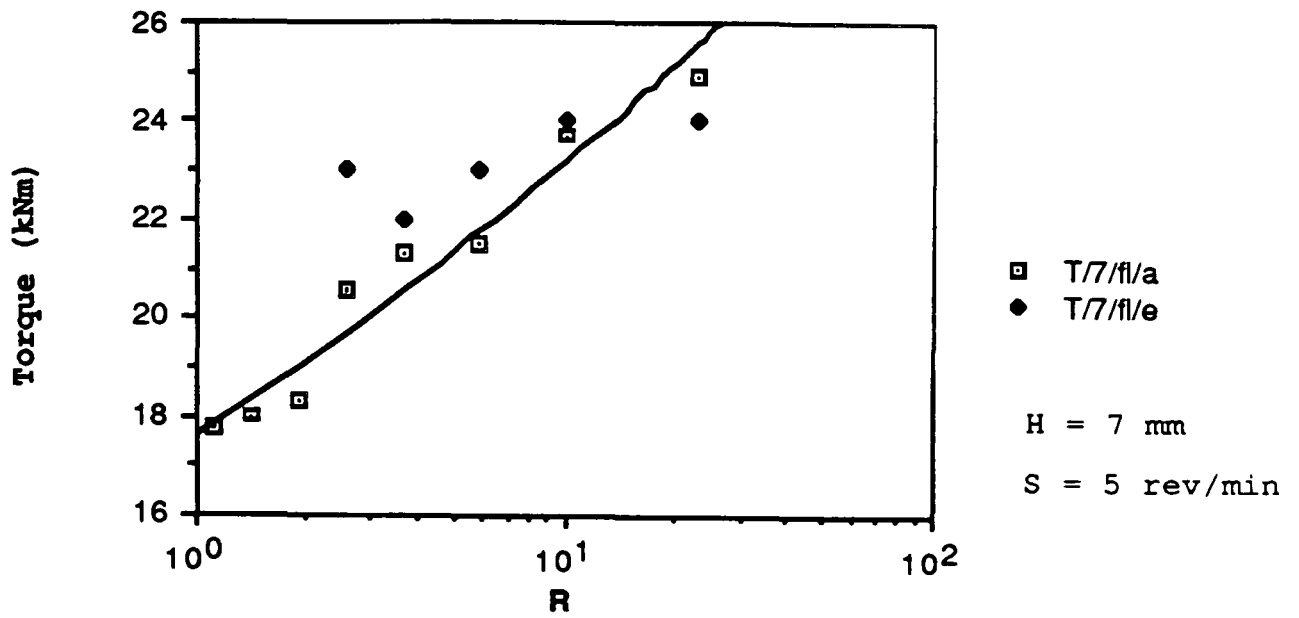


Figure 7.25 The graphs show the relationship between theoretical and experimental torque against reduction ratio corresponding to various abutment depths 7, 8, 9 mm and constant wheel speed, using the annealed feed stock.

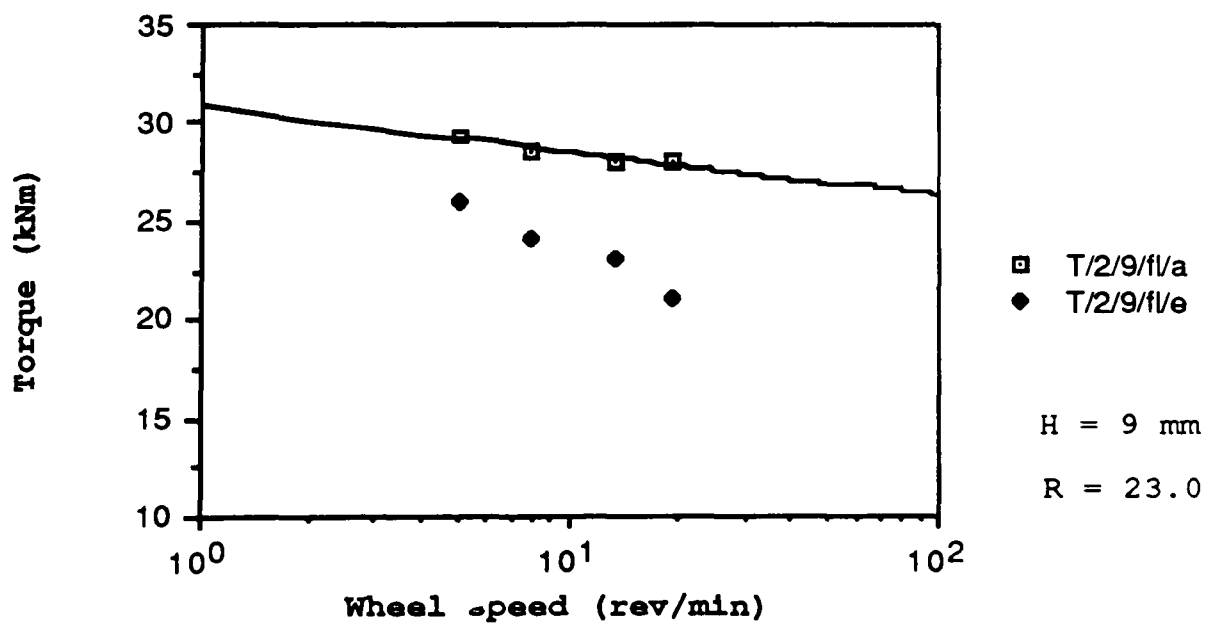
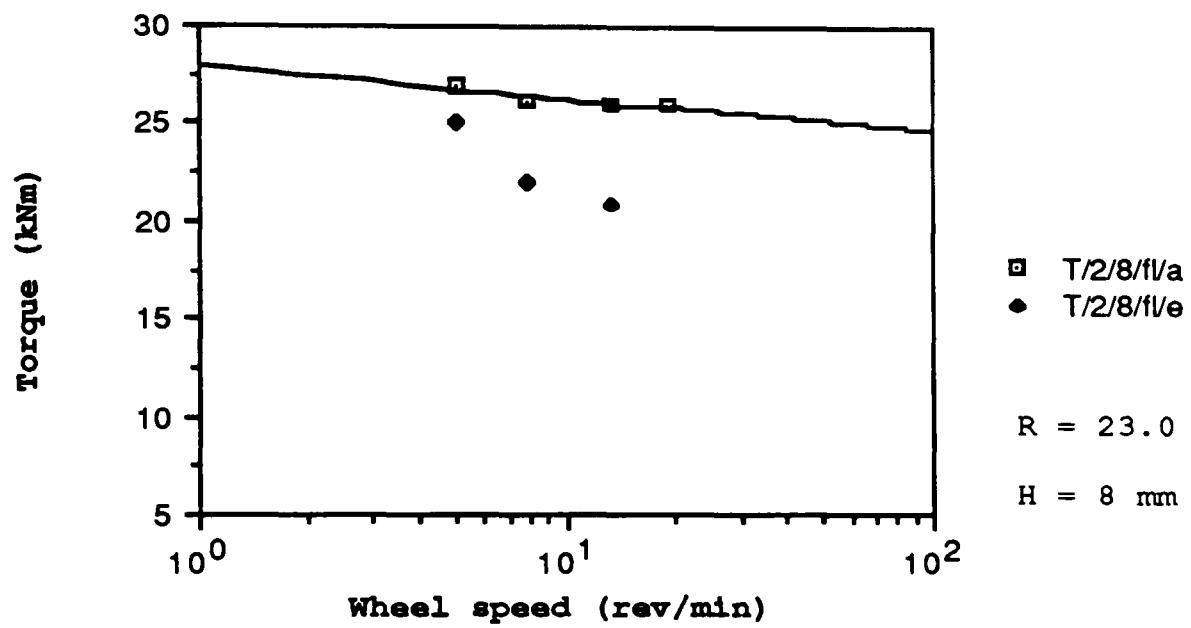
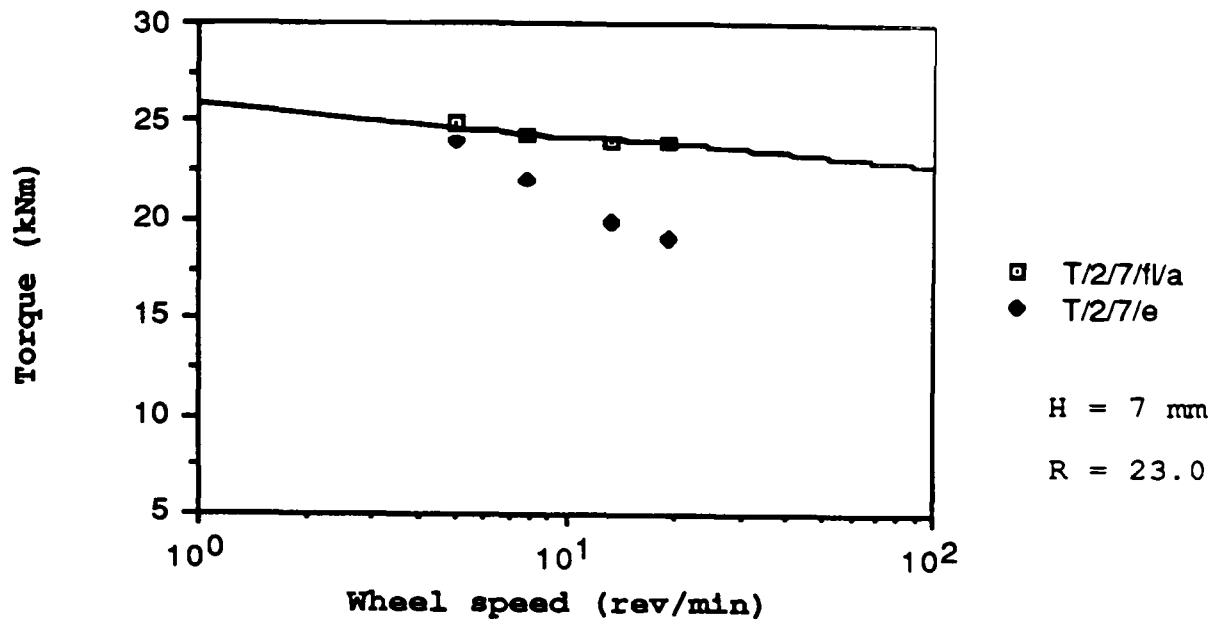


Figure 7.26 The graphs show the relationship between theoretical and experimental torque against wheel speed corresponding to various abutment depths 7, 8, 9 mm and constant reduction ratio, using the annealed feed stock.

It is recalled that the predicted torque is determined from the product of the total tangential force and wheel speed. It is suggested therefore that the the predicted die and abutment loads should account for a greater reduction in force corresponding to an increase in wheel speed. However, it is also recalled from the experimental measurements of abutment and die force that no significant reduction in force accompanying an increase in wheel speed was recorded for the range of reduction. It is also possible that the sensitivity of the respective loadcells is not sufficient to detect changes in force corresponding to variations in wheel speed within the band width of experimental error.

Another possibility is that the flash friction which exists between the stationary tooling in the shoe and the rotating wheel, will experience an increase in temperature corresponding to an increase in wheel speed. Subsequently, a reduction in friction force accompanies an increase in flash temperature and thereby reduces the torque accordingly. The effect of flash friction in the present theoretical analysis is considered with heat transfer. However, it is noted that a limitation within the theory in this respect is that the small variation in flash friction corresponding to an increase in wheel speed had only a minimal effect on torque.

Finally, it is recalled from the theoretical analysis in section 5, that an increase in temperature accompanies an increase in wheel speed. In addition, it has been demonstrated that proportionally more heat is retained in the feed metal than is given to the tooling chamber⁽⁴⁴⁾ as it is plastically deformed with increasing speed. This effect was incorporated in the heat transfer equation 5.22, i.e. $T_f = T_i / f(\theta)$ where $f(\theta)$ reduces corresponding to an increase in wheel speed. However, it is noted that the variation in $f(\theta)$ is small in the range 1.2 - 1.05 for increasing wheel speed in the range 5 - 20 rev/min. It is suggested therefore that a limitation of the theory is the range of heat loss denoted by $f(\theta)$. In other words, $f(\theta)$ could be interpreted from

experimental torque data to yield a wider band i.e. 1.05 - 1.5, subsequently providing the equivalent reduction in abutment force corresponding to an increase wheel speed, at the expense of increasing the abutment force at reduced wheel speed.

The $f(\theta)$ was however, not incorporated in the expression 5.20 for the temperature increase in the feed metal along the primary deformation zone. Alternatively, the constant β_2 denoted by equation 5.26 is used to ascertain the effect of the heat retained in the feed metal after heat transfer from experimental data.

The constant β_2 is determined from two variables, namely the mean diameter of the primary extrusion chamber and the surface area of the wheel groove in contact with the abutment tool. The limitation of the constant in the present theoretical analysis is that no allowance has been made for speed variations. Indeed, the constant β_2 has been determined from experimental force data for the constant wheel speed condition corresponding to 5 rev/min. This is because the computer program detailed in section 5.10 becomes unstable due to further increases in temperature at high wheel speed. In other words, the temperature and, subsequently, stress state will not converge to an acceptable level of desired accuracy but infact diverge. The reason for this is most likely attributable to the limited knowledge of the changing metallurgical structure of the feed metal in the deformation zone and the subsequent precise determination of the changing stress state from flow hardening to that of flow softening.

It is noted that the total energy equation 5.9 is balanced for the predicted abutment force at lower wheel speeds. As the wheel speed increases the energy equation becomes less balanced. However, it is considered that the determination of abutment and die force from the upper bound equation provides a reasonable indication of the true load. The experimental data complement the predicted data within the margin of

experimental error. To confirm this, attention is drawn to fig 7.27 which illustrates the analytical relationship between torque and reduction for varying abutment depth settings and constant wheel speed. The trend of the curves indicates that increasing torque accompanies an increase in abutment depth setting. This is considered to be a sensible measurement since an increase in available area must justify a corresponding increase in force as indicated by the predicted and experimental measurement of abutment force, see fig 7.2.

Also, it is noted from fig 7.7 that the total pressure measurement is high, of the order of 1130 MPa, corresponding to high reduction for all abutment depth settings. It was observed after tool removal, that the abutment tool had suffered plastic deformation at the leading edge which is seated to the root of the wheel groove. The deformation was in the form of a small bulge which protruded by a small amount from the face of the abutment tool particularly for the higher abutment depth setting 9 mm. The depth of the groove in the wheel in which the abutment tool is located was measured in order to ensure that sufficient clearance was available to prevent contact at high operating temperature. Since the abutment tool is manufactured from a high strength tool steel with an equivalent yield stress in the range 1100 - 1400 MPa for the high operating temperature condition, it is reasonable to expect that yielding of the abutment tool may result with high reduction (noting that the landed region of the abutment tool was minimised in order to reduce the influence of friction on the abutment tool force, and as a result, it is likely that this modification resulted in the premature failure of the abutment tool caused by the onset of plastic yielding at high reduction).

In addition, because the scraper tool profile was removed for the tests 30e - 55e, the oxidised surface layer of feed metal deposited on the wheel groove surface was removed by the abutment tool, consequently increasing the abutment tool force due to the increased friction at the landed region.

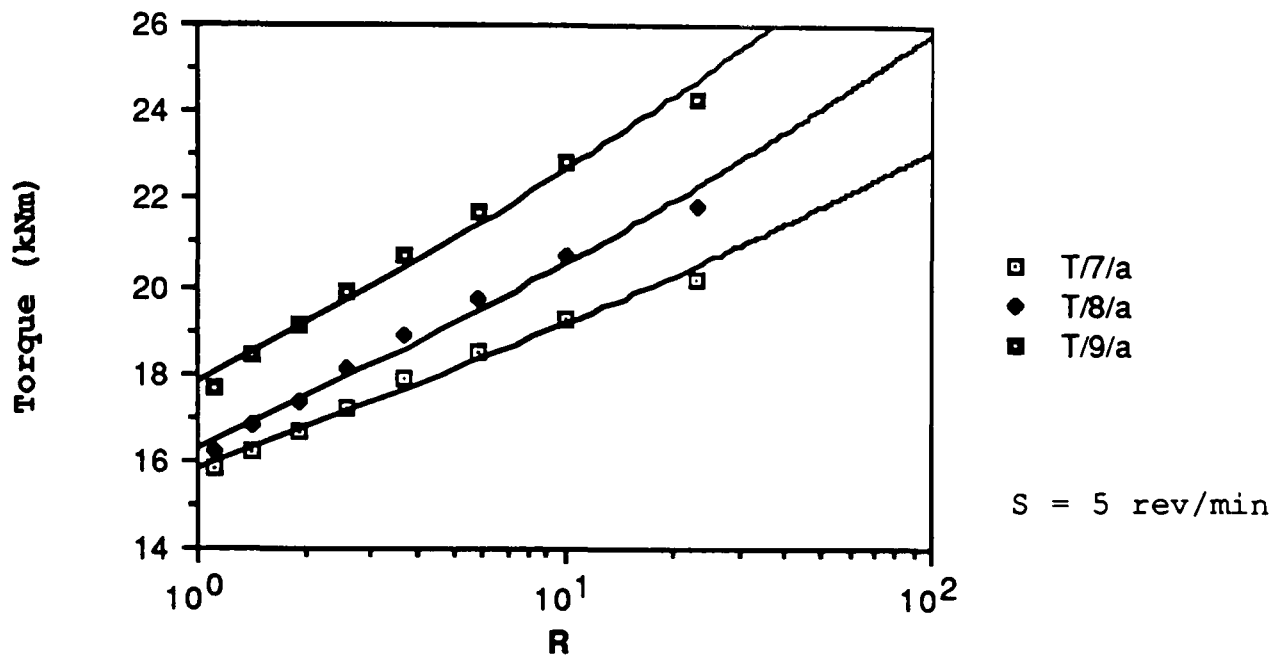


Figure 7.27 The graph shows the analytical relationship between the torque against reduction ratio corresponding to various abutment depths 7, 8, 9 mm and constant wheel speed, using the annealed feed stock.

7.5 GRIP LENGTH

The length of grip in the primary extrusion chamber is an important consideration with respect to machine tooling design. Figure 7.28 illustrates the analytical relationship between grip length and reduction for varying abutment depth settings and constant wheel speed. It is observed from the graph that no direct relationship exists between the abutment depth setting and grip length. It is clear, that the trend of the curves illustrated in fig 7.28 follow a logarithmic relationship.

The theoretical determination of the grip length is given by expression 5.28. It is noted, that the grip length is a function of the total work done, the stress state at stages 2a - 3 and the geometry of the primary extrusion chamber. The influence of the work done at stage 1 - 2a is considered to have a negligible effect on the grip length, see section 5.3, however the stress level determined from the strain level at stage 2a will influence the grip length. The total work done is, in turn, a complex function based on the changing stress state and strain at each stage in the deformation zone.

It is recalled that the level of strain developed in the feed metal in the primary extrusion chamber stage 2a - 3 is greatest for the abutment depth setting 7 mm and lowest for the 8 mm, with the 9 mm setting at an intermediate level. This allows a direct relationship to be established between the stress state (or strain since the feed metal is assumed to be at ambient temperature) in the primary extrusion chamber and the grip length, as illustrated in fig 7.28. That is, with increasing the level of strain at stage 2a (2a corresponds to the start of the primary extrusion chamber) a reduction in the length of grip required to maintain extrusion is observed. To complement this, attention is drawn to the cold worked analytical test data in which the stress level at stage 2a is greater due to the initial pre-strain in the feed metal. It is observed that there is a significant reduction in grip length for the abutment depth setting 8 mm compared

with the 7 and 9 mm settings.

The measured arc length of the tooling chamber is 125 mm from the chamber entrance to the face of the abutment tool (135 mm inclusive of the small tapered portion at the tooling chamber entrance). It is noted that the predicted grip length for all abutment depth settings does not exceed the measured arc length of the tooling chamber.

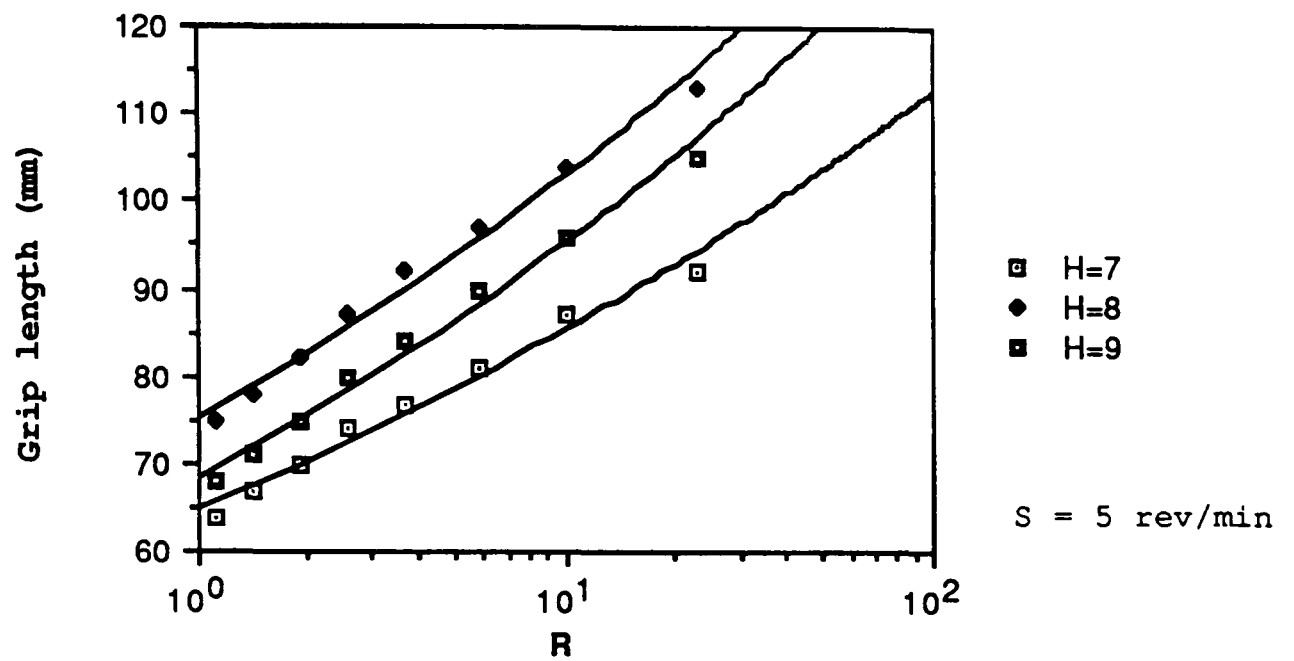


Figure 7.28 The graph illustrates the analytical relationship between the length of grip and reduction for varying abutment depth setting and constant wheel speed.

8.0 CONCLUDING SUMMARY

The following conclusions are drawn from the present investigation which involved the extrusion of commercial purity aluminium on the Conform process.

8.1 DEFORMATION MODES

To allow full analysis, the deformation zone is divided into definable stages of plastic deformation between entry and exit planes.

The modified uniaxial stress-strain experimental test data (after Alder and Philips), has been shown to provide an expression for the stress state corresponding to each stage in the deformation zone for the range of strain, strain rate and temperature, i.e.,

$$\sigma = A(1 - BT_H) \epsilon^n \dot{\epsilon}^m$$

where $m = C(10^{DT_H})$ and, $0.1 < \epsilon < 0.7$, $1/s < \dot{\epsilon} < 40/s$,
 $18^\circ\text{C} < T < 550^\circ\text{C}$

and, $T_H = T/T_M$ where T_M is the melting point temperature for commercial purity aluminium (details of constant values are given in appendix C3).

For higher levels of strain and strain rate i.e. $\epsilon > 0.5$, and $\dot{\epsilon} > 40/s$ and $T > 200^\circ\text{C}$, or, assuming dynamic recovery is the deformation mechanism then the equation for stress can take the following form,

$$\sigma = A(1 - BT_H) \dot{\epsilon}^m$$

The grip length is determined by equating the external forces to the internal work of deformation thus providing a measure of the length of tooling chamber required to maintain extrusion i.e.,

$$L_{(2a-2c)} = \left((W_T - W_{t(1-2a)} A_a) / \tau_{m(1-3)} (SA - W) \right)$$

Also, it has been demonstrated that the grip length is directly related to the initial stress (or strain) level at the start of the grip length zone where the feed metal is plastically deformed to take the shape of the tooling chamber cross-section.

8.2 FORCE AND PRESSURE MEASUREMENT

It has been shown that the upper bound expression after Avitzur⁽²⁷⁾ for the total work done per unit volume and time in the die chamber is applicable as follows,

$$\begin{aligned} W_{t(3-5)} &= \int_3^5 \sigma_{(3-5)} f(\alpha_2) \delta \epsilon && \{W_h\} \\ &+ 2K_{(3-5)} \left((\alpha_2 / \sin^2(\alpha_2)) - \cot(\alpha_2) \right) && \{W_R\} \\ &+ 2K_{(3-5)} \cot(\alpha_2) \epsilon_c && \{W_f\}_d \\ &+ 2\tau_{(3-5)} \left((2L_{(3-5)} / d_3) - (1 - d_5/d_3) \cot(\alpha_2) \right) && \{W_f\}_c \end{aligned}$$

where, $\tau = mK$

The die pressure is described by the following equation,

$$\begin{aligned} P_d &= \int_3^5 \sigma_{(3-5)} f(\alpha_2) \delta \epsilon && \{W_h\} \\ &+ 2K_{(3-5)} \left((\alpha_2 / \sin^2(\alpha_2)) - \cot(\alpha_2) \right) && \{W_R\} \\ &+ 2K_{(3-5)} \cot(\alpha_2) \epsilon_c && \{W_f\}_c \end{aligned}$$

The modified upper bound expression for the work done per unit volume and time in the primary extrusion chamber where the feed metal is constrained to flow into the die chamber is described as follows,

$$\begin{aligned}
 W_{t(2b-3)} &= \int_{2b}^3 \sigma_{(2b-3)} \delta \epsilon && \{W_h\} \\
 &+ 2K_{(2b-3)} (1.25 + (\alpha_1 / \sin^2(\alpha_1)) - \cot(\alpha_1)) && \{W_R\} \\
 &+ 2K_{(2b-3)} \cot(\alpha_1) \epsilon_c && \{W_f\}
 \end{aligned}$$

It follows that the total work done on the abutment tool is equal to the sum of the energy equations as follows,

$$W_T = W_{t(2b-3)} + W_{t(3-5)}$$

The dead zone angle in the die chamber is determined by differentiation of equation $W_{t(3-5)}$ with respect to α_2 and equating the subsequent expression to zero.

It was observed that the dead zone angle in the die chamber which is determined from the minimum upper bound equation, will increase corresponding to a reduction in the friction factor in the range 0.5 - 1.

The pressure value determined from the minimum upper bound equation provide a reliable indication of the die and abutment forces for the broad range of reduction and abutment depth settings, at lower wheel speeds.

The pressure measurement is less reliable at higher speeds, from observations of the experimental torque data.

The total pressure corresponding to different abutment depth settings does not vary significantly for the range of reductions studied.

The measured values of abutment and die force agree with the predicted values for the broad range of reduction, abutment depth setting and wheel speed within the band width of experimental error.

It was observed that a reduction in the friction factor in the range 0.5 - 1 will lead to a comparatively small reduction in abutment and die force of the order of 10 % for $m = 0.5$.

8.3 TEMPERATURE CONSIDERATIONS

For high reductions, the temperature measured by a thermocouple probe on the die, correlates well with the predicted mean temperature of the product emerging from the die. The relationship does not hold for low reductions.

It is clear, from both analytical and experimental data that a substantial increase in temperature of the order of 80°C, will accompany a reduction in abutment depth setting (from 9 to 7 mm) for the range of reductions. Similarly, an increase in temperature will accompany an increase in wheel speed.

Within the range 0.5 - 1, a reduction in friction factor leads to a comparatively small reduction in product temperature of the order of 10% for $m = 0.5$.

It is evident that the temperature will vary across a section of the product directly it emerges from the die. A limitation with the present model is in its ability to predict bulk (or mean) temperature and not account for these variations which arise in the real process.

8.4 MEASURING EQUIPMENT

The initial decision to select tungsten carbide as the loadcell material instead of the standard EN 24 was substantiated. A tungsten carbide loadcell creates a more uniform temperature distribution when used in conjunction with a heat source on the upper face and heat sink on the lower face. The carbide material enables the design of a smaller and more compact loadcell compared with EN 24 due to its superior material strength and stiffness.

However, difficulties were experienced with regard to the second calibration of the tungsten carbide die loadcell. The carbide loadcell was used in conjunction with test no. 1e. Subsequently, recalibration on completion of test 1e revealed an output from the bridge circuit not comparable with the first calibration under similar set-up and loading conditions. Indeed, further calibration revealed quite different results from the second calibration. This suggested that damage had occurred to the tungsten carbide die-loadcell at some stage, and it should be discarded from being used in subsequent experimentation.

In view of the time required for the manufacture of a replacement carbide die loadcell (i.e. 14 to 16 weeks manufacture of spring element, with a further 2 to 4 weeks required for installation of strain gauges), and in addition, the total cost, it was felt that the EN 24 die loadcell should be used for following experimentation. Indeed, frequent recalibration of the EN 24 die loadcell revealed that only marginal variations in the calibration conversion factor occurred as detailed under section 4.4.1.

The first EN 24 die loadcell ceased to provide reliable data after test no. 39e and again was discarded. A replacement loadcell was manufactured and installed for test numbers 40e onwards. Examination of the first EN 24 die loadcell revealed that high temperature (of the order 260 °C) in conjunction with MoS₂-based lubricating oil, had rapidly degraded the

coating material which protects the strain gauges.

9.0 SUGGESTIONS FOR FURTHER WORK

From a modelling viewpoint, it is considered useful to extend the present analysis by using a more complex form of constitutive equation based on the changing metallurgical structure within the feed metal as it traverses the deformation zone. From this knowledge it may then be feasible to determine precisely where the condition for strain softening prevails over strain hardening. This feature would then obviate the need for the assumption that strain softening is initiated by a change in geometry (i.e. strain) alone at the entrance to the die chamber. It is likely that strain softening will occur at an earlier stage in the deformation zone rather than on entry to the die chamber where either an increase in wheel speed (strain rate) or reduction ratio (die size) will generate an increase in temperature.

It would be useful to determine the temperature and stress state change corresponding to a change in die chamber geometry. Further experimentation by way of macro-examination of discards removed from the die chamber after completion of tests, using different extrusion schedules, would yield a better understanding of dead-zone formation. These data will, in turn, contribute an understanding of the deformation mechanisms in particular, strain rate, stress state, temperature and subsequently work done (pressure) in the die chamber.

It would be useful to repeat the experimental programme using a copper feed stock. Determination of constitutive equations based on copper as the model feed metal would provide a means of assessing the reliability of the upper bound and constitutive equations, for the prediction of abutment and die forces together with temperature distribution.

The determination of the heat transfer constants in equations 5.23, 5.24 and 5.26 could be further examined by experimentation. Thermocouples could be positioned at strategic points along the tool grip length and die chamber in

order to observe heat transfer to the tooling. This is useful in determining the amount of heat energy retained in the tooling close to the deformation zone, and subsequently given back to the feed metal. In other words, a steady-state operation will be observed when the rate of heat given to the tooling reduces to a near constant value.

The use of particulate feed should warrant further examination by way of modelling. This is because the compacting process which takes place in the deformation zone implies changes in the metallurgical structure of the feed metal. Also, appreciably lower temperatures and forces are generated by using particulate feed stock compared with rod feed. This is, in the main, attributed to the lower volume through-put in a given period of time. The main disadvantage with particulate feed, setting aside metallurgical requirements, is related to lower production rates. However, the possibility of using harder alloy feed metals may exist due to a reduction in tooling wear.

The instrumentation used for generating the necessary experimental data was considered satisfactory for this research programme. The use of a computer based data-logging system proved time consuming with regards preparation, assembly and programming. However, the benefits gained by reducing the workload in terms of calibration conversion factors for the range of measuring equipment are significant, and considered to be worthwhile. Also, an understanding was gained with computational methods in data transfer, with appreciation of difficulties relating to none compatibility in hardware and software, and limitations associated with the storage of large amounts of data. It is suggested that the application of a computer-based data-logging system and associated sensing devices i.e. abutment force, die force, torque, speed and various thermocouples could be used in conjunction with a development/production Conform machine. The benefits of real-time data processing in association with small scale development work is demonstrated by way of a hard copy print out directly accessible to the operator, with the

variables displayed in the appropriate units.

Further work is, however, required in terms of loadcell design in conjunction with operation in a high temperature environment. But simply redesigning the shoe, with provision for a column loadcell placed further away from the heat source, would reduce the difficulties associated with a low strain gauge cycle life.

REFERENCES

REFERENCES

1. Green D.J., Institute of Metals, 1972. 100, 295-300. Also, UKAEA TRG report 2364(s), 1974.
2. Slater H. K., Conform - The continuous extrusion process. Int. Sym. modern metal forming techniques, New Delhi, 1979.
3. Marsh D. J., The extrusion of copper by the Conform continuous extrusion process. UKAEA TRG - Report 3007 (s), August 1977.
4. UKAEA - Advanced Metal Forming Group, Springfields. Paper No. 2, May 1975. Commercially Confidential.
5. BKL Extrusions (GKN Group) Kings Norton, Birmingham. GT Almax (Die Makers), Redditch.
6. Pardoe J. A., Non ferrous tube production by the Conform extrusion process. Int. Wire and Mach. Assoc. (Tube production conference). Birmingham, April 1978.
7. UKAEA - Advanced Metal Forming Group, Springfields. Paper No. 4, Feb. 1976. Commercially Confidential.
8. UKAEA - Advanced Metal Forming Group, Springfields. Paper No. 5, Aug. 1976. Commercially Confidential.
9. UK patent 1566152
10. UKAEA - Advanced Metal Forming Group, Springfields. Paper No. 10, Feb. 1981. Commercially Confidential.
11. Marsh D. J., A study of wheel and tool component life in the Conform extrusion of copper. UKAEA SL-Con-13, Dec., 1977.
12. Slater H. K., Development experience with the Conform continuous extrusion process on copper. UKAEA type ND-R-242 (s). Aug. 1978.

- 13 Epsilonics, measurements group Inc., Raleigh, North Carolina, 1982, 2, issue 3.
- 14 Wood P.K.C., The Mechanics of the Conform Continuous Extrusion Process (2nd report), Aston University, England, 1987, section 2, 6-11.
15. Private correspondence with Marshalls Hard Metals in Sheffield, England.
16. Private correspondence with Welwyn Strain Measurement, Basingstoke, Berkshire, England.
17. Etherington C., Journal of Engineering for Power, Trans. ASME, 1974. 96, 3, 893-900. Also, UKAEA RFL-CON-143, 1974, (Commercial in Confidence).
18. Tirosh J., Grossman G., and Gordon G.. Theoretical and Experimental Study of the Conform Metal Forming Process, July 1977. Faculty of Mech. Eng. Technion Israel Inst. of Tech. Haifa, Israel.
19. Haleem A.S., Cole I.M. and Sansome D.H.. Measurement of Contact Pressures in Tube Rolling, J.Mech. Working Tech., 1977, 1, 153-168.
20. Gorokhov Yu. V., Sergeev V. M., Gilevitch F. S., Kornilov V. N.. Capacity Parameters of Conform Continuous Extrusion Process. Tsvetn. Met. (4). 1987, 73-75.
21. Hodierne F. A.. A Torsion test for use in Metalworking studies, J. Inst. Met., 1962-63, 91, 267-273.
22. Bowden F. P., Tabor D., The Friction and Lubrication of Solids, 1950, Clarendon Press, Oxford.
23. van Rooyen G. T. and Backofen W.A., A study of interface friction in plastic deformation, Jan 1960, Int. J. Mech. Sci., 1-27.

24. van Rooyen G. T. and Backofen W.A., Distribution of interface stress in plain strain and Axial symmetric compression, 1959, J. Mech. Phys. Solids, 7, 163.
25. Drucker D. C., Coulomb friction, Plasticity and Limit Loads. J. App. Mech, 21. Trans ASME, 1954, 76, 71-74.
26. Hill, R., The Mathematical Theory of Plasticity, 1950, Clarendon Press, Oxford.
27. Avitzur B., Flow Characteristics through Conical Converging Dies. Trans ASME, Nov. 1966, 410-420. Also, Analysis of Wire Drawing and Extrusion Through Conical Converging Dies of Small Cone Angles, Trans ASME, Feb. 1963, 89-96.
28. Motamura, M., A New Plastic Working Art, J. Jpn Inst. Light Met., Oct. 1984, 34, (10), 591-606.
29. Kuhn H. A., Workability in Hot and Cold Deformation Process, Test Methods, Criteria and, Applications. University of Pittsburgh.
30. Orowan E., The Cam Plastometer, 1950. B.I.S.R.A. Report MW/F/22/50. Lueg W., Muller H.G., Krause U., The Hydraulic Forging Press, 1957, Arch. Eisenhutt Wes, 28, (8), 505.
31. Alder J.P., Philips V.A., The Resistance of Strain Rate and Temperature on the Resistance of Aluminium, Copper and Steel to Compression. J. Inst. Met., 1954-55, 83, 80-86.
32. Samanta S.K., On relating the Flow Stress of Aluminium and Copper to Strain, Strain Rate and Temperature, Inst. J. Mech. Sci., 1969, 11, 433-453.
33. Hockett J.E., On relating the Flow Stress of Aluminium to Strain, Strain Rate and Temperature, 1969, Los Alamos Scientific Lab. of Univ. of California (Report LA-3544).

34. Johnson W., Mellor P.B., Engineering Plasticity, Empirical equations to represent the Strain Curve, 1972, 267-270.
35. Akeret R., Untersuchungen uber die Warmverformbarkeit von Aluminiumlegierungen, S. auch Zeitschrift Metallkunde 61, 1970, S, 3-10.
36. Dieter G.E., Mechanical Metallurgy, 1986 Third ed., 532-538, 627-629.
37. Winston A.W., Jonas J.J., Aluminium Extrusion as a Thermally Activated Process, Trans. Met. Soc. AIME, Nov. 1968, 242, 2271-2280.
38. Conrad H., Thermally Activated Deformation of Metals, J. Met., July 1964, 582-588
39. Avitzur B., Analysis of Metal Flow through Conical Converging Dies as a Adiabatic Process, Proc. of the 4th NAMRC Con., 1976, 206-212.
40. Feltam P., Extrusion of Metals, Metal Treatment and Drop Forging, Nov. 1956, 440-444, See also Dieter op. cit. pp 628-629.
41. Farren W.S., Taylor G.I., Proc. Roy. Soc., 1925, (A), 107, 422.
42. Altan T., Gegel H. L., Metal Forming, American Soc. for Metals, 1983, Metals Park, Ohio.
43. Singer A.R.E., Al-Samarrai S.H.K., Temperature Changes Associated with Speed Variation during Extrusion. J. Inst. Met., 1960-61. 89, 225-231.
44. Gemant A., J. Appl. Physics, 1946, 17, 1076.

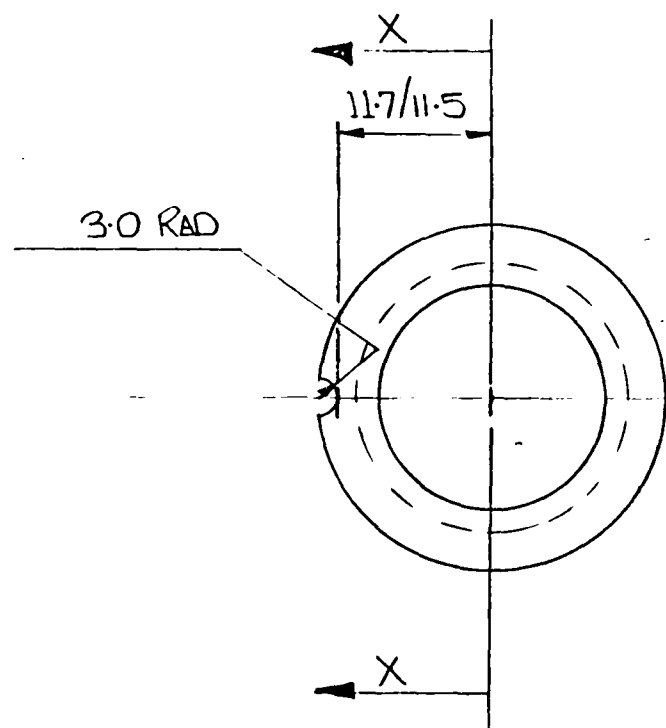
45. Grigull U., Sandner H., Heat Conduction, Sec. 6.3, Nonsteady One-Dimensional Heat Conduction, 1984, 76.

46. Sheppard T., Temperature and Speed effects in the Hot Extrusion of Aluminium Alloys, Metals Technology, April 1981, 130-141

APPENDICES

APPENDIX A1

$H/2.2 = 1.1$



ITEM 1

0.2/0.4 x 45°
INTERNAL CHAMFER

0.4/0.6 x 45°
(EXT. CHAM)

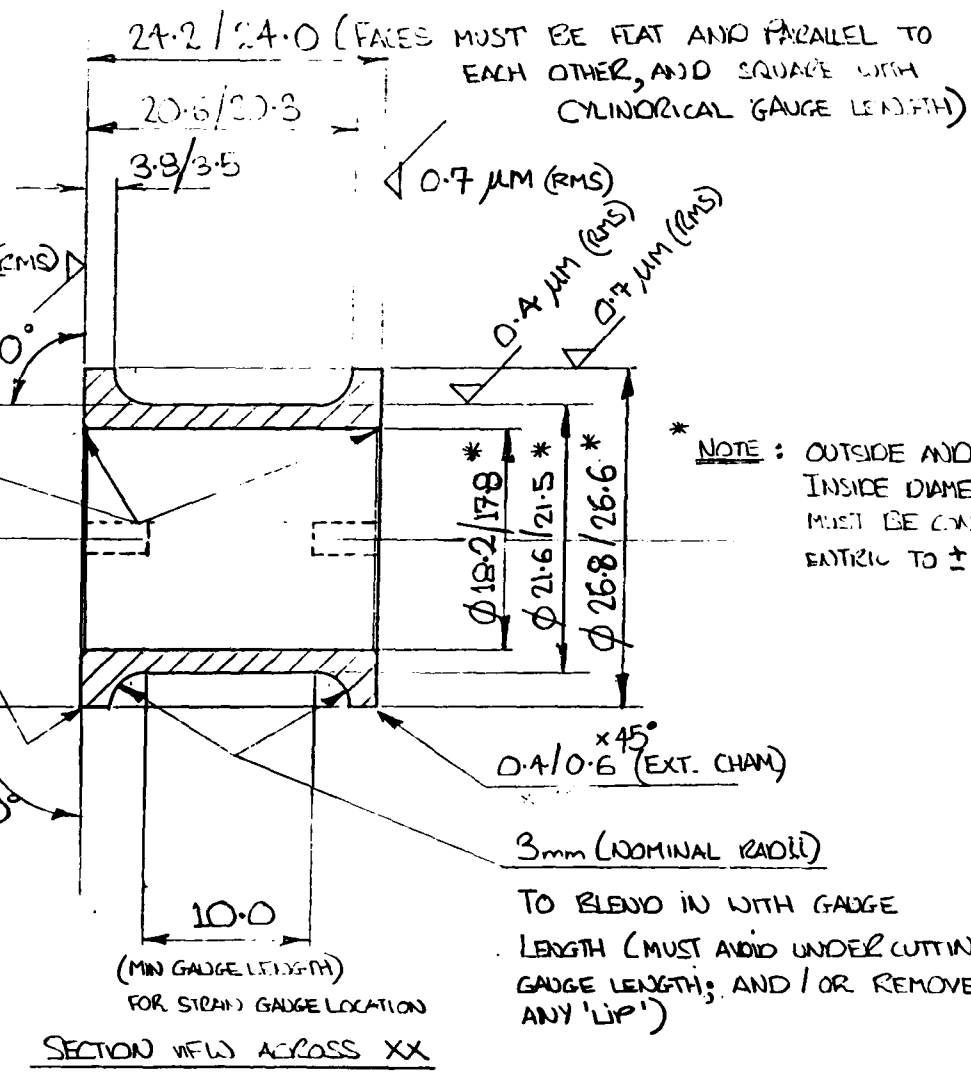
NOTE: CAREFULLY REMOVE ALL EXTERNAL SHARP CORNERS

MATERIAL SPEC :

SPECIAL TREATMENT - ISOSTATIC HOT PRESSING (TO ELIMINATE POROSITY)

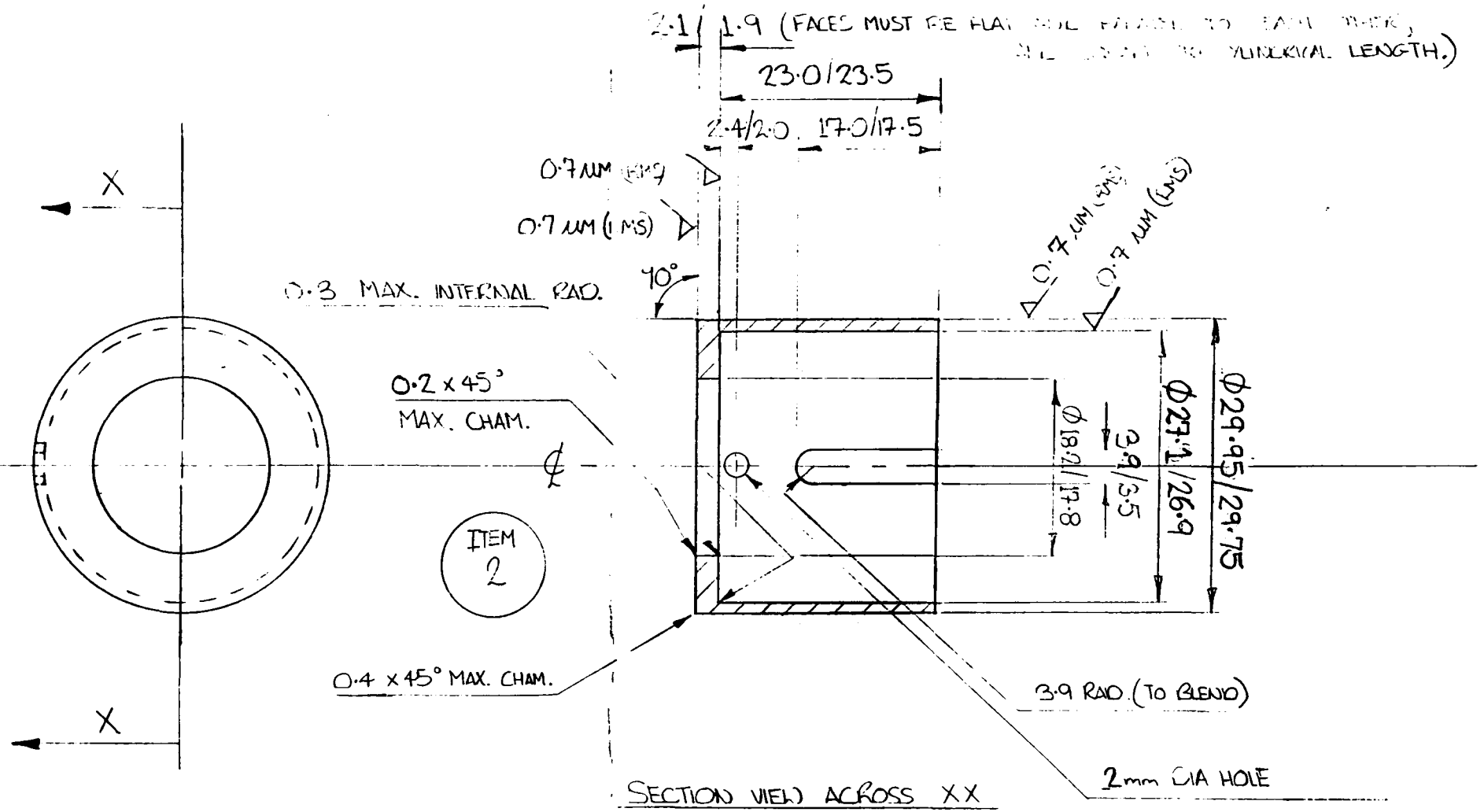
Nº OFF - (1)

COMPONENT DRAWING



SHEET NO. OF

SCALE 2:1	DRW BY P.K. WOOD
ALL DIMENSIONS ARE IN MM UNLESS STATED OTHERWISE	TITLE RADIAL - LOAD/FILL BODY
DEPT OF MECH. AND PROD. ENIG. ASTON UNIVERSITY	DATE 12/2/27
PROJECTION 3rd ANGLE	



NOTE: CAREFULLY REMOVE ALL EXTERNAL SHARP CORNERS

MATERIAL SPEC: EN 24

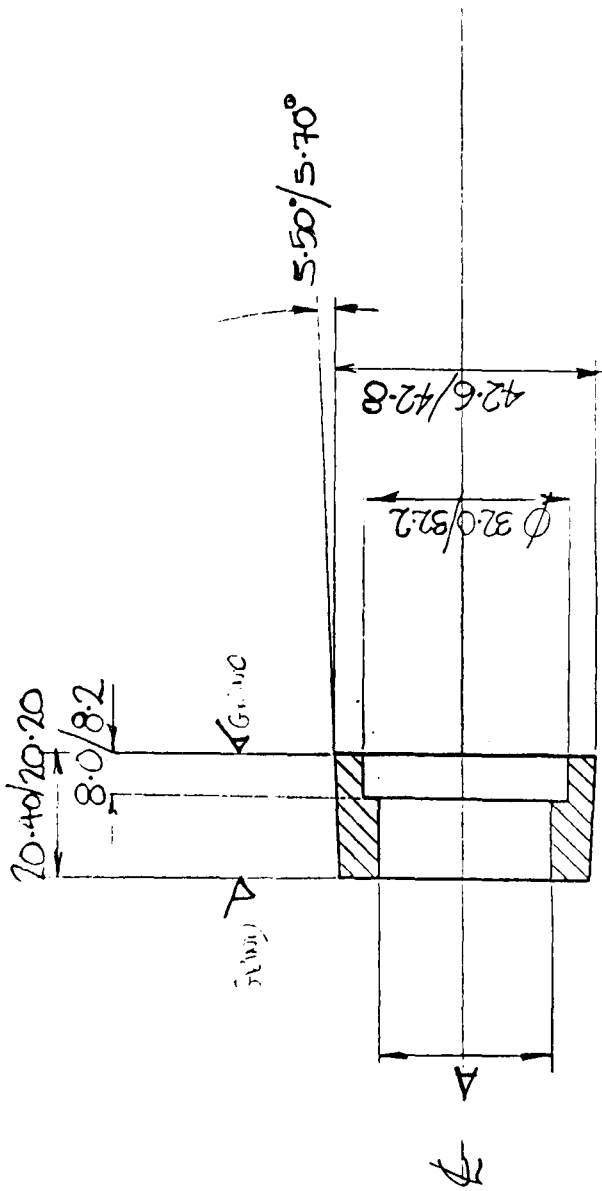
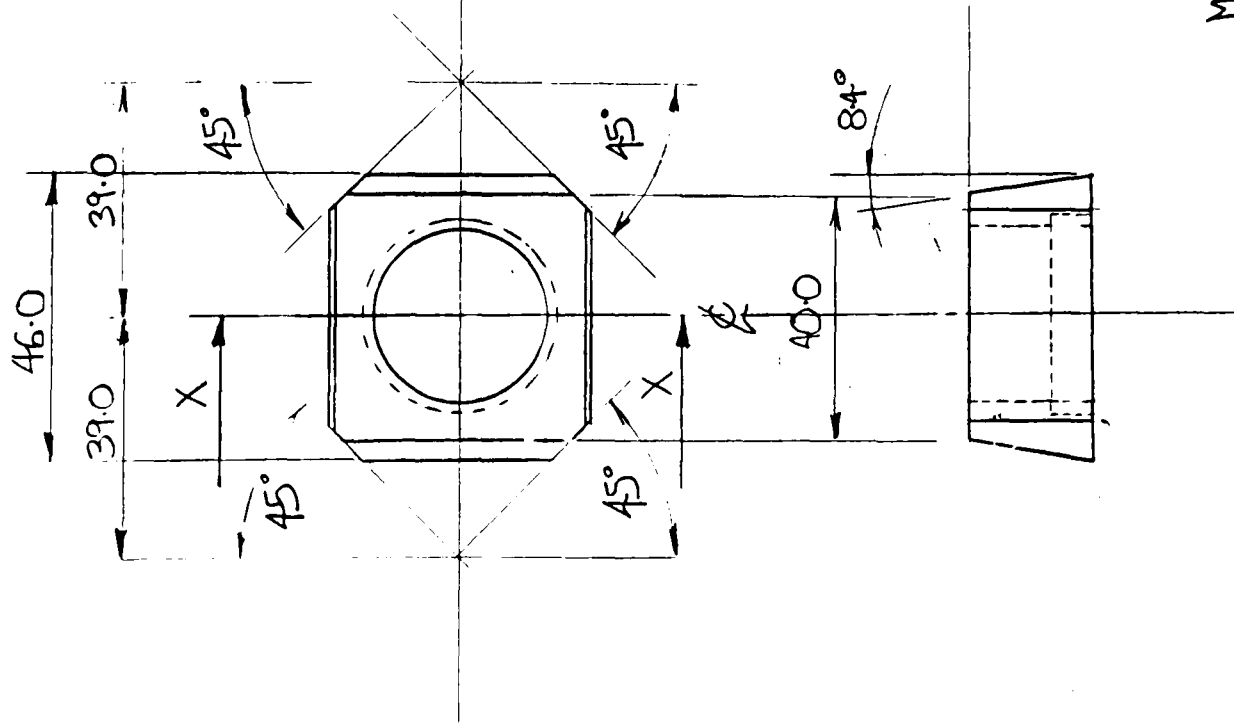
TREATMENT: H/T TO 375 VPN

Nº OFF - (1)

COMPONENT DRAWING - TO MATCH ITEM (1)

SHEET NO. OF

SCALE 2 : 1	DES BY PRC LIND
ALL DIMENSIONS ARE TO MM UNLESS STATED OTHERWISE	TITLE
DEPT OF MECH. AND. PROD. ENG. ASTON UNIVERSITY	LOAD CELL (SEE ITEM CAVING 1)
PRODUCTION BY NYIE	DATE 1/1/17



SECTION VIEW ACROSS XX

DIE HOLDER PART NO.	Ø A
1	28.7/28.8
2	32.5/32.6

ITEM N^o 5

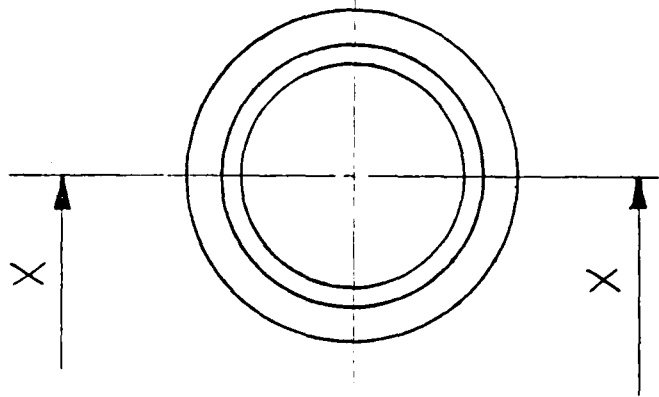
MATERIAL SPEC: EN 30B

HEAT TREATMENT: H/T FOR TOUGHNESS

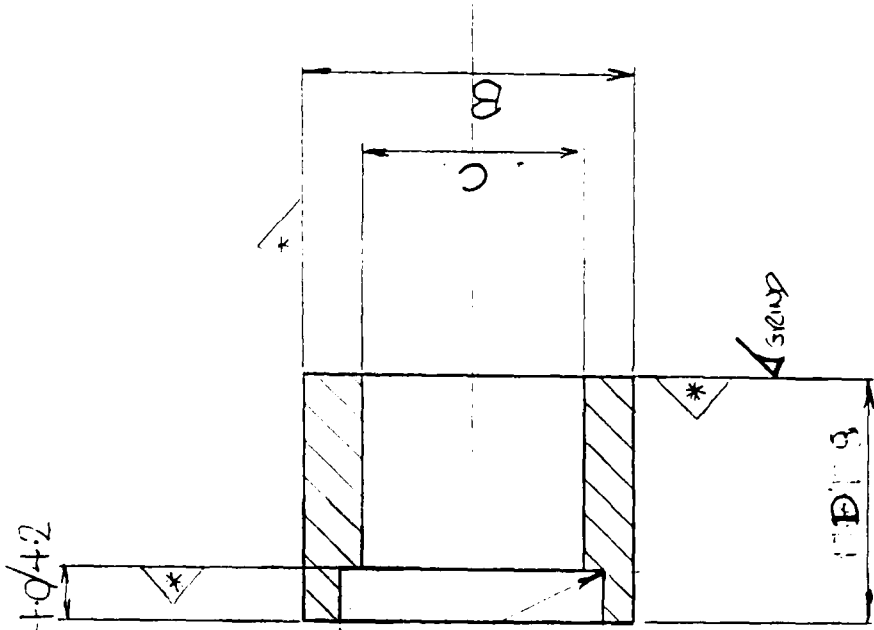
REMOVE ALL SHARP EDGES

SHEET 12 OF 5

DESIGNER	PROF. A. L. V. D. S.	PROJECTION	3rd ANGLE
DEPT. OF MECH. A	UNIVERSITY OF ZAMBIA	TITLE	DIE HOLDER
ALL DIM. ARE IN MM		SUBJECT	COURSE
DATE: 12/11/86		SCALE	



0.25/0.5 U' CUT



SECTION VIEW ACROSS XX

DIE CASE PART NO.	Φ A	Φ B	Φ C	DIM D
1	21.0/21.2	28.0/28.2	16.0/16.2	12.3/12.5
2	30.0/30.2	31.8/32.0	17.0/17.2	9.3/9.5

MATERIAL SPEC: EN30B

HEAT TREATMENT: H/T FOR TOUGHNESS

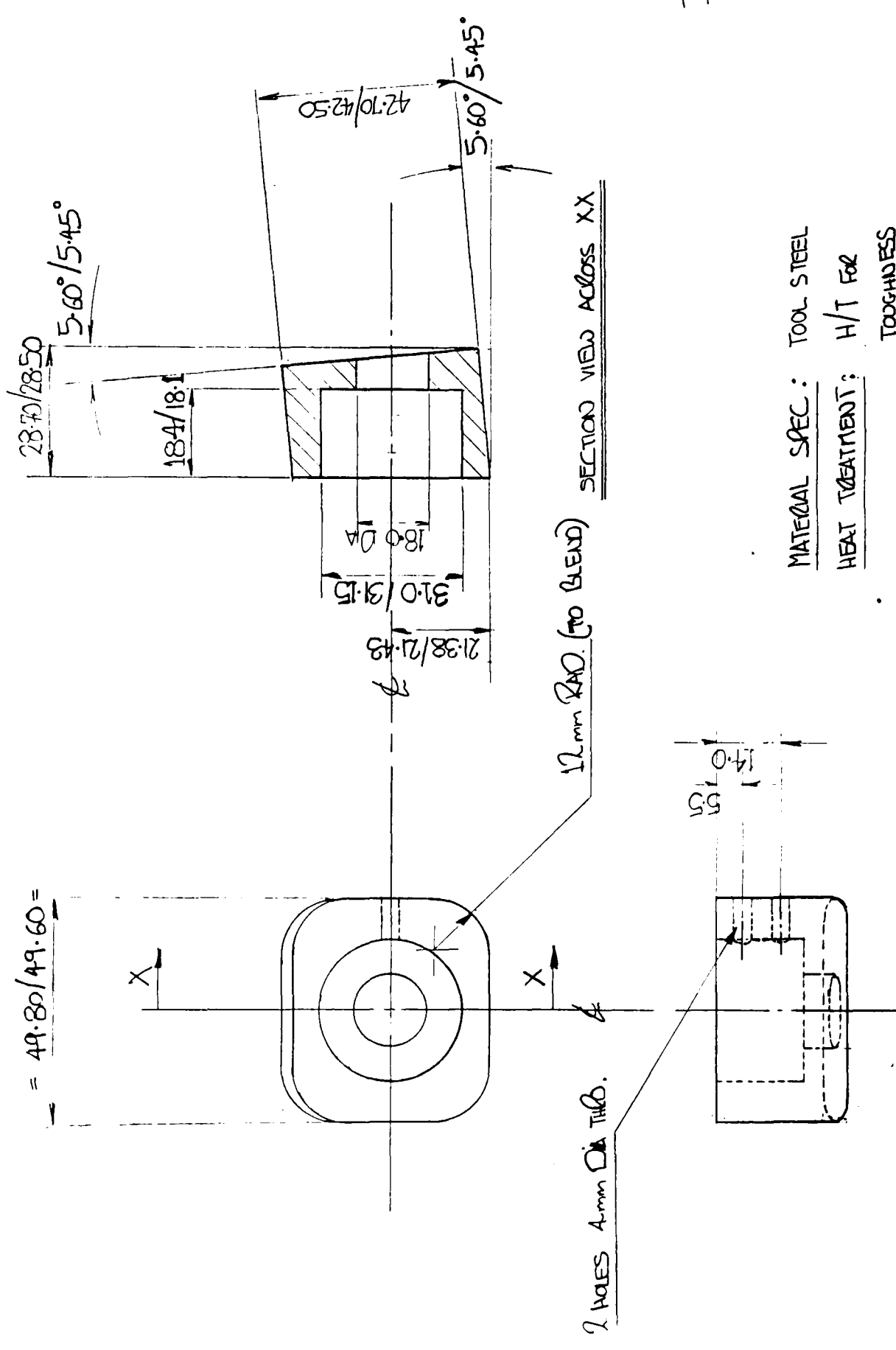
NOTE: FACES MARKED "A" MUST BE FLAT, PARALLEL AND SQUARE.

REMOVE SHARP EDGES

ITEM NO. ④

SHEET NO. 3 OF 5

PROJECTION SYMBOL	DATE
ALL DIM. GIVE IN MM UNLESS STATED OTHERWISE	13/11/86
DIR. OF MECH. AND PROD. ENG. INSTN. UNIVERSITY	TITLE
DRAWN BY	TRANSMITTING
SCALE	FORGE RING

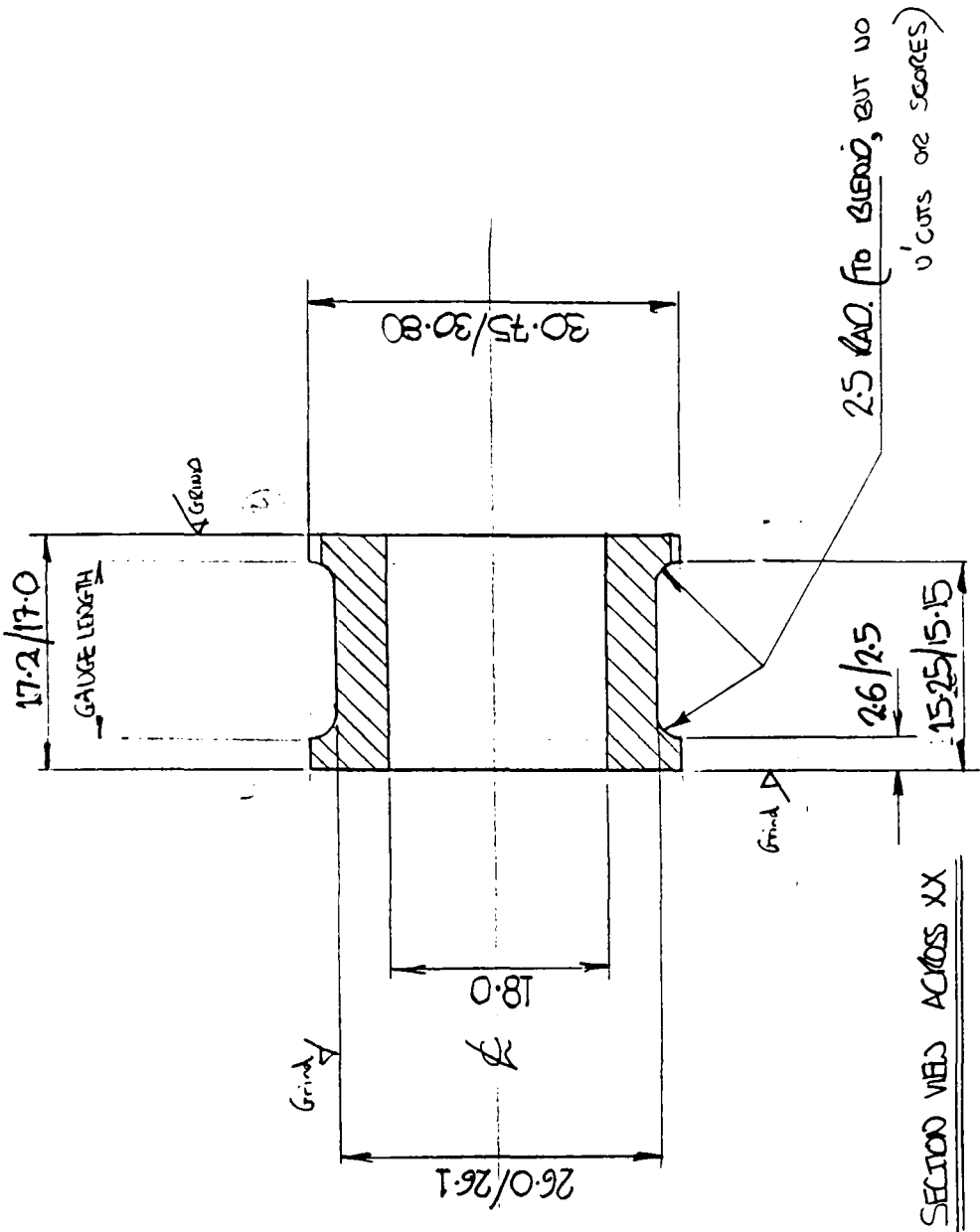


ITEM N° ③

SHEET N° 4 OF 5

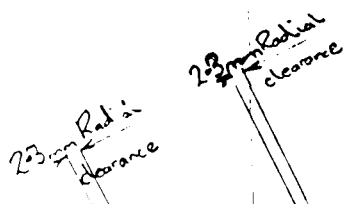
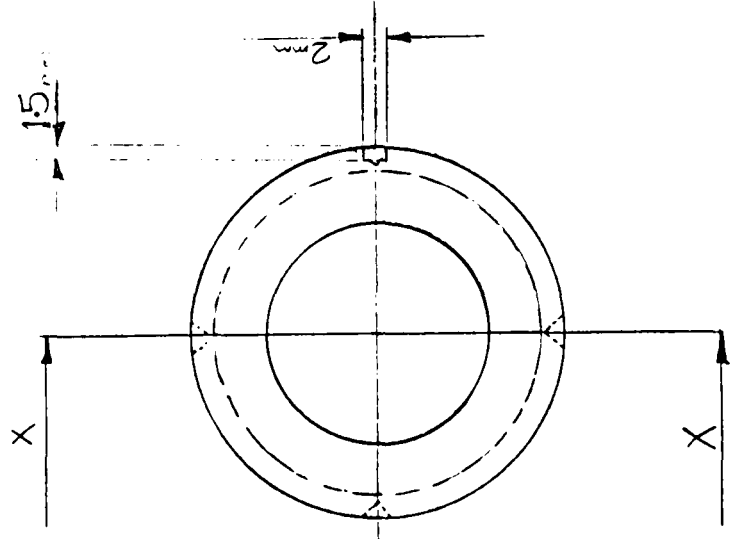
DRAWN BY	PREL. WOOD	DATE	13/11/17
ALL DIM. ARE IN MM UNLESS OTHERWISE STATED		TITLE	DIE HOLDER
DEPT. OF MECH. & FABR. ENG. ASTON UNIVERSITY		BASE	
PROJECTION			3rd ANGLE
			SCALE

REMOVE ALL SHARP EDGES
 SEE ITEM ③ ASSEMBLY DRAWING FOR FURTHER DETAILS



ITEM N^o. ①

SHEET N^o. 5 OF 5



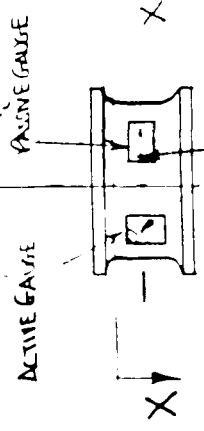
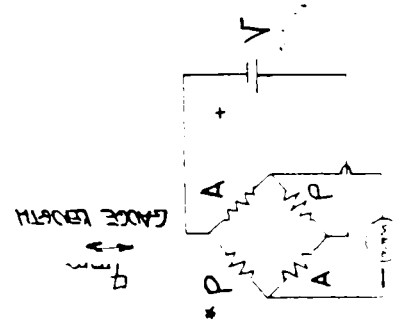
MATERIAL SPEC: EN 24

HEAT TREATMENT: HARDEN & TEMPER FOR TOUGHNESS { V_{PN} = 374 (YIELD STRESS @ 600 N/mm²) }

REMOVE SHARP EDGES

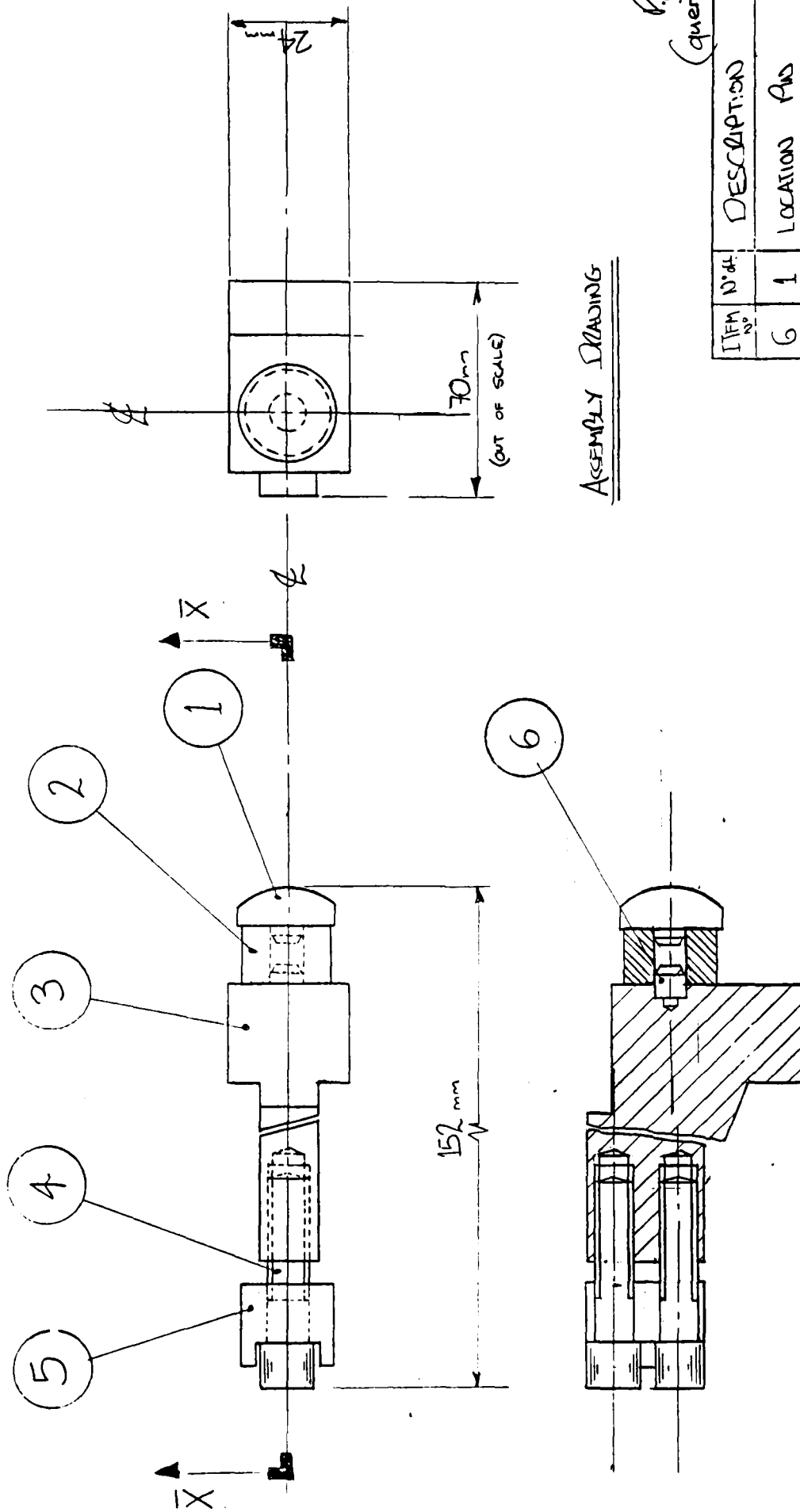
BRIDGE CIRCUIT DETAILS

BRIDGE SUPPLY VOLTAGE IS 10 V DC.
 GAUGE RESISTANCE IS 500Ω
 BRIDGE CIRCUIT TYPE - FULL BRIDGE ARRANGEMENT FOR TEMP COMP N
 OPERATING TEMPERATURE IS 250°C MAX. NORMAL IS 200°C
 MAXIMUM RADIAL CLEARANCE 2.4mm TO ALLOW INSTALLATION OF GAUGE AND LEAD CONNECTIONS.
 FLUING LEAD LENGTH = 6 METRES
 * A = ACTIVE P = PASSIVE.



DRW BY	ACLD000	PROJECTION	3rd ANGLE
ALL DIM	ARE IN MM	TITLE	RADIAL
UNLESS	STATED OTHERWISE	DESIGNER	MAXWELL BODY
DATE	13/11/86	SCALE	

APPENDIX A2



ASSEMBLY DRAWING

AP
(queries - Feb 1983)

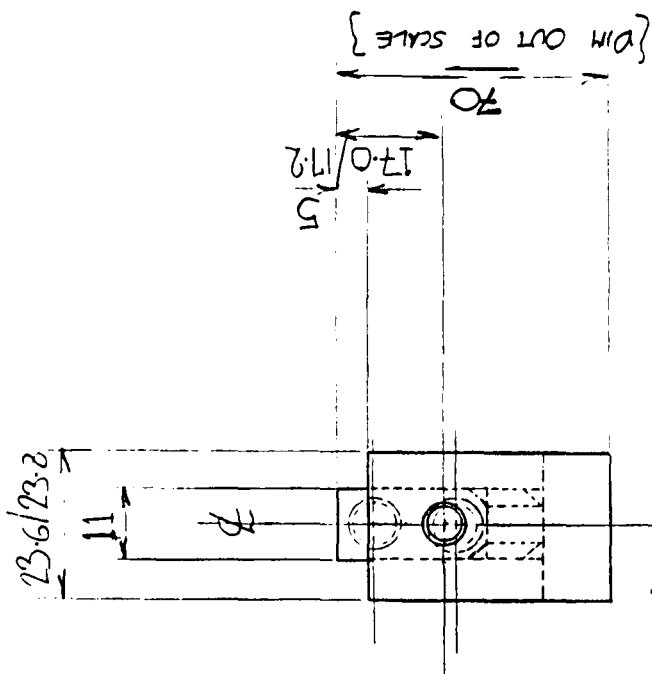
ITEM No	DESCRIPTION
6	1 LOCATION PIN
5	1 MOUNTING UNIT HOLDER
4	2 MBX 32mm LG ALLAN SCREW
3	1 LOAD CELL MOUNTING UNIT
2	3 LOAD CELL * SEE COMPONENT DRAWING
1	1 FORCE TRANSMITTING PIN
PROJECTION THIRD ANGLE	
SCALE 1:1	
DATE	21/1/87
DRAWN BY: PRC LIND	
SHEET NO	1 OF 3
TITLE	
ABSTMENT	
LOAD CELL	

SECTION VIEW ACROSS XX

MATERIAL SPEC: MILD STEEL

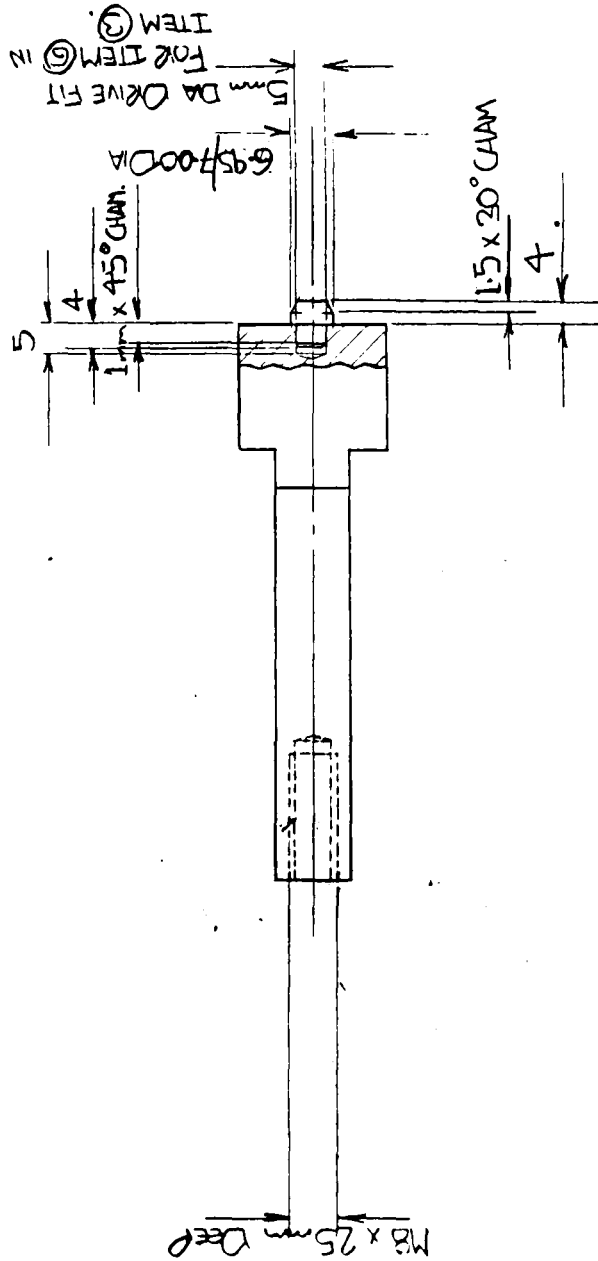
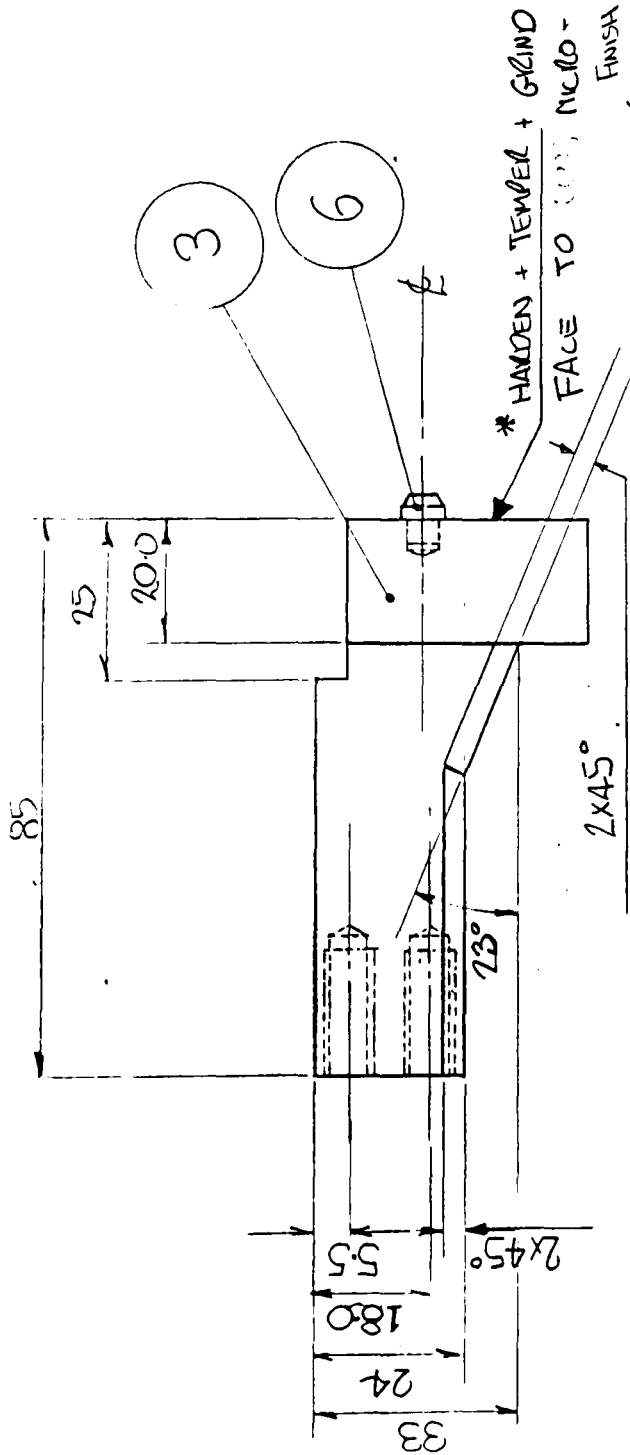
HEAT TREATMENT { CASE HARDENED + HARDEN SURFACE }

ALL DIMENSIONS IN MM



REMOVE ALL SHARP EDGES

ALL DIMENSIONS IN MM



COMPONENT DRAWING

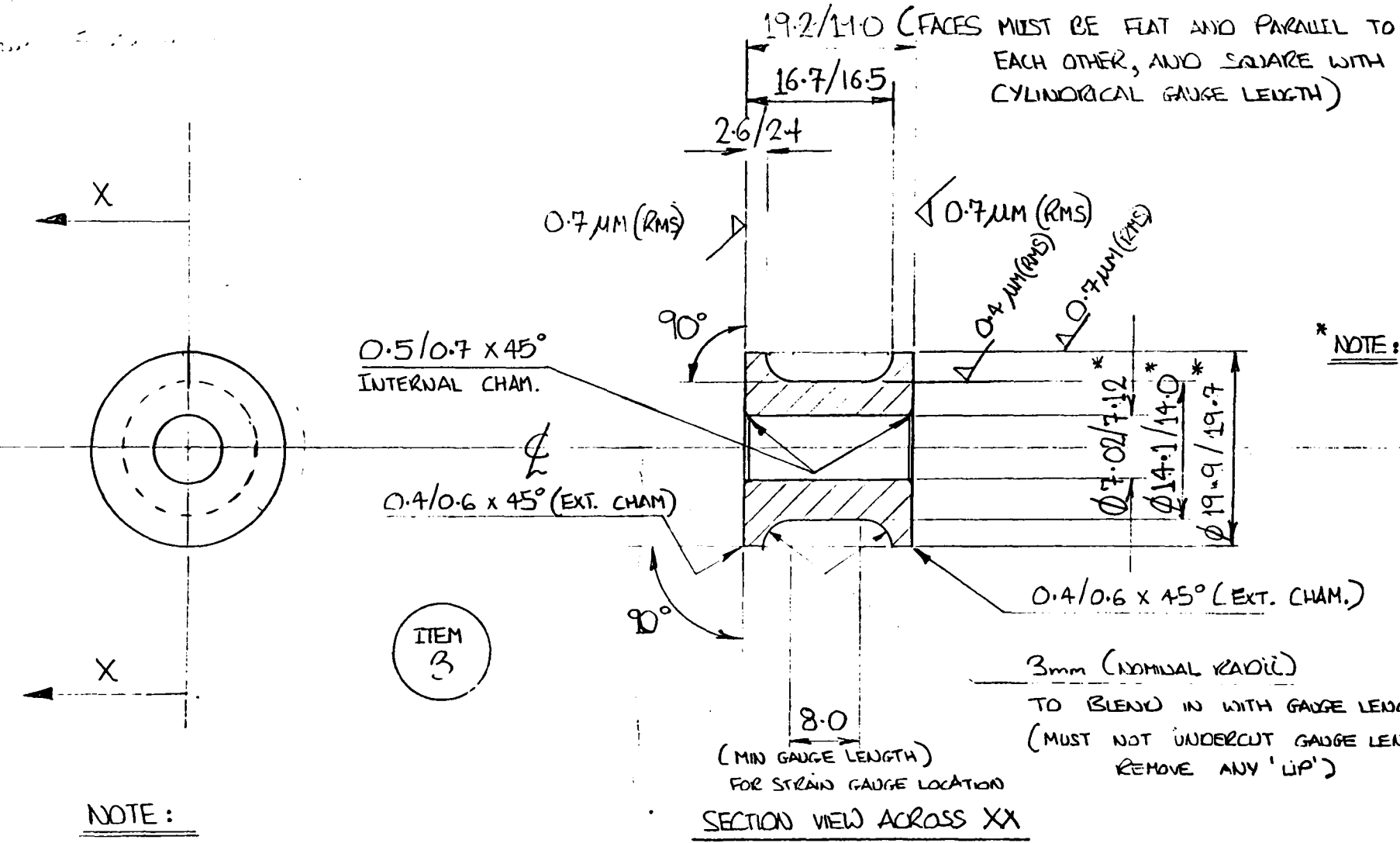
NOTE: MAX FORCE EXERTED ON FACE IS 150 kN (15 tonf)

6	1	LOCATION PIN	HARDEN + TEMPER TOOL STEEL
3	1	LOADCELL MOUNT UNIT	TO SUIT H.T. SEE (#)
ITEM NO	OFF	DESCRIPTION	MAT + H.T.
PROJECTION CHANGE			SCALE 1:1
ASTON UNIVERSITY MECH + PROD EDG.			TITLE ADJUSTMENT
DATE: 22/1/87			LOADCELL (COMP'D)
Dwg BY PKC (2000)			SHEET NO 2 OF 3

MAX. CPE AT ...
 ... < 4 ... (20%)

Eq. 2 ...
 ...
 $H/2.0 = 1.4$

293



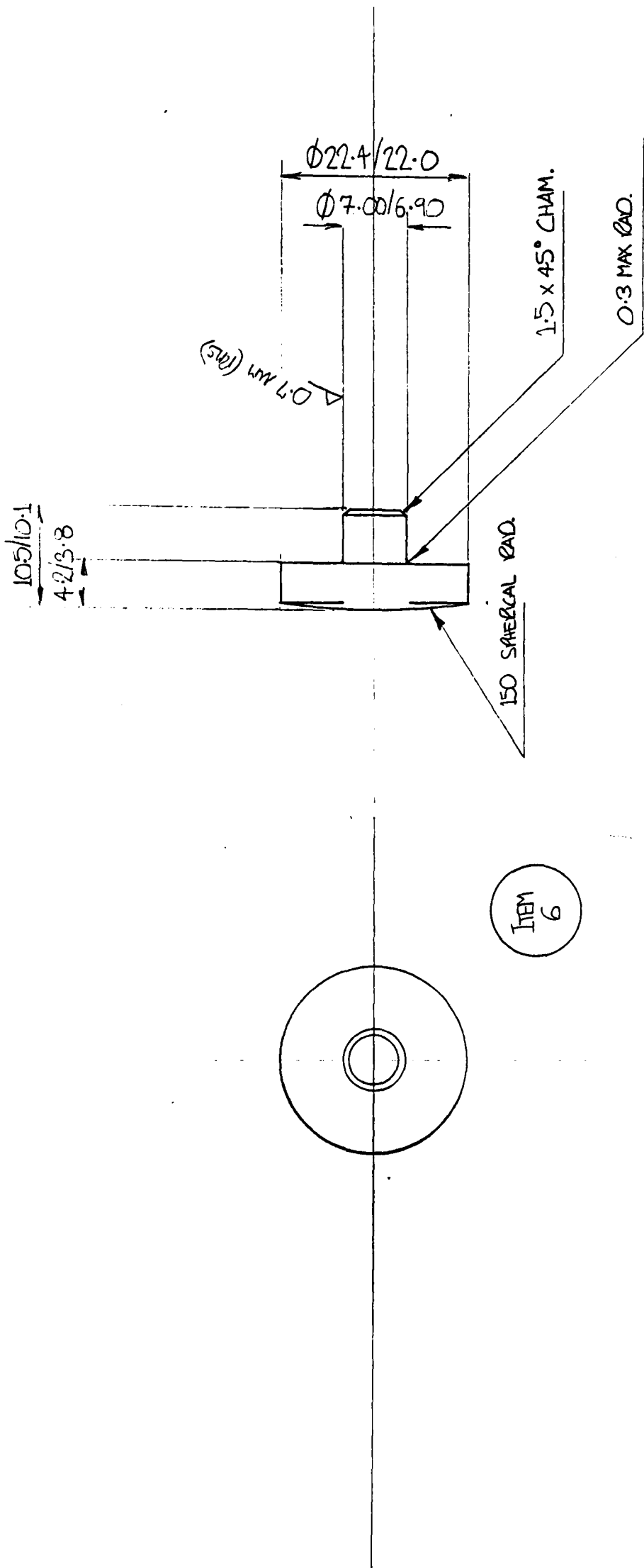
NOTE:
 CAREFULLY REMOVE ALL EXTERNAL SHARP CORNERS

MATERIAL SPEC:
SPECIAL TREATMENT - ISOSTATIC HOT PRESSING
 (TO ELIMINATE HIRSBITY)
 NO. OFF - (1)

COMPONENT DRAWING

SHEET NO OF

SCALE 2:1	DRAWN BY PRC. (1000)
ALL DIMENSIONS ARE IN MM UNLESS STATED OTHERWISE	TITLE TANGENTIAL
DEPT OF MECH. AND PROD. ENG. ASTON UNIVERSITY	LOAD/ILL. PEROY
PROFESSOR 3 rd AYRE	DATE 12/11/27



NOTE : REMOVE ALL SHARP EDGES

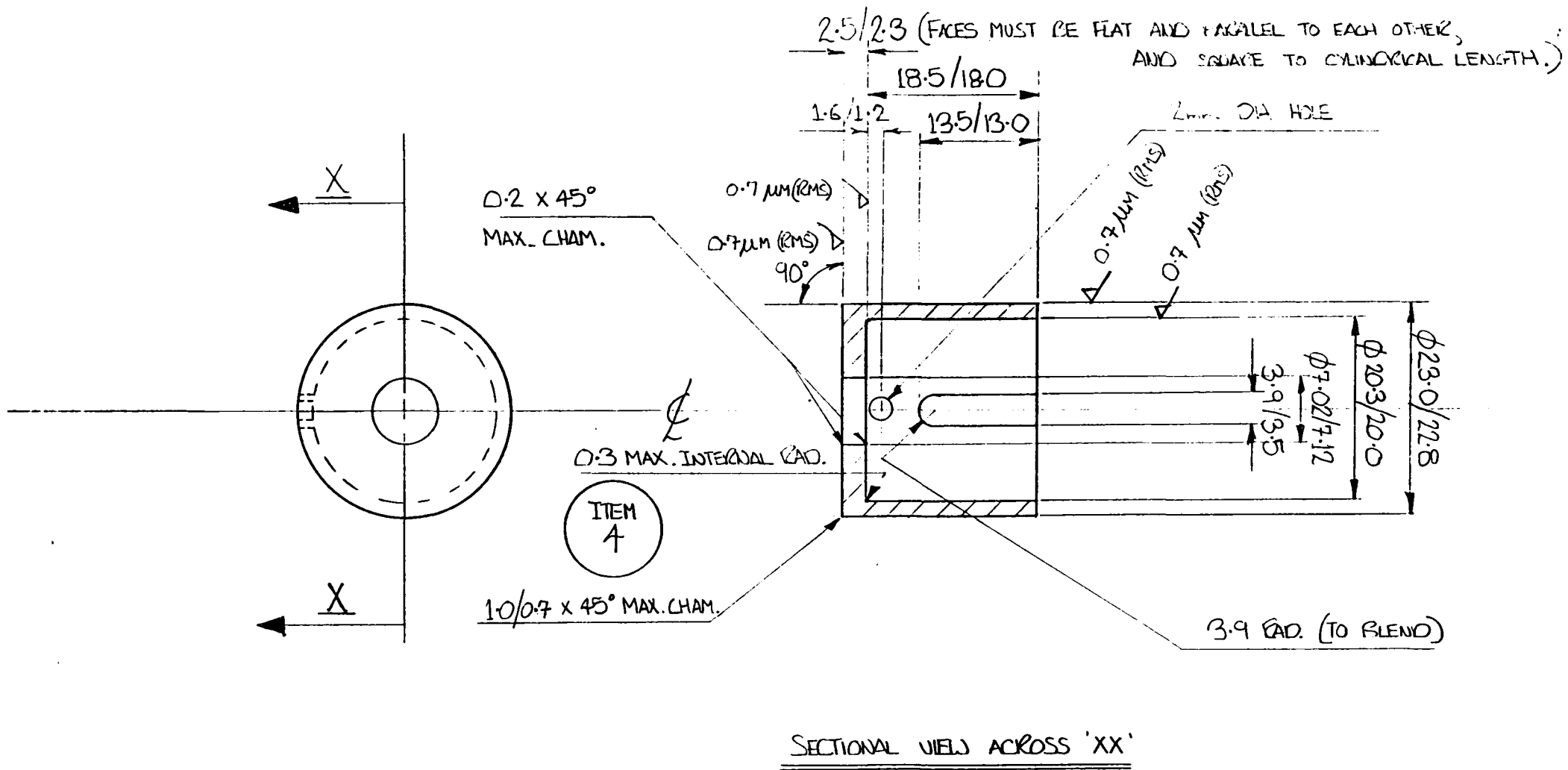
MATERIAL SPEC :

N° OF - (1)

COMPONENT DRAWING

SHEET N° OF

SCALE 2:1	DNW BY AKL 0200
ALL DIMENSIONS ARE IN MM UNLESS STATED OTHERWISE	TITLE PIN
DEPT. OF MECH. AND PROD. ENG. ASTON UNIVERSITY	(DRAWING ITEM 3 AND 4)
PROFESSOR J.A. NIXE	DATE 17/1/87



NOTE: CAREFULLY REMOVE ALL EXTERNAL SHARP CORNERS

MATERIAL SPEC: EN 24 No. OFF - (1)

TREATMENT: H/T TO 375 VPV

COMPONENT DRAWING TO MATCH ITEM (3)

SHEET NO OF

SCALE 2:1	DEN BY PRC WOOD
ALL DIMENSIONS ARE IN MM UNLESS STATED OTHERWISE	TITLE LOADCELL - CASING (SEE ITEM 3)
DEPT OF MECH. AND PROD. ENGR. ASTON UNIVERSITY	DATE 12/8/87
PROFESSIONAL ENGINEER	

APPENDIX A3

Appendix A3

The details of the strain gauges, bonding material and coating provided by Welwyn Strain Measurement are given below.

Strain gauge installation for high-temperature loadcell, maximum temperature 260°C.

Installation of 4 strain gauges type WK-06-062AQ-350 to Tungsten carbide loadcell spring element.

Installation of 4 strain gauges type WK-18-062AQ-350 to EN 24 loadcell spring element.

Wire to form full bridge, balance, protect and temperature compensation.

One metre of flying lead attached to loadcell, type 430-FST (4 conductor, teflon with screen - max 260°C).

Adhesive:	'M' Bond 610
Interbridge Wire:	134-AWQ (Polyimide enamel - max. 325 °C)
Coating:	GA-61 (max. temp 315°C) or RTV-3145 (max, temp 260°C)
Solder:	570-20S

APPENDIX B1

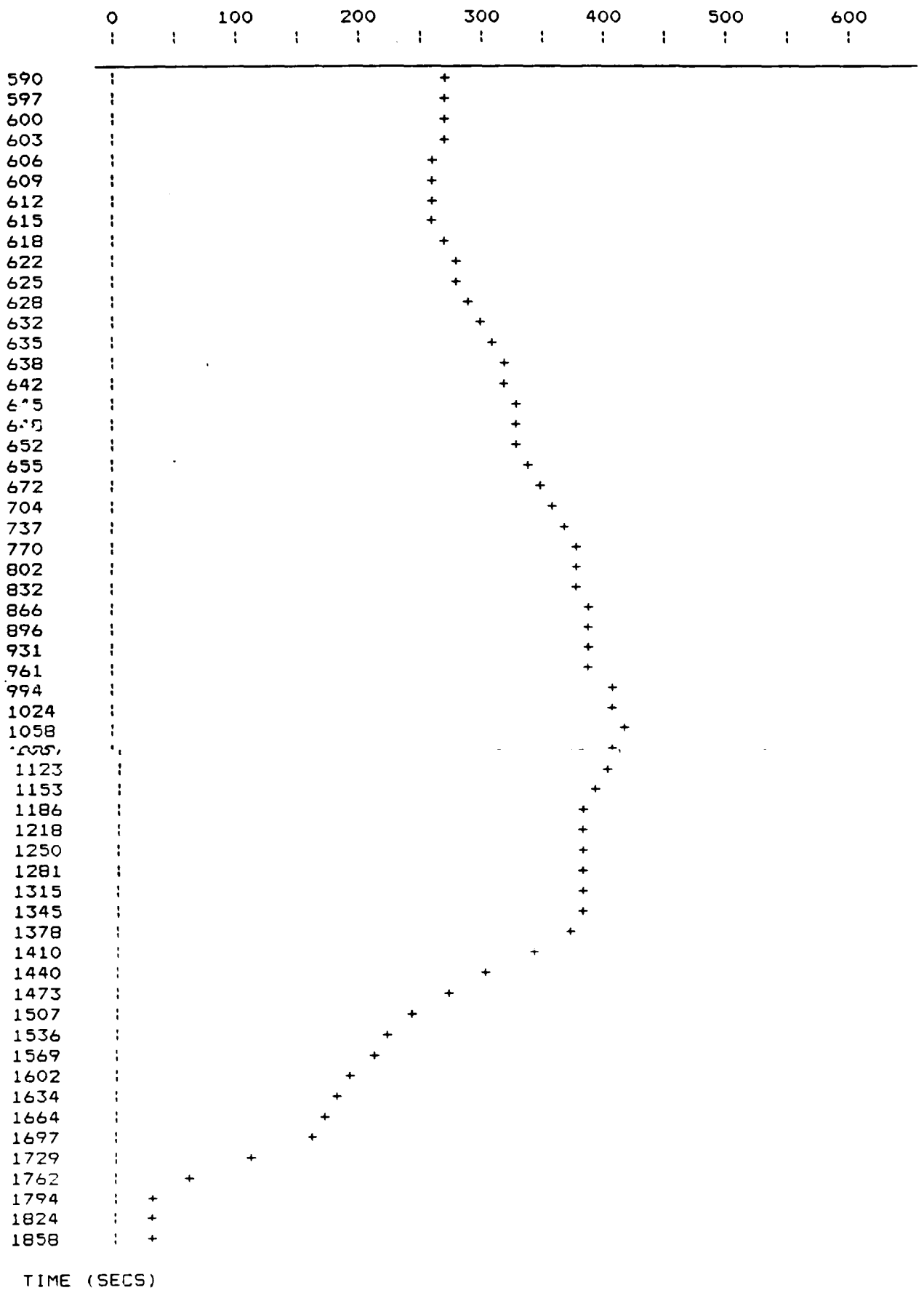
TEST NO.
 DATE 24.10.88
 Feed technique employed was continuously cast rod (spec. AA1050)
 Extrusion ratio =
 Abutment height =
 shoe angle = degrees
 Die diameter =
 Rod diameter = 9.6
 Expansion chamber type: S
 Weight of rod feed stock = 11.11 kg

TIME2 SEC	ALC(B) (CEL)	ALC(F) (CEL)	ABUT (CEL)	DLC(B) (CEL)	DLC(F) (CEL)	DIE (CEL)	TORQUE (kNm)	SPEED (RPM)	RLOAD (KN)	ALOAD (KN)
0	19.2	18	20.4	20.4	19.2	20.4	0	0	0	0
590	57.6	59.9	288.6	115.6	187	278	11.15	0	18.92	48.93
597	55.8	59.3	286.3	116.2	185.7	276.9	0	0	12.97	43.34
600	57	59.3	281.6	113.8	185.7	273.3	11.81	0	24.32	53.87
603	55.4	59.3	279.8	114.4	185.1	271.5	11.42	0	20.15	50.11
606	55.4	60.5	277.6	114.2	183.7	269.4	13.32	0	17.66	48.5
609	54.6	61.7	277.2	112.7	181.6	267.8	19.63	0	32.34	61.61
612	54.6	59.3	278	112.7	180.8	266.2	23.08	0	54.95	79.23
615	54.6	61.7	279.2	112.7	178.4	269.8	24.41	0	54.68	79.45
618	55.8	59.3	280.4	113.8	178.4	274.5	30.82	4.19	53.17	78.8
622	54.6	61.7	287.5	112.7	175.9	281.6	28.58	4.78	52.08	78.8
625	55.8	60.5	296.8	112.7	177.2	288.6	30.66	4.88	51.67	78.02
628	54.6	61.7	309.7	112.7	175.9	296.8	34.71	4.83	51.67	78.59
632	55.8	60.5	317.9	111.4	177.2	305.1	35.19	4.99	49.89	78.37
635	54.6	59.3	330.7	111.4	177.2	313.3	34.04	5.05	49.62	78.37
638	57	60.5	337.8	110.2	178.4	320.3	35.71	5.05	48.93	78.8
642	54.6	59.3	345.9	111.4	178.4	324.9	38.72	5.13	48.8	79.23
645	55.8	60.5	348.2	110.2	180.8	330.7	37.46	5.1	47.98	79.56
648	54.6	60.5	356.3	111.4	182	334.3	35.46	4.72	46.75	79.88
652	58.2	60.5	361	110.2	183.3	338.9	37.27	5.05	47.84	80.74
655	55.8	60.5	366.8	112.7	184.5	342.4	37.65	4.94	45.79	80.74
672	58.2	63.1	378.8	114.6	190.1	352.9	36.02	5.12	45.35	81.14
704	58.8	64.7	395.2	117.6	201.2	367.5	35.1	5.23	45.35	81.14
737	63.2	67.9	407.3	124	211.7	377.8	34.36	5.23	45.35	81.14
770	66.1	72.2	413.5	129.8	219.8	387.2	33.34	5.19	45.35	81.14

802	69.5	74.3	416.9	134.4	224.9	386.6				
832	70.7	77.5	418.7	138.3	229	388.5	33.07	5.12	45.63	83.92
866	72.7	78.5	421.2	141.5	232.2	390.7	33.06	5.12	45.97	83.65
896	74.4	81.4	422.7	144.4	234.8	392.3	31.97	5.12	45.61	83.25
931	76.3	82.3	424	147.4	237.1	394.1	32.52	5.12	45.93	82.98
961	77.3	84.5	421.3	149.7	239.1	398.6	31.55	5.14	45.89	82.17
994	81.1	86.4	454.2	151.8	243.8	414.3	30.73	6.75	45.96	82.93
1024	87.2	93.4	459.5	156	249.2	419.3	28.19	7.76	45.02	85.71
1058	94	99	459.8	158.7	252.7	420.2	27.07	7.88	45.25	87.01999
1089	93.2	99.9	449.5	161.5	255.6	416.8	26.11	7.92	45.02	85.86
1123	93	98.9	427.9	164.1	255.7	403.9	22.79	7.66	44.65	81.89
1153	91.1	98.7	411.2	164.7	252.9	391.5	23.76	5.13	45.67	77
1186	90.8	97.6	404.8	164.9	250	386.3	24.83	5.05	45.97	75.36
1218	90.7	97.2	398.5	165	247.6	382.2	23.88	5.09	45.8	74.33
1250	90.4	97.3	406.2	164.8	246.1	384.4	25	5.02	47.38	74.93
1281	91.9	97.3	400.1	165.1	246.7	383.4	28.8	4.96	46.68	76.49
1315	92.2	99.1	398.5	165.8	246.4	381.4	25.53	5	45.45	76.17
1345	94.1	99.6	398	165.8	246.2	381.6	26.86	5.01	46.09	76.58
1378	94	100.1	398.4	167	247.6	377.6	25.95	5.14	44.53	74.91
1410	92.8	97.7	349.8	166.4	241.5	342.5	11.03	5.26	22.77	47.99
1440	89	93.9	314.7	161.8	224.9	306.9	0	5.61	9.429999	24.6
1473	84.9	90.9	285.6	156.2	208.7	275	0	0	5.05	17.03
1507	81.5	86.6	261	149.3	194	249.5	0	0	0	11.13
1536	78	84.6	241.5	142.8	183.8	229.6	0	0	0	7.43
1569	76.4	81.2	225.8	137.7	173.7	214.2	0	0	0	4.97
1602	73.3	79.5	210.3	132.1	165.4	199.7	0	0	0	0
1634	70.2	77.1	195.5	126.9	154.9	187.2	0	0	0	0
1664	67.6	73.6	185	122.4	147.5	174.9	0	0	0	0
1697	66	72.6	185.3	117.9	144.3	160.4	0	0	0	0
1729	63.2	70.3	66.9	113.3	105.8	118.1	0	0	0	0
1762	63.3	68.4	46.2	109.2	49.2	63.6	0	0	0	0
1794	61.1	66.4	32.7	105.2	33.8	38.3	0	0	0	0
1824	59.7	63.9	32	99.5	28.2	35	0	0	0	0
1858	57.7	62.7	32.6	95.1	26.4	37.3	0	0	0	0

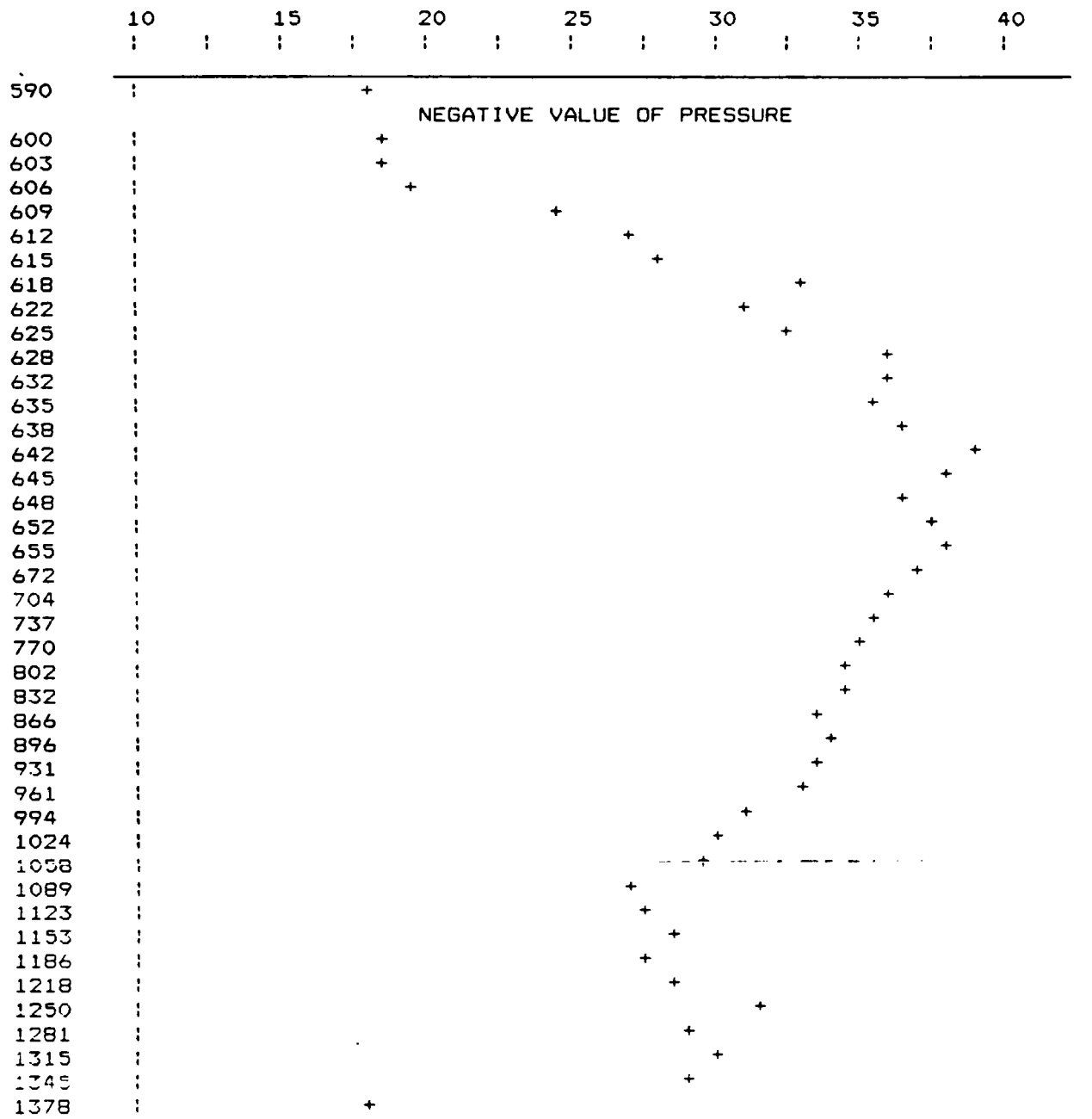
VARIATION OF DIE TEMPERATURE WITH TIME

TEMP. (deg.C)



CHANGE IN WHEEL TORQUE OUTPUT WITH TIME

TORQUE (kNm)

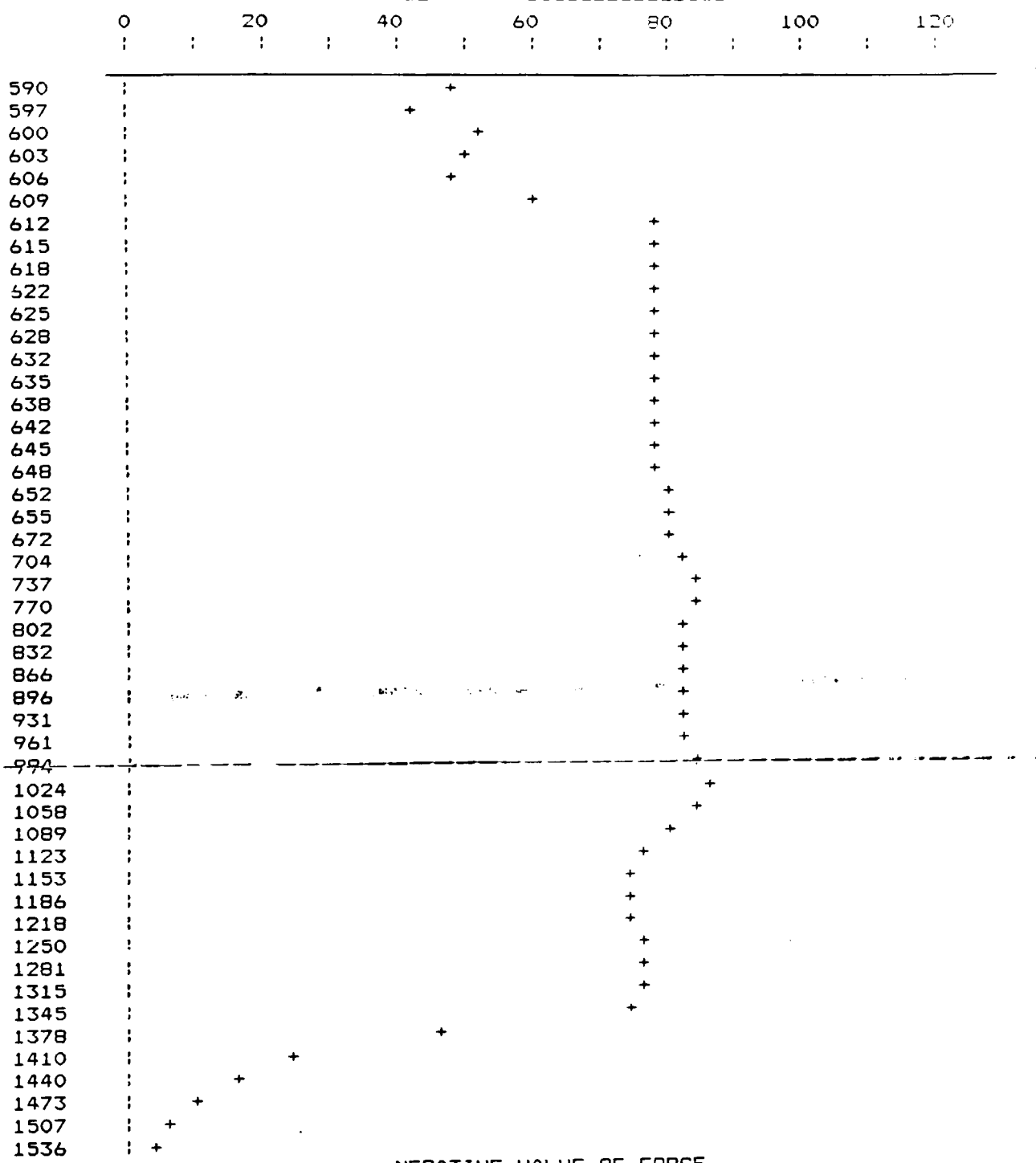


NEGATIVE VALUE OF PRESSURE
 NEGATIVE VALUE OF PRESSURE

TIME (SECS)

VARIATION OF 'ALC' FORCE WITH TIME

FORCE (KN)



NEGATIVE VALUE OF FORCE
 NEGATIVE VALUE OF FORCE

TIME (SECS)

APPENDIX B2

```

10 CLS
20 COLOR 4,0,0
30 LOCATE 8,20:PRINT"INSTRUMENTATION SYSTEM FOR THE CONFORM"
40 LOCATE 9,13:PRINT"CONTINUOUS EXTRUSION PROCESS INCLUDES DATA ACQUISITION"
50 LOCATE 10,12:PRINT"FOR GRAPHICAL REAL-TIME DISPLAY, DATA LOGGING FOR DISPLAY"

60 LOCATE 11,18:PRINT"OF POST PROCESSED GRAPHS AND TABULATED DATA"
62 LOCATE 13,12:PRINT"INTERFACE MEASURING EQUIPMENT TO BE PROCESSED INCLUDES"
63 LOCATE 14,14:PRINT"THERMOCOUPLE PROBES, PRESSURE GAUGES, LOADCELLS AND"
64 LOCATE 15,32:PRINT"TACHOMETER"
70 COLOR 7,0,0
80 LOCATE 18,23:PRINT"SOFTWARE COMPILED BY P.K.C.WOOD
90 CALL INIT
.91 CALL PAUSE'(10,"SEC")
92 CLS
93 COLOR 2,0,0
94 PRINT "INPUT test no."
95 INPUT TN
96 PRINT "INPUT date 00.00.00"
97 INPUT DA$
98 PRINT""
99 PRINT"
"
100 PRINT""
103 PRINT"INPUT the following machine setting variables"
104 REM machine setting variables determining the physical geometry of the
105 REM deformation zone in the extrusion chamber.
106 REM setting variable calculations, reduction ratio, chamber geometry.
107 COLOR 3,0,0
108 PRINT"INPUT feed rod diameter in mm (if particulate enter 0)"
109 INPUT D1
110 PRINT"INPUT die or product diameter in mm"
111 INPUT D5
112 PRINT"INPUT abutment height from grip segment face in mm"
113 INPUT H
114 PRINT"INPUT shoe angle in degrees"
115 INPUT ANGLE
116 PRINT"Is the die expansion chamber used in this test LARGE or SMALL ?"
117 INPUT K$
118 PRINT"INPUT feed technique employed. i.e particulate (1) or rod (2)"
119 INPUT G
120 IF G>2 THEN GOTO 118
122 PRINT "INPUT mass of rod feed stock used in units of lb"
124 INPUT Q
128 CLS
129 COLOR 12,0,0
130 LOCATE 1,10:PRINT"This program is designed to be used with the various"
140 LOCATE 2,10:PRINT"interface sensing devices detailed in the user option"
150 LOCATE 3,10:PRINT"menu."
160 LOCATE 5,10:PRINT"The user is required to insert the necessary geometric"
163 LOCATE 6,10:PRINT"setting conditions as the prompt will indicate at the"
165 LOCATE 7,10:PRINT"start of this program."
168 LOCATE 9,10:PRINT"The program will operate in either the real-time or"
170 LOCATE 10,10:PRINT"data logging mode only. The user must define at the"
172 LOCATE 11,10:PRINT"prompt the duration of data logging expected, which"
175 LOCATE 12,10:PRINT"must not exceed a maximum value of ?? minutes (this"
178 LOCATE 13,10:PRINT"is because of the maximum space reserved by the array"
180 LOCATE 14,10:PRINT"dimensions).".
183 COLOR 3,0,0
185 LOCATE 16,10:PRINT"In order to minimize zero drifts. the data values at"

```

```

187 LOCATE 17,10:PRINT"zero load will be displayed for several minutes before"
190 LOCATE 18,10:PRINT"the start of the experiment. With the option of repea-
200 LOCATE 19,10:PRINT"ting the procedure."
260 COLOR 7,0
270 LOCATE 23,25:PRINT"PRESS ANY KEY TO CONTINUE"
280 A$=INKEY$ : IF A$="" THEN 280
370 DIM A1(600),A2(600),A3(600),A4(600),A5(600),A6(600),A7(600),A8(600)
380 DIM A9(600),A10(600),A11(600)
390 CALL INIT
580 CALL ANIN'("ARRAY%",2.,"COLDJUNC,THERMA,THERMB,THERMC,THERMD,THERME,THERMF,T
RANSA,TRANSB,TACHO,CELLA,CELLB",1,-1,"DEMO")
590 CALL WARNOFF
591 CALL TIMERSTART'(0,"wgo")
600 CALL INTON'(800,"MIL")
710 TO#=0
720 VA7=0:VAB=0:VA9=0:VA10=0:VA11=0:VA1=0
725 VC7=0:VC8=0:VC9=0:VC10=0:VC11=0:VC1=0:I=0
728 VD7=0:VDB=0:VD9=0:VD10=0:VD11=0:VD1=0:J=0
730 K1=0
740 TIME1=0
750 CLS
755 COLOR 4,0,0
760 PRINT"TIME1" TAB(8) "PRESSURE1" TAB(20) "PRESSURE2" TAB(32) "SPEED" TAB(42)
"RCCELL" TAB(52) "ACE!L" TAB(61) "TEMP1"
770 PRINT"(SEC)" TAB(11) "(V)" TAB(23) "(V)" TAB(33) "(V)" TAB(42) "(mV)" TAB(52)
) "(mV)" TAB(61) "deg.C"
775 PRINT"
"
780 COLOR 7,0,0
840 CALL ARGETVAL'("ARRAY%",1.,"TRANSA",VA7,0)
845 CALL ARGETVAL'("ARRAY%",1.,"THERMA",VA1,11)
850 CALL ARGETVAL'("ARRAY%",1.,"TRANSB",VAB,0)
860 CALL ARGETVAL'("ARRAY%",1.,"TACHO",VA9,0)
870 CALL ARGETVAL'("ARRAY%",1.,"CELLA",VA10,30)
880 CALL ARGETVAL'("ARRAY%",1.,"CELLB",VA11,30)
881 IF TIME1=0 THEN GOTO 980
882 I=I+1
883 VC7=VC7+VA7:VC8=VC8+VAB:VC9=VC9+VA9:VC10=VC10+VA10:VC11=VC11+VA11:VC1=VC1+VA
1
886 IF TIME1<K1 THEN GOTO 990
890 VC7=VC7/I:VC8=VC8/I:VC9=VC9/I:VC10=VC10/I:VC11=VC11/I:VC1=(VC1/I)-20
892 A7=(INT((VC7*1000)+.5))/1000: A8=(INT((VC8*1000)+.5))/1000
900 A9=(INT((VC9*1000)+.5))/1000: A10=(INT((VC10*1000)+.5))/1000
910 A11=(INT((VC11*1000)+.5))/1000
915 A1=(INT((VC1*100)+.5))/100
930 TIME1=INT(TIME1+.5)
932 J=J+1
933 VD7=VD7+VC7:VDB=VDB+VC8:VD9=VD9+VC9:VD10=VD10+VC10:VD11=VD11+VC11:VD1=VD1+VC
1
950 PRINT TIME1 TAB(10) A7 TAB(20) A8 TAB(30) A9 TAB(40) A10 TAB(50) A11 TAB(60)
A1
960 VC7=0:VC8=0:VC9=0:VC10=0:VC11=0:VC1=0:I=0
980 K1=K1+2
990 TIME1=TIME1+.4
1000 CALL TIMERREAD'(0,TO#)
1010 IF TO#<25 THEN GOTO 840
1015 BASE7=VD7/J: BASE8=VDB/J: BASE9=VD9/J: BASE11=VD11/J
1016 BASE10=(VD10/J)-(-15) : REM CALIBRATION OFFSET ZERO IS -15
1017 PRINT "VD11="VD11
1020 PRINT "BASE11="BASE11
1050 CALL INTOFF
1060 COLOR 4,0,0
1070 PRINT
1080 INPUT"ARE THE REFERENCE VALUES INCONSISTENT: WOULD YOU RATHER REPEAT THE PF
OCEDURE (Y/N)";A$
1090 IF A$="Y" THEN GOTO 390

```

```

1100 ERASE A1,A2,A3,A4,A5,A6,A7,A8,A9,A10,A11
1110 CLS
1120 COLOR 2,0,0
1130 LOCATE 10,23:PRINT"EXPERIMENT WILL NOW COMMENCE"
1135 CALL PAUSE'(2,"SEC")
1140 CLS
1150 COLOR 3,0,0
1160 INPUT"DURATION OF DATA-LOGGING REQUIRED FOR EXPERIMENT (input time required
in minutes)";J1
1170 JJ1=J1*57:REM ie T4 = JJ1 after count conversion has been introduced
1230 CALL TIMERSTART'(1)
1240 CALL INTON'(840,"MIL")
1371 CLS
1380 DIM WTIME2(600), W4(600), WDP(600), W10(600), W11(600)
1390 OPEN "SEQUEL" FOR OUTPUT AS #1
1400 T1#=0
1405 COUNT=0
1406 TIME=0
1407 TIME2=0
1408 T4=INT(JJ1)
1409 T5=INT(T4*.5)
1410 K2=0
1415 K3=0
1420 VB1=0:VB2=0:VB3=0:VB4=0:VB5=0:VB6=0:VB7=0:VB8=0:VB9=0:VB10=0:VB11=0:T=0
1430 VE1=0:VE2=0:VE3=0:VE4=0:VE5=0:VE6=0:VE7=0:VE8=0:VE9=0:VE10=0:VE11=0
1450 CALL ARGETVAL'("ARRAY%",1.,"THERMA",VB1,11)
1460 CALL ARGETVAL'("ARRAY%",1.,"THERMB",VB2,11)
1470 CALL ARGETVAL'("ARRAY%",1.,"THERMC",VB3,11)
1480 CALL ARGETVAL'("ARRAY%",1.,"THERMD",VB4,11)
1490 CALL ARGETVAL'("ARRAY%",1.,"THERME",VB5,11)
1500 CALL ARGETVAL'("ARRAY%",1.,"THERMF",VB6,11)
1510 CALL ARGETVAL'("ARRAY%",1.,"TRANSA",VB7,0)
1520 CALL ARGETVAL'("ARRAY%",1.,"TRANSB",VB8,0)
1530 CALL ARGETVAL'("ARRAY%",1.,"TACHO",VB9,0)
1540 CALL ARGETVAL'("ARRAY%",1.,"CELLA",VB10,30)
1550 CALL ARGETVAL'("ARRAY%",1.,"CELLB",VB11,30)
1551 CALL TIMERREAD'(1,T1#)
1552 IF COUNT=0 THEN GOSUB 1770
1553 COUNT=COUNT+1
1554 IF COUNT=T5 THEN GOSUB 1770
1560 I=I+1
1565 VE1=VE1+VB1:VE2=VE2+VB2:VE3=VE3+VB3:VE4=VE4+VB4:VE5=VE5+VB5:VE6=VE6+VB6
1566 VE7=VE7+VB7:VE8=VE8+VB8:VE9=VE9+VB9:VE10=VE10+VB10:VE11=VE11+VB11
1570 IF K2<TIME2 THEN K2=INT(TIME2)
1575 IF TIME2<K2 THEN GOTO 1665
1580 VE1=VE1/I:VE2=VE2/I:VE3=VE3/I:VE4=VE4/I:VE5=VE5/I:VE6=VE6/I:VE7=VE7/I
1582 VE8=VE8/I:VE9=VE9/I:VE10=VE10/I:VE11=VE11/I
1583 PRINT #1, K2,TIME2,VE1,VE2,VE3,VE4,VE5,VE6,VE7,VE8,VE9,VE10,VE11
1585 VE8=386*(VE8-BASE8)+99
1586 DB=(.0143*VE8)-1.98
1587 IF DB<0 THEN DB=0
1588 VE9=(5.51*(VE9-BASE9))-.39
1589 VE10=(1.4*(VE10-BASE10))+21.9
1591 VE11=(2.2*(VE11-BASE11))+2.12
1592 VE1=INT(VE1+.5)-20:VE2=INT(VE2+.5)-20:VE4=INT(VE4+.5)-20
1593 VE5=INT(VE5+.5)-20:VE6=INT(VE6+.5)-20
1595 DB=INT(DB+.5)
1600 VE9=INT(VE9+.5)
1605 VE10=INT(VE10+.5)
1610 VE11=INT(VE11+.5)
1645 LOCATE 18,4:PRINT TIME TAB(12) VE1 TAB(19) VE2 TAB(26) VE4 TAB(33) VE5 TAB(
40) VE6 TAB(47) DB TAB(55) VE9 TAB(62) VE10 TAB(69) VE11
1648 VE1=0:VE2=0:VE3=0:VE4=0:VE5=0:VE6=0:VE7=0:VE8=0:VE9=0:VE10=0:VE11=0:I=0
1650 K2=K2+3
1665 TIME2=TIME2+1
1670 TIME=INT(TIME2+.5)

```

```

1675 IF (T1#*1.67)>TIME2 THEN GOTO 1665
1687 LOCATE 11,38:PRINT COUNT
1690 IF COUNT<T4 THEN GOTO 1450
1705 KK=K2
1706 TIMESAVE=INT(TIME2)
1708 CALL INTOFF
1730 COLOR 2,0,0
1731 CLS
1732 LOCATE 11,28:PRINT"DATA LOGGING COMPLETED"
1733 PRINT "COUNT="COUNT
1734 PRINT "TIMESAVE="TIMESAVE
1735 PRINT"T1#="INT(T1#*1.67)
1736 PRINT "KK="KK
1737 O=0
1738 O=O+1
1739 IF O<5000 THEN GOTO 1738
1750 GOTO 2660
1770 SCREEN 2: SCREEN 0
1780 CLS
1790 LOCATE 3,9:PRINT"+++++++CHOOSE AN OPTION BY PRESSING APPROPRIATE KEY+++++
++++"
1800 COLOR 4,0,0
1803 LOCATE 5,9:PRINT"FOR REAL-TIME GRAPHICAL DISPLAY OF DATA FROM THE FOLLOWING
"
1804 LOCATE 6,9:PRINT"SENSING DEVICES;"
1810 LOCATE 8,9:PRINT"M) : TEMPERATURE ON UPPER AND LOWER FACE OF ABUTMENT LOADC
ELL"
1811 LOCATE 9,9:PRINT"N) : TEMPERATURE ON ABUTMENT TOOL FACE"
1812 LOCATE 10,9:PRINT"P) : TEMPERATURE ON UPPER AND LOWER FACE OF DIE LOADCELL"

1820 LOCATE 11,9:PRINT"Q) : TEMPERATURE OF DIE PERIPHERY"
1830 LOCATE 12,9:PRINT"R) : OUTPUT FROM HIGH AND LOW PRESSURE TRANSDUCERS"
1840 LOCATE 13,9:PRINT"S) : RELATIVE SPEED OF CONFORM WHEEL"
1850 LOCATE 14,9:PRINT"T) : OUTPUT FROM ABUTMENT AND DIE LOADCELLS"
1860 COLOR 13,0,0
1870 LOCATE 16,9:PRINT"U) : FOR DATA LOGGING AND PROCESSING"
1880 COLOR 3,0,0
1890 LOCATE 20,4:PRINT"NOTE : PRESS ESCape TO ABORT REAL-TIME GRAPHICAL DISPLAY
AND, RETURN TO MENU"
1900 INPUT I$
1910 CLS
1912 COLOR 4,0,0
1914 LOCATE 4,15: PRINT"PLEASE WAIT, DATA LOGGING IS NOW BEING CONTINUED"
1916 COLOR 6,0,0
1918 LOCATE 6,11: PRINT"WHEN COUNT IS EQUAL TO";T5;"THEN REAL TIME GRAPH MENU WI
LL"
1920 LOCATE 7,11: PRINT "BE RETURNED TO THE SCREEN"
1925 LOCATE 9,11: PRINT "WHEN COUNT IS EQUAL TO";T4;"THEN DATA LOGGING IS COMPLE
TED"
1927 COLOR 4,0,0
1929 LOCATE 11,32:PRINT "COUNT;"
1932 LOCATE 14,5:PRINT "TIME" TAB(13) "AL(B)" TAB(20) "AL(F)" TAB(27) "DL(B)" TA
B(34) "DL(F)" TAB(41) "DIE" TAB(48) "TORQUE" TAB(56) "SPEED" TAB(63) "RLOAD" TAB
(70) "ALOAD"
1935 LOCATE 15,5:PRINT "SECS" TAB(13) "(cel)" TAB(20) "(cel)" TAB(27) "(cel)" TA
B(34) "(cel)" TAB(41) "(cel)" TAB(48) "(kNm)" TAB(56) "(rpm)" TAB(63) "(kN)" TAB
(70) "(kN)"
1937 LOCATE 16,2:PRINT"
"
1940 COLOR 7,0,0
1960 IF I$="M" THEN GOTO 2010
1963 IF I$="N" THEN GOTO 2028
1965 IF I$="P" THEN GOTO 2160
1967 IF I$="Q" THEN GOTO 2190
1969 IF I$="R" THEN GOTO 2300
1970 IF I$="S" THEN GOTO 2420

```

```

1780 IF I$="U" THEN GOTO 2530
1990 IF I$="U" THEN GOTO 2000
2000 RETURN
2010 CLS
2012 SCREEN 1
2013 COLOR 1,0
2020 LOCATE 1,1:PRINT"400 (CELS)"
2021 LOCATE 22,1:PRINT"0"
2022 LOCATE 22,40:PRINT"8"
2023 LOCATE 23,2:PRINT"CHANGE IN TEMPERATURE WITH TIME (mins)"
2025 LINE (8,9)-(310,166),1,B :REM Draws a box on the screen
2026 CALL GRAPHRT ("DEMO","2,3","1,2","PAGEC",0.,400.,11)
2027 GOTO 1770
2028 CLS
2029 SCREEN 1
2030 COLOR 1,0
2040 LOCATE 1,1:PRINT"400 (CELS)"
2050 LOCATE 22,1:PRINT"0"
2060 LOCATE 22,40:PRINT"8"
2070 LOCATE 23,2:PRINT"CHANGE IN TEMPERATURE WITH TIME (mins)"
2080 LINE (8,9)-(310,166),1,B :REM Draws a box on the screen
2085 CALL GRAPHRT ("DEMO","4","1","PAGEC",0.,400.,11)
2086 GOTO 1770
2160 CLS
2162 SCREEN 1
2163 COLOR 1,0
2164 LOCATE 1,1:PRINT"600 (CELS)"
2165 LOCATE 22,1:PRINT"0"
2166 LOCATE 22,40:PRINT"8"
2167 LOCATE 23,2:PRINT"CHANGE IN TEMPERATURE WITH TIME (mins)"
2171 LINE (8,9)-(310,166),1,B :REM Draws a box on the screen
2172 CALL GRAPHRT ("DEMO","5,6","1,2","PAGEC",0.,600.,11)
2175 GOTO 1770
2190 CLS
2200 SCREEN 1
2210 COLOR 1,0
2220 LOCATE 1,1:PRINT"600 (CELS)"
2230 LOCATE 22,1:PRINT"0"
2240 LOCATE 22,40:PRINT"8"
2250 LOCATE 23,2:PRINT"CHANGE IN TEMPERATURE WITH TIME (mins)"
2260 LINE (8,9)-(310,166),1,B
2280 CALL GRAPHRT ("DEMO","7","1","PAGEC",0.,600.,11)
2290 GOTO 1770
2300 CLS
2310 SCREEN 1
2320 COLOR 1,0
2330 LOCATE 2,1:PRINT"4_ (PSI)*1000"
2333 LOCATE 7,1:PRINT"3-----"
2335 LOCATE 12,1:PRINT"2-----"
2337 LOCATE 17,1:PRINT"1-----"
2340 LOCATE 22,1:PRINT"0-"
2350 LOCATE 22,40:PRINT"8"
2360 LOCATE 23,4:PRINT"CHANGE IN HIGH AND LOW TRANSDUCER"
2365 LOCATE 24,8:PRINT"PRESSURE WITH TIME (mins)"
2370 LINE (10,8)-(310,165),1,B
2390 REM are 0 and 10V.
2400 CALL GRAPHRT ("DEMO","8,9","1,2","PAGEC",0.,10.,0)
2410 GOTO 1770
2420 CLS
2430 SCREEN 1,0
2440 COLOR 1,0
2445 LOCATE 2,1:PRINT"(RPM)"
2450 LOCATE 3,1:PRINT"32-"
2455 LOCATE 7,1:PRINT"24-----"
2460 LOCATE 12,1:PRINT"16-----"
2463 LOCATE 17,2:PRINT"8-----"

```

```

2465 LOCATE 22,2:PRINT"0-"
2470 LOCATE 22,40:PRINT"8"
2480 LOCATE 23,8:PRINT"CHANGE IN TACHOMETER SPEED"
2485 LOCATE 24,13:PRINT"WITH TIME (mins)"
2490 LINE (15,9)-(310,166),1,B
2510 CALL GRAPHRT("DEMO","10","2","PAGEC",0.,6.,0)
2520 GOTO 1770
2530 CLS
2540 SCREEN 1
2550 COLOR 1,0
2560 LOCATE 2,1:PRINT"2*100 (kN)"
2565 LOCATE 12,1:PRINT"1"
2570 LOCATE 22,1:PRINT"0"
2580 LOCATE 22,40:PRINT"8"
2590 LOCATE 23,3:PRINT"CHANGE IN DIE AND ABUTMENT FORCE"
2595 LOCATE 24,9:PRINT"WITH TIME (mins)"
2600 LINE (8,9)-(310,166),1,B
2630 CALL GRAPHRT("DEMO","11,12","1,2","PAGEC",0.,100.,30)
2640 GOTO 1770
2660 CLS
2661 CLOSE #1
2662 COLOR 4,0,0
2663 LOCATE 3,31:PRINT "MASTER MENU"
2664 LOCATE 5,7:PRINT"++++++POST-PROCESSED EXPERIMENTAL RESULTS FROM TEST++++
+++"
2665 COLOR 11,0,0
2666 LOCATE 8,15:PRINT"CHOOSE AN OPTION BY PRESSING APPROPRIATE KEY"
2667 COLOR 4,0,0
2670 LOCATE 12,15:PRINT"P) DATA AND GRAPHS RETURNED TO THE SCREEN"
2672 LOCATE 13,15:PRINT"Q) DATA AND GRAPHS RETURNED TO THE PRINTER"
2674 COLOR 14,0,0
2676 LOCATE 16,15:PRINT"F) TO TERMINATE SESSION"
2677 PRINT""
2680 INPUT A$
2690 IF A$="P" THEN GOTO 2870
2700 IF A$="Q" THEN GOTO 8000
2710 IF A$="F" THEN GOTO 5070
2870 RODAREA=3.142*D1*D1*.25
2880 DIEAREA=3.142*D5*D5*.25
2890 REDRATIO=RODAREA/DIEAREA
2900 IF RODAREA=0 THEN GOTO 2920
2910 EXPRATIO=DIEAREA/RODAREA
2920 ABUTAREA=4.75*4.75*3.142*.5+(H-4.75)*9.5
2930 REDRATIOPART=ABUTAREA/DIEAREA
2940 EXPRATIOPART=DIEAREA/ABUTAREA
2950 WEIGHT=(INT(((Q*.4536)*100)+.5))/100
2980 CLS
2990 COLOR 4,0,0
2991 PRINT "TEST NO. ";TN
2992 PRINT "DATE "; DA$
3000 IF G=2 THEN GOTO 3090
3010 PRINT"Feed technique employed was particulate (spec. AA1050)"
3020 PRINT" Grannulated mesh size is ??"
3030 PRINT "Extrusion ratio =";REDRATIOPART
3040 PRINT "Abutment height =";H;"mm"
3050 PRINT "Shoe angle =";ANGLE;"degrees"
3060 PRINT "Die diameter =";D5;"mm"
3070 PRINT "Expansion chamber type: ";K$
3080 IF D1=0 THEN GOTO 3167
3090 PRINT "Feed technique employed was continuously cast rod (spec. AA1050)"
3100 PRINT "Extrusion ratio =";REDRATIO
3110 PRINT "Abutment height =";H;"mm"
3120 PRINT "shoe angle =";ANGLE;"degrees"
3130 PRINT "Die diameter =";D5;"mm"
3140 PRINT "Rod diameter =";D1;"mm"
3150 PRINT "Expansion chamber tvoe: " :K$

```

```

3155 PRINT "Weight of rod feed stock =";WEIGHT;"kg"
3167 COLOR 7,0,0
3170 LOCATE 12,1:PRINT"TIME2" TAB(10)"ALC(B)" TAB(17)"ALC(F)" TAB(24)"ABUT" TAB(
31)"DLC(B)" TAB(38)"DLC(F)" TAB(45)"DIE" TAB(51)"TORQUE" TAB(58) "SPEED" TAB(65)
"RLOAD" TAB(72) "ALOAD"
3180 LOCATE 13,1:PRINT"SEC"TAB(10)"(CEL)" TAB(17)"(CEL)" TAB(24)"(CEL)" TAB(31)"
(CEL)" TAB(38)"(CEL)" TAB(45)"(CEL)" TAB(52)"(kNm)" TAB(58)"(RPM)" TAB(65) "(kN)
"TAB(72)"(kN)"
3190 PRINT"
"
3200 OPEN "SEQUEL" FOR INPUT AS #1
3210 J=1 :REM      "J" is used to count the no. of values printed.
3220 K2=0
3225 K3=0
3230 TIME2=0
3240 I=0
3250 VB1=0:VB2=0:VB3=0:VB4=0:VB5=0:VB6=0:VB7=0:VB8=0:VB9=0:VB10=0:VB11=0
3260 VE1=0:VE2=0:VE3=0:VE4=0:VE5=0:VE6=0:VE7=0:VE8=0:VE9=0:VE10=0:VE11=0
3300 INPUT #1, K2, TIME2, VE1,VE2,VE3,VE4,VE5,VE6,VE7,VE8,VE9,VE10,VE11
3305 I=I+1
3308 VB1=VB1+VE1:VB2=VB2+VE2:VB3=VB3+VE3:VB4=VB4+VE4:VB5=VB5+VE5:VB6=VB6+VE6
3310 VB7=VB7+VE7:VB8=VB8+VE8:VB9=VB9+VE9:VB10=VB10+VE10:VB11=VB11+VE11
3315 IF TIME2<K3 THEN GOTO 3850
3320 VB1=VB1/I:VB2=VB2/I:VB3=VB3/I:VB4=VB4/I:VB5=VB5/I:VB6=VB6/I
3325 VB7=VB7/I:VB8=VB8/I:VB9=VB9/I:VB10=VB10/I:VB11=VB11/I
3330 VB1=VB1-20:VB2=VB2-20:VB3=VB3-20:VB4=VB4-20:VB5=VB5-20:VB6=VB6-20
3370 Z1=(VB4+VB5)*.5
3375 Z2=(VB1+VB2)*.5
3390 VB10=(1.4*(VB10-BASE10))+21.9      :REM DIE LOADCELL
3428 IF Z1=<0 THEN VB10=0
3430 REM      ABUTMENT LOADCELL
3440 IF (Z2>0) AND (Z2=<166) THEN VB11=(2.2*(VB11-BASE11))+2.12
3460 IF (Z2>166) AND (Z2=<186) THEN VB11=(2.19*(VB11-BASE11))+1.39
3465 IF (Z2>186) THEN VB11=(2.19*(VB11-BASE11))+.29
3487 IF Z2=<0 THEN VB11=0
3490 VB7=422.6*(VB7-BASE7)+115.9      :REM Calibrate LP transducer.
3500 VB8=386.2*(VB8-BASE8)+98.7      :REM Calibrate HP transducer.
3505 DP=VB8-VB7
3510 DP=(.0143*DP)-1.978
3515 IF DP<10 THEN DP=0
3520 VB9=5.505*(VB9-BASE9)-.39
3530 IF VB9<4 THEN VB9=0 :REM CALIBRATION NOT APPLICABLE IN THIS RANGE
3540 IF VB10<4 THEN VB10=0
3545 IF VB11<4 THEN VB11=0
3590 VB1=(INT((VB1*10)+.5))*1: VB2=(INT((VB2*10)+.5))*1
3600 VB3=(INT((VB3*10)+.5))*1: VB4=(INT((VB4*10)+.5))*1
3610 VB5=(INT((VB5*10)+.5))*1: VB6=(INT((VB6*10)+.5))*1
3620 DP=(INT((DP*100)+.5))*01
3630 VB9=(INT((VB9*100)+.5))*01: VB10=(INT((VB10*100)+.5))*01
3640 VB11=(INT((VB11*100)+.5))*01
3645 TIME2=(INT((TIME2*10)+.5))*1
3650 W4(J)=VB6
3660 WDP(J)=DP: W10(J)=VB10 : W11(J)=VB11
3700 PRINT TIME2 TAB(9) VB1 TAB(16) VB2 TAB(23) VB3 TAB(30) VB4 TAB(37) VB5 TAB(
44) VB6 TAB(50) DP TAB(57) VB9 TAB(64) VB10 TAB(72) VB11
3705 VB1=0:VB2=0:VB3=0:VB4=0:VB5=0:VB6=0:VB7=0:VB8=0:VB9=0:VB10=0:VB11=0:I=0
3710 J=J+1
3720 K3=K3+3
3850 TIMETOTAL=TIMESAVE-(5*1):REM OTHERWISE INPUT PAST 3370 (ie 4*TIME INCREMENT
)
3855 IF J>598 THEN GOTO 3870
3860 IF TIME2<TIMETOTAL THEN GOTO 3300
3870 COLOR 14,0,0
3890 PRINT"PRESS ANY KEY AND MENU WILL BE RETURNED TO SCREEN"
3892 F$=INKEY$: IF F$="" THEN GOTO 3892
3895 COLOR 4,0,0

```

```

3470 CLS
3980 LOCATE 2,10:PRINT" THE MENU PROVIDES THE USER WITH THE FACILITY TO VIEW"
3990 LOCATE 3,10:PRINT" THE DATA POINTS WHICH CORRESPOND TO THOSE PREVIOUSLY"
3991 LOCATE 4,10:PRINT" LOGGED"
4000 PRINT
4010 SCREEN 0
4020 COLOR 11,0,0
4030 LOCATE 6,6:PRINT"+++++++CHOOSE AN OPTION BY PRESSING APPROPRIATE KEY+++++
+++
4033 COLOR 4,0,0
4035 LOCATE 8,10:PRINT" FOR DISPLAY OF THE FOLLOWING TEST DATA WITH TIME"
4050 LOCATE 10,10:PRINT" A) : TEMPERATURE OF DIE PERIPHERY"
4060 LOCATE 11,10:PRINT" B) : WHEEL TORQUE"
4070 LOCATE 12,10:PRINT" C) : RADIAL LOADCELL FORCE"
4080 LOCATE 13,10:PRINT" D) : ABUTMENT LOADCELL FORCE"
4082 COLOR 3,0,0
4085 LOCATE 15,10:PRINT" E) : MONOCHROME PRINT OF NUMERIC DATA AND GRAPHS"
4090 COLOR 14,0,0
4100 LOCATE 17,10:PRINT" F) : TO TERMINATE SESSION"
4110 INPUT M$
4120 IF M$= "A" THEN GOTO 4180
4130 IF M$= "B" THEN GOTO 4420
4140 IF M$= "C" THEN GOTO 4650
4150 IF M$= "D" THEN GOTO 4860
4155 IF M$= "E" THEN GOTO 2660
4160 IF M$= "F" THEN GOTO 5070
4170 REM Now start plotting graphs
4180 COLOR 7,0,0
4190 CLS
4200 SCREEN 2
4210 KEY OFF
4220 LOCATE 25,35: PRINT" TIME (sec)"
4230 LOCATE 25,47: PRINT TIME2
4235 LOCATE 1,1 : PRINT"TEMPERATURE"
4240 LOCATE 1,22 : PRINT"VARIATION OF DIE TEMPERATURE WITH TIME"
4250 LOCATE 2,3 : PRINT"(deg.C)"
4252 LOCATE 3,2 :PRINT"600-"
4255 LOCATE 2,22 : PRINT"+++++++PRESS ANY KEY FOR MENU+++++++
4256 LOCATE 8,2:PRINT"450-"
4260 LOCATE 13,2:PRINT"300-"
4265 LOCATE 18,2:PRINT"150-"
4270 LOCATE 23,4 : PRINT"0-"
4280 LINE (40,20)-(40,180)
4290 LINE (40,180)-(640,180)
4300 W4(1)=180-INT(W4(1)*180/600)+INT(W4(1)*20/600)
4310 LINE (40,W4(1))-(40,W4(1)) :REM plot the 1st point.
4320 X=41
4330 FOR J=2 TO 600
4340 Y=W4(J)
4350 Y=180-INT(Y*180/600)+INT(Y*20/600) : REM Scales Y to fit the screen with
4370 LINE -(X,Y),,,&HAAAA: REM Draws a line from the 1st to the next point.
4380 X=X+1
4390 NEXT J
4400 F$=INKEY$: IF F$="" THEN GOTO 4400
4410 GOTO 3970
4420 CLS
4430 COLOR 7,0,0
4440 SCREEN 2
4450 KEY OFF
4460 LOCATE 25,35: PRINT"TIME (sec)"
4470 LOCATE 25,47: PRINT TIME2
4475 LOCATE 1,1:PRINT"TORQUE"
4480 LOCATE 1,22: PRINT"CHANGE IN WHEEL TORQUE OUTPUT WITH TIME"
4490 LOCATE 2,3: PRINT"(kNm)"
4495 LOCATE 2,22: PRINT"+++++++PRESS ANY KEY FOR MENU+++++++
4496 LOCATE 3,3:PRINT"40-"

```

```

4500 LOCATE 7,3: PRINT"32-"
4501 LOCATE 11,3:PRINT"24-"
4502 LOCATE 15,3:PRINT"16-"
4503 LOCATE 19,4:PRINT"8-"
4510 LOCATE 23,4: PRINT"0-"
4520 LINE (40,20)-(40,180)
4530 LINE (40,180)-(640,180)
4540 WDP(1)=180-INT(WDP(1)*180/40)+INT(WDP(1)*20/40)
4550 LINE (40,WDP(1))-(40,WDP(1))
4560 X=41
4570 FOR J=2 TO 600
4580 Y=WDP(J)
4590 Y=180-INT(Y*180/40)+INT(Y*20/40)
4600 LINE -(X,Y),,,&HAAAA
4610 X=X+1
4620 NEXT J
4630 F$=INKEY$: IF F$="" THEN GOTO 4630
4640 GOTO 3970
4650 CLS
4660 COLOR 7,0,0
4670 SCREEN 2
4680 LOCATE 25,35: PRINT" TIME (sec)"
4690 LOCATE 25,47: PRINT TIME2
4695 LOCATE 1,2 :PRINT"FORCE"
4700 LOCATE 1,20 : PRINT"CHANGE IN RADIAL-DIE LOADCELL FORCE WITH TIME"
4705 LOCATE 2,3:PRINT"(kN)"
4706 LOCATE 2,20 : PRINT"+++++++PRESS ANY KEY FOR MENU+++++++"
4710 LOCATE 3,2 : PRINT"150-"
4711 LOCATE 7,2:PRINT"120-"
4712 LOCATE 11,3:PRINT"90-"
4713 LOCATE 15,3:PRINT"60-"
4715 LOCATE 19,3:PRINT"30-"
4720 LOCATE 23,4 : PRINT"0-"
4730 LINE (40,20)-(40,180)
4740 LINE (40,180)-(640,180)
4750 W10(1)=180-INT(W10(1)*180/150)+INT(W10(1)*20/150)
4760 LINE (40,W10(1))-(40,W10(1))
4770 X=41
4780 FOR J=2 TO 600
4790 Y=W10(J)
4800 Y=180-INT(Y*180/150)+INT(Y*20/150)
4810 LINE -(X,Y),,,&HAAAA
4820 X=X+1
4830 NEXT J
4835 F$=INKEY$: IF F$="" THEN GOTO 4835
4850 GOTO 3970
4860 CLS
4870 COLOR 7,0,0
4880 SCREEN 2
4890 KEY OFF
4900 LOCATE 25,35: PRINT"TIME (sec)"
4910 LOCATE 25,47: PRINT TIME2
4915 LOCATE 1,2:PRINT"FORCE"
4920 LOCATE 1,21 : PRINT"CHANGE IN ABUTMENT LOADCELL FORCE WITH TIME"
4925 LOCATE 2,3:PRINT"(kN)"
4930 LOCATE 3,2 : PRINT"150-"
4935 LOCATE 2,21 : PRINT"+++++++PRESS ANY KEY FOR MENU+++++++"
4936 LOCATE 7,2:PRINT"120-"
4937 LOCATE 11,3 :PRINT"90-"
4938 LOCATE 15,3:PRINT"60-"
4939 LOCATE 19,3:PRINT"30-"
4940 LOCATE 23,4 : PRINT"0-"
4950 LINE (40,20)-(40,180)
4960 LINE (40,180)-(640,180)
4970 W11(1)=180-INT(W11(1)*180/150)+INT(W11(1)*20/150)
4980 LINE (40,W11(1))-(40,W11(1))

```

```

4770 ^-+1
5000 FOR J=2 TO 600
5005 Y=W11(J)
5010 Y=180-INT(Y*180/150)+INT(Y*20/150)
5020 LINE -(X,Y),,,&HAAAA
5030 X=X+1
5040 NEXT J
5050 F$=INKEY$: IF F$="" THEN GOTO 5050
5060 GOTO 3970
5070 CLS
5090 COLOR 14,0,0
5100 LOCATE 8,10:PRINT"ARE YOU SURE YOU WANT TO DELETE ALL DATA FROM PREVIOUS T
ST (Y/N)"
5110 INPUT K$
5120 IF K$="N" THEN GOTO 2660
5130 CLOSE #1
5140 END
5700 LPRINT ""
8000 CLS
8010 COLOR 14,0,0
8011 LOCATE 12,18:PRINT"POST PROCESS DATA PRINTING NOW IN PROGRESS"
8012 LPRINT "TEST NO.";TN
8013 LPRINT "DATE "; DA$
8020 IF G=2 THEN GOTO 8110
8030 LPRINT"Feed technique employed was particulate (spec. AA1050)"
8040 LPRINT" Grannulated mesh size is ??"
8050 LPRINT "Extrusion ratio =";RODTIOPART
8060 LPRINT "Abutment height =";H;"mm"
8070 LPRINT "Shoe angle =";ANGLE;"degrees"
8080 LPRINT "Die diameter =";D5;"mm"
8090 LPRINT "Expansion chamber type: ";K$
8100 IF D1=0 THEN GOTO 8167
8110 LPRINT "Feed technique employed was continuously cast rod (spec. AA1050)"
8120 LPRINT "Extrusion ratio =";REDRATIO
8130 LPRINT "Abutment height =";H;"mm"
8140 LPRINT "shoe angle =";ANGLE;"degrees"
8150 LPRINT "Die diameter =";D5;"mm"
8155 LPRINT "Rod diameter =";D1;"mm"
8160 LPRINT "Expansion chamber type: ";K$
8162 LPRINT "Weight of rod feed stock =";WEIGHT;"kg"
8167 LPRINT""
8168 LPRINT""
8170 LOCATE 6,1:LPRINT"TIME2" TAB(10)"ALC(B)" TAB(17)"ALC(F)" TAB(24)"ABUT" TAB
31)"DLC(B)" TAB(38)"DLC(F)" TAB(45)"DIE" TAB(51)"TORQUE" TAB(58) "SPEED" TAB(65
"RLOAD" TAB(72) "ALOAD"
8180 LOCATE 13,1:LPRINT"SEC"TAB(10)"(CEL)" TAB(17)"(CEL)" TAB(24)"(CEL)" TAB(31
"(CEL)" TAB(38)"(CEL)" TAB(45)"(CEL)" TAB(52)"(kNm)" TAB(58)"(RPM)" TAB(65) "(K
)"TAB(72)"(KN)"
8190 LPRINT"
"
8195 CLOSE #1
8200 OPEN "SEQUEL" FOR INPUT AS #1
8210 J=1 :REM "J" is used to count the no. of values printed.
8220 K2=0
8225 K3=0
8230 TIME2=0
8240 I=0
8250 VB1=0:VB2=0:VB3=0:VB4=0:VB5=0:VB6=0:VB7=0:VB8=0:VB9=0:VB10=0:VB11=0
8260 VE1=0:VE2=0:VE3=0:VE4=0:VE5=0:VE6=0:VE7=0:VE8=0:VE9=0:VE10=0:VE11=0
8300 INPUT #1, K2, TIME2, VE1,VE2,VE3,VE4,VE5,VE6,VE7,VE8,VE9,VE10,VE11
8305 I=I+1
8308 VB1=VB1+VE1:VB2=VB2+VE2:VB3=VB3+VE3:VB4=VB4+VE4:VB5=VB5+VE5:VB6=VB6+VE6
8309 VB7=VB7+VE7:VB8=VB8+VE8:VB9=VB9+VE9:VB10=VB10+VE10:VB11=VB11+VE11
8315 IF TIME2<K3 THEN GOTO 8618
8320 VB1=VB1/I:VB2=VB2/I:VB3=VB3/I:VB4=VB4/I:VB5=VB5/I:VB6=VB6/I
8325 VB7=VB7/I:VB8=VB8/I:VB9=VB9/I:VB10=VB10/I:VB11=VB11/I

```

```

8330 VB1=VB1-20:VB2=VB2-20:VB3=VB3-20:VB4=VB4-20:VB5=VB5-20:VB6=VB6-20
8370 Z1=(VB4+VB5)*.5
8375 Z2=(VB1+VB2)*.5
8395 VB10=(1.4*(VB10-BASE10))+21.9 :REM DIE LOADCELL
8405 IF Z1<=0 THEN VB10=0
8430 REM ABUTMENT LOADCELL
8440 IF (Z2>0) AND (Z2<=166) THEN VB11=(2.2*(VB11-BASE11))+2.12
8460 IF (Z2>166) AND (Z2<=186) THEN VB11=(2.19*(VB11-BASE11))+1.39
8465 IF (Z2>186) AND (Z2<=212) THEN VB11=(2.19*(VB11-BASE11))+.29
8485 IF (Z2>212) THEN VB11=0
8487 IF Z2<=0 THEN VB11=0
8490 VB7=422.6*(VB7-BASE7)+115.9
8500 VB8=386.2*(VB8-BASE8+.04)+98.7
8505 DP=VB8-VB7
8510 DP=(.0143*DP)-1.978
8515 IF DP<10 THEN DP=0
8520 VB9=5.505*(VB9-BASE9)-.39
8530 IF VB9<4 THEN VB9=0
8540 IF VB10<4 THEN VB10=0
8545 IF VB11<4 THEN VB11=0
8590 VB1=(INT((VB1*10)+.5))*1: VB2=(INT((VB2*10)+.5))*1
8600 VB3=(INT((VB3*10)+.5))*1: VB4=(INT((VB4*10)+.5))*1
8601 VB5=(INT((VB5*10)+.5))*1: VB6=(INT((VB6*10)+.5))*1
8602 DP=(INT((DP*100)+.5))*1
8603 VB9=(INT((VB9*100)+.5))*1: VB10=(INT((VB10*100)+.5))*1
8605 VB11=(INT((VB11*100)+.5))*1
8608 TIME2=(INT((TIME2*10)+.5))*1
8609 WDP(J)=DP: W10(J)=VB10: W11(J)=VB11
8611 WTIME2(J)=TIME2: W4(J)=VB6
8613 LPRINT TIME2 TAB(9) VB1 TAB(16) VB2 TAB(23) VB3 TAB(30) VB4 TAB(37) VB5 TAB
(44) VB6 TAB(50) DP TAB(57) VB9 TAB(64) VB10 TAB(71) VB11
8614 VB1=0:VB2=0:VB3=0:VB4=0:VB5=0:VB6=0:VB7=0:VB8=0:VB9=0:VB10=0:VB11=0:I=0
8615 J=J+1
8616 K3=K3+32
8618 TIMETOTAL=TIMESAVE-(5*1)
8620 IF J>598 THEN GOTO 8630
8621 IF TIME2<TIMETOTAL THEN GOTO 8300
8630 COLOR 4,0,0
8720 CLS
8730 LOCATE 2,10:PRINT" THE MENU PROVIDES THE USER WITH THE FACILITY TO PRINT"
8740 LOCATE 3,10:PRINT" THE DATA POINTS WHICH CORRESPOND TO THOSE PREVIOUSLY"
8741 LOCATE 4,10:PRINT" LOGGED"
8760 SCREEN 0
8770 COLOR 11,0,0
8780 LOCATE 6,6:PRINT"+++++++CHOOSE AN OPTION BY PRESSING APPROPRIATE KEY+++++
+++
8785 COLOR 4,0,0
8790 LOCATE 8,10:PRINT" FOR A PRINT OF THE FOLLOWING TEST DATA WITH TIME"
8792 LOCATE 10,10:PRINT" A) : TEMPERATURE OF DIE PERIPHERY"
8800 LOCATE 11,10:PRINT" B) : WHEEL TORQUE"
8810 LOCATE 12,10:PRINT" C) : RADIAL LOADCELL FORCE"
8820 LOCATE 13,10:PRINT" D) : ABUTMENT LOADCELL FORCE"
8830 COLOR 3,0,0
8835 LOCATE 15,10:PRINT" E) : RETURN TO MASTER MENU"
8836 COLOR 14,0,0
8840 LOCATE 17,10:PRINT" F) : TO TERMINATE SESSION"
8870 INPUT M$
8880 IF M$= "A" THEN GOTO 8950
8890 IF M$= "B" THEN GOTO 9190
8900 IF M$= "C" THEN GOTO 9420
8910 IF M$= "D" THEN GOTO 9640
8920 IF M$= "E" THEN GOTO 2660
8930 IF M$= "F" THEN GOTO 5070
8940 REM Now start plotting graphs
8950 COLOR 14,0,0
8960 CLS

```

```

8980 KEY OFF : REM Turn BASIC keys on line 25 off.
9000 LPRINT""
9011 LPRINT""
9013 LOCATE 12,18:PRINT"POST PROCESS GRAPH PRINTING NOW IN PROGRESS"
9020 LPRINT TAB(19) "VARIATION OF DIE TEMPERATURE WITH TIME" TAB(66) "TEMP. (deg
.C)"
9025 LPRINT TAB(19) "-----"
9030 LPRINT TAB(10) "0" TAB(19) "100" TAB(29) "200" TAB(39) "300" TAB(49) "400"
TAB(59) "500" TAB(69) "600"
9040 LPRINT TAB(10) ":" TAB(15) ":" TAB(20) ":" TAB(25) ":" TAB(30) ":" TAB(35)
":" TAB(40) ":" TAB(45) ":" TAB(50) ":" TAB(55) ":" TAB(60) ":" TAB(65) ":" TAB(
70) ":"
9050 LPRINT TAB(9) "
"
9080 FOR J=2 TO 600
9100 Y=INT((60/600)* W4(J))+10
9101 IF WTIME2(J)=0 THEN GOTO 9165
9130 IF Y>10 THEN GOTO 9135
9133 LPRINT TAB(30) "NEGATIVE VALUE OF TEMPERATURE"
9134 GOTO 9160
9135 IF Y<76 THEN GOTO 9150
9136 LPRINT TAB(30) "OVERSHOOT ON TEMPERATURE AXIS"
9140 GOTO 9160
9150 LPRINT WTIME2(J) TAB(10) ":" TAB(Y) "+"
9160 NEXT J
9165 LPRINT""
9170 LPRINT TAB(3) "TIME (SECS)"
9180 GOTO 8720
9190 CLS
9200 COLOR 14,0,0
9220 KEY OFF
9230 LPRINT""
9240 LPRINT""
9250 LOCATE 12,13:PRINT"POST PROCESSED GRAPH PRINTING NOW IN PROGRESS"
9270 LPRINT TAB(19) "CHANGE IN WHEEL TORQUE OUTPUT WITH TIME" TAB(64) "TORQUE (k
Nm)"
9280 LPRINT TAB(19) "-----"
9290 LPRINT TAB(10) "10" TAB(20) "15" TAB(30) "20" TAB(40) "25" TAB(50) "30" TAB
(60) "35" TAB(70) "40"
9300 LPRINT TAB(10) ":" TAB(15) ":" TAB(20) ":" TAB(25) ":" TAB(30) ":" TAB(35)
":" TAB(40) ":" TAB(45) ":" TAB(50) ":" TAB(55) ":" TAB(60) ":" TAB(65) ":" TAB(
70) ":"
9310 LPRINT TAB(9) "
"
9320 FOR J=2 TO 600
9325 IF WTIME2(J)=0 THEN GOTO 9370
9330 Y=INT((60/40)*WDP(J))+10
9340 IF Y>10 THEN GOTO 9343
9341 LPRINT TAB(30) "NEGATIVE VALUE OF PRESSURE"
9342 GOTO 9360
9343 IF Y<76 THEN GOTO 9350
9344 LPRINT TAB(30) "OVERSHOOT ON PRESSURE AXIS"
9345 GOTO 9360
9350 LPRINT WTIME2(J) TAB(10) ":" TAB(Y) "+"
9360 NEXT J
9370 LPRINT ""
9380 LPRINT TAB(3) "TIME (SECS)"
9390 GOTO 8720
9420 CLS
9430 COLOR 14,0,0
9440 LPRINT""
9450 LPRINT""
9460 LOCATE 12,13:PRINT"POST PROCESSED GRAPH PRINTING NOW IN PROGRESS"
9470 LPRINT TAB(20) "VARIATION OF 'RLC' FORCE WITH TIME" TAB(66, "FCPCE (kN)
9480 LPRINT TAB(20) "-----"
9490 LPRINT TAB(10) "0" TAB(19) "20" TAB(29) "40" TAB(39) "60" TAB(49) "80" TAB(

```

```

59) "100" TAB(69) "120"
9500 LPRINT TAB(10) ":" TAB(15) ":" TAB(20) ":" TAB(25) ":" TAB(30) ":" TAB(35)
      ":" TAB(40) ":" TAB(45) ":" TAB(50) ":" TAB(55) ":" TAB(60) ":" TAB(65) ":" TAB(
70) ":"
9510 LPRINT TAB(9) " _____
      "
9515 FOR J= 2 TO 600
9520 IF WTIME2(J)=0 THEN GOTO 9570
9530 Y=INT((60/120)*W10(J))+10
9532 IF Y>10 THEN GOTO 9535
9533 LPRINT TAB(30) "NEGATIVE VALUE OF FORCE"
9534 GOTO 9560
9535 IF Y<76 THEN GOTO 9550
9540 LPRINT TAB(30) "OVERSHOOT ON FORCE AXIS"
9545 GOTO 9560
9550 LPRINT WTIME2(J) TAB(10) ":" TAB(Y) "+"
9560 NEXT J
9570 LPRINT""
9580 LPRINT TAB(3) "TIME (SECS)"
9590 GOTO 8720
9640 CLS
9650 COLOR 14,0,0
9660 LPRINT""
9670 LPRINT""
9680 LOCATE 12,13:PRINT"POST PROCESSED GRAPH PRINTING NOW IN PROGRESS"
9690 LPRINT TAB(20) "VARIATION OF 'ALC' FORCE WITH TIME" TAB(66) "FORCE (kN)"
9705 LPRINT TAB(20) "-----"
9710 LPRINT TAB(10) "0" TAB(19) "20" TAB(29) "40" TAB(39) "60" TAB(49) "80" TAB
59) "100" TAB(69) "120"
9720 LPRINT TAB(10) ":" TAB(15) ":" TAB(20) ":" TAB(25) ":" TAB(30) ":" TAB(35)
      ":" TAB(40) ":" TAB(45) ":" TAB(50) ":" TAB(55) ":" TAB(60) ":" TAB(65) ":" TAB
70) ":"
9730 LPRINT TAB(9) " _____
      "
9740 FOR J=2 TO 600
9745 IF WTIME2(J)=0 THEN GOTO 9790
9750 Y=INT((60/120)*W11(J))+10
9755 IF Y>10 THEN GOTO 9758
9756 LPRINT TAB(30) "NEGATIVE VALUE OF FORCE"
9757 GOTO 9780
9758 IF Y<76 THEN GOTO 9770
9762 LPRINT TAB(30) "OVERSHOOT ON FORCE AXIS"
9765 GOTO 9780
9770 LPRINT WTIME2(J) TAB(10) ":" TAB(Y) "+"
9780 NEXT J
9790 LPRINT""
9800 LPRINT TAB(3) "TIME (SECS)"
9810 GOTO 8720
10072 LOCATE 13,10:PRINT"must not exceed a maximum value of ?? minutes (this"
10073 LOCATE 14,10:PRINT"is because of the maximum space reserved by the array"
10074 LOCATE 15,10:PRINT"dimensions)."

```

APPENDIX C1

The expression after Avitzur equation (5.6) can be expressed as follows,

$$\begin{aligned}
 W_{t(3-5)} &= \sigma_{m(3-5)} f(\alpha_2) \epsilon_{(3-5)} && \{W_R\} \\
 &+ 2K_{m(3-5)} \left(\alpha_2 / \sin^2(\alpha_2) - \cot(\alpha_2) \right) && \{W_R\} \\
 &+ K_{m(3-5)} \cot(\alpha_2) \epsilon_{(3-5)} && \{W_f\}_d \\
 &+ 2\tau_{m(3-5)} \left(2L_{(3-5)} / d_3 - (1 - d_5/d_3) \cot(\alpha_2) \right) && \{W_f\}_c
 \end{aligned}$$

where a mean value for $\sigma_{m(3-5)}$ in the term W_R has been assumed.

The components of strain are described under section 5.2.1

APPENDIX C2

The redundant work done term in equation (5.9) i.e.,

$$\begin{aligned}
 W_{t(2b-3)} &= \sigma_{m(2b-3)} f(\alpha_1) \epsilon_{(2b-3)} && \{W_h\} \\
 &+ 2K_{m(2b-3)} \left(1.25 + \alpha_1 / \sin^2(\alpha_1) - \cot(\alpha_1) \right) && \{W_R\} \\
 &+ K_{m(2b-3)} \cot(\alpha_1) \epsilon_{(2b-3)} && \{W_f\}
 \end{aligned}$$

incorporates the additional component $2.5 K_{m(2b-3)}$ in order to account for the metal change in direction ($\approx 90^\circ$) for a plane boundary at stages 2b to 3 see fig. 5.1.

Appendix C3

Values for constants in constitutive equations

The following data corresponding to the constitutive relationships have been derived from the compression test with the exception © from the hot torsion test.

Equation No	A	B	C	D	E	m	n
(5.11) {.1 < ϵ < .7}	166	1.13	.014	1.22	-	-	.23
(5.12)	153	-	-	-	†		.25
(5.13)	166	1.13	.014	1.22	†		.23
© (5.14) {.5 < (ϵ + E) < 2.5}	101	.98	-	-	-	.12	-
(5.15) {.7 < (ϵ + E) < 2.5}	153	1.13	.014	1.22	-	-	.23

† E = variable depending on the amount of prior cold work where $E = 0.44E_i$ and, E_i holds the value in the range $0 \leq E_i \leq 1$. For example, $E_i = 0.25, 0.5, 0.75$ and 1 for commercial purity aluminium in the 1/4, 1/2, 3/4 and full hard condition respectively. The expression $E = 0.44E_i$ has been derived from data provided in reference (34) for commercial purity aluminium in the zero and half hard condition.

T = temperature

T_H = homologous temperature = T/T_M

T_M = melting point temperature of feed metal selected in this case as 645 °C.

Appendix C4

Derivation of strain rate at stages 2b to 3

The strain rate can be determined by considering the control volume bounded by the planes of deformation after Motamora⁽¹⁷⁾, the volume flow rate and, the effective strain in the following relationship i.e.,

$$\dot{\epsilon} = \frac{\dot{\epsilon} \Delta_{cv}}{\dot{\Delta}_{cv}}$$

where, subscript cv refers to the control volume see fig C1

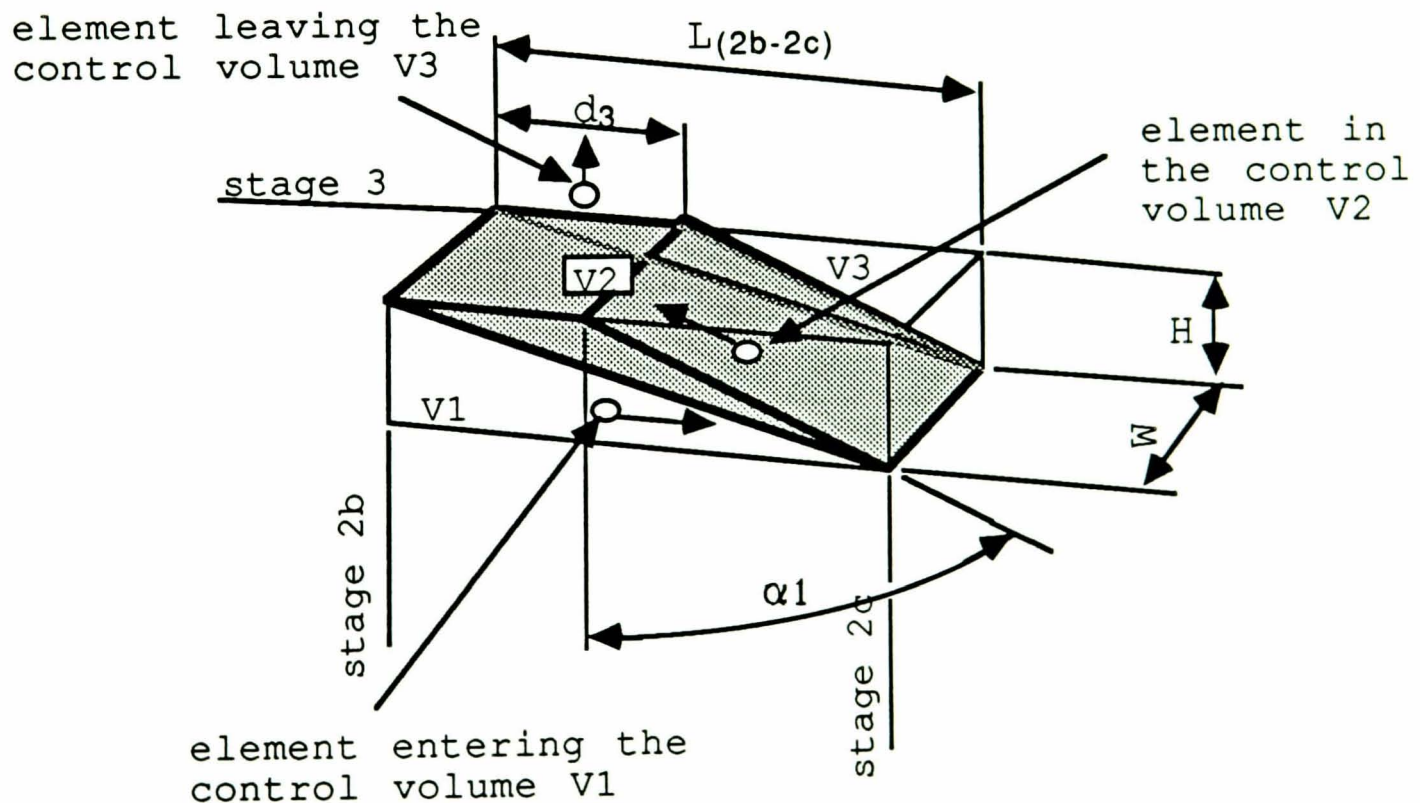


Figure E.1

The diagram illustrates plane boundaries of deformation

assuming constant density across the deformation zone then,

$$\epsilon = \epsilon V / V$$

evaluation yields, $V = A_2 d_3 / 2$

and, $V = A_2 \tan(\alpha_1) \dot{V}_2$

then, $\epsilon = 2 \dot{V}_2 \tan(\alpha_1) \epsilon / d_3$

$$\alpha_1 = \tan^{-1} \left((L_{(2b-2c)} - d_3/2) / H \right)$$

$$d_3 = 13.5 \text{ mm}$$

$$\dot{V}_2 = \zeta \dot{V}_2$$

where, ζ = fraction of feed metal remaining in the deformation zone at stage 3 as a function of the total feed metal entering the primary extrusion chamber.

The fraction value for ζ , can be determined from the equation of continuity as follows,

$$\text{mass}_i = \text{mass}_f + \text{mass}_{f1}$$

where, the mass flow of feed metal entering the deformation zone = mass flow leaving the deformation zone + mass flow lost through metal leakage (or flash).

Assuming constant density then the continuity equation becomes,

$$\dot{V}_1 A_1 = \dot{V}_5 A_5 + \dot{V}_{f1} A_{f1}$$

noting, that $\zeta = (A_1 - A_{f1}) / A_1$

and, $\dot{V}_5 A_5 = \dot{V}_{2b} A_2$

also, $\dot{V}_1 \approx \dot{V}_{f1}$

then evaluation yields, $\dot{V}_2 = \zeta \dot{V}_2$

will provide a measure of the spread of flash, over the periphery of the wheel as the metal leaks from the clearance along the primary extrusion zone i.e.,

$$\text{Width of flash} = A_1(1 - \zeta)/h$$

where h = thickness of flash (or the pre-set clearance between the rotating wheel and stationary tooling). Noting that the clearance setting can be measured before the start of each test, then, providing there is negligible elastic movement between the wheel and the tools under load i.e. assuming the machine components are rigidly held in their respective positions under the applied load, the measured value for h can be inserted into the above equation in order to determine the theoretical value for the spread of flash.

Appendix C5

Values for constants in heat loss equations

Feed metal spec. commercial purity aluminum 99.3 % < Al < 99.75 %

equation No	A	B	C
(5.23)	1.13	.351	-.375
(5.24)	.162	-	-.511
(5.26)	2.8	-	2

$$\beta_1 = 0.95$$

$$k = 230 \text{ W/m}^2$$

$$\rho_f = 2710 \text{ Kg/m}^3$$

$$C_f = 880 \text{ J/kg.K}$$

$$J = 4185 \text{ J/kcal} \quad (\text{noting that, } J = 1 \text{ if the units } \rho_f C_f = \text{J/m}^3\text{K})$$

A_a = cross-sectional area of primary extrusion chamber (abutment area)

$$\text{where, } A_a = ((H - PR)d_1 + PR^2\pi/2 + PR)$$

and, the profile radius (PR) on the abutment tool = 4.25 mm
SA = surface area of the wheel groove per unit length where,

$$SA = (P\pi + 1) + 2(H - PR)$$

$d_d = d_s = 13.5 \text{ mm}$ (where, d_s is the exposed die cross-sectional area noting also that, d_1 = initial diameter before deformation at a particular stage)

$$d_1 = 9.6 \text{ mm} \quad (\text{noting, that } W \approx d_1)$$

d_2 = mean diameter of the primary extrusion chamber where,

$$d_2 = \left(\frac{4A_a}{\pi} \right)^n \quad \text{where, } n = 1/2$$

Appendix D1

```

1 PRINT "To determine the minimum power required for steady-state radial extrusion"
2 PRINT "from knowledge of feed spec under certain conditions, geometry of extrusion"
3 PRINT "vessel, speed of operation, and friction conditions."
4 PRINT "The optimum dead-zone angle can then be determined and hence die pressure."
5 PRINT "-----"
6 PRINT "Commercial purity aluminium feed rod (spec. AA1050) "
10 PRINT "INPUT DIE DIAMETER in mm"
20 INPUT D5
30 PRINT "INPUT ABUTMENT SET in mm"
40 INPUT Ah
70 PRINT "INPUT WHEEL SPEED in rev/min"
80 INPUT S1
90 PRINT "INPUT FRICTION FACTOR for container wall i.e.  $1 \geq m \geq 0$ "
100 INPUT m
102 PRINT "INPUT PERCENTAGE OF FLASH DEVELOPED"
105 INPUT FLASH
CLS

200 REM GEOMETRY (CONFIGURATION TABLE)
205 FLASH=FLASH/100
210 PFLASH=1-FLASH
220 D1= 9.6
230 NA=(((Ah-4.25)*D1)+((4.25^2)*3.142*.5)+4.25)
240 SA=((3.142*4.25)+1)+((Ah-4.25)^2) :REM per unit length of chamberl
250 D2=SQR(4*NA/3.142)
260 D4= 13.5
270 D3= D4
280 e3=2*LOG(D4/D2)
290 IF D1<D2 THEN GOTO 310
300 e1=2*LOG(D1/D2) :GOTO 320
310 e1=2*LOG(D2/D1)
320 Lc=8+6
330 DD=D4/D5
340 RED=(D1/D5)^2
350 e4 =2*LOG(DD)
360 V=(D1/D5)^2
370 W=1/SQR(3) :REM Tresca yield criterion
380 TH1=30/645
390 YM1=166*(1-(1.13*TH1)) :REM after A&P -- strain rate small
400 PRINT "HAS THE FEED ROD BEEN WORK-HARDENED ENTER (Y=1/N=2)"
405 INPUT FF
408 IF FF = 2 THEN GOTO 470
410 PRINT "INPUT PERCENTAGE PRE-STRAIN (or COLD-WORK) IN FEED ROD"
420 INPUT PS
430 PSS=LOG(100/(100-PS))
440 WV1=YM1*(PSS^.23)*(e1+.23*(e1^2)/(2*PSS))-(.77*(e1^3)/(6*(PSS^2)))
450 YM1=YM1*(PSS^.23)*(1+.23*e1/PSS)-(.77*(e1^2)/(2*(PSS^2))) :REM true stress modified aft
er J & M.
460 PRINT "YM1*YM1"
465 GOTO 480
470 WV1=YM1*(e1^1.23)/1.23
475 YM1=YM1*(e1^.23) :REM mean true stress for true strain at ambient temp.
480 YM33a=80 :REM assume initial value for iteration
490 GG=0
495 IF DD<2.7 THEN GOTO 509
500 PPT=290 :REM assume initial value for iteration
505 DP=480 :REM assume initial value for iteration
508 AP=850 :GOTO 510
509 PPT=200
DP=250
AP=550
510 YMfla=80
511 r=18 :REM distance between abut tool face and centre of die

520 D1=D1/1000
530 D2=D2/1000
540 D3=D3/1000
550 D4=D4/1000
560 D5=D5/1000

```

```

570 Lc=Lc/1000
580 DM=(D4+D3)*.5

590 V1=((S1*3.142*2)/60)*.1675
600 V2=((D1/D2)^2)*V1*PFLASH
610 V4=((D2/D4)^2)*V2
620 time3= Lc/(6*V4) : REM INITIAL VALUE average time based on mean values ?
630 S11=S1*3.142*2/60 : REM wheel speed units= rad/s

650 Tor=19440*(S11^-.16)*((RED)^(-.071+(.15*Ah/(D1*1000)))) : REM Nm
660 TPOW=Tor*S11
670 FT=Tor/.1675
680 DPex=152*((Ah/(D1*1000))^-.722)*(RED^(.51-(.25*(Ah/(D1*1000)))) REM at 5 rev/min
690 APex=540*(RED^.14)*((Ah/(D1*1000))^-.22) REM at 5 revs/min

800 GOTO 5000

900 GG=GG+1
910 IF m=0 THEN GOTO 1000
920 ANG=10000
930 POW=10000
940 DIEPRESS=10000

1000 Z1=e4
1010 Z2=2*W
1020 Z3=W*e4
1030 Z4=4*W*m*Lc/D4
1040 Z5=2*W*m*(1-(D5/D4))
1050 Aa=(6*V4*(D4^2)*e4*.5)/((D4^3)-(D5^3)) : REM mean strain rate

1060 IF m=0 THEN GOTO 1080
1070 PRINT "D'Angle" ;TAB(8) "Pressure";TAB(47) "SR";TAB(52) "YM4";TAB(57) "TM"
1080 B=180/3.142
1090 l=0
1100 l=l+.0698
1110 X=(D4-D5)/(2*(Lc-.006))
1120 IF X>TAN(l) THEN GOTO 1100
1130 J=TAN(l) : REM TO SIMPLIFY MATHS
1140 Jj=Aa*J
1150 YM4=166*(1-(1.13*TH4))^(Jj^(.014*(10^(1.22*TH4)))) : REM YM4=101*(1-(.98*TH4))*Jj^.12
1151 e4a=e4+e3a
1152 YM4=YM4*(e3a^.23)
1155 YM44=YM4*e4 : REM workdone/unit volume - limits for large strains i.e. constant stress
1160 PHA=(1+(l/16)-(5*(l^2)/36)+(2*(l^3)/19))
1170 PH=PHA*YM44*10^6
1180 PR=Z2*((l/(SIN(l)^2))-(1/TAN(l)))*YM4*10^6
1190 PF1=Z3*(YM4*10^6)/(TAN(l))
1200 PF2=Z4*YM4*10^6
1210 PF3=Z5*(YM4*10^6)/(TAN(l))
1220 PT=PH+PR+PF1+PF2+PF3
1230 PT=PT/(10^6)
1240 K=(INT(((l*B)+.1)*10))/10 : REM convert to DEGREES
1250 K1=(INT(PT*10))/10
1260 K2=INT(PH/(10^6))
1270 K3=INT(PR/(10^6))
1280 K4=INT(PF1/(10^6))
1290 K5=INT(PF2/(10^6))
1300 K6=INT(PF3/(10^6))
1310 K7=INT(Jj) : REM effective strain rate
1320 K8=INT(YM4)
1330 K9=INT(TM4)
1340 IF GG>1 THEN GOTO 1360
1350 PRINT K;TAB(7) K1;TAB(15) K2;TAB(21) K3;TAB(27) K4;TAB(34) K5;TAB(41) K6;TAB(46)
K7;TAB(51) K8;TAB(56) K9
1360 G=l*B
1370 IF m>0 THEN GOTO 1400
1380 IF K>ANG THEN GOTO 1420
1390 DIEPRESS=K1: YM4=K8 : GOTO 1420
1400 IF K1>POW THEN GOTO 1420

```

```

1410 ANG=K : POW=K1 : JJ1=K7 : JO=J
1420 IF G<60 THEN GOTO 1100
1430 IF m=0 THEN GOTO 9000
1440 IF q=1 THEN GOTO 9000
1450 CLS
1460 PRINT "To determine work done per unit volume on the die (die pressure)"
1470 PRINT "and subsequently abutment pressure enter 1"
1480 INPUT q
1490 IF q=1 THEN GOTO 8000
1500 END

5000 L2e=(AP-WV1)*NA/((YM1+YM33a)*.5*W*(SA-(D1*1000))) :REM assuming temp rise, note:
equate Tf & L22 directly and YM1,2,3 cancel
PRINT "L2e="L2e
5042 Tf=(YM1+YM33a)*.5*W*L2e/(2.37*(D2*1000)) :REM friction at shoe interface
5043 T2=(3.3*((D1*1000/SA)^2)*Tf)+30 :REM bulk feed temp incl. tool cond. back to deforming
feed
5046 I2=ATN((r-((D4*1000)/2))/Ah)
PRINT "angle 2-3" I2
5047 Aaa=2*V2*e3*.5/D4 :REM Aaa= ((6*V2*((D2)^2)*e3)/((D4^3)-((D2)^3)))
5048 JJJ=Aaa*TAN(I2) :REM strain rate 2 - 3
5049 time2= e3*.5*TAN(I2)/JJJ
PRINT "time2="time2
5051 T3a=(1.273+(.023*D2*1000))*time2^-.377
5053 T3b=(.162*(time2^-.511))
5054 Speed=V2*100 :REM units m/s to cm/s
5055 T3c=T3a*.55/(((2.7*.21*Speed)^2)*NA*.01) :REM units cm
PRINT "T3c="T3c
5056 T3d=T3b/(2.7*.21*Speed)
PRINT "T3d="T3d
5057 Ti= ((PPT*.95)/2.37) :REM assume 98 % adiabatic heat initially; check temp. i.e. abut temp =
AP-POW; neglecting friction at abut. and dead zone.
5058 T3=(Ti/(1+T3c+T3d))+T2
5059 TM3=((T3+T2)/2) :REM T2 is accounted for in equation for T versus wheel speed. however
, heat conduction to feed is greater at higher speed
PRINT "TM3="TM3
5060 TH3=TM3/645
5061 YM3=166*(1-(1.13*TH3))^(JJJ*(.014*(10^(1.22*TH3))))
LET e1a=e1+PSS
LET e3a=e3+e1a
5062 YM33=YM3*(((e3/2)+e1a)^.23) :REM average true stress over suitable range of true strain
for use with redundant and friction work
PRINT "YM33a="YM33a
PRINT "YM33="YM33 :REM true stress after A&P for strain hardening
5063 HH= YM33a-YM33
5070 IF ABS(HH)<1 THEN GOTO 5090
5080 YM33a=YM33 :GOTO 5000
5090 GOSUB 7000
5100 TM4=(T5+T3)/2
5110 TH4=TM4/645
5120 TH1=T3/645
5130 GOTO 900

7000 Tid= DP*.95/2.37
7005 IF GG=0 THEN GOTO 7020 :REM ASSUME ADIABATIC HEATING
7010 time3=e4*.5*JO/JJ1
7020 PRINT "time3="time3
7025 T5a=(1.273+(.023*D4*1000))*time3^-.377
7030 T5b=.162*(time3^-.511)
7040 T5c=.55*T5a/((2.7*.21*V4*100)^2*1.43)
PRINT "T5c="T5c
7050 T5d=T5b/(2.7*.21*V4*100)
7060 T5=(Tid/(1+(1.3*T5c)))+T3
7105 TH2=T5/645
7150 PRINT "T3="INT(T3) :TAB (20) "T5="INT(T5)
7200 RETURN

8000 PRINT "min power/volume = 1.68*(20) *dead-zone angle"

```

```

8020 PRINT TAB(4)"N/mm2"; TAB(24)"DEG"
8025 PRINT"_____ "
8030 PRINT TAB(4) POW; TAB(24)ANG
8040 PRINT""
8045 PRINT "ABUT PRESS=" INT(AP) ;TAB(20) "DIE PRESS.:" INT(DP)
8048 PRINT "T3="INT(T3) ;TAB (20) "T5:"INT(T5)
8049 PRINT"_____ "
8050 GOTO 900

9000 CLS
9005 PRINT"To determine the work done per unit volume on the abutment (i.e."
9010 PRINT"abutment pressure)"
9020 PRINT"_____ "
fricarea=(((D3*1000)/2)+r)*(SA-(D1*1000))^2/3+(SA^2)
fricforce=fricarea*YM33*W
PP12=fricforce/NA
CLS
rr1=((12/((SIN(I2))^2))-(1/TAN(I2)))
PP11=((1/TAN(I2))^e3)

9108 PPRF=(2+PP11+(2*rr1))*W*YM33
9110 PPH=YM33*e3 : REM plastic homog. workdone per unit vol.
9120 PPT=PPRF+PPH+VW1
9123 AAP=POW+PPT
9125 L2=(AAP-WV1)*NA/((YM1+YM33a)*.5*W*(SA-(D1*1000)))
9126 abutpress=INT(AAP+PP12) : abutload=(INT((abutpress*NA)/100))/10
diearea=(((D4*1000)^2)-(D5*1000)^2)*3.142/4 : dielead=(INT((DP*diearea)/100))/10
L2fl=L2+r-((D3*1000)/2)
9127 IF FLASH=0 THEN GOTO 9136

9128 tt=(.2*(D4/D5)^1.1) :REM thickness
efl=LOG(D1*1000)/tt
9129 Widthfl=FLASH*(3.142*((D1*1000)^2))/(4*tt)
PRINT"Flash width="Widthfl
TWDfl=2*YMfla*efl/2.37 :REM two sides
9131 Tflb=YMfla*W*.5*Widthfl/(2.37*tt)
Tflc=YMfla*W*L2fl/(2.37*tt)
Tfla=((1)*Tflb)+(.32*Tflc)
time1fl= L2fl/(S11*.1715*1000)
alpha=(1.273+(.023*tt*1000))*time1fl^-.377
Vfl=Widthfl/(2*time1fl*1000)
Tcc=alpha*.55/(((2.7*.21*Vfl*100)^2)*L2fl*tt*.01)
PRINT"Tcc=Tcc"
Tfl=(Tfla/(1+Tcc))+((T2-30)/2)+30
PRINT"Tfl=Tfl"
THfl=Tfl/645
jfl=(efl*Vfl*1000)/(2*Widthfl) :REM rate of deformation
PRINT"Jfl=jfl"
YMfl=166*(1-(1.13*THfl))*(jfl^(.014*(10^(1.22*THfl))))
PRINT"YMfl=YMfl"
Flashfric=L2fl*Widthfl*.5*YMfl*W
Torqflb=Flashfric*.1715
LET III=YMfla-YMfl
IF ABS(III)<1 THEN GOTO 9136
LET YMfla=YMfl : GOTO 9128
9136 Torqfla=(YM33a+YM1)*.5*W*(D1*1000*L2fl)*.1675
PRINT"Torqfla=Torqfla"
Torq=Torqfla+Torqflb+(abutpress*NA*.1675)
PRINT "ABUT PRESS (exp);" INT(APex) ;TAB(23) "DIE PRESS.(exp);" INT(DPex);TAB(45) "Torque (exp
);"(INT(Tor/100)/10)
9137 PRINT"abut area=";(INT((NA*10)+.1))/10;"mm2" TAB(25) "abutmean dia=";(INT(D2*10000))/1
0;"mm"
PRINT"abutment load (theo);"abutload;"kN";TAB(28) "abutment pressure (theo);"abutpress;"N mm2"
PRINT"die load (theo);"dielead;"kN"
P R I N T "-----"
9140 PRINT"abut. press:"TAB(12)"L2";TAB(17)"SR ;TAB(23)"YM2-3";TAB(31) "Y1";TAB(33)"T2" TA
E(44) "T3"; TAB(49) "wheel";TAB(56) "Torque"
9141 PRINT TAB(50) "speed"
9143 PRINT"N/mm2";TAB(12)"mm"; TAB(17)"1/s";TAB(23)"N/mm2";TAB(31) "mm"
A S(44) "C" TAB(49) "rev/min";TAB(57) "KNm"

```

```

9146 PRINT*
9150 PRINT INT(AAP);TAB(11) INT(L2);TAB(16) INT(JJJ);TAB(22) INT(YM33);TAB(30) INT(YM1);T
AB(38) INT(T2);TAB(43) INT(T3);TAB(49) S1;TAB(56) (INT(Torq/100)/10)
9155 PRINT*
-----
9160 PRINT"die press";TAB(10) "dead-zone";TAB(21) "power";TAB(28)"SR";TAB(33) "die";TAB(39)
"YM3-5";TAB(46) "T5";TAB(52) "T3"
9165 PRINT TAB(12) "angle";TAB(23) "die"
9170 PRINT "N/mm2";TAB(12)"deg";TAB(21) "N/mm2";TAB(28) "1/s";TAB(33) "mm";TAB(39)"N/mm
2";TAB(46) "C";TAB(52) "C"
9180 PRINT*
-----
9190 PRINT INT(DIEPRESS);TAB(11) ANG;TAB(21) INT(POW);TAB(27) JJ1;TAB(32) (D5*1000);TAB
(39) INT(YM4);TAB(45) INT(T5);TAB(51) INT(T3)
PRINT"jfl";(INT(jfl*10))/10;TAB(15) "tt";(INT(tt*100))/100;TAB(25) "Widthfl";(INT(Widthfl*10)
)/10;TAB(40)"YMfla";INT(YMfla)
9192 IF m=0 THEN GOTO 9250
9192 XX=AAP-AP
9193 IF ABS(XX)<2 THEN GOTO 9200
9195 LET AP=AAP :GOTO 5000
9200 m=0 : GOTO 900
9250 XXX=DIEPRESS-DP
9255 IF ABS(XXX)<2 THEN GOTO 9300
9260 LET DP=DIEPRESS
9270 m=1 : GOTO 5000
9300 PRINT*To determine the force components i.e. dead-zone friction
END

```